Les bactéries comme actrices du microbiote intestinal entre inflammation, métabolisme des acides biliaires et interaction avec les bactériophages

Lorenzo Chaffringeon

Sorbonne Université

Ecole doctorale 394 : Physiologie, Physiopathologie et Thérapeutique

Centre de recherche Saint-Antoine / Equipe Microbiote, intestin et inflammation

Institut Pasteur / Unité Bactériophage, Bactérie, Hôte

Les bactéries comme actrices du microbiote intestinal entre inflammation, métabolisme des acides biliaires et interaction avec les bactériophages

Par Lorenzo Chaffringeon

Thèse de doctorat de Microbiologie

Dirigée par Jean-Pierre Grill et Laurent Debarbieux

Présentée et soutenue publiquement le 8 juillet 2022

Devant un jury composé de :

M. Vincent Maréchal, PU	Président du Jury
Mme. Catherine Schouler, DR	Rapportrice
M. Philippe Langella, DR	Rapporteur
Mme. Bénédicte Pigneur, MCU-PH	Examinatrice
M. Frédéric Laurent, PU-PH	Examinateur
M. Jean-Pierre Grill, PU	Directeur de Thèse
M. Laurent Debarbieux, DR	Co-directeur de Thèse
Mme. Luisa De Sordi, MCU	Co-encadrante de Thèse

« Le hasard ne favorise que les esprits préparés »

- *Mon père citant Louis Pasteur quand j'étais petit*

Titre : Les bactéries comme actrices du microbiote intestinal entre inflammation, métabolisme des acides biliaires et interaction avec les bactériophages.

Résumé : Le microbiote intestinal et la santé humaine sont étroitement liés. Les bactéries et leur virus, les bactériophages, sont les plus abondants microorganismes de ce microbiote. Ces différents acteurs sont en relation entre eux mais aussi avec l'hôte, formant de dynamiques complexes qui restent encore peu comprises.
Au cours de cette thèse, nous avons d'abord étudié les interactions entre bactériophages et bactéries dans l'intestin à l'état basal. Premièrement, nous avons constaté que l'environnement intestinal modulait l'expression génétique des bactéries. Parmi les gènes différentiellement exprimés, certains modifiaient leurs interactions avec les bactériophages. Deuxièmement, nous avons observé dans l'intestin que la répartition spatiale différentielle entre bactériophages et bactéries se manifestait par la présence de refuges pour les bactéries. Ces observations, en accord avec le modèle écologique « source-puits », permettent d'expliquer la coexistence entre ces deux populations antagonistes sans provoquer l'émergence de bactéries résistantes.
Enfin, nous avons étudié l'effet de l'acide ursodésoxycholique, un acide biliaire épimérisé, sur l'inflammation intestinale. Un nouveau modèle d'inflammation intestinale induite par le pathogène murin *Citrobacter rodentium* a été mis au point et caractérisé chez des souris gnotobiotiques. La capacité anti-inflammatoire de cet acide biliaire passe par l'inhibition de la voie de l'IL-22, une cytokine clé de la réponse à l'infection par *C. rodentium*.
Ces résultats nous ont permis de mieux comprendre comment les bactéries intestinales participent à l'homéostasie du tractus digestif et comment elles coexistent avec leurs virus prédateurs.

Mot clés : Inflammation, Microbiote intestinal, Bactériophages, Infections intestinales, Acides biliaires

Title: Bacteria as actors of the intestinal microbiota between inflammation, bile acid metabolism and interaction with bacteriophages.

Abstract: The intestinal microbiota and human health are closely linked. Bacteria and their viruses, bacteriophages, are the most abundant microorganisms of the microbiota. These different actors are in relation with each other but also with the host, forming complex dynamics that are still poorly understood.
In this thesis, we first studied the interactions between bacteriophages and bacteria in the gut in physiological condition. First, we found that the gut environment modulated bacterial gene expression. Among the differentially expressed genes, some modified their interactions with bacteriophages. Second, we observed that the differential spatial distribution between bacteriophages and bacteria in the gut was manifested by the presence of refuges for the bacteria. These observations, in agreement with the "source-sink" ecological model, explain the coexistence between these two antagonistic populations without causing the emergence of resistant bacteria.
Finally, we studied the effect of ursodeoxycholic acid, an epimerized bile acid, on intestinal inflammation. A new model of intestinal inflammation induced by the murine pathogen *Citrobacter rodentium* was developed and characterized in gnotobiotic mice. The anti-inflammatory capacity of this bile acid is mediated through the inhibition of the IL-22 pathway, a key cytokine in the response to *C. rodentium* infection.
These results have allowed us to better understand how intestinal bacteria participate in the homeostasis of the digestive tract and how they coexist with their predatory viruses.

Keywords: Inflammation, Gut microbiota, Bacteriophages, Intestinal infections, Bile acids

Remerciements

Cette thèse a été une formidable aventure scientifique, mais avant tout humaine. J'ai pu rencontrer tant de personnes formidables que je tiens à remercier ici.

Je souhaiterais tout d'abord remercier les membres du jury pour avoir pris le temps d'évaluer ce travail.

Ensuite je tiens à remercier Laurent pour m'avoir fait confiance et accepté dans son équipe dès mon stage de M2 alors que, il faut bien l'avouer, je n'avais aucune expérience. Tu as su me guider, m'encourager, me conseiller tout en me laissant une grande liberté.

Un grand merci à Jean-Pierre qui m'a ramené jusqu'au CRSA et sans qui je n'aurais pas pu faire cette thèse. Tes conseils m'ont été d'une grande aide pendant toute la thèse. Les discussions que nous avons eues allaient bien souvent au-delà de la science et m'ont aidé à comprendre le monde académique d'aujourd'hui.

Luisa, tu as été ma directrice adoptive dès le début de cette thèse. Tes conseils et tes remarques m'ont accompagné tout le long de cette aventure et tu m'as permis de progresser bien au-delà de ce que j'aurais pu espérer.

Je remercie également les professeurs Philippe Seksik et Harry Sokol pour m'avoir accueilli dans leur équipe à Saint-Antoine.

Je voudrais évidemment dire merci à tous les membres de l'unité BBH. Quentin, tu as su m'accompagner et me transmettre tant de choses au cours de ces années, mais tu m'as surtout montré que la thèse pouvait être une aventure plus qu'amusante ! Merci Marta de m'avoir accueilli dans la « gut team » avec Quentin en M2 et de m'avoir embarqué dans tous tes projets passionnants. Merci à toi Devon pour nous avoir joyeusement rejoints dans cette aventure et pour avoir enfin révélé au monde que je suis « nicer than Quentin ».

Je tiens à remercier aussi Thierry et Marie pour leur aide, leurs conseils et pour avoir su me transmettre une part de leur expérience. Céline, tu viens tout juste d'arriver, mais tu fais déjà partie de l'équipe !

Je n'oublie pas les membres de la « team lung », Quentin n°2 (et oui), Sophia, Xavière pour les moments conviviaux que nous avons partagés. Je remercie particulièrement Baptiste pour toutes les discussions médicales, scientifiques et tes râleries qui nous ont bien amusés !

Je remercie aussi les anciens membres de l'unité : Mathieu, Raphaëlle, Tanguy pour toutes nos discussions, scientifiques ou non. Une pensée pour toi Rokhaya, je me souviendrai toujours des moments joyeux passés avec toi et de ton rire communicatif.

Je suis particulièrement reconnaissant envers Ana pour m'avoir aidé dans la plus grande épreuve de cette thèse : l'administration.

En restant à Pasteur, je pense aussi aux voisins de l'unité Arvir pour leur gentillesse et leur aide. Je remercie également Julian pour avoir amené sa bonne humeur jusque dans notre laboratoire. Merci à toute l'équipe de l'animalerie Lwoff, particulièrement Martine et Eddie, sans qui ce projet de thèse n'aurait pas pu être mené à bien, mais surtout pour leur

bienveillance. Enfin, au monsieur qui fait les pizzas à la cantine de Pasteur : je ne connais pas votre nom, mais vous occupez une place importante dans ma vie.

Je remercie toute l'équipe MII pour m'avoir accueilli en début de thèse, que ce soient les gens « du six » comme « du douze », vous avez fait de Saint-Antoine un endroit accueillant alors même qu'il n'y a pas de cantine là-bas.

Loïc pour m'avoir supporté et encouragé dans tous mes projets, même les plus farfelus, merci pour ta patience et ta gentillesse (si si, ta gentillesse j'ai dit). Merci Coline de m'avoir donné un kinder Bueno une fois. Spéciale dédicace à Nathalie et ses super pâtisseries ! Merci à Charlotte d'avoir accepté de participer à mon étude très bien construite sur les effets du café (n=1).

Merci à Véronique pour avoir eu la patience de m'apprendre à cultiver les Caco alors que je n'en avais même pas la patience moi-même. Je tiens aussi à remercier Olivier pour ses précieux conseils qui m'ont aidé à être plus rigoureux.

Merci à tous.tes les copaines et les colocs : Anaïs, Anaëlle, Manzo, Léa, Tania, Aurélien, Dorian, Dorian (le chat), Coline, Noa, Camille, Étienne, Sébastien, Garance, Marion, Thomas et à tous les colocataires temporaires passés par la « maison du bonheur de Bagneux ». Merci à Mohamed de m'avoir encouragé à me dépasser et aller au-delà de ce que je pensais être capable.

À toi Diane, qui m'a accompagné pendant toutes les épreuves de la vie. Pour tous les moments de joie, de tristesse, de surprise et d'inquiétude que nous avons partagés. Chaque jour avec toi est agréablement inattendu et si je devais traduire cela en musique cela donnerait l'Etude Op. 25 No. 5 de ton pianiste préféré.

Je remercie mes parents et mes frères pour m'avoir soutenu pendant toutes ces années et sans qui je n'aurais jamais pu accomplir tout ça. Grâce à vous je n'ai jamais hésité à m'engager dans de longues études. Merci à toi Clara pour ton soutien inconditionnel depuis toujours. À mon grand-père Émile : tu pensais que j'étais encore en médecine et ne comprenais pas vraiment ce que je faisais, mais tu étais quand même fier de moi. Je pense à toi.

Sur ces belles paroles je dois vous laisser, il est 11h30, l'heure d'aller manger !

Table des matières

Introduction

I – L'appareil digestif

L'appareil digestif est un ensemble d'organes permettant l'assimilation de nutriment du milieu extérieur afin qu'ils soient utilisés comme source d'énergie ou participant au métabolisme de nouvelles molécules. Il permet aussi l'élimination de produits du catabolisme. Pour étudier cet appareil complexe, nous prendrons comme modèle de l'être humain un autre mammifère : la souris.

A) Organisation générale du l'appareil digestif

Anatomie

L'appareil digestif est constitué du tractus digestif s'entendant de la bouche à l'anus ainsi que d'organes en relation avec ce tractus : le foie, la vésicule biliaire et le pancréas.

L'œsophage, l'estomac, l'intestin grêle, le colon et le rectum font partie du tractus digestif. Lors de cette thèse, nous ne nous intéresserons qu'au tractus digestif à partir de l'intestin grêle ainsi qu'au foie et voies biliaires. L'intestin grêle est un organe en forme de tube creux de six à huit mètres de long chez l'humain. Il est séparé en trois parties : le duodénum, le jéjunum et l'iléon du plus proximal au plus distal. Chez l'humain le caecum n'est que légèrement plus large que le colon qui lui fait suite tandis qu'il est très développé et formant un organe bien délimité chez la souris, organisme modèle que nous étudierons. Chez l'humain, colon est également décrit en trois parties, le colon ascendant à droite, transverse puis descendant à gauche. Enfin le tractus se termine par le rectum et le sphincter anal. Le foie est en communication avec la vésicule biliaire par le canal hépatique commun et le canal cystique. La réunion de ces deux canaux forme le canal cholédoque qui s'abouche au niveau du duodénum par le sphincter d'Oddi. (Fig. 1)

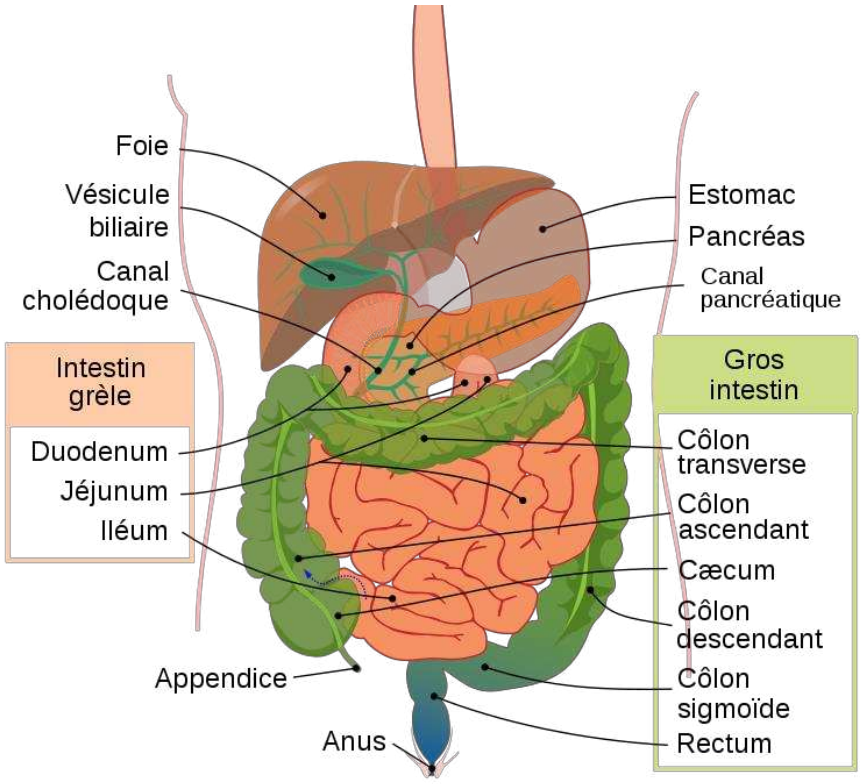

Figure 1 : Schéma du système digestif humain. Schéma de Mariana Ruiz (1)

Histologie

Bien que les caractéristiques histologiques varient le long du tractus digestif, certaines structures persistes tout au long de l'intestin. On retrouve ainsi les mêmes couches concentriques avec, de l'extérieur vers l'intérieur : la séreuse, la couche musculaire externe, la sous-muqueuse et enfin la muqueuse. La muqueuse comporte elle-même plusieurs couches concentriques : la musculaire muqueuse, la *lamina propria* (composé de tissu conjonctif), la lame basale et l'épithélium. L'épithélium est composé de nombreux types cellulaires avec des structures et des fonctions variées qui seront détaillés ci-après (2) (Fig. 2).

Au-delà de l'aspect tubulaire, des éléments caractéristiques différencient les sections intestinales. Au niveau de l'intestin grêle, on retrouve des projections de la muqueuse dans la lumière intestinale, appelées villosités, ainsi que des invaginations de celle-ci appelées cryptes de Lieberkühn augmentant la surface en contact avec la lumière intestinale. Le colon se différencie de l'intestin grêle par l'absence de villosité.

Parmi les différents types cellulaires, les cellules souches situées à la base de la crypte se différencient en cellules amplificatrices de transit, qui cessent de proliférer aux deux tiers des cryptes pour devenir des cellules épithéliales matures.

Les entérocytes constituent les cellules majoritaires de l'épithélium intestinal. Elles ont pour fonction l'absorption des nutriments qui est facilité par leur pôle apical avec de nombreuse microvillosités formés de replis de la membrane plasmique augmentant grandement leur surface. Elles sont parfois appelées colonocytes dans le colon. Les entérocytes sont renouvelés très rapidement, avec une durée de vie de trois à cinq jours (3).

Les cellules caliciformes, ou cellules à mucus ouvert, produisent les mucines qui sont le constituant majeur du mucus. Leur abondance augmente le long de l'intestin de l'intestin grêle, où elles sont absentes des villosités, au colon. Les cellules caliciformes, comme les entérocytes, migrent de la base des cryptes vers la lumière intestinale.

Les cellules de Paneth sont regroupées au fond des cryptes intestinales de l'intestin grêle et produisent des peptides anti-microbiens (PAM).

Les cellules entéro-endocrines sont des cellules isolées les unes des autres tous le long de l'intestin. Elles sont responsables de la sécrétion d'hormones et transmettent les signaux mécaniques et chimiques (4).

Les cellules M font partis du tissu lymphoïde associé au tube digestif et du tissu lymphoïde associé aux muqueuses (ou GALT et MALT de l'anglais « gut associated lymphoid tissue » et « mucosal associated lymphoid tissue ») et sont regroupés au sein des plaques de Peyer. Elles se différencient des entérocytes par l'absence ou la faible concentration de microvillosités à leur pôle apical. Elles ont pour rôle le transport d'antigène de la lumière intestinale vers la *lamina propria* afin d'interagir avec le système immunitaire au niveau des follicules permettant d'initier rapidement une réponse face à une infection (5).

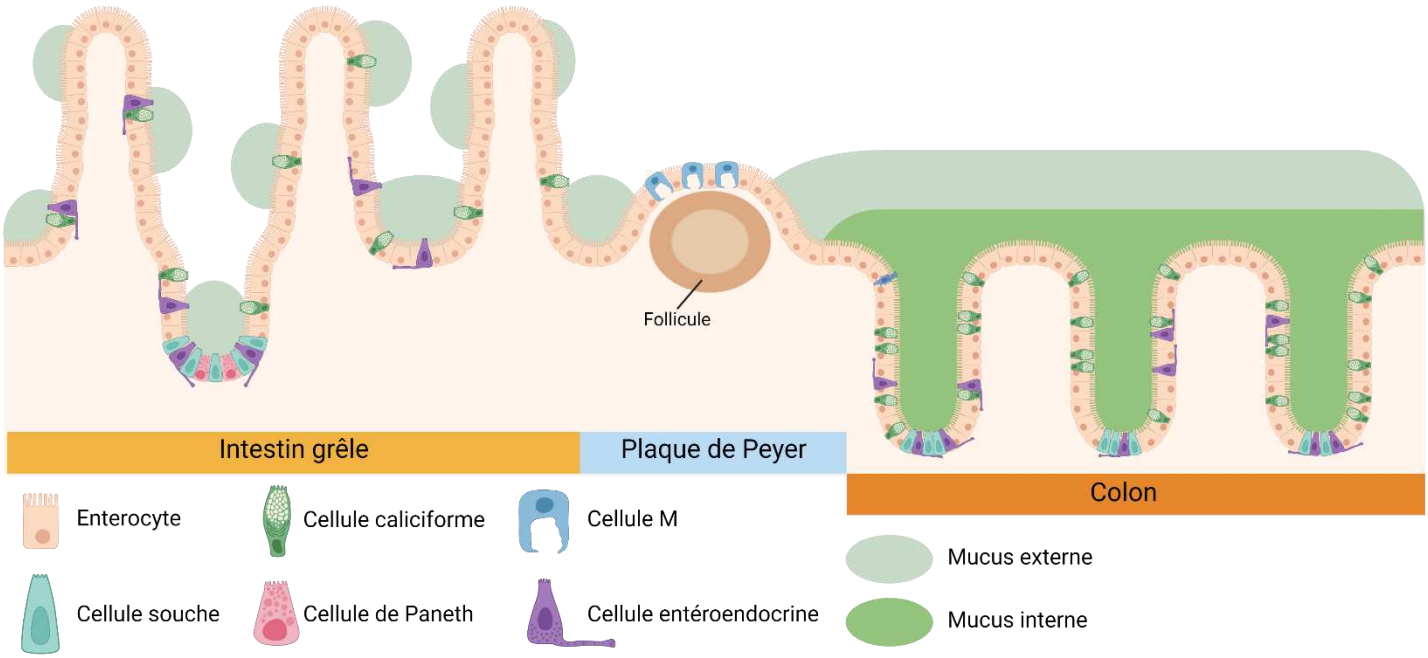

Figure 2 : Composition cellulaire de l'épithélium intestinal.

Physiologie générale

Les fonctions principales de l'intestin sont la digestion et l'absorption. La digestion regroupe les mécanismes permettant la transformation des aliments en nutriments qui pourront ensuite être absorbés. L'absorption des nutriments est réalisée par les entérocytes, cellules majoritaires de l'épithélium intestinal, transportant les nutriments de la lumière intestinale (pôle apical) vers le réseau sanguin et lymphatique (pôle basolatéral).

De nombreuses hormones régulent ces deux fonctions, digestion et absorption, participant à la fonction endocrine de l'intestin. Ces hormones sont sécrétées par les cellules entéro-endocrines influençant la physiologie intestinale comme le métabolisme du glucose. Par exemple, le Glucagon-Like Peptide 1 (GLP1) stimule la sécrétion d'insuline après le repas. Inversement, la ghréline inhibe la sécrétion d'insuline entre les repas (6). Les hormones jouent également un rôle important dans le métabolisme des acides biliaires.

B) Le métabolisme des acides biliaires

Les acides biliaires jouent un rôle important dans la physiologie intestinale, aussi bien dans la digestion que dans l'absorption des nutriments. Grace à leur propriété amphiphile, ils émulsifient les lipides et les vitamines liposolubles (A, D, E et K) en formant des micelles, augmentant la surface de contact pour les enzymes permettant leur digestion et facilitant leur

absorption (7). Ils forment également une voie du catabolisme du cholestérol. Ils interviennent également dans le métabolisme de glucides (8) et la prolifération cellulaire (9).

Métabolisme intrahépatique des acides biliaires

Le foie intervient dans la physiologie intestinale *via* la production de la bile. La bile est un liquide visqueux stocké dans la vésicule biliaire et sécrété sous l'action de la Cholécystokinine à la suite du passage d'aliments dans le duodénum (10). Elle participe à la digestion et à l'absorption des lipides et des vitamines liposolubles (A, D, E et K) ainsi qu'à l'excrétion de molécules issues des voies du catabolisme, comme la bilirubine issue de la dégradation de l'hème de l'hémoglobine et autres hémoprotéines ou encore de certains médicaments. Elle est composée à 97% d'eau, le reste étant formé d'acides biliaires, de cholestérol, de phospholipide, de bilirubines, d'ions et de vitamines (11).

Les acides biliaires sont des petites molécules dérivées du cholestérol produites par le foie et sécrétées dans la bile. Chez l'humain, il existe deux voies du métabolisme des acides biliaires : une voie classique formant 90% des acides biliaires et une voie alternative formant les autres 10%. La voie classique aboutit à une production équivalente d'acides choliques (CA) et d'acides chénodésoxycholiques (CDCA) tandis que la voie alternative ne produit que du CDCA (12). Chez la souris, le CDCA est en partie transformé en acide α-muricholique (αMCA) (13). Les souris produisent aussi de l'acide ursodéoxycholique (UDCA) qui est en grande partie transformé en acide β-muricholique (βMCA) avant d'être excrété (14). Ils sont alors sous forme de sels conjugués avec un acide aminé, glycine ou taurine. Les acides biliaires conjugués ont une capacité importante d'émulsification des lipides, les rendant plus accessibles à la lipase pancréatique et facilitant leur digestion (7).

Métabolisme des acides biliaires par le microbiote intestinal

Les acides biliaires produits du foie et sécrétés dans la lumière intestinale sont nommés acides biliaires primaires. Ils sont ensuite métabolisés par le microbiote intestinal formant les acides biliaires secondaires. Chez l'humain, seul de CA et le CDCA sont considérés comme étant primaire alors que chez la souris, l'αMCA et le βMCA le sont aussi. Étant produit par la souris, l'UDCA est aussi parfois catégorisé comme acide biliaire primaire, mais n'étant que faiblement excrété dans l'intestin et en grande partie issue de la transformation bactérienne, il est parfois considéré comme secondaire (15).

Les acides biliaires primaires sécrétés sont conjugués à un acide aminé (glycine ou taurine). La première étape nécessaire à toutes les autres transformations microbiennes est la déconjugaison. Cette réaction nécessite la présence d'une enzyme bactérienne : la bile salt hydrolase (BSH). La BSH libère une molécule de taurine ou de glycine d'une part et une

molécule d'acide biliaire d'autre part, qui est toujours considérée comme primaire à cette étape. Cette enzyme est très repandue parmi les bactéries du microbiote et a notamment déjà été identifiée dans plusieurs genres : *Lactobacillus*, *Bifidobacterium*, *Enterococcus*, *Clostridium* spp., et *Bacteroides* (16). Ces acides biliaires déconjugués sont majoritairement réabsorbés au niveau de l'iléon terminal où ils sont transportés vers le foie par la veine porte. Ils sont ensuite reconjugués dans le foie et sécrétés de nouveau dans l'intestin, c'est le cycle entéro-hépatique (Fig. 3) (17).

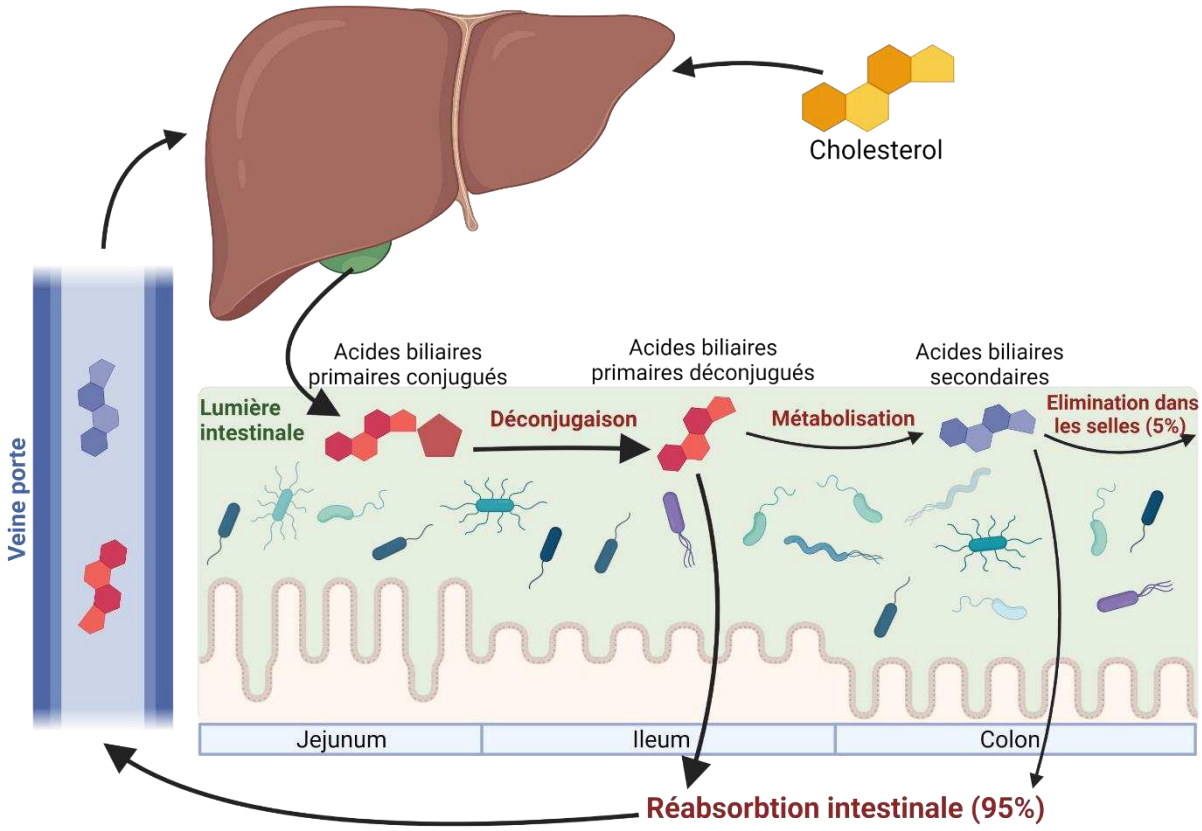

Figure 3 : Cycle entéro-hépatique des acides biliaires.

Au niveau du colon, les acides biliaires vont subir différentes transformations aboutissant à la production d'acides biliaires secondaires (18). L'une des réactions clés est la déshydroxylation du carbone 7, transformant le CA et le CDCA en acide désoxycholique (DCA) et acide lithocholique (LCA), respectivement. Cette réaction est réalisée par un ensemble d'enzymes réunies dans l'opéron *bai* présent dans certaines bactéries du genre *Clostridium* et notamment *C. scindens, C. hylemonae et C. hiranoni* (19,20). Une autre réaction importante est l'épimérisation qui nécessite deux étapes : une oxydation puis une réduction d'un groupement hydroxyle. Ainsi, le groupement hydroxyle du carbone 7 du CDCA est oxydé en 7-oxoLCA puis

réduit pour former de l'UDCA. Ces deux étapes nécessitent l'action de deux enzymes distinctes : la 7α-hydroxysteroid deshydrogenase et la 7β-hydroxysteroid deshydrogenase (7α et 7β HSDH) présentes chez *Clostridium baratii* (21). D'autres bactéries ne disposent que d'une des deux enzymes comme *Ruminococcus gnavus* (22). Des épimérisations sont aussi possibles sur les groupements hydroxyles des carbones 3 et 12. Par exemple, le DCA peut être transformé en 3oxo-DCA puis en iso-DCA par d'autres bactéries comme *Eggerthella lenta* et *Ruminoccocus gnavus* (23,24). L'UDCA peut aussi être transformé en LCA *via* une 7β-dehydroxylation (Fig. 4) (25). Une très grande partie des acides biliaires secondaires est réabsorbée au niveau du colon et rejoint la circulation entéro-hépatique puisqu'en général, 95% des acides biliaires sont réabsorbés (Fig. 3).

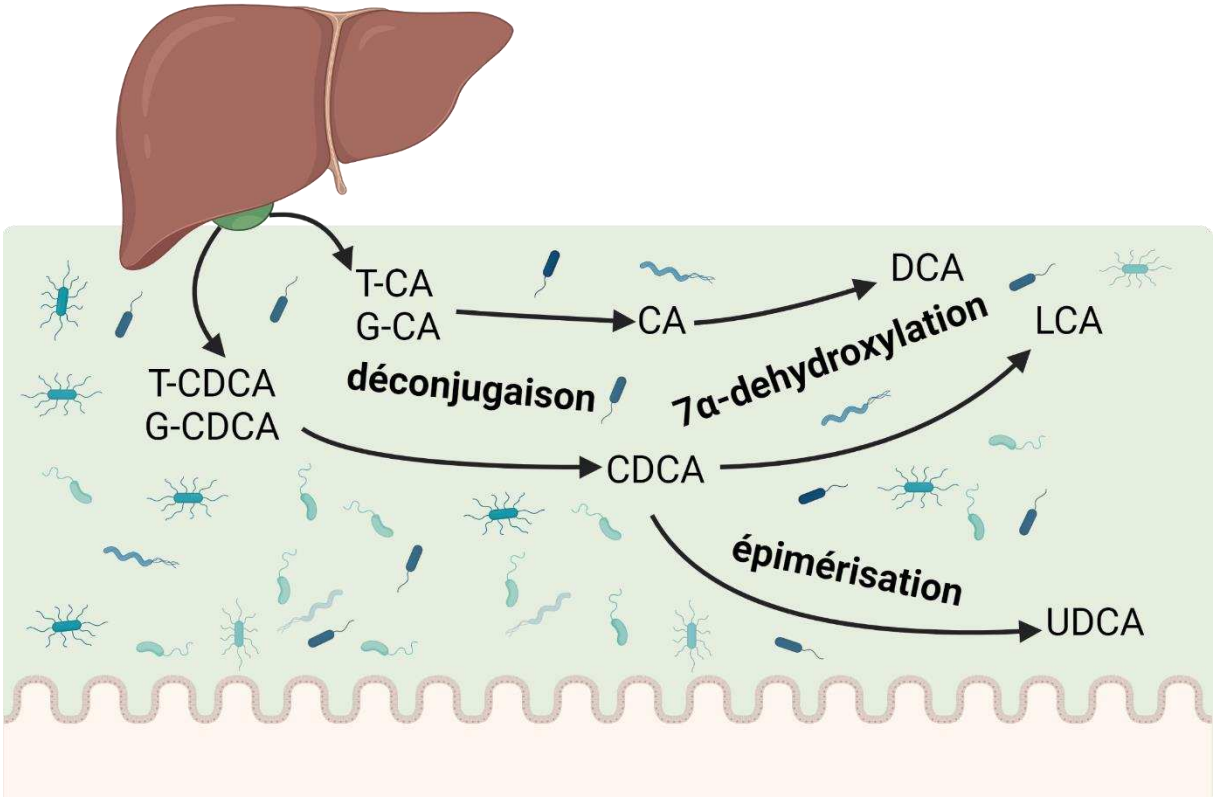

Figure 4 : Principales voies métaboliques bactériennes des acides biliaires. T-CDCA : acide taurochénodésoxycholique ; G-CDCA : acide glycochénodésoxycholique ; T-CA : acide taurocholique ; G-CA : acide glycocholique ; CA : acide cholique ; CDCA : acide chénodésoxycholique ; DCA : acide désoxycholique ; LCA : acide lithocholique ; UDCA : acide ursodésoxycholique

C) La muqueuse intestinale, une barrière perméable

Étant en continuité avec le milieu extérieur, l'intestin est l'hôte d'une population microbienne diverse composé de bactéries, de virus, d'archées, de champignons et de protistes formant ensemble le microbiote intestinal. La plupart des bactéries présentes dans l'intestin sont commensales ; elles ne provoquent pas d'infection et participent au métabolisme intestinal. Cependant certaines bactéries peuvent être à l'origine d'infections. Ces agents peuvent être des pathogènes strictes ou opportunistes s'ils provoquent des infections sur un terrain déjà pathologique ou avec un système immunitaire déficient. Les bactéries pathogènes opportunistes, aussi appelé pathobiontes, peuvent coloniser un individu sain sans provoquer de symptôme ou de maladie. Pour se protéger de ces bactéries, de multiples barrières et défenses sont mises en place par l'hôte. Ces barrières ne sont cependant pas parfaitement étanches, permettant le passage de petites molécules. Ces barrières jouent donc un rôle de filtre. On décrit plusieurs barrières successives : écologique et chimique. Le système immunitaire agit en parallèle de ces barrières, et peut être activé davantage lorsque celles-ci sont franchies.

Barrière écologique

Les ressources nutritionnelles étant riches et diverses, mais limitées, seules les bactéries les plus compétitives parviennent à coloniser le tractus digestif, réduisant la probabilité d'une infection par un pathogène qui serait moins compétitif. Les bactéries influent aussi sur les paramètres physico-chimiques tels que le pH et la concentration en oxygène empêchant la colonisation de certaines bactéries pathogènes (26). Ainsi, les bactéries commensales adaptées à l'intestin sont capables former une barrière écologique. Ce rôle spécifique du microbiote sera abordé dans la partie II-C.

Barrière physique

Recouvrant l'épithélium intestinal, le mucus forme la première barrière physique dans l'intestin permettant de maintenir à distance le microbiote de l'épithélium. Le mucus est produit par les cellules caliciformes et est composé de mucines, majoritairement MUC2. Les mucines sont des glycoprotéines formant des polymères par l'intermédiaire de ponts disulfures. Au niveau de l'intestin grêle, le mucus est sécrété à la base des cryptes et progresse le long des villosités. Il est discontinu et ne recouvre pas l'entièreté de l'épithélium, notamment les extrémités des villosités (27). Chez la souris, le caecum est également recouvert d'un mucus discontinu (28). Le mucus du colon est composé de deux couches, un mucus interne dense et fermement adhérent à l'épithélium et profond de 50 à 100µm. Ce mucus est une barrière physique séparant la lumière intestinale de la muqueuse et présente une forte concentration de PAM,

expliquant qu'il est exempt de bactérie (29,30). Ce mucus dense est lui-même recouvert d'un mucus peu dense régulièrement renouvelé et abritant de nombreuses bactéries. Il est d'une profondeur très variable (Fig. 2).

Les cellules épithéliales sont unies par différentes jonctions. Les desmosomes relient les filaments intermédiaires entre les cellules, permettant de répartir les forces mécaniques sur tout l'épithélium (31). Les jonctions adhérentes relient l'actine des cellules adjacentes, formant une continuité morphologique au sein de l'épithélium (32). Enfin, les jonctions serrées forment la *zonula occludens,* composée des protéines ZO-1 et ZO-2, qui empêche le passage incontrôlé de macromolécules par voie paracellulaire (33). Les molécules traversant l'épithélium sont finement contrôlées, empruntant deux voies : la voie paracellulaire et la voie transcellulaire. La voie paracellulaire permet à l'eau et les petites molécules chargées comme les ions de diffuser à travers l'épithélium. La voie transcellulaire permet l'absorption de molécules activement ou passivement par le biais de canaux et de récepteurs spécifiques. De plus grosses molécules peuvent aussi traverser l'épithélium avec une faible capacité par voie paracellulaire (34).

Barrière chimique

A l'état basal, les microorganismes du microbiote sont isolés dans la lumière intestinale, séparés de l'hôte par l'intermédiaire de plusieurs mécanismes. Les cellules de Paneth sont primordiales pour accomplir cela. Elles sécrètent de nombreux peptides antimicrobiens (PAM) dans la lumière. Il existe plusieurs catégories de PAM qui agissent selon différents modes d'action.

Les défensines induisent une déstabilisation de la membrane bactérienne en formant des pores. Chez l'humain et la souris, il existe deux types de défensines, α et β. Les α-défensines, appelées cryptidines chez la souris, sont sécrétées par les cellules de Paneth tandis que les β-défensines le sont par les entérocytes de l'intestin grêle et du colon (35). Proches des défensines, les cathélicidines ne sont produites que par les colonocytes. Un défaut de production des cathélicidines entraine une plus forte susceptibilité aux infections par des entérobactéries comme *Escherichia coli* ou *Citrobacter rodentium* (36,37).

Comme les défensines, les lectines de types C sont bactéricides. Elles sont composées de la famille des protéines REG, notamment REG3α et REG3γ chez l'humain (REG3β et REG3γ chez la souris), qui agissent en formant des pores au niveau de la paroi bactérienne, ciblant principalement les bactéries Gram + (38). Cependant, certaines études montrent que REG3β peut aussi cibler les bactéries Gram - (39). En conditions physiologiques, REG3γ participe à

la barrière chimique séparant les bactéries du microbiote de l'épithélium intestinal (40). En cas d'infection, la production de REG3γ et REG3β est augmentée en réponse à la sécrétion d'IL-22 (41).

Sécrété par les cellules de Paneth, le lysozyme a une action de dégradation enzymatique de la membrane bactérienne ciblant préférentiellement les bactéries Gram +, mais agissant aussi sur les Gram - (42).

Récemment, il a été montré que les chimiokines, molécules de signalisation du système immunitaire permettant la migration cellulaire, peuvent jouer un rôle antimicrobien. Les modes d'action des chimiokines sont diversifiés, ciblant la membrane bactérienne, la production d'enzymes ou les protéines transmembranaires (43,44).

Certains PAM agissent en séquestrant des nutriments et cofacteurs essentiels à la croissance bactérienne et potentialisent la barrière écologique en favorisant la compétition. Les métaux de transitions sont une cible de choix étant nécessaires dans de nombreux processus cellulaires et étant finement régulé (45). Ainsi, le fer est souvent un facteur limitant au cours de l'infection par une bactérie pathogène (46). Pour améliorer la captation de fer dans l'environnement, les bactéries produisent des sidérophores, des protéines ayant une forte affinité pour le fer. En réponse, l'hôte produit de la lipocaline-2 qui séquestre les sidérophores bactériens, limitant la croissance des bactéries (47). En cas d'inflammation, la sécrétion de lipocalin-2 est stimulée par l'IL-17 et l'IL-22 (48,49).

La réponse immunitaire innée

Au-delà des fonctions décrites précédemment, les cellules épithéliales transmettent aussi des signaux au système immunitaire en produisant des cytokines et chimiokines (50). Une liste des cytokines et chimiokines produites par les cellules épithéliales humaines est présentée dans la Table 1. Pour détecter la présence de bactéries, les cellules épithéliales disposent de Pattern Recognition Receptor (PRR) qui peuvent être transmembranaires comme les Toll like receptor (TLR) ou intracellulaire comme les NOD like receptor (NLR). Les PRR reconnaissent des motifs moléculaires associés aux microorganismes (MAMP) ou aux pathogènes (PAMP), très conservés parmi les microorganismes. Il existe plusieurs types de TLR comme de NLR reconnaissant chacun des motifs non spécifiques différents. Par exemple, le TLR2 reconnait le peptidoglycane des bactéries Gram + tandis que le TLR4 reconnait le LPS des bactéries Gram -.

Types de cytokine	Exemples d'Effets sur l'immunité	Référence
CXCL1 CXCL3 CXCL5 CXCL 8 (IL-8)	Chimioattractant pour neutrophiles	(Kagnoff, 2014)
CCL2 (monocyte chemotactic protein-1) CCL3 (macrophage inflammatory protein 1-α) CCL5 (RANTES)	Chimioattractant pour macrophages et cellules dendritiques	(Kagnoff, 2014; Vijay-Kumar *et al.*, 2014)
CCL20	Chimioattractant pour cellules dendritiques et lymphocytes T mémoire	(Kagnoff, 2014)
CCL22	Chimioattractant pour cellules dendritiques et lymphocytes Th2	(Kagnoff, 2014)
CXCL9 CXCL10 CXCL11	Chimioattractant pour lymphocytes Th1	(Kagnoff, 2014)
CCL28	Chimioattractant pour cellules plasmatiques	(Kagnoff, 2014)
TNFα	Amplifie la réponse pro-inflammatoire	(Jung *et al.*, 1995; Kagnoff, 2014; Vijay-Kumar *et al.*, 2014)
GM-CSF	promotes the survival and activation of macrophages and granulocytes	(Jung *et al.*, 1995; Kagnoff, 2014)
IL-6	Stimule une réponse pro-inflammatoire	(Vijay-Kumar *et al.*, 2014)
IL-1β	Stimule une réponse pro-inflammatoire	(Stadnyk, 2002)
TGFβ	Stimule la prolifération des lymphocyte T et la production d'IgA par les cellules plasmocytes	(Stadnyk, 2002)

Table 1 : Liste non exhaustive des cytokines et chimiokines sécrétées par les cellules épithéliales intestinales humaines. Table réalisée par Garance Coquant (51).

Les PRR sont aussi exprimés par les cellules de l'immunité innée : les cellules dendritiques, les monocytes et macrophages, les granulocytes (comprenant les neutrophiles, éosinophiles et basophiles) et les cellules lymphoïdes innées (ILC). Les cellules dendritiques, les macrophages et les granulocytes sont des phagocytes, ingérant débris cellulaires, corps étranger et microorganismes (52).

Contrairement aux autres lymphocytes, les ILC ne nécessitent pas d'activation préalable et peuvent donc engendrer une réponse rapide face à une infection (53). Les ILC sont regroupées en trois catégories selon les cytokines qu'elles produisent. Les ILC1 produisent de l'IFN-γ tandis que les ILC2 et 3 produisent des cytokines coordonnant la défense contre les infections parasitaires et les pathogènes extracellulaires, respectivement. Les ILC3 produisent notamment de l'IL-17 et de l'IL-22, cytokines clés dans la réponse inflammatoire contre certaines bactéries comme *Citrobacter rodentium* (41). Ces cytokines entrainent la production des PAM comme la lipocaline-2 et les protéines REG3 (38,54).

La réponse immunitaire adaptative

En complément du système immunitaire inné, d'autres cellules peuvent répondre à une infection, reparties selon deux lignages, les lymphocytes T et les lymphocytes B.

Ces cellules font partie du système immunitaire adaptatif, qui apporte une réponse plus tardive que le système immunitaire inné, mais aussi plus efficace et spécifique. La réponse adaptative est mise en place lorsque des cellules présentatrices d'antigène entrent en contact avec un lymphocyte au sein des ganglions lymphatiques et des plaques de Peyer. Toutes les cellules présentent des antigènes, mais les cellules du système immunitaire inné, en particulier les cellules dendritiques, sont spécialisées dans ce rôle. Chaque lymphocyte est spécifique d'un antigène en particulier. À la suite de cette reconnaissance, le lymphocyte va se multiplier et s'activer (52).

Lorsqu'ils sont activés, les lymphocytes B se différencient en plasmocytes capables de produire des immunoglobulines (Ig) et notamment des IgA qui sont transportés dans la lumière intestinale par voie transcellulaire *via* un transporteur spécifique (55). Les IgA vont alors former une couche protectrice à la surface des muqueuses avec le mucus, neutralisant les bactéries en s'adsorbant à leur surface.

Les lymphocytes T se divisent en deux types, les lymphocytes T CD4+ et les lymphocytes T CD8+ qui déterminent le type de cellules pouvant les activer. Les CD8 sont activés en réponse à une infection d'un pathogène intracellulaire, se transforment en lymphocytes T cytotoxiques capables de tuer une cellule infectée.

De manière complémentaire, les CD4 sont activés lors d'une infection par un pathogène extracellulaire. A la différence des CD8, elles n'interviennent pas directement, mais coordonnent la réponse immunitaire de la même manière que les ILC au cours de la réponse immunitaire innée. On retrouve d'ailleurs des CD4 correspondant aux types des ILC : les lymphocytes T CD4+ Th1 correspondent au ILC1, les Th2 aux ILC2 et les Th17 aux ILC3, répondant aux mêmes types de pathogènes et produisant un panel de cytokines similaire. Le rôle des CD4 est donc de produire des cytokines afin de recruter des cellules effectrices comme les neutrophiles. Comme les ILC3, les Th17 sont caractérisés par la production d'IL-17 et d'IL-22 (52).

Un dernier sous-type de lymphocytes T, les lymphocytes Treg, a pour rôle de contrôler la réaction immunitaire et de médier la tolérance immunitaire. Les Treg agissent en sécrétant des cytokines anti-inflammatoires comme l'IL-10, le TGF-β ou l'IL-35. La différenciation d'un lymphocyte T en Treg nécessite l'expression du gène FOXP3 (56).

D) Les acides biliaires en interaction avec l'hôte

Les récepteurs des acides biliaires

En plus de leurs actions sur la digestion, les acides biliaires agissent comme une molécule de signalisation par l'intermédiaire des récepteurs aux acides biliaires, les plaçant à l'interface entre l'hôte et le microbiote intestinal. Les récepteurs sont aussi bien transmembranaires comme le G-protein-coupled bile acid receptor 1 (GPBAR1, anciennement TGR5) que nucléaires comme le farnesoid X receptor (FXR) qui constituent les deux principaux récepteurs des acides biliaires. GPBAR1 est exprimé de manière quasi-ubiquitaire mais est très abondant chez les cellules épithéliales intestinales ainsi que chez certaines cellules immunitaires comme les monocytes/macrophages et les cellules dendritiques (57). Il est également exprimé par les cellules entéro-endocrines où son activation entraine la sécrétion de GLP-1 (58). L'activation de GPBAR1 entraine une augmentation d'AMP cyclique intracytoplasmique qui va enclencher une cascade de signalisation aboutissant à l'inhibition de la voie NF-κB, à la phosphorisation de AKT et à l'activation de ERK1 et 2 (59).

FXR a une distribution tissulaire similaire à GPBAR1 à l'exception de l'épithélium du colon ou il n'est présent qu'en faible proportion. Les acides biliaires ont des affinités différentes selon les récepteurs. Les acides biliaires primaires montrent une plus grande affinité pour FXR et les secondaires pour GPBAR1. Une exception notable est l'UDCA qui est neutre envers FXR et montre une faible affinité pour GPBAR1 (60).

Les acides biliaires primaires et secondaires activent d'autres récepteurs nucléaires, notamment le pregnane X receptor (PXR) (61), le constitutive androstane receptor (CAR) (62) et le vitamin D receptor (VDR) (63) ainsi que des récepteurs couplés aux protéines G, notamment le sphingosine 1-phosphate receptor (SP1R2) (64) et les récepteurs muscariniques M3. Il a aussi été démontré que le 3oxo-LCA pouvait se lier au retinoid-related orphan receptor γt (RORγt) (65). L'UDCA semble également pouvoir de se lier au récepteur aux glucocorticoïdes, inhibant la production d'IFN-γ (66).

Les acides biliaires influencent la réponse immunitaire

Par leurs récepteurs, les acides biliaires semblent avoir une action pléiotropique sur le système immunitaire. Les acides biliaires secondaires exercent une activité anti-inflammatoire tandis que les acides sulfatés inhibent cette activité (67,68). Le 3-OxoLCA inhibe la différenciation des cellules Th17 en se liant directement RORγt tandis que l'isoalloLCA favorise la différenciation des cellules Treg par la production d'espèces réactives de l'oxygène mitochondrial, ce qui conduit à une expression accrue de FOXP3 (65). L'iso-DCA, en inhibant l'immunostimulation des cellules dendritiques *via* le récepteur FXR, favorise aussi la

différenciation de cellules Treg (69). La présence de bactérie avec une activité de déconjugaison dans des souris axéniques contribuait à la différenciation des Treg par l'intermédiaire des récepteurs FXR et VDR (70).

Les acides biliaires influencent également la réponse inflammatoire. Le LCA et le DCA favorisent la régénération d'organoïdes intestinaux via l'activation de GPBAR1 dans les cellules souches intestinales. Des souris dont GPBAR1 a été inhibé développent des colites plus sévères tandis que les souris traitées avec un agoniste de GPBAR1 présentent une meilleure régénération de leurs cellules souches (71). De plus, l'administration intra-rectal de DCA et de LCA démontre une activité anti-inflammatoire dans trois modèles murins (68). Cependant, dans certains modèles murins, le DCA semble avoir un effet pro-inflammatoire (72). Des effets anti-inflammatoires ont aussi été rapportés pour le LCA et l'UDCA dans un modèle de souris traité avec du dextran sulfate sodium (DSS) (73). L'UDCA inhibe également la progression tumorale dans un modèle de souris développant un cancer colorectal après un traitement par DSS (74).

Inversement, un contexte inflammatoire modifie la composition intestinale en acides biliaires. Chez des patients atteints de Maladie Inflammatoire Chronique de l'Intestin (MICI), le ratio acides biliaires primaires sur acides biliaires secondaires est augmenté (67,75).

II – Les bactéries du microbiote

A) Historique

Longtemps inaccessible à l'œil humain, l'étude des microorganismes a débuté avec l'invention du microscope par Antonie van Leeuwenhoek dans les années 1670-80. Il observe alors des « animacules » qui seront appelés plus tard bactéries. Il décrit et compare les bactéries présentes dans sa bouche et ses selles (Fig. 5). Sans le savoir, il vient de faire la première description du microbiote.

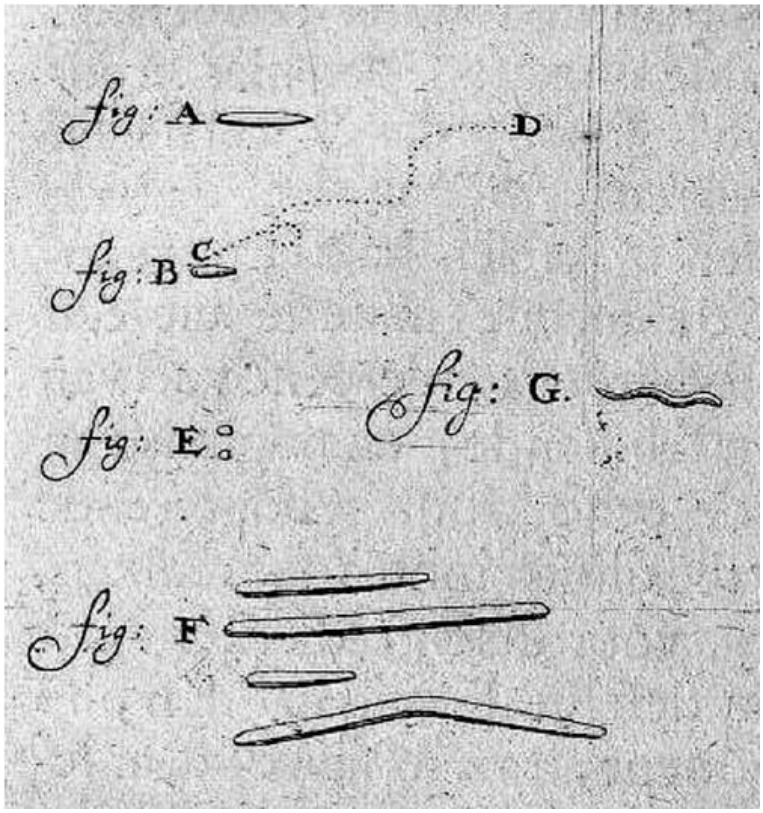

Figure 5 : **Dessin des premières observations des "animalcules" de A. Leeuwenhoek provenant de sa propre bouche**

En 1846, Friedrich Theodor von Frerichs met en avant l'hypothèse que les microorganismes observés dans le tractus digestif sont inoffensifs (76). Dans les années 1880, Théodore Escherich isola une bactérie dans les selles d'enfants sains qu'il nomma *Bacterium coli commune,* qui deviendra *Escherichia coli* par la suite, confirmant l'hypothèse de Frerichs. Escherich pensait alors que *E. coli* constituait la bactérie la plus abondante présente dans l'intestin (77).

Dans les décennies suivantes, Koch, Pasteur, Metchnikoff et bien d'autres se sont intéressés au microbiote ouvrant la voie à l'étude des interactions entre microbiote et hôte. Cependant la plupart des recherches se limitaient encore aux bactéries aérobies, facilement cultivables en laboratoire, qui, on le sait aujourd'hui, ne représentent qu'une infime partie de la diversité des espèces bactériennes.

Ce n'est qu'à partir des années 1940-50 que la culture des bactéries anaérobies se développa, entrainant un essor considérable de ce domaine. Certaines bactéries restaient tout de même récalcitrantes à la culture en laboratoire telle que *Helicobacter pylori,* agent causal d'ulcères gastroduodénaux. Cette bactérie a été retrouvée par des observations histologiques dans l'estomac de patients atteints d'ulcères dès 1906 (78,79). Ce n'est que dans les années 80 que Marshall et Warren réussirent à cultiver *H. pylori* en microaérobie. Cependant, ne parvenant pas à transmettre l'infection à un modèle animal, Berry Marshall décida d'ingérer lui-même une culture de *H. pylori* et développa un ulcère gastrique, démontrant définitivement le lien de causalité entre la bactérie et les ulcères gastriques (80,81).

Au milieu du 20ème siècle, de nombreux microorganismes demeuraient invisibles aux yeux des scientifiques. Aucune méthode ne permettait d'identifier toutes les espèces bactériennes présentes au sein d'une population plurimicrobienne telle que le microbiote intestinal. Le bon technologique apporter par le séquençage de l'ADN permit de palier à ce problème. Il n'était plus nécessaire de cultiver ou d'observer une bactérie pour la caractériser. Il était même possible de retracer leur arbre phylogénétique. En 1985, Carl Woese tira profit de cette avancée pour mettre au point une nouvelle technique. Les gènes codant pour les ARN ribosomiques des bactéries étant très conservés parmi toutes les bactéries, il démontra que les quelques mutations présentent dans les séquences codant les ARN ribosomiques 16S et 5S permettaient d'identifier les différents phyla bactériens, remontant parfois jusqu'à l'espèce (82). Cette technique révolutionna la microbiologie, permettant l'étude des populations, mais aussi de l'évolution des bactéries, cultivables ou non.

De grands projets internationaux tel que le « Human Microbiota Project », débuté en 2007, tentent désormais de caractériser la complexité du microbiote (83). Aujourd'hui, les enjeux se portent sur le fonctionnement du microbiote et notamment ses interactions avec l'hôte. Le microbiote est considéré aujourd'hui comme un organe à part entière (84). L'implication du microbiote est également étudiée dans diverses pathologies telles que l'obésité (85), les Maladies Inflammatoires Chroniques de l'Intestin (MICI) (67,86), le cancer colorectal (87), le diabète (88) et bien d'autres encore.

B) Formation et composition du microbiote humain

Toutes les muqueuses en contact avec le milieu extérieur sont colonisées par des microorganismes : des champignons, des archées, des protistes et, mais aussi des bactéries et des virus formant ensemble le microbiote (Fig. 6).

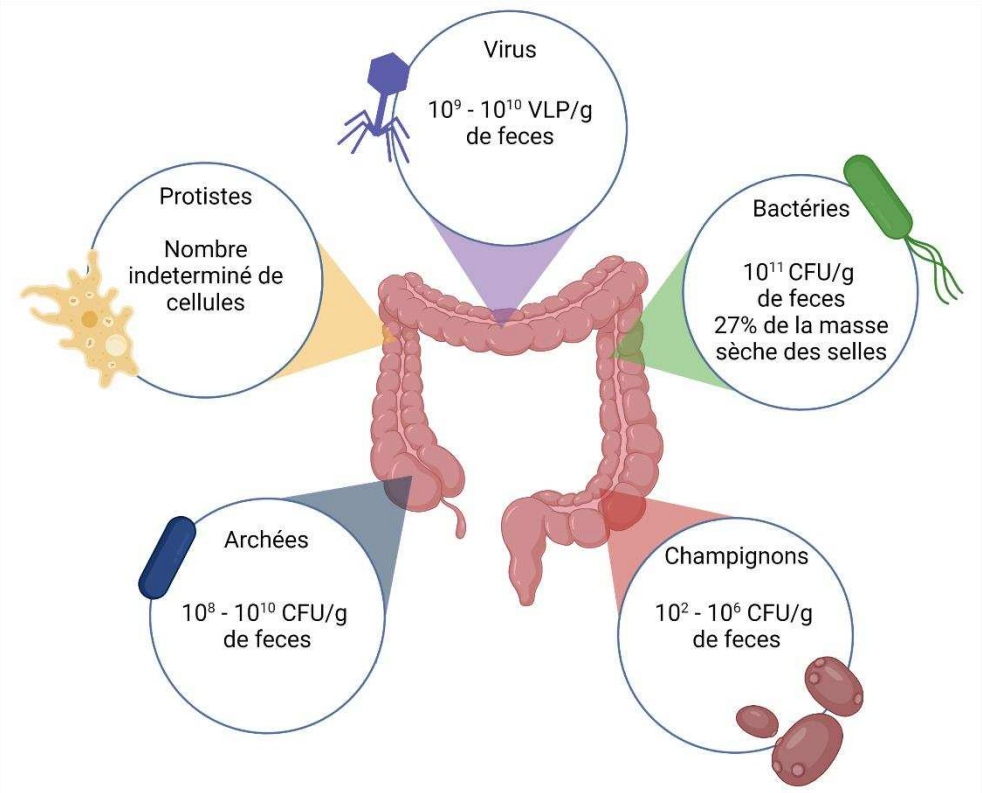

Figure 6 : **Abondances des différents microorganismes présents dans l'intestin**. Figure adaptée de (89) et (90).

Ainsi, la peau, les voies respiratoires, le tractus urinaire, vaginal et digestif sont de véritables écosystèmes à l'échelle microscopique. (Fig. 7) Parmi ceux-ci, le microbiote intestinal est le plus riche en termes de diversité et de densité. Par la suite, nous n'étudierons que ce microbiote en particulier. La partie bactérienne du microbiote intestinal est la plus abondante avec 10^{11} bactéries par gramme de fèces et demeure la plus étudiée à ce jour.

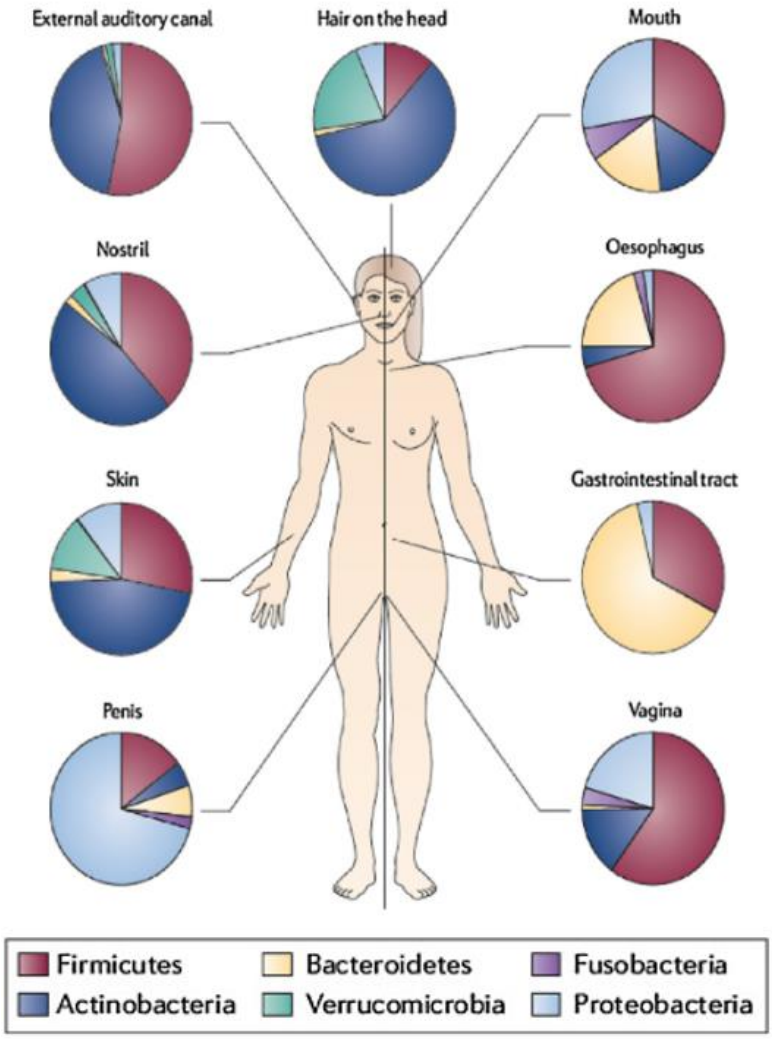

Figure 7 : **Diversités bactériennes des différents microbiotes du corps humain.** Figure de (248).

La structure du microbiote intestinal est déterminée dès l'enfance et particulièrement à la naissance. Le mode d'accouchement influe fortement sur la composition du microbiote et aura un retentissement sur celle-ci à l'âge adulte (91). Lors d'un accouchement par voie basse, le nouveau-né est en contact avec la flore vaginale, fécale et de la peau de la mère. Durant les mois suivants la naissance, le lait maternel, contenant également une flore microbienne, participe à la formation du microbiote du nourrisson (92). Ainsi, un accouchement par césarienne, l'alimentation du nourrisson par du substitut de lait maternel (lait en poudre) ou un traitement antibiotique chez la femme enceinte ou pendant l'allaitement ont un impact sur la composition du microbiote de l'enfant (93–96). Juste après la naissance, les bactéries anaérobies facultatives comme les *Entérobactéries* sont prédominantes (97). Leur présence entraine une diminution la concentration en oxygène dans la lumière intestinale facilitant la colonisation du tractus digestif par des bactéries anaérobies strictes. La composition du

microbiote intestinal se stabilise autour à l'âge de 2,5-3 ans (98,99). À l'âge adulte, la composition du microbiote est stable au cours du temps chez un individu donné. Le microbiote intestinal bactérien d'un individu sain est composé à 90% par deux phyla : les *Bacteroidetes* (73.13 ± 22.16%) et les *Firmicutes* (22.2 ± 18.66%). Les 10% restant sont composés de *Proteobacteria*, *Actinobacteria*, *Fusobacteria* et *Verrucomicrobia* (83,100,101). Cependant, il existe une forte variabilité interindividuelle.

En plus des facteurs influençant le microbiote dans l'enfance, la composition du microbiote adulte est impactée par de nombreux autres facteurs, le principal étant l'alimentation et, dans une plus faible mesure, l'âge, la pollution, la prise de médicament, le tabagisme et d'autres agents environnementaux (102,103). Le facteur génétique semble avoir un effet modéré sur le microbiote (104).

Bien que certains travaux se soient basés sur l'étude de biopsies intestinales, la plupart des études portant sur le microbiote intestinal analysent des échantillons de selles reflétant la diversité présente au niveau du colon. Ces études ont permis d'observer une plus grande abondance des *Enterobacteriaceae* et des *Lactobacillaceae* au niveau de l'intestin grêle où la concentration en oxygène et en sucre est plus élevée et le pH bas (105). Au niveau du colon, les *Bacteroidetes* et les *Firmicutes*, principalement des *Clostridiales,* sont prédominants. Au sein d'une même section intestinale, il existe également une forte hétérogénéité spatiale. En effet, le mucus externe abrite une population bactérienne spécifique, comprenant majoritairement des *Firmicutes*, différente de celle présente dans la lumière intestinale, contenant plus de *Bacteroidetes* (Fig. 8) (106). Ainsi l'intestin n'est pas un environnement homogène, mais peut être décrit comme étant un ensemble de biotopes en communication les uns avec les autres, et avec le milieu extérieur.

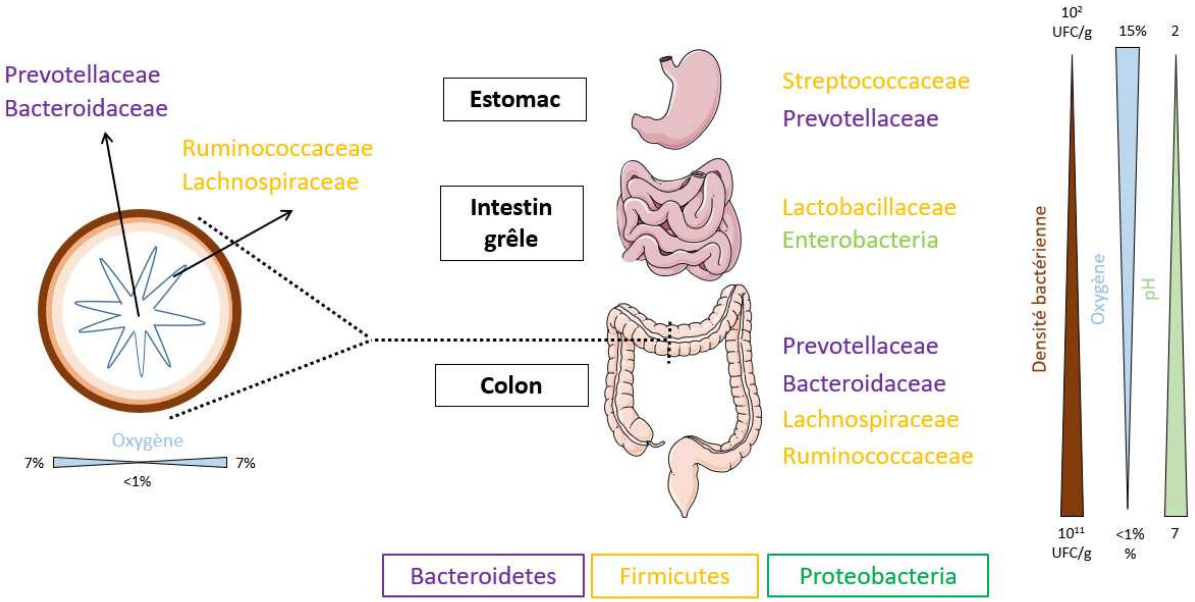

Figure 8 : Composition et structure du microbiote intestinal humain. Le long des sections intestinales, on peut observer un gradient de pH, d'oxygène et de densité bactérienne. Parallèlement, le microbiote humain est dominé par les *Bacteroides*, *Firmicutes*, *Proteobacteria*, mais la composition exacte diffère selon chaque section. Cette hétérogénéité est également présente entre les parties luminales et mucosale de chaque section. UFC : Unité formant colonie. Figure adaptée depuis la thèse de Quentin Lamy-Besnier

C) Les fonctions du microbiote intestinal

Les microorganismes du microbiote intestinal et leur hôte ont une relation symbiotique : l'hôte offre aux microorganismes un environnement favorable à leur croissance ainsi que des nutriments tandis que le microbiote a un rôle important dans la physiologie d'un individu sain (Fig. 9).

Rôle dans le métabolisme intestinal :

L'une des premières fonctions du microbiote à avoir été identifiée est sa capacité à métaboliser certaines molécules d'origine alimentaire. Les Firmicutes sont capables de fermenter les glucides complexes non digérés par l'hôte en acides gras à chaine courte (AGCC) parmi lesquels on peut citer le butyrate, l'acétate ou le propionate. Les AGCC ont des rôles variés ; le butyrate, et dans une moindre mesure le propionate, sont une source d'énergie pour les cellules épithéliales intestinales et notamment les colonocytes (107). Les AGCC sont également une source d'énergie importante pour les autres bactéries du microbiote, par exemple *Faecalibacterium prausnitzii* ne pousse qu'en présence d'acétate (108). *F. prausnitzii* produit également du butyrate qui influence la colonisation de certaines bactéries et réduit la

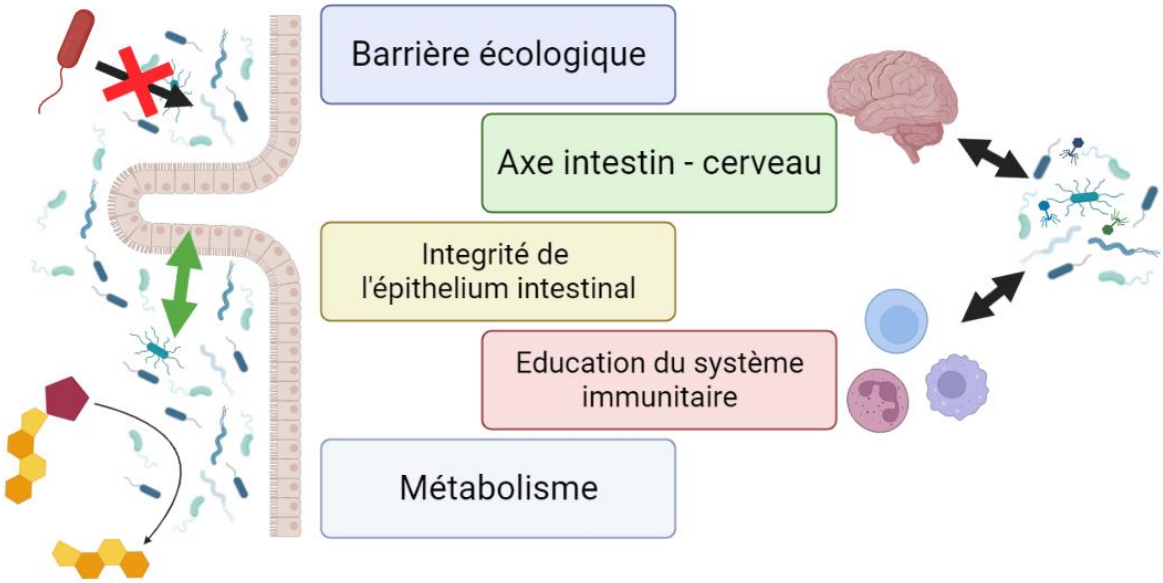

Figure 9 : Les principales fonctions du microbiote intestinal.

pathogénicité de *Salmonella enterica* (109). De plus, les AGCC produits par les bactéries participent à leur compétitivité. Par exemple les bactéries du genre *Bifidobacterium* métabolisent de l'acétate empêchant l'infection de souris par une *E. coli* entérohémorragique (110). Les AGCC peuvent ensuite être absorbés par l'hôte *via* la veine porte et intégrer d'autres voies métaboliques comme celle du cholestérol pour l'acétate ou de la néoglucogenèse pour le butyrate et le propionate (111). L'acétate a aussi été lié à une masse corporelle plus faible due à son effet sur l'appétit (112).

Le microbiote intestinal participe au métabolisme du tryptophane, un acide aminé essentiel retrouvé dans les protéines d'origines animales. Le tryptophane peut être métabolisé en dérivés de l'indole qui sont des ligands des aryl hydrocarbon receptor (AhR) impliqués dans la réponse immunitaire (113).

Les bactéries du microbiote sont aussi impliquées dans la synthèse de vitamines. Dès les années 60, des chercheurs se sont aperçus que des rats axéniques avec un régime pauvre en vitamine K développaient un déficit en prothrombine et étaient plus susceptibles de développer des hémorragies que des rats avec un microbiote sain (114). Chez l'humain, un traitement antibiotique peut avoir le même effet (115). Le microbiote a un rôle dans la production de la plupart des vitamines B (1, 2, 3, 5, 6, 7, 9, et 12) autrement non synthétisables par l'hôte et il est estimé que 25% des vitamines B absorbées par les êtres humains sont produites par le microbiote (allant jusqu'à 86% pour la vitamine B6), le reste étant apporté par l'alimentation (116). Comme décrit dans la partie I, le microbiote intestinal intervient aussi dans le métabolisme des acides biliaires.

Rôle dans le maintien de l'intégrité de l'épithélium intestinal :

Dès la naissance, le microbiote intestinal interagit avec son hôte et participe au développement et au maintien de l'intégrité de l'épithélium intestinal qui forme une barrière physique séparant la lumière intestinale du reste de l'organisme (voir partie I-C). La présence de molécules d'origines bactériennes telles que le peptidoglycane et l'acide lipotéichoïque active les TLR2 favorisant le maintien des jonctions serrées de l'épithélium intestinal (117). La bactérie *Bacteroides thetaiotaomicron* promeut la maintenance des desmosomes et ainsi la résistance mécanique des villosités intestinales en induisant la production de la protéine SPR-2A par les cellules épithéliales (118). Le microbiote participe aussi à l'angiogenèse de la microvascularisation au niveau de l'intestin en induisant la production d'angiogenin-3 *via* les cellules de Paneth (119).

Rôle de barrière écologique :

En plus de l'épithélium, les bactéries présentent dans la lumière intestinale sont séparées du reste de l'organisme par de nombreuses barrières présentées dans la partie I-C. Mais le microbiote lui-même peut être considéré comme une barrière empêchant la colonisation de bactéries ne sont pas adaptées à cet environnement compétitif.

Pour coloniser et persister dans l'intestin, bactéries disposent d'un système de sécrétion de type VI (T6SS) permettant de sécréter des toxines directement dans le cytoplasme d'une bactérie adjacente. Ces effecteurs présentent de nombreuses propriétés, notamment l'hydrolyse du peptidoglycane, la formation de pores membranaires et la fixation d'ions métalliques, ce qui confère un avantage compétitif aux bactéries possédant un T6SS (120–122). Dans le microbiote, ce système de sécrétion est très rependu parmi les phyla des Bacteroidetes et des Proteobacteria (123,124). Le maintien d'un équilibre sain du microbiote intestinal, appelé eubiose, est donc nécessaire à la fonction de barrière écologique. Un microbiote riche et diversifié occupe toutes les niches écologiques disponibles dans l'intestin, empêchant la colonisation par de nouvelles bactéries. Ainsi, dans un modèle murin de microbiote contrôlé ne disposant pas d'entérobactéries, *S. enterica* sérovar Typhimurium est capable de coloniser et d'engendrer une infection intestinale. Par contre, les mêmes souris préalablement colonisées par *E. coli* deviennent résistantes à la colonisation par *S.* Typhimurium (125). Il a aussi été montré que la production d'acides biliaires secondaires par *Clostridium scindens* entraine une résistance à la colonisation par *Clostridioides difficile* (15). La perturbation de cet équilibre par la prise d'antibiotique peut favoriser la survenue d'infection intestinale comme la colite à *C. difficile* ou les infections par *S.* Typhimurium (126).

Les bactéries colonisant l'intestin ont ainsi développé de nombreux mécanismes pour occuper la plupart des niches écologiques et pour entrer en compétition avec d'autres microorganismes affluant *via* la nourriture.

Interaction avec le système immunitaire :

Le microbiote est en interaction constante avec son hôte rendant nécessaire une certaine tolérance immunitaire. Cependant, l'hôte doit aussi se prémunir des infections bactériennes. Une réponse immunitaire adaptée et ciblée et donc indispensable au maintien de l'eubiose.

En fait, le microbiote intestinal participe à l'éducation du système immunitaire afin que celui-ci tolère les bactéries commensales tout en gardant la capacité de répondre efficacement à une infection. Cette maturation du système immunitaire est limitée à une courte période dans l'enfance pendant la forte diversification du microbiote intestinal qui a lieu lors du sevrage. L'absence de cette maturation entraine une plus forte susceptibilité aux maladies inflammatoire à l'âge adulte (127).

Toutes les bactéries présentent à leur surface des motifs moléculaires (PAMP et MAMP) reconnus par le système immunitaire inné (voir partie I-C). Celles du microbiote ne font pas exception. La reconnaissance des PAMP permet la maturation du système GALT. La production bactérienne d'AGCC influence le système immunitaire en promouvant la production d'IL-22 par les lymphocytes T CD4+ et les ILC3 (128). Le butyrate augmente aussi la concentration d'IgA dans le colon en induisant la production de TGF-β par les cellules dendritiques (129).

Les acides biliaires métabolisés par le microbiote peuvent aussi modifier la réponse immunitaire. La transplantation de plusieurs espèces de *Bacteroides* possédant l'enzyme BSH, permettant la déconjugaison des acides biliaires, dans des souris axéniques induit la prolifération des lymphocytes Treg RORγ+ par l'intermédiaire des récepteurs VDR et FXR. Lorsque ces bactéries sont génétiquement modifiées pour ne plus exprimer la BSH et inoculées dans des souris axéniques, l'effet est perdu (70).

Chez les souris axéniques, l'absence de microbiote entraine un défaut de maturation du système GALT avec une baisse de la concentration des plaques de Peyer et de ganglions lymphatiques ainsi qu'une plus faible production d'immunoglobulines démontrant l'importance du microbiote intestinal dans le développement du système immunitaire (130).

L'axe microbiote-intestin-cerveau :

De nombreuses études ont mis en évidence des liens entre l'intestin et le système nerveux central ayant un impact sur le développement de maladies ou même sur le comportement.

Ces liens sont regroupés sous le terme d'axe intestin-cerveau. Par exemple, des animaux peuvent développer une préférence pour des aliments sucrés, alors même qu'ils ne disposent pas de récepteurs du gout sucré, *via* l'activation d'une population de neurone du nerf vague (131). Plus récemment, des interactions entre le microbiote et le cerveau ont été mises en évidence, formant le concept d'axe microbiote-intestin-cerveau. Le microbiote peut interagir avec le système nerveux par la production de neurotransmetteur (dopamine, sérotonine) (132) ou de métabolites (AGCC) (133) qui seront transportés dans le sang jusqu'au cerveau. De nombreuses études ont démontré le rôle du microbiote dans la physiopathologie de certaines maladies neurodégénératives, comme Alzheimer et Parkinson, ou psychiatriques (134–136).

En plus de ses rôles physiologiques, le microbiote peut avoir d'autres effets comme celui de métaboliser certains composés pharmacologiques. 271 médicaments administrés oralement dans des souris sont ainsi chimiquement modifiés (137). La métabolisation des médicaments par le microbiote pourrait expliquer une part de la variabilité interindividuelle observée en réponse aux traitements. Par exemple l'Irinotecan, un anticancéreux, peut être métabolisé par l'enzyme bactérienne β-glucoronidase en une forme toxique pour les cellules épithéliales, engendrant alors des diarrhées. Un inhibiteur de la β-glucoronidase offre une protection contre cet effet secondaire (138).

D) Dysbiose et infection bactérienne intestinale

Les bactéries intestinales peuvent aussi être associées à des états pathologiques, directement ou indirectement. Certaines bactéries provoquent des infections aiguës tandis que d'autres sont corrélées à des maladies non infectieuses.

Les infections intestinales aiguës

L'intestin, très riche en nutriments, est un environnement propice à la croissance de bactéries commensales ou pathogènes. L'ingestion d'eau ou de nourriture contaminées représentent les principales portes d'entrées par des pathogènes. Dans des environnements sans point d'eau potable et avec un manque d'hygiène, les contaminations par voie oro-fécale sont particulièrement fréquentes. Les contaminations sont aussi possibles dans l'alimentation produites industriellement comme ce fut le cas récemment avec les produits Kinder® contaminés par *S.* Typhimurium et les pizzas Buitoni® contaminées par des *E. coli* entrainant un syndrome hémolytique et urémique (139,140). La gravité des infections intestinales varie grandement selon le pathogène en cause ainsi que de la personne infectée. Les âges extrêmes (enfants de moins de cinq ans et personnes âgées), ainsi que les personnes ayant

une immunodéficience sont particulièrement vulnérables à la déshydratation provoquée par les diarrhées. L'accès aux antibiotiques joue un rôle majeur sur le pronostic de ces infections. Ainsi, la plupart des cas graves sont concentrés dans les pays en voie de développement où l'accès à une eau de qualité et aux traitements est difficile. Ainsi, les infections intestinales responsables de diarrhée aiguë sont un problème de santé publique mondial avec plus de 1,7 milliard de cas pédiatriques chaque année entrainant la mort de plus de 500 000 enfants de moins de cinq ans (141).

Parmi les pathogènes intestinaux, la bactérie *E. coli* est la plus étudiée. De nombreuses souches sont regroupées sous ce nom d'espèce présentant une immense diversité génétique témoignant d'une grande capacité d'adaptation. *E. coli* est accompagnée d'une multiplicité d'interactions avec l'hôte. Présente chez 90% de la population humaine, la plupart des souches sont commensales, mais d'autres sont des pathogènes opportunistes et quelques-unes sont des pathogènes strictes (142,143). Au sein des *E. coli* entrainant une infection, il existe plusieurs pathotypes dont six sont responsables d'infections intestinales (144).

Les *E. coli* entéropathogéniques (EPEC) ainsi que les *E. coli* entéro hémorragiques (EHEC) adhèrent aux microvilli des entérocytes et entrainent des lésions d'attachement/effacement (lésions A/E). Les EHEC produisent en plus des shigatoxines (*stx*1 et *stx*2) qui cible la N-glycosidase de l'ARN des cellules de l'hôte. Ces shigatoxines sont codés par des bactériophages et peuvent être transmises horizontalement (145). Les *E. coli* entéro toxinogènes (ETEC) ne provoquent pas de lésion A/E, mais produise des entérotoxines. Les *E. coli* entéroaggrégatives (EAEC) forment un biofilm adhérent à l'épithélium intestinal et sont aussi capables de produire des entérotoxines et cytotoxines. Les *E. coli* entéroinvasives (EIEC) sont capables d'envahir les colonocytes et de se déplacer latéralement au sein de l'épithélium sans revenir dans la lumière intestinale. Les *E. coli* adhérentes diffuses (DAEC) provoquent la formation d'extension cytoplasmique qui enveloppent les bactéries.

D'autres pathothypes sont décrits dans la littérature, comme les *E. coli* adhérentes invasives (AIEC) associées à la maladie de Crohn, mais aucun marqueur génétique ne permet de les identifier à ce jour. Les AIEC sont caractérisées par leur capacité à envahir et se répliquer au sein de macrophages et des cellules épithéliales (146).

Citrobacter rodentium, anciennement *Citrobacter freundii* biotype 4280 est un pathogène intestinal murin très proche génétiquement de *E. coli,* à tel point qu'il fut nommé « mouse pathogenic *Escherichia coli* » par Itoh *et al.* lorsqu'ils l'ont isolé en 1988 (147). *C. rodentium* est un pathogène modèle dans l'étude des infections intestinales chez la souris entrainant des lésions d'attachements/effacement proches de celles provoquées par des EPEC et des EHEC (148). Sa pathogénicité dépend en partie du fond génétique des souris infectées, les C57BL/6

et les Swiss ne présentent qu'une colite résolutive spontanément, tandis que les souris C3H, FVB et AKR développent une maladie sévère et succombe en quelques jours (149).

Une infection résolutive spontanément à *C. rodentium* peut être divisée en quatre phases : 1 – la phase d'implantation 2 – la phase d'expansion 3 – l'état d'équilibre 4 – la clairance ; détaillées dans la figure 10. *C. rodentium* possède un ilot de pathogénicité similaire à celui retrouvé chez les EPEC et EHEC : le locus of enterocyte effacement (LEE) qui code pour un système de sécrétion de type III (T3SS) et des protéines effectrices. Cet ilot de pathogénicité est exprimé *in vivo* lors de la colonisation du caecum (150). LEE est régulé par Ler codé par dans l'unité de transcription *LEE1* (151,152). Des signaux comme la température ou le butyrate produits par le microbiote ainsi que des contraintes mécaniques régulent l'expression de LEE (153–155). De plus, des ions, la cystéine et la sérine, des hormones et d'autres métabolites bactériens comme la biotine influencent la capacité de *C. rodentium* à coloniser l'intestin (156–159).

Pendant la phase d'expansion, *C. rodentium* entraine des lésions A/E dans la partie distale du colon. Ces lésions sont caractérisées par l'effacement de la bordure en brosse des colonocytes et l'attachement de la bactérie à la surface de l'épithélium. Les lésions A/E nécessite l'action du T3SS et de son effecteur translocated intimin receptor (Tir) en plus d'autres effecteurs (160). La clairance de *C. rodentium* se fait en deux étapes. Une première fait intervenir le système immunitaire adaptatif, et notamment les lymphocytes T helper de type 1 (Th1) et T helper producteurs d'IL-17 (Th17) (Fig. 10) (161). La seconde, plus tardive, met en jeu les autres bactéries du microbiote et notamment les *Enterobacteriaceae* dont *E. coli*, qui entrent en compétition avec *C. rodentium* et parviennent à l'éliminer définitivement. Il faut donc une action combinée du microbiote et de l'hôte pour éliminer *C. rodentium* (162).

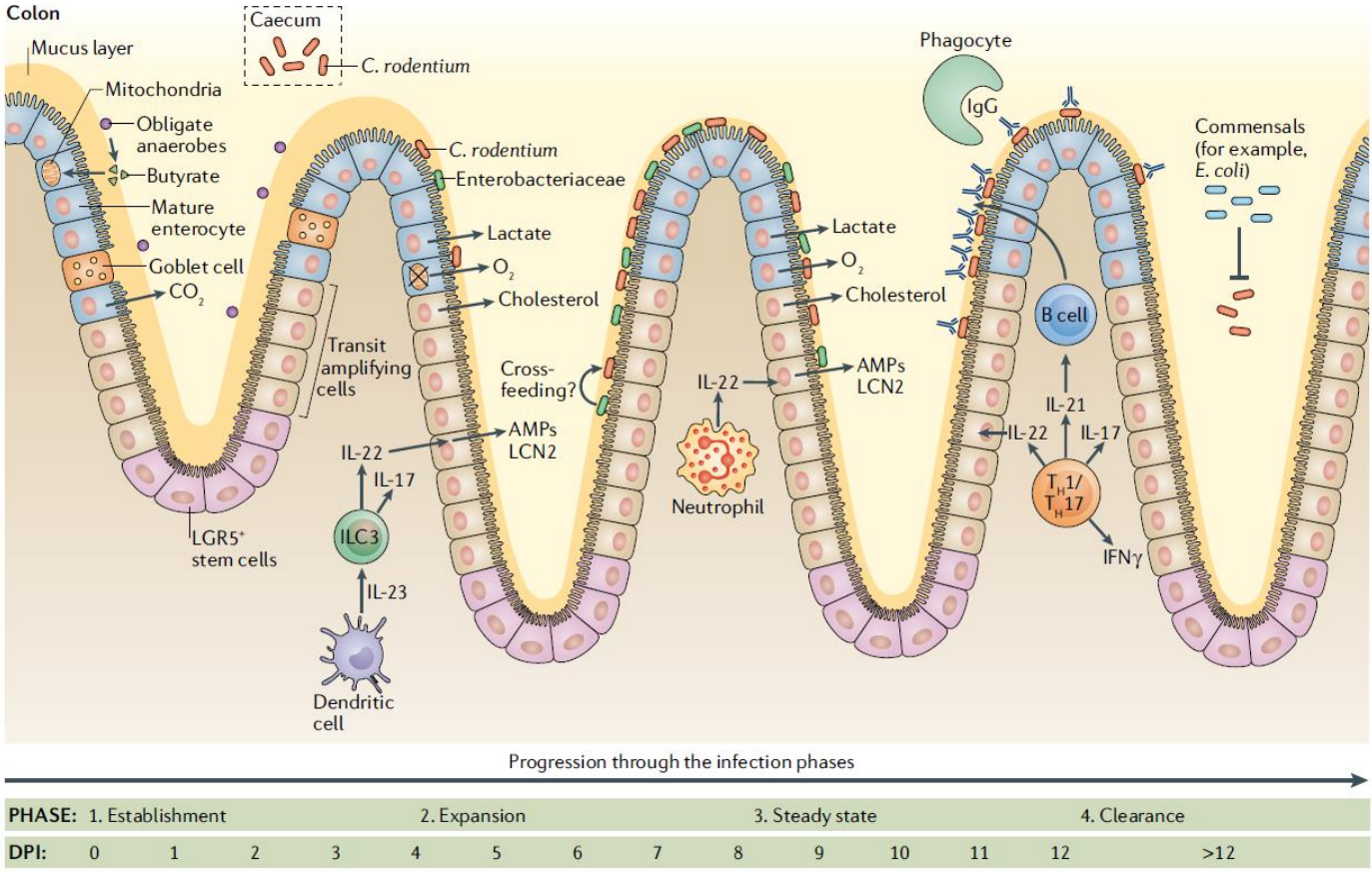

Figure 10 : La colonisation de *C. rodentium* dans le cas d'une infection spontanément résolutive. Pendant la phase d'établissement (1 à 3 jours post infection - JPI), *C. rodentium* réside dans les patchs du cæcum (Wiles et al., 2004). Avant la colonisation du colon, les bactéries commensales (notamment les espèces de *Clostridia*) produisent du butyrate, qui est oxydé par les mitochondries des cellules épithéliales intestinales (CEI). Dans la phase d'expansion (4-8 JPI), *C. rodentium* colonise la muqueuse colique à partir de 4 JPI. Cela induit une régulation négative de la phosphorylation oxydative mitochondriale dans les CEI et un passage à la glycolyse aérobie, ce qui entraine une augmentation de la concentration en oxygène et de la sécrétion de lactate dans la lumière intestinale. Une hausse de la biosynthèse et de l'efflux du cholestérol dans les CEI se produit à partir de 4 JPI, entrainant une augmentation de l'excrétion du cholestérol. Ces changements sont associés à une diminution des bactéries anaérobies strictes associées aux tissus et à une expansion des bactéries anaérobies facultatives (par exemple, *Enterobacteriaceae*), qui peuvent être nécessaires à l'alimentation croisée de *C. rodentium* et également aider l'hôte à éliminer l'agent pathogène. Les CEI présentent une expression accrue des marqueurs de prolifération cellulaire à partir de 4 JPI, mais l'hyperplasie de la crypte colique (c'est-à-dire la prolifération des cellules amplificatrices de transit et des cellules souches, et la perte des cellules épithéliales matures, y compris les entérocytes et les cellules en gobelet) ne se développe pas avant 6 JPI. Au cours de l'infection précoce, les cellules dendritiques sécrètent de l'IL-23, qui induit la production de cytokines pro-inflammatoires IL-22 et IL-17. L'IL-22 agit sur les CEI et induit la sécrétion de peptides antimicrobiens (PAM ; par exemple, REG3β, REG3γ et lipocaline 2 (LCN2)). Dans la phase d'état stable (8-12 JPI), *C. rodentium* continue à coloniser la muqueuse du colon et sa concentration dans les selles se stabilise à environ 10^9 UFC/g de selles. Les neutrophiles tissulaires contribuent à la réponse IL-22. Dans la phase de clairance (à partir de 12 JPI), *C. rodentium* associé à la muqueuse est opsonisé par les immunoglobulines G (IgG) et phagocyté. Par la suite, les bactéries luminales sont éliminées par compétition *via* les bactéries commensales, dont *Escherichia coli*. Les lymphocytes T helper de type 1 (Th1) et T helper producteurs d'IL-17 (Th17) sécrètent de l'IL-22, de l'IL-21, de l'interféron-γ (IFNγ) et de l'IL-17. La surprolifération des cellules amplificatrices de transit et des cellules souches (entrainant une hyperplasie de la crypte colique) se poursuit après l'élimination des bactéries. On ne sait pas si et quand le métabolisme de la CEI revient à l'homéostasie préinfection.

Figure de (148).

La dysbiose au sein du microbiote

Les altérations en termes de composition et de fonction sont réunies sous le terme de dysbiose. La dysbiose se distingue de la simple variabilité interindividuelle lorsqu'elle est associée à une pathologie ou lorsque le microbiote ne remplit plus ses fonctions. Les dysbioses sont ainsi associées à de nombreuses pathologies, intestinales ou non : l'asthme (163), l'autisme (164), les maladies neurodégénératives (165), mais elles sont particulièrement étudiées et décrites pour le diabète (88), l'obésité (85) et les maladies inflammatoires chroniques de l'intestin (MICI) que nous prendrons pour exemple (86,166).

Les MICI sont séparées en deux entités, la maladie de Crohn qui correspond une inflammation transmurale pouvant toucher l'ensemble du tube digestif, et la rectocolite hémorragique ne touchant que la partie superficielle du colon. La dysbiose dans les MICI est d'abord compositionnelle avec une diminution de la diversité, une baisse des Firmicutes, dont les *Clostridium,* et une augmentation des *Enterobacteriaceae* (167). On peut noter que des AIEC sont retrouvés plus fréquemment dans les selles de patients atteints de la maladie de Crohn que chez des individus sains (168). L'abondance de la bactérie *F. prausnitzii*, qui possède de propriétés anti-inflammatoires, est diminuée aussi bien dans la maladie de Crohn que dans la rectocolite hémorragique (169). Les *Bacteroidetes* et les autres *Proteobacteria* voient leur abondance augmenter ou diminuer selon les études (170,171).

Cette dysbiose compositionnelle est elle-même associé à une dysbiose fonctionnelle. Les acides biliaires sont en majorité des acides biliaires primaires chez les patients atteints de MICI alors qu'ils sont majoritairement métabolisés en acides biliaires secondaires chez les individus sains. On observe aussi une augmentation des acides biliaires sulfatés (67). Ce changement est à la fois une cause de la dysbiose compositionnelle, car moins de bactéries métabolisent les acides biliaires, mais il permet aussi un maintien de l'état inflammatoire, car les acides biliaires secondaires qui ont des propriétés anti-inflammatoires sont moins abondants (67). De même, les AGCC sont diminués chez les patients atteints de MICI, conséquence de la baisse des bactéries productrices d'AGCC comme *F. prausnitzii* ou les *Clostridium* (166). La diminution de l'abondance de *F. prausnitzii* est aussi associée à la diminution de la concentration du peptide microbial anti-inflammatory molecule (MAM) qui possède une activité anti-inflammatoire en inhibant la voie NF-κB (172). On observe aussi une diminution de l'épaisseur du mucus dû à l'abondance de bactéries mucolytiques comme *Runinococcus gnavus* et *R. torques* (173). Enfin, l'inflammation provoque une augmentation de la perméabilité de l'épithélium intestinal ce qui entraine une infiltration bactérienne au sein de la muqueuse (174).

E) Modèles d'études du microbiote

Les chercheurs disposent d'un large éventail de modèles expérimentaux pour étudier la complexité des interactions au sein du microbiote. Les modèles cellulaires, comme les cellules épithéliales intestinales humaines différenciées Caco2/Tc7, permettent d'élucider les mécanismes moléculaires de certaines voies métaboliques (175). Des modèles plus complexes comme les organoïdes permettent de recréer un tissu fonctionnel (176). Les modèles « organ-on-chip », comme le « gut-on-chip » récapitule une unité fonctionnelle d'un organe en entier et peut même accueillir une population microbienne similaire à un microbiote (177). Un des modèles *in vitro* les plus complexe à ce jour est le « simulator of the human intestinal microbial ecosystem » (SHIME) qui consiste en une succession de fermenteurs finement régulés afin de simuler un intestin entier (178). Ces modèles *in vitro* présentent cependant des limitations comme des difficultés d'entretenir des communautés bactériennes complexes pour les modèles les plus simples ou de coût pour les plus complexes comme le SHIME. Cependant, chaque modèle permet de répondre à des questions spécifiques

Seuls les modèles *in vivo* permettent l'étude des différentes composantes en interaction les unes avec les autres. Il existe différents modèles *in vivo* pour étudier le microbiote intestinal. Étant proches des êtres humains génétiquement et anatomiquement, les souris sont de loin les animaux modèles les plus utilisés pour étudier les relations hôte-microbiote. Il existe cependant certaines différences importantes. La première est la présence d'un caecum large et anatomiquement distinct du colon chez les souris tandis qu'il n'y a qu'un vestige de cet organe chez l'être humain. En revanche, les humains possèdent un appendice absent chez les souris. Histologiquement, les souris disposent de cellules de Paneth uniquement dans l'intestin grêle alors qu'elles sont présente jusque dans le colon proximal chez l'être humain (179).

De multiples modèles murins ont été mis au point, répondant chacun à des besoins particuliers. Le premier est le modèle de souris conventionnelles. La plupart des souris commercialisées à des fins de recherche sont passées au crible afin d'éliminer de potentiels pathogènes murins ou humains, elles sont alors qualifiées spécific pathogen free (SPF). Les souris SPF présentent un microbiote diversifié et, comme le microbiote humain, avec de fortes variations interindividuelles, dépendant notamment du fournisseurs (180). Les souris comme les humains présentent une majorité de bactéries appartenant aux phyla *Bacteroidetes* et de *Firmicutes*. Il existe en revanche des différences au sein de ces phyla avec une plus grande abondance de bactéries appartenant aux genres des *Lactobacillus*, *Alistipes* et *Turicibacter* chez la souris et aux genres des *Prevotella*, *Faecalibacterium* et *Ruminococcus* chez l'humain (181).

La variabilité interindividuelle de composition du microbiote des souris SPF représente une limite expérimentale évidente, impactant la reproductibilité des expériences. De plus, l'ajout de bactéries au sein d'un microbiote riche déjà formé est difficile, la plupart des niches écologiques étant déjà occupées, et nécessite souvent l'utilisation d'antibiotiques entrainant une dysbiose majeure.

Pour pallier ces limitations, des souris axéniques, ne disposant pas de microbiote et élevées dans un environnement stérile ont été largement utilisées, limitant la variabilité. Ces souris ont également permis d'étudier l'importance du microbiote dans la physiologie et certaines pathologies (182). Les souris axéniques permettent aussi l'ajout d'une, ou plusieurs, bactéries permettant l'étude de la relation entre ces bactéries spécifiquement et l'hôte (183). En revanche, les souris axéniques ne disposent pas d'un système immunitaire mature, car le microbiote est crucial pour la maturation de celui-ci (voir partie II-C), ce qui constitue une limite majeure dans l'étude des interactions hôte-microbiote.

Afin de modéliser un microbiote sain et fonctionnel tout en maintenant une grande reproductibilité et modularité, des souris gnotobiotiques ont vu le jour. Le premier, connu sous le nom de flore de Schaedler a été obtenu par la combinaison de bactéries cultivées provenant de l'intestin de souris (183). Plus récemment, des souris disposant d'un microbiote « humanisé » ont été mise au point. Ces souris ont été inoculé par un consortium de bactéries représentatives du microbiote humain et non murin afin d'étudier des conditions plus proche de l'être humain (184). Cependant ces souris ne représentent ni le fonctionnement d'un microbiote humain ni d'un microbiote murin qui sont le résultat de millions d'années de coévolution. Les souches sélectionnées pour constituer le microbiote d'une souris gnotobiotique sont choisies en fonction de la question posée. Pour l'étude du rôle des acides biliaires, étudié dans ce travail de thèse, un modèle ne métabolisant pas les acides biliaires constitue une plateforme idéale. Le modèle Oligo Mouse Model 12 (OMM^{12}) répond à ces critères et a donc été utilisé. Le microbiote des souris OMM^{12} dispose de 12 bactéries représentatives des cinq principaux phyla bactériens présents chez les souris conventionnelles. Ce microbiote est inoculé à des souris C57BL/6 axéniques. Le consortium OMM^{12} est ensuite transmis de la mère à la progéniture et est stable au cours des générations (Fig. 11). Cette stabilité permet une grande reproductibilité. De plus, la présence du microbiote dès la naissance les rapproche d'un modèle de souris conventionnelle avec une maturation du système immunitaire. Enfin, il est possible d'ajouter une ou plusieurs espèces bactériennes sans utilisation d'antibiotique. Les souris OMM^{12} constituent donc un modèle modulable et contrôlé dans l'étude du microbiote (125).

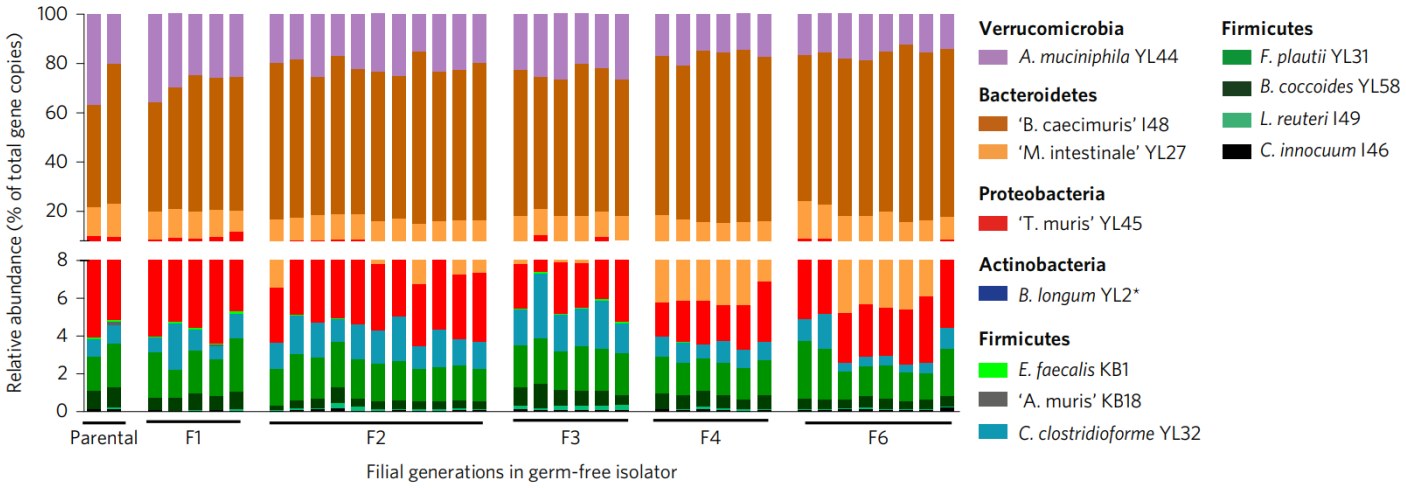

Figure 11 : Composition du microbiote bactérien des souris OMM[12] au cours de sept générations. Abondances relatives des 12 souches du consortium OMM[12], *Bifidobacterium animalis* YL2 et *Acutalibacter muris* KB18 n'ont pas atteints la limite de détection. Figure de (125).

III – Les bactériophages

A) Historique

La découverte des bactériophages est souvent attribuée aux travaux de Félix d'Hérelle (185) et Frederick Twort (186), mais avant cela, certains articles mentionnaient déjà l'existence d'agents capables de lyser les bactéries. Le plus ancien remonte à 1896 lorsque Hankin démontra que les eaux filtrées du Gange et de la Jumna possédaient une activité antibactérienne. Cette activité était perdue lorsque l'eau était portée à ébullition, cependant il est difficile d'attribuer avec certitude l'effet antibactérien à l'action de bactériophages (187). Les premières observations effectuées par Frederick Twort en 1915 l'ont amené à émettre l'hypothèse de l'existence de « virus ultramicroscopiques » qui pouvaient être considérés comme des agents infectieux des bactéries. Cependant, il a privilégié d'autres hypothèses et notamment celle d'une action enzymatique (186).

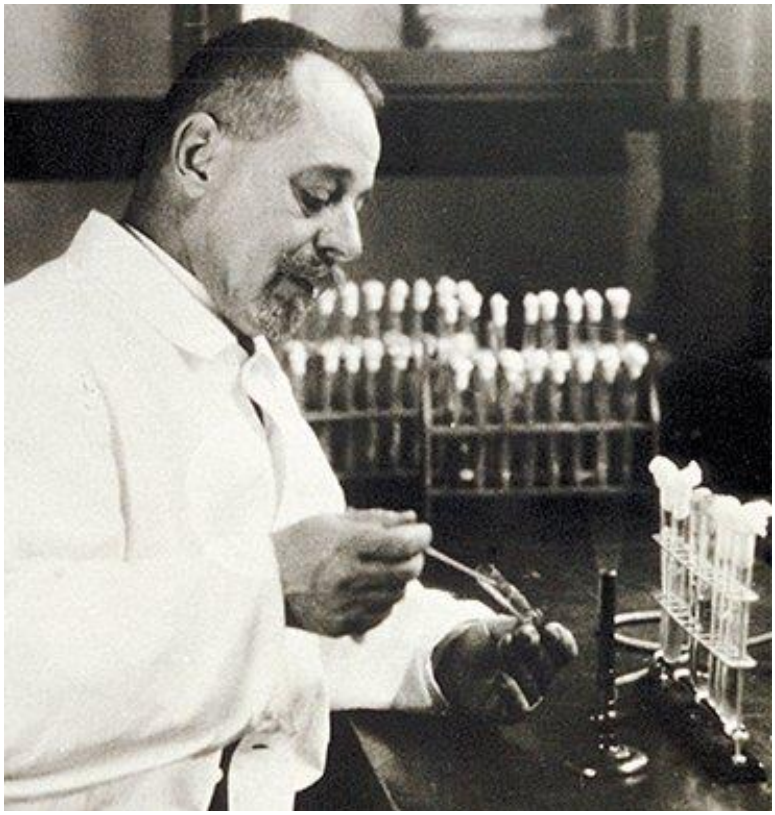

Figure 12 : Félix d'Hérelle travaillant à la paillasse. La photo a probablement été prise dans son laboratoire de production de bactériophages thérapeutiques créé en 1936.

Indépendamment, Félix d'Hérelle (Fig. 12) découvrit en 1917 un agent antagoniste des bactéries dans les selles filtrées de patients atteints de dysenterie. Cet agent provoque la lyse des bactéries en culture liquide et l'apparition de plages de lyse sur milieu solide. Il remarque également que cette action antimicrobienne est limitée à une seule espèce bactérienne même s'il suppose ce phénomène plus général. Différemment à Twort, il est persuadé qu'il s'agit d'un « microbe antibactérien » qu'il appela : bactériophage, dérivé du grec « phagein » (manger) (188). D'Hérelle poursuivit ses premières observations et chercha à appliquer les effets antibactériens des bactériophages en clinique, créant alors le concept de phagothérapie. En 1919, il étudia pour la première fois les effets des bactériophages *in vivo* en administrant en prophylaxie des bactériophages de *Salmonella gallinarum.* En 1921 il effectua ses premiers traitements chez des patients atteints de dysenterie (189). La nature virale des bactériophages fut controversée jusqu'en 1940, date des premières observations directes en microscopie électronique effectuées par Ernst Ruska (Fig. 13) (190).

.

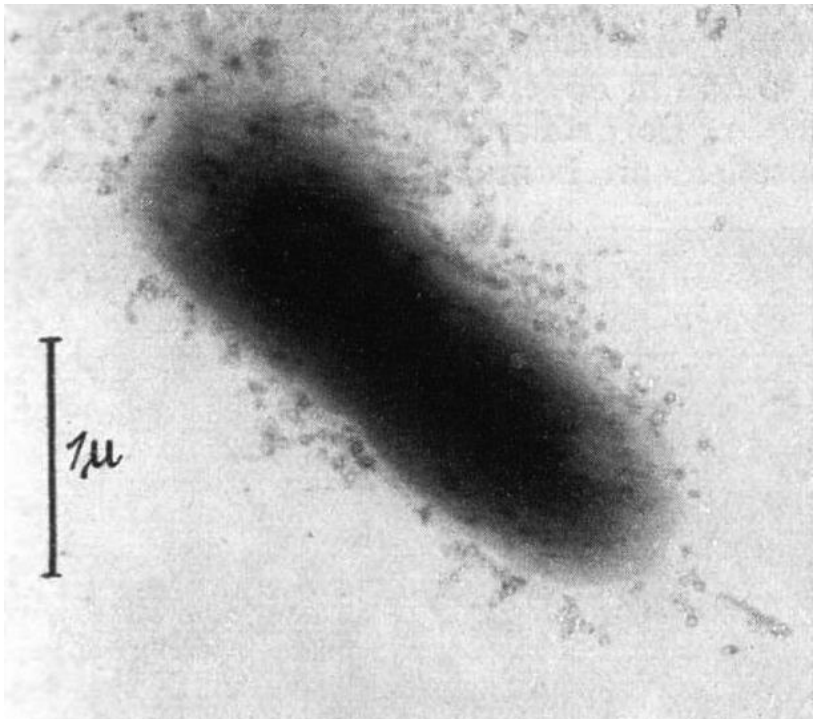

Figure 13 : Première photo de bactériophages par microscopie électronique par Ernst Ruska en 1940. Des bactériophages sont visibles à la surface de la bactérie *E. coli*.

La phagothérapie fut très largement utilisée dans les années 1930 avant de tomber en désuétude face à l'apparition de nouveaux traitements antimicrobiens, les antibiotiques, qui présentaient les avantages d'être facilement produits en grande quantité et d'avoir un spectre large qui les rendaient efficaces dans de nombreuses situations (191). L'utilisation de la phagothérapie persista en URSS après la Seconde Guerre mondiale puis dans les pays d'Europe de l'Est pour des raisons économiques et d'indépendance vis-à-vis des puissances occidentales. Cet héritage prend sa source en Géorgie où un institut, aujourd'hui dénommé

l'Institut Eliava, fût fondé au milieu des années 20 suite à la visite de Georgyi Eliava à l'Institut Pasteur où il rencontra Félix d'Hérelle. Cet institut demeure spécialisé dans le traitement de maladies infectieuses par phagothérapie (192).

La découverte des bactériophages a permis l'essor d'une recherche centrée sur la compréhension des mécanismes essentiels au vivant, donnant naissance au domaine de la biologie moléculaire. Hershey et Chase ont par exemple effectué en 1952 des expériences avec des bactériophages pour démontrer que l'ADN était le support de l'information génétique, travaux qui furent récompensés par un prix Nobel (193). De manière remarquable, six autres prix Nobel ont été attribués à des découvertes impliquant des bactériophages, la plus récente étant la découverte du système de défense bactérien CRISPR/Cas9 dont l'application dérivée facilite l'édition de génomes (194).

Récemment, un regain d'intérêt pour la phagothérapie s'est manifesté à cause de l'émergence de la résistance aux antibiotiques et l'absence d'alternative qui posent un problème de santé publique majeur (195). L'utilisation massive d'antibiotiques, notamment pour l'élevage, entraine une modification des écosystèmes bactériens et favorise l'émergence de résistance. Plus largement, la réduction de l'utilisation des antibiotiques au profit d'alternatives plus ciblées s'inscrit dans le cadre d'une approche « santé globale » (« One health » en anglais) qui vise à réduire l'impact de l'être humain sur la biodiversité, notamment la biodiversité microbienne, afin de limiter l'émergence de bactéries résistantes aux antibiotiques (196).

Au-delà de leur utilisation en thérapeutique ou comme outil de biologie moléculaire, les bactériophages sont également étudiés pour leurs rôles dans les écosystèmes microbiens. Ces prédateurs naturels des bactéries sont impliqués dans les dynamiques des populations bactériennes, que ce soit dans l'océan ou l'intestin (197,89).

B) Diversité et classification

Les bactériophages sont l'entité biologique la plus abondante sur terre avec une estimation de 10^{31} particules virales, un nombre dont il est difficile d'apprécier la grandeur à l'échelle humaine. Il y aurait en moyenne 10 milliards de bactériophages par litre d'eau dans l'océan, soit plus que la population humaine sur terre (198,199). Il existe aussi une très grande diversité au sein des bactériophages, mais l'absence de marqueur universel, contrairement au 16S pour les bactéries, rend difficile le suivi de la phylogénie des bactériophages et donc leur classification. La première classification proposée, et encore largement utilisée aujourd'hui, repose sur l'aspect morphologique des bactériophages ainsi que le support de leur information génétique (Fig. 14) (200). La majorité des bactériophages caractérisés ont une molécule

d'ADN double brin, mais il existe des bactériophages ayant un ADN simple brin ou encore de l'ARN simple ou double brin. Leur taille varie de 20 à 200 nm de long et ils peuvent présenter des formes variées. Environ 95% des bactériophages observés en microscopie électronique font partie de l'ordre des *Caudovirales* (du latin « cauda » signifiant queue). Cela signifie qu'ils sont composés schématiquement d'une tête (la capside) contenant une molécule d'ADN double brin et d'une queue protéique à laquelle des fibres caudales sont attachées. Cet ordre viral est composé de trois familles : les *Myoviridae* avec une queue contractile, les *Siphoviridae* avec une queue souple et non contractile et les *Podoviridae* avec une queue courte et non contractile.

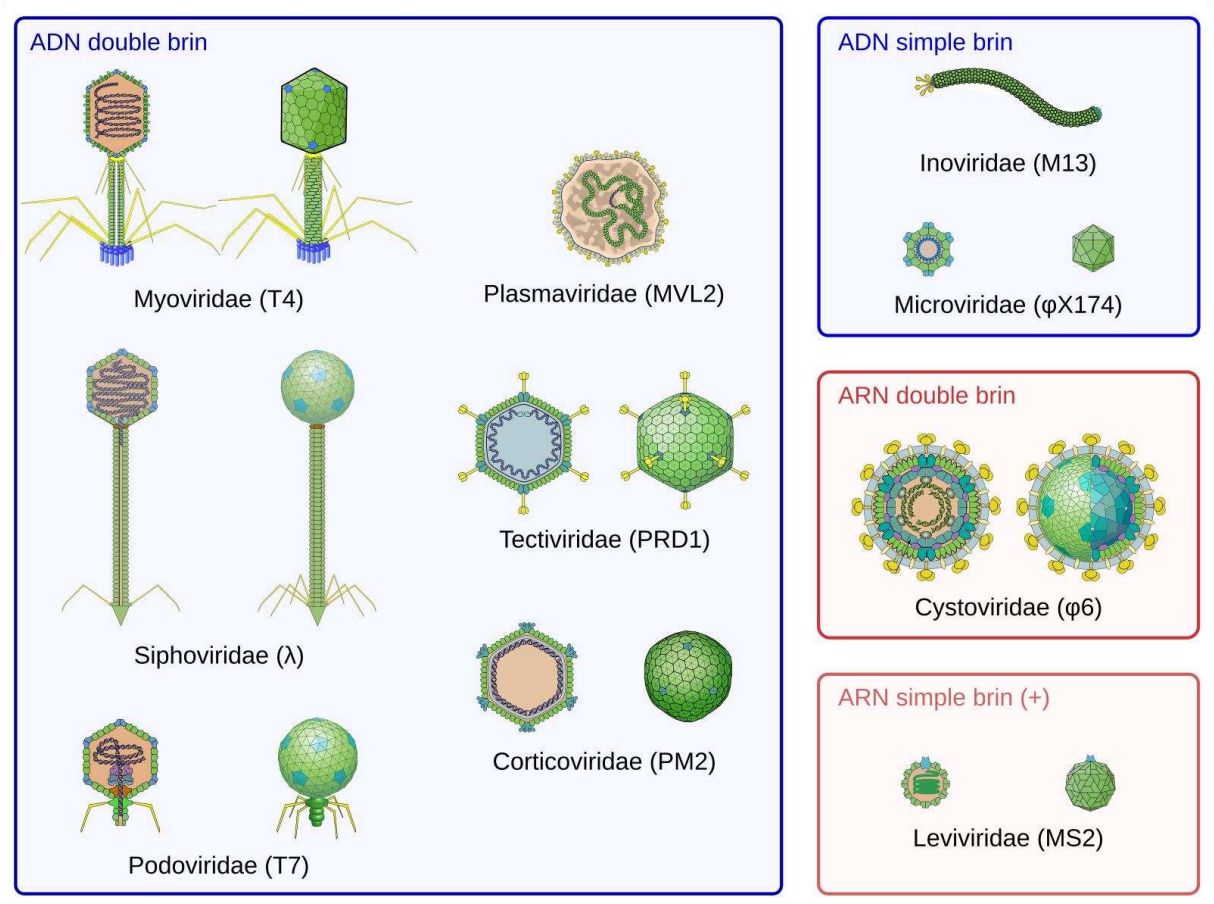

Figure 14 : Diversité et classification des bactériophages selon leur morphologie et le support moléculaire de leur matériel génétique. Chaque famille est illustrée par l'un de ses membres les mieux caractérisés. Figure provenant de (201)

Comme pour les bactéries, l'immense diversité des bactériophages n'a pu être appréhendée qu'avec la révolution métagénomique. Les bactériophages étant dépourvus de gènes universellement présents, des approches par comparaison de génomes entiers (202,203) ou basées sur des marqueurs protéiques (204) ont été proposées. Actuellement, la classification de l'International Committee for the Taxonomy of Viruses (ICTV) est en pleine évolution pour

prendre en compte de manière prioritaire la proximité génétique en lieu et place de la morphologie (205).

C) Les cycles infectieux des bactériophages

Au-delà de leur morphologie et de leur séquence, les bactériophages se différencient aussi selon leur type de cycle infectieux. Les deux principaux types sont les bactériophages virulents et les bactériophages tempérés (Fig. 15).

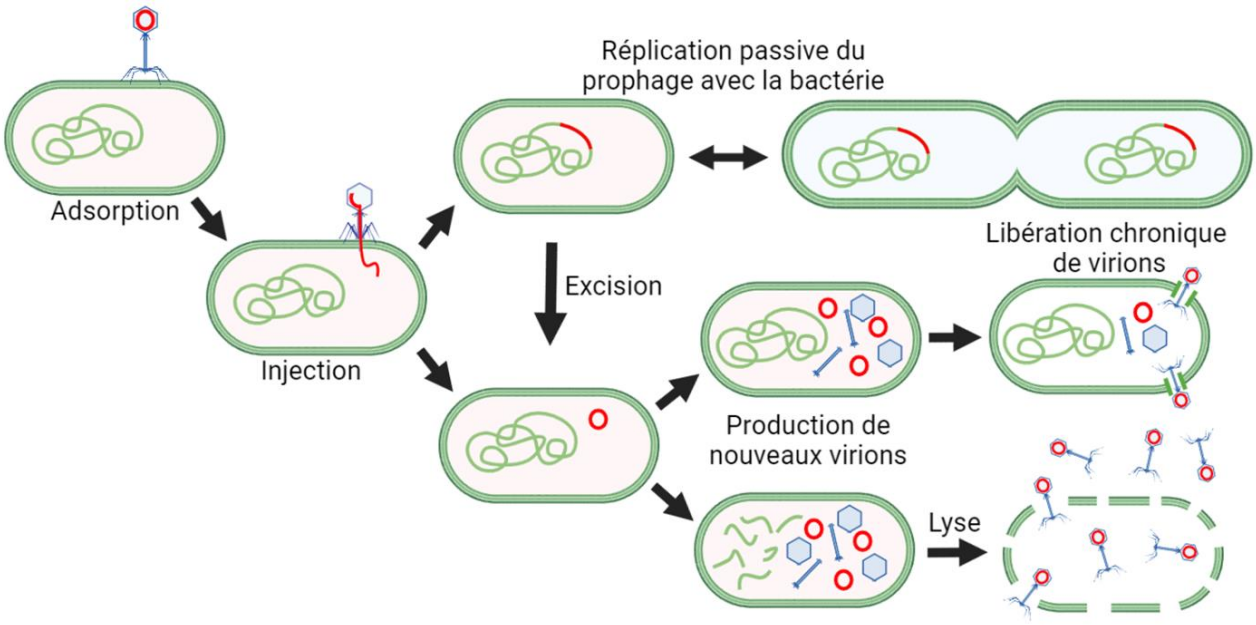

Figure 15 : Les principaux cycles infectieux des bactériophages. Tous les cycles infectieux des bactériophages commencent par l'adsorption d'une particule virale à une bactérie et l'injection de leur génome. Certains bactériophages peuvent intégrer leur génome dans celui de leur hôte et commencer un cycle lysogénique. D'autres entament directement la production de nouveaux virions qui sont libérés lors de la lyse de la bactérie ou chroniquement sans entrainer la mort de leur hôte bactérien.

Cycle infectieux d'un bactériophage virulent

Les bactériophages virulents accomplissent un cycle lytique qui aboutit à la lyse de la bactérie et qui peut être décomposé en trois étapes : l'adsorption, l'infection (aussi appelée phase de latence) et la lyse avec libération de nouveaux virions (206). Un cycle lytique commence par la rencontre aléatoire d'un bactériophage et d'une bactérie. Les bactériophages n'ayant pas d'activité métabolique propre, ils sont incapables de s'approcher activement d'une bactérie cible et ne peuvent donc que diffuser dans l'environnement. Les interactions entre bactériophages et bactéries sont donc favorisées par une forte densité des deux populations. Le cycle se poursuit uniquement si le phage s'adsorbe à la surface de la bactérie grâce à la

reconnaissance d'un motif moléculaire spécifique. Ces récepteurs moléculaires sont très divers et dépendent de chaque couple bactériophage/bactérie ; des exemples sont listés dans la table 2.

Gram -			
Bactériophage	**Hôte**	**Récepteurs**	**Référence**
Sf6	*Shigella flexneri*	OmpA/OmpC	Parent et al. 2014
SfMu	*Shigella flexneri*	Antigène O du LPS	Jakhetia et al. 2015
KSF-1	*Vibrio choleraa*	Pili de type IV	Faruque et al. 2005
ICP1	*Vibrio choleraa*	Antigène O1 du LPS	Seed et al. 2012
PP01	*Escherichia coli* O157:H7	OmpC	Morita et al. 2002
ϕiV10	*Escherichia coli* O157:H7	Antigène O157	Perry et al. 2009
P22	*Salmonella* Typhimurium	Antigène O du LPS	Baxa et al. 1996
9NA	*Salmonella* Typhimurium	Antigène O du LPS	Schmidt et al. 2016
F336	*Campilobacter jejuni*	Capsule	Sørensen et al. 2011
F341	*Campilobacter jejuni*	Flagelle	Baldvinsson et al. 2014
JG004	*Pseudomonas aeruginosa*	Antigène O du LPS	Le et al. 2013
Phage K8	*Pseudomonas aeruginosa*	Antigène O du LPS	Mcshan et al. 2016
Gram +			
Bactériophage	**Hôte**	**Récepteurs**	**Référence**
Gamma Phage	*Bacillus anthracis*	GamR	Gillis et al. 2016
AP50c	*Bacillus anthracis*	CsaB	Bishop-Lilly et al. 2012
ϕi11	*Staphilococcus aureus*	Acide théicoique	Xia et al. 2011
iSLT	*Staphilococcus aureus*	Acide lipothéicoique	Kaneko et al. 2009
A118	*Listeria monocytongenes*	Acide théicoique	Bielmann et al. 2015
P35	*Listeria monocytongenes*	Acide théicoique	Bielmann et al. 2015

Table 2 : Exemples de bactériophages infectant des bactéries pathogènes et leurs récepteurs. Table adaptée de (207)

Le motif présent à la surface des bactéries est reconnu par les fibres caudales du bactériophage. Ainsi chaque bactériophage ne peut infecter qu'un nombre limité d'hôtes, définissant un « spectre d'hôtes ». Le bactériophage va ensuite injecter son matériel génétique dans la bactérie cible, laissant généralement son enveloppe protéique à l'extérieur de la bactérie. Le matériel génétique va alors permettre de pirater la machinerie cellulaire de l'hôte afin de répliquer le génome du bactériophage et de produire des protéines virales qui seront assemblées en nouveaux virions. Au cours de ce processus, le génome de la bactérie est parfois dégradé pour fournir des ressources supplémentaires à la production des nouveaux bactériophages. Le nombre de virions produits au cours d'un cycle varie en fonction du bactériophage, il est par exemple de 300 pour le bactériophage T4. Une fois les virions formés, la bactérie est lysée par l'action de protéines virales spécialisées telles que la holine qui forme

des pores dans la membrane plasmique et l'endolysine qui dégrade le peptidoglycane, aboutissant à la libération des virions.

Ce cycle infectieux à une durée variable selon le bactériophage et l'hôte, il est de 30 minutes pour le bactériophage T4 infectant la bactérie *E. coli* et de 6 heures pour le bactériophage LE4 infectant *Leptospira biflexa* (208).

Lors de la formation de nouvelles particules virales, des fragments du génome de la bactérie hôte peuvent être encapsidés par erreur. Une fois libérés, ces nouveaux virions ne seront pas capables de produire un cycle infectieux, mais pourront injecter ce fragment dans un nouvel hôte. Ce phénomène que l'on appelle transduction, peut être généralisé lorsque les fragments sont encapsidés au hasard, ou spécialisés lorsqu'il s'agit de bactériophages tempérés.

Cycles infectieux d'un bactériophage tempéré

Les bactériophages tempérés suivent en général les mêmes étapes que les bactériophages virulents lors de leur cycle infectieux. Cependant, après l'étape d'injection de leur ADN, ils possèdent la capacité d'insérer leur génome dans le chromosome de la bactérie hôte et prennent alors le nom de prophages. Le prophage se réplique alors en même temps que son hôte bactérien de manière quasi indéfinie. Sous certaines conditions, le prophage perçoit des signaux qui vont l'amener à reprendre un cycle infectieux lytique. Cette décision, dénommée induction, provoque l'excision du prophage afin que de nouveaux virions soient formés puis libérés. Le choix entre cycle lytique et cycle lysogénique a été très étudié pour le phage lambda où il dépend de l'état métabolique de l'hôte et du nombre de bactériophages co-infectant une même bactérie (209,210). Plus récemment, une molécule, l'arbitrium, impliquée dans la décision entre les deux cycles infectieux, a été identifiée au cours de l'étude de bactériophages infectant *Bacillus subtilis.* L'arbitrium est produit lors d'un cycle lytique et renseigne ainsi sur le nombre de nouvelles infections récentes dans l'environnement proche. Lorsque la concentration en arbitrium est élevée, le bactériophage entrera dans un cycle lysogénique (211).

Les prophages peuvent être bénéfiques pour leur hôte. Par exemple, ils apportent généralement une protection contre l'infection de phages similaires. Ce mécanisme est appelé l'exclusion de surinfection ou homo-immunité (212). Ils peuvent également apporter des facteurs de pathogénicité comme les shigatoxines *stx*1 et *stx*2, présentes dans les EHEC et ETEC (voir partie II-C).

Une partie du génome de l'hôte connexe à un prophage peut être excisé par erreur en même temps que le génome du prophage. Cela aboutie à l'empaquetage d'un génome chimère bactériophage/bactérie dans une particule virale qui peut rester infectieuse. Ce génome pourra

s'intégrer dans un nouvel hôte, transduisant ainsi une partie du génome de la bactérie d'origine du prophage. C'est la transduction spécialisée. De plus, un bactériophage peut échanger des gènes avec autre phage par recombinaison formant un génome mosaïque. La recombinaison est souvent médiée par des recombinases codées par les bactéries qui sont détournées par les bactériophages ou directement codées par les bactériophages (213). Ce phénomène participe activement à la diversité des bactériophages.

Autres cycles infectieux

Deux autres cycles infectieux ont été décrits dans la littérature, mais sont bien moins connus. Le premier, découle de l'observation de la persistance au sein de la bactérie, sous la forme d'un épisome, du génome du bactériophage. Sans lyse ni immobilisation dans le chromosome bactérien, ce cycle infectieux est qualifié de « pseudo-lysogénique » (214).

Le deuxième concerne les bactériophages filamenteux de la famille des *Inoviridae*, qui présentent la particularité de ne pas lyser la bactérie, tout en produisant de nouvelles particules qui sont sécrétées en permanence. Cette situation est définie comme une infection chronique (215).

D) Les systèmes de résistance bactériens aux bactériophages

Loin de subir passivement la prédation des bactériophages, les bactéries ont développé de nombreux mécanismes de défense (Fig. 16).

Mécanismes ciblant l'adsorption

L'un des premiers mécanismes identifiés est lié à l'affinité des bactériophages pour le récepteur qu'ils reconnaissent à la surface des bactéries. Il suffit en effet de changer parfois un seul acide aminé du récepteur bactérien pour que l'adsorption soit fortement réduite, voire inexistante. Lorsque le récepteur du bactériophage est le produit d'une série de réactions enzymatiques impliquant de nombreuses protéines, comme c'est le cas pour le LPS chez les bactéries Gram -, une seule mutation peut aboutir à une modification de cette molécule et rendre ainsi les bactéries résistantes aux bactériophages (216). Un autre moyen d'empêcher l'adsorption est de masquer les sites d'adhésions aux bactériophages. Par exemple, la protéine TraT d'*E. coli* se lie aux protéines de membrane externe OmpA et OmpE et empêche ainsi l'infection par le bactériophage K3 (217). D'autres bactéries produisent des vésicules exposant des récepteurs aux bactériophages afin de les leurrer (218). Certains de ces mécanismes peuvent avoir un coût évolutif élevé lorsque les récepteurs impliqués remplissent un rôle prépondérant dans la physiologie bactérie (219).

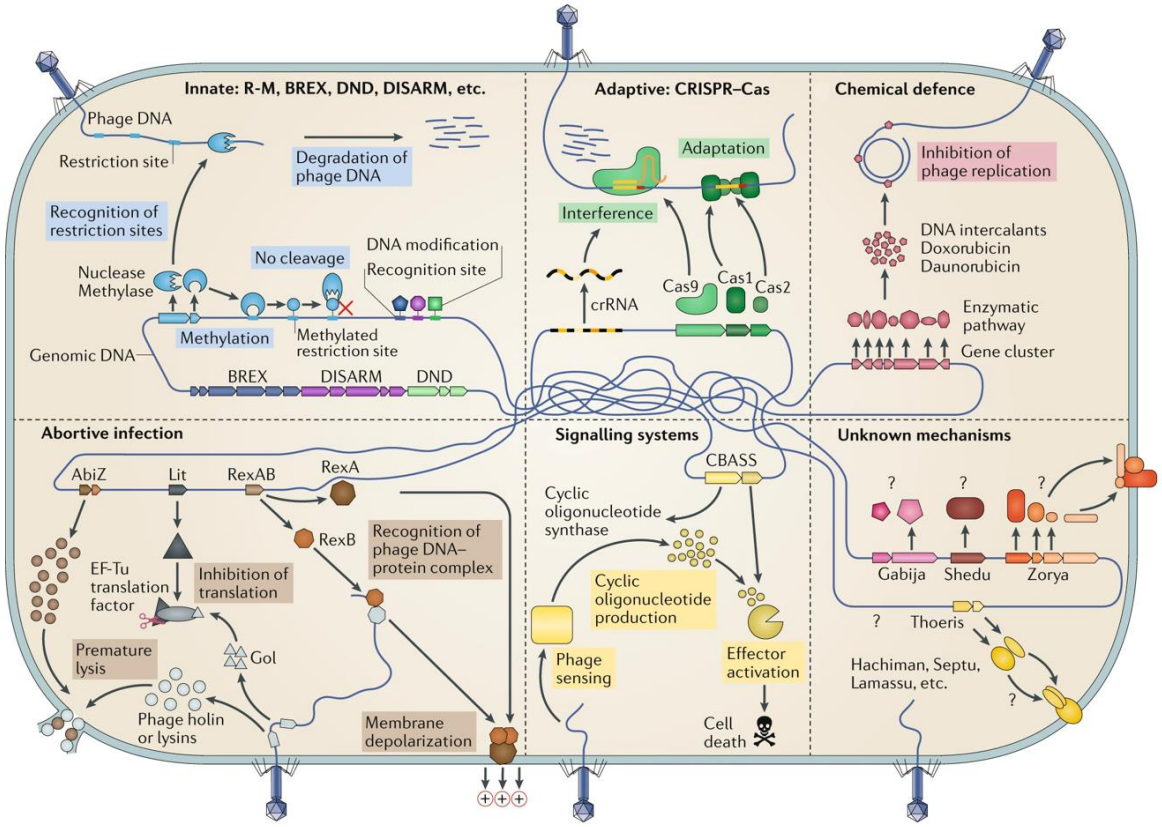

Figure 16 : Les principaux mécanismes de résistance aux bactériophages. Les systèmes de restriction-modification et les systèmes CRISPR ciblent des motifs d'ADN spécifiques. Les mécanismes d'infection avortée déclenchent une mort bactérienne prématurée. D'autres mécanismes, médiés par des agents chimiques ou des systèmes de signalisation, sont également représentés, en plus d'autres systèmes de résistance putatifs. Adapté de (220).

Mécanisme ciblant la production de nouveaux acides nucléiques

Une fois adsorbé à la surface des bactéries, le bactériophage injecte son génome dans le cytoplasme, l'exposant à des mécanismes de défense intracellulaire. Les systèmes de restriction-modification ciblent et dégradent l'ADN « non-hôte » *via* la reconnaissance de courtes séquences. Dans le génome de l'hôte, ces séquences sont généralement méthylées afin qu'elles ne soient pas prises pour cible par les enzymes de restriction. D'autres manières de différencier le génome de l'hôte de celui du bactériophage ont été identifiées, comme l'ajout d'un groupe soufre à l'ADN bactérien (221). Le mécanisme de restriction-modification est très repandu parmi les bactéries puisque 74% des génomes procaryotes sont dotés d'au moins un système de restriction/modification (222). Ce système de défense n'est pas spécifique d'un bactériophage, ni même de l'ADN viral et il est donc considéré comme un système immunitaire inné (220).

Tout comme les systèmes de restriction-modification, le système CRISPR-Cas cible l'ADN viral. À la suite d'une infection par un bactériophage, un fragment du génome viral peut être incorporé au génome bactérien. Lorsque la bactérie survit à cette première infection, via l'action d'un système de restriction-modification par exemple, cette séquence peut alors être transcrite pour servir de guide à la machinerie enzymatique Cas afin de cibler et dégrader spécifiquement le génome d'un autre bactériophage présentant une séquence identique à celle intégrée au chromosome. Ce système en deux étapes est assimilé à un système immunitaire adaptatif (223). Il existe une grande diversité de systèmes CRISPR-Cas avec plus de 20 sous-types, certains ciblant les bactériophages à ADN et d'autres les bactériophages à ARN (224).

L'infection abortive

Les bactéries ont aussi développé des mécanismes de défense au niveau populationnel. Lorsqu'une bactérie est infectée par un bactériophage, ces mécanismes, apparentés à un suicide cellulaire, empêchent le bactériophage d'accomplir un cycle infectieux productif et évitent qu'il n'infecte d'autres bactéries. Le principal mécanisme, appelé système d'infection abortive (Abi), a été identifié chez de nombreuses espèces bactériennes, mais aussi chez les archées. Il repose généralement sur des protéines toxine-antitoxine (225). La plupart des toxines ciblent la traduction des ARNs chez les bactéries (226).

Le système Abi peut être complémentaire à d'autres mécanismes de résistance. Par exemple chez certaines souches de *E. coli*, l'ARN bactérien est dégradé lorsque le système de restriction-modification est réprimé (227). Récemment, un nouveau système appelé Cyclic oligonucleotide Based Anti-phage Signalling System (CBASS) a été découvert. Dans ce système, une protéine cGAS détecte la présence d'ADN viral cytosolique et induit la production d'AMP et GMP cycliques qui vont à leur tour activer une phospholipase. Une fois activée, la phospholipase dégrade la membrane bactérienne, entrainant la mort de la bactérie (228).

Nouveaux mécanismes de défense

Récemment, un mécanisme de défense basé sur une molécule, la daunorubicine, a été identifié chez les *Streptomyces.* Cette molécule s'intercale dans l'ADN du bactériophage sans pour autant affecter la croissance de la bactérie hôte (229).

Un autre mécanisme atypique, ne constituant pas un système de défense à proprement parler, consiste à interférer avec le cycle viral des bactériophages. Il s'agit des phage-inducible chromosomal islands (PICIs) mis en évidence chez les bactéries Gram + et plus récemment chez les bactéries Gram - (230). Ce mécanisme exploite la présence de bactériophages tempérés afin de transmettre par transfert horizontal de gènes une partie spécifique de leur

génome. Les virions formés vont ainsi empaqueter aussi bien leur propre génome que les PICIs de la bactérie hôte, entrainant la production de nombreuses particules virales défectives. (231). Ce phénomène de transduction latérale explique que certains éléments génétiques, souvent des ilots de pathogénicité, aient une fréquence de transduction multipliée par 10^5 comparée à d'autres parties du génome (230).

Enfin, comme pour l'homo-immunité, un nombre croissant d'autres systèmes de défense putatifs ont été identifiés par des approches bio-informatiques, mais leurs mécanismes moléculaires restent à élucider (232).

Résistance phénotypique

Au sein d'une population, les bactéries ne forment pas un ensemble homogène. Certaines expriment des gènes de manière stochastique. Lorsque ces gènes sont nécessaires à l'infection virale d'un bactériophage, ces bactéries peuvent alors manifester une résistance dite phénotypique à ce bactériophage (233,234). *B. thetaiotaomicron* alterne l'expression de huit lipoprotéines de capsules entrainant une modification de son spectre de susceptibilité aux bactériophages (235). Dans le cas du phage crAss001, les variations d'expression peuvent aussi entrainer un délai de la lyse de la bactérie *B. intestinalis* engendrant une persistance du bactériophage. Un mécanisme similaire de variation de phase a été observé chez *Campylobacter jejuni* qui peut modifier son expression génétique afin de s'adapter à son environnement. Ceci entraine une modification des protéines présentes à sa surfaces et empêche ainsi l'adsorption de certains bactériophages (236). Ce mécanisme permet au bactériophage et à la bactérie de se multiplier en parallèle et de coexister au sein d'un même environnement (237).

Échappement des systèmes de défense bactériens par les bactériophages

Malgré tous les systèmes de défense cités, les bactériophages demeurent nombreux, preuve en est qu'ils parviennent à se multiplier. Les bactéries sont en fait résistantes à l'immense majorité des bactériophages auxquels elles sont exposées. Cependant, une fraction de ceux-ci a évolué conjointement avec un hôte bactérien, en développant des mécanismes de contournement des systèmes de défense. Ces bactériophages sont alors devenus spécialisés dans l'infection d'un spectre limité d'hôtes.

Pour ce faire, les bactériophages disposent de plusieurs solutions. Ils peuvent muter leurs protéines de queue en réponse à une mutation du récepteur bactérien (238). Pour contourner les systèmes de restriction/modification, le bactériophage T4 incorpore dans son génome une base modifiée, l'hydroxymethylcytosine, au lieu de la cytosine (239). Certains bactériophages sont capables de détourner un système d'infection abortive en produisant une antitoxine (240).

Le phage ΦKZ infectant *Pseudomonas aeruginosa* peut former un compartiment protéique entourant son ADN le protégeant des DNAse de l'hôte, notamment celles associées aux systèmes CRISPR-Cas et de restriction-modification (241). Plus directement, certains bactériophages produisent des protéines inhibant le système CRISPR-Cas selon plusieurs mécanismes : en se liant à la protéine Cas, empêchant son recrutement dans le complexe CRISPR-Cas ou en bloquant l'attachement du complexe CRISPR-Cas à l'ADN viral (242).

Afin de s'adapter au mieux à leur environnement et à leurs hôtes, les bactériophages sont en constante évolution, avec des mécanismes générant activement des mutations et des phénomènes de recombinaison (243). Les bactériophages sont ainsi capables d'échanger des régions fonctionnelles aboutissant à la formation de génomes mosaïques (244).

E) Les bactériophages en interaction avec leur environnement

Les bactériophages ont un impact majeur sur leur écosystème

En tant que prédateurs des bactéries, les bactériophages participent à la régulation des populations bactériennes et à leur diversité. Les bactéries les plus abondantes et les plus homogènes génétiquement sont plus susceptibles aux bactériophages. Cette dynamique « kill the winner » limite l'expansion d'une population bactérienne dans un environnement donné (245). Un exemple parmi d'autre est le rôle particulièrement importantes des bactériophages dans l'océan où ils sont responsables de la mort d'environ 20% de la biomasse microbienne chaque jour, impactant grandement le cycle du carbone océanique (198,246). Les bactériophages participent également à la diversité et à l'évolution bactérienne en réalisant la transduction de plus de 10^{28}pb d'ADN chaque année dans l'océan (247).

L'environnement influence les interactions entre bactériophages et bactéries

Réciproquement, l'environnement influence le cycle infectieux des bactériophages. Par exemple, le phage ΦS1 infecte *P. fluorescens* de manière optimale à 26°C, mais a une efficacité drastiquement diminuée à 4°C et nulle à 37°C. Ce même bactériophage est capable d'infecter son hôte dans un milieu riche, mais pas dans un milieu minimum supplémenté en glucose (248). Les conditions physico-chimiques et les conditions nutritionnelles peuvent donc exercer une influence sur l'efficacité des bactériophages.

Cependant la majorité des études sur les interactions entre bactériophages et bactéries ont été réalisées au laboratoire dans un environnement riche, contrôlé et homogène, avec une forte concentration de bactérie et souvent avec un seul couple bactériophage – bactérie. Ces conditions ne sont pas celles présentent dans le tube digestif des mammifères qui est un

environnement abritant plus de 500 espèces bactériennes différentes (249). Au sein même de l'intestin, les conditions environnementales (pH, oxygène) varient et influencent la nature et le niveau d'expression des gènes bactériens (250). Ces différences de transcription de gènes peuvent directement impacter le cycle infectieux des bactériophages.

Ainsi, des résultats observés au laboratoire ont montré que certains bactériophages ont une efficacité moindre à infecter la même bactérie *in vivo* que *in vitro*. Au sein même de l'intestin, certains sont plus efficaces dans l'intestin grêle (251,252) ou dans le colon (253). Des dynamiques nouvelles entre bactériophages et bactéries peuvent donc prendre place lorsque les conditions environnementales varient, pouvant aboutir à des situations de coexistence (251). De manière intéressante, cette coexistence n'est pas accompagnée d'une baisse importante du nombre de bactéries infectées ni de la sélection de clones résistants (253,254). Quels sont alors les mécanismes permettant la coexistence de ces deux populations antagonistes dans l'intestin ? Nous apporterons une partie des réponses au cours de ce travail.

F) Composition et rôle du virome intestinal

De la même manière que pour les bactéries, l'étude des bactériophages a connu un nouvel essor avec les avancées en bio-informatiques et en séquençage permettant l'étude du virome, c'est-à-dire l'ensemble des génome viraux retrouvés par séquençage métagénomique dans un environnement donné. Dès les premiers travaux, il a été remarqué que la composition virale dans l'intestin est dominée par les bactériophages (255,256). Même s'il est estimé qu'il y a environ 10 à 100 fois moins de bactériophages que de bactéries dans l'intestin, ils représentent 10^9 à 10^{10} unité formant plage (UFP) par gramme de contenu intestinal (89). La majorité des bactériophages dans l'intestin appartient aux ordres des *Caudovirales* et des *Microviridae*. Malgré leur abondance la caractérisation expérimentale de ces bactériophages n'est pas aisée. Les analyses métagénomiques ont permis la découverte d'un bactériophage, le crAssphage, présent dans plus de la moitié de la population et représentant jusqu'à 90% des bactériophages de l'intestin chez certains individus (257,258) . Il a fallu plus de 4 ans entre sa découverte *in silico* et son isolement au laboratoire.

Pathologie	Echantillon	Alteration du virome observée	Référence
Auto-immunité de la maladie cœliaque	Fèces	Diversité virale réduite	Reyes *et al.* 2015
MICI	Fèces	Enrichissement en entérovirus	Lindfors *et al.* 2019
MICI	Fèces	Enrichissement en *Caudovirales*	Norman *et al.* 2015
MICI	Fèces	Enrichissement en *Caudovirales*	Fernades *et al.* 2019
MICI diagnostiquée précocement	Biopsies intestinales	Augmentation des Hepadnaviridae et Hepeviridae ; réduction des Polydnaviridae, Tymoviridae et Virgaviridae	Ungaro *et al.* 2019
MICI à un stade précoce	Fèces	Augmentation du ratio *Caudovirales* sur *Microviridae*	Liang *et al.* 2020
Maladie de Crohn	Fèces	Basculement des populations de bactériophages de virulents à tempérés	Clooney *et al.* 2019
Rectocolite hémorragique	Biopsies intestinales	Augmentation de l'abondance des *Caudovirales*	Zuo *et al.* 2019
Cancer colorectal	Fèces	Augmentation de la diversité virale	Nakatsu *et al.* 2018
Diabète de type 1	Fèces	Diversité virale réduite	Zhao *et al.* 2017
Diabètes type 1 pendant la grossesse	Fèces	Enrichissement en picobirnavirus et tobamovirus	Kim *et al.* 2019
Diabète de type 2	Fèces	Modification des populations de bactériophages du virome intestinal	Ma*et al.* 2018
SIDA	Fèces	Enrichissement en adenovirus	Monaco *et al.* 2016
Transplantation de cellules souches hématopoïétiques	Fèces	Augmentation en picobirnavirus	Legoff *et al.* 2017

Table 3 : Exemples de modification du virome intestinal au cours de pathologies. Table adaptée de (259)

Des études suivant des individus au cours du temps ont démontré qu'il y a une forte variabilité interindividuelle du virome mais que pour une personne donnée, le virome est très stable au cours du temps (260). Malgré cette variabilité interindividuelle, un « core virome » commun à plus de 50% de la population a pu être découvert (261). Chez un individu sain, les bactériophages virulents sont majoritaires (262).

Un nombre croissant de facteurs influencent la composition du virome, tels que l'alimentation, la prise de médicaments, le contexte génétique et l'âge (259). Pour résumer, on peut s'attendre à ce que toute modification de l'équilibre bactérien au sein du tube digestif ait un impact sur la composition du virome. D'ailleurs les études comparatives entre sujets sains et patients confirment cette hypothèse. Des différences de composition entre des patients atteints de MICI et des individus sains ont rapporté une augmentation de l'abondance des bactériophages tempérés qui surpasse l'abondance des bactériophages virulents (262). Le virome est perturbé dans de nombreuses autres pathologies récapitulées dans la table 3. Cependant il est difficile de déterminer l'éventuelle présence de liens de causalités à partir d'études observationnelles chez l'humain. La nécessité de développer des modèles animaux pour étudier le virome est donc essentielle. L'intérêt de tels modèles est développé ci-après dans une revue publiée dans *Current Opinion in Virology* (263).

Available online at www.sciencedirect.com

ScienceDirect

Current Opinion in Virology

The intestinal virome: lessons from animal models

Lorenzo Chaffringeon[1,2,3], Quentin Lamy-Besnier[2,4], Laurent Debarbieux[2] and Luisa De Sordi[1,3]

Mucosal surfaces in contact with the environment host specific microbiota. The intestinal tract harbours the most abundant and diverse bacterial and viral populations interacting with each other as well as with the host. Viruses of the microbiota are important components of this ecosystem, as shown by viral alterations associated with various pathologies. However, practical and ethical constraints limit functional studies of the virome in humans, making animal models invaluable experimental tools to understand its impact on intestinal physiology. In this review, we present the recent advances in the study of virome in animal models. We focus on the strategies used to characterise viral changes in disease models and approaches to modulate the microbiota using viruses. In reviewing the interplay between viruses, bacteria, and the animal host, we highlight the potential and limitations of these models in elucidating the role of the virome in determining human health and disease.

Addresses
[1] Sorbonne Université, INSERM, Centre de Recherche St Antoine, UMRS_938, Paris, France
[2] Department of Microbiology, Institut Pasteur, Paris, F-75015, France
[3] Paris Center for Microbiome Medicine (PaCeMM) FHU, AP-HP, Paris, France
[4] Université de Paris, Paris, France

Corresponding author:
De Sordi, Luisa (luisa.de_sordi@sorbonne-universite.fr)

Current Opinion in Virology 2021, **51**:141–158

This review comes from a themed issue on **The virome in health and disease**

Edited by **Evelien Adriaenssens** and **Jelle Matthijnssens**

For complete overview about the section, refer "The virome in health and disease (2022)"

Available online 23rd October 2021

https://doi.org/10.1016/j.coviro.2021.09.016

Introduction

Several organs and mucosal membranes of animals are colonised by symbiotic microbes, known as microbiota, which include bacteria, archaea, fungi, protozoa and viruses [1]. Viruses of the microbiota are highly diverse and infect either eukaryotic or prokaryotic cells as obligate parasites. Although viruses have mostly been studied as pathogens, they can establish a mutualistic symbiosis with infected cells. This is well illustrated with bacteriophages (phages), viruses that infect bacteria, the most abundant viruses in the microbiota. Their life cycle is often either virulent, leading to phage replication and bacterial death, or temperate, conferring a possible fitness advantage, acting as mobile genetic elements.

Differently from cellular organisms, the genetic information of viruses is stored in DNA or RNA, single or double-stranded, and lacks common genetic markers, considerably limiting their study. Shotgun metagenomics partially overcomes these limitations by being able to access genomic information of different nature and is currently the gold-standard approach to study many microbial environments [2]. Although virome analysis is still challenging, bioinformatics tools are rapidly improving. Indeed, several studies have associated variations in virome composition with human disease, raising questions about their underlying mechanisms. Most have focused on intestinal phages and their overall impact on the bacteriome and gut physiology [3], whereas a few have also examined eukaryotic viruses, which appear to play similar roles as bacteria, affecting the development of host physiology and immunity [4].

Pre-clinical approaches using animal models present several advantages (ethics, costs, and reproducibility) in preliminary investigations on the role of the virome in host physiology and disease. In this review, we present and discuss the most recent advances in the characterisation of the virome in animal models, the factors involved in its variation, its mechanisms of interaction with the host, and the possible clinical and therapeutic consequences, with a focus on phages.

The intestinal virome of laboratory mice

The use of mice as robust models of virome-associated disorders requires that the baseline viral composition is known and comparable to that observed in clinical studies. Professional providers of laboratory mice raise them under specific pathogen-free (SPF) conditions, which implies that they are only screened for the absence of certain eukaryotic viruses. A major difference in the virome of laboratory mice compared to wild ones is indeed the much lower abundance of eukaryotic viruses, a factor that should be taken into account when discussing the outcome of functional microbiome studies [5].

To date, no facilities control for the presence of phages, as they are *generally recognised as safe* (GRAS) for animals,

including humans. The composition of intestinal phages reflects the composition of the intestinal bacteria, which varies between animal facilities and mouse lines. Recent studies have consistently showed that most phages in SPF mice belong to the *Microviridae* family (from 1–10 to 60–85%, depending on the mouse supplier) and Caudovirales order (1–10 to 80–99%), whereas a minority are still unknown or unclassified (1–10 to 25%) [5,6•,7•].

These results are coherent with observations in humans, in whom phages, *Microviridae* and Caudovirales, are the major viral component of the intestinal microbiota relative to eukaryotic viruses, as reviewed extensively elsewhere [8,9], further justifying the use of mice in preclinical research. Also, certain phage taxa are consistently found in mice from the same vendor, suggesting the existence of a core virome specific to breeding facilities [6•].

However, the lack of common standards in virome extraction, sequencing and analysis makes it hard to compare the high variability in composition observed in these studies. Sources of differences include the nature of the starting material (intestinal content [6•], faeces [7•] or caecal content [5]), the filtration method, the nucleic acid extraction (DNA and RNA viruses [5] or DNA viruses only [6•,7•]) and the sequencing technology (Illumina [5,6•] or Ion Torrent [7•]). Increasing cycles of DNA amplification during the preparation of Illumina sequencing libraries was also shown to enrich single-stranded viral DNA, which is consistent with the variability found in the proportion of *Microviridae* [2].

Overall, the impact of the virome on most animal studies is still unclear. It is possible that experimental reproducibility within and between laboratories could be perturbed by differences in the composition of the virome, as already shown for the bacterial microbiota [10,11]. Exploring virome diversity in these studies would have the double function of improving experimental practice and our understanding of the impact of viruses on host physiology.

The influence of diet on the animal virome

The diet is a source of microbiome variability [12] and a major parameter of several widely used models, such as those employing high-fat (HFD) and low-fat diets (LFD) to study diseases such as obesity or type-2 diabetes. Thus, the effect of diet on the virome is of particular interest.

After dietary intervention with a HFD or LFD, a study of six mice showed no significant differences in the composition of the core faecal virome [6•] but a significant change in the alpha diversity (Box 1) of phage populations. The bacteria, however, did not vary in alpha diversity in caecal samples after 13 weeks, although the different taxonomic level of analysis (strains versus genera) prevents a direct comparison between the viral and the bacterial component [6•]. However, Schulfer *et al.* obtained different results for the faeces of 24 mice, 16 weeks after transitioning to a HFD, showing a non-significant increase in alpha diversity of the viral community but a significant reduction in that of the bacterial population [7•]. In terms of beta diversity (Box 1), there was a significant shift after transitioning to a HFD from a standard diet (SD) in both the bacterial and viral populations in both studies [6•,7•]. A drop in the ratio of temperate to virulent phages was also observed in mice transitioning to a HFD [7•]. The results of these studies are consistent concerning HFD-related changes in the relative abundance of phage, showing an increase in *Microviridae* [6•,7•] and a decrease in Caudovirales, especially *Siphoviridae*, relative to a LFD [7•].

Box 1 Definitions of viral diversities from virome data

In ecology, **diversity** reflects the relative abundance of different species while the **richness** represents the number of different species. Within a specific ecosystem, the diversity is defined as **alpha diversity**, whereas **beta diversity** measures differences in diversity between two or more ecosystems. For the microbiota, the local ecosystem is the intestinal tract of a specific individual, therefore the alpha diversity represents the intra-individual diversity while the beta diversity represents the inter-individual diversity.

The virome of mice is not only affected by diet but is also altered in several pathological conditions. Moreover, in certain diseases, such as diabetes, the microbiota is a key factor in the development of the pathology [13]. Although current evidence suggests a connection between the microbiota and disease, the role of the virome in this context is still unknown.

Models of disease and their impact on the virome

Mice are often used as a proxy for human diseases to decipher their pathophysiology or test new therapeutics. Virome diversity correlates with several pathological conditions, such as inflammatory bowel disease [14], arthritis [15], and child growth impairment [16].

In a mouse model, neurotoxic chemicals were administered to induce symptoms of Gulf War illness, a chronic multisystemic disorder characterised by inflammatory bowel disease and neuroinflammation, among other conditions. The authors observed significant changes in the richness and composition of the virome associated with neuroinflammation driven by a decrease in the levels of the proteins which ensure epithelial cell–cell junctions in the gut and blood brain barrier. Additional antibiotic treatment did not significantly affect these differences but a wide-spectrum anti-viral agent partially reversed them to a level similar to that of the healthy control group

[17]. Overall, these results suggest a role of the virome in neuroinflammation and thus in the 'gut-brain' axis [17,18].

In another mouse model, Cao *et al.* examined the effect of vaccination with a full-length spike protein on the virome of mice infected with SARS-CoV2. Metagenomics showed a significant increase in alpha diversity in the virome of vaccinated mice relative to controls, without evidence of viral infection in the gastrointestinal tract, suggesting either an undetectable infection or modulation of the immune landscape that altered the gut microbiome [19].

Given the known involvement of the virome in the physiopathology of diseases associated with intestinal dysbiosis, the use of viruses to re-establish the microbial equilibrium has been proposed. Strategies of faecal viral transfer have thus been developed in animal models.

Modifying the microbiota of animal models in virome studies

Faecal microbiota transplantation (FMT) and faecal viral transfer (FVT) (Figure 1) are used to modify the gut microbiota of animal models, either to correct dysbiosis or to study the resulting specific perturbations.

A HFD induces glucose intolerance and weight gain in mice [20•]. These symptoms are significantly reduced after FVT from LFD mice. However, depleting gut bacteria with antibiotics neutralises the efficacy of FVT treatment, suggesting a crucial role for the gut bacteria of the recipient in the success of FVT in controlling the symptoms of diabetes [20•].

Mice fed a standard diet (SD) and treated by FMT or FVT from mice fed a HFD for 30 days had a significantly different bacterial composition in the small intestine than untreated mice and a beta diversity of bacteria comparable to that of mice fed a HFD. This shows that FMT and FVT can specifically shift the gut microbiota towards the donor composition with similar efficacy [21].

Thus, the effect of FVT depends on both the recipient and the donor [21] and the choice of donors is of utmost importance [22]. As mentioned previously, the composition of the murine virome is highly variable depending on environmental factors, such as the vendors or diet. Differences in the transferred material (faecal of caecal) also lead to grafting different viral populations. To minimise these factors in animal studies, mixing caecal contents or faeces of mice from different origins has been proposed [7•,20•].

The FVT can also originate from the recipient itself. Autochthonous FVT was shown to restore the antibiotic-treated microbiota of mice to a closer composition to that of the pre-antibiotic status relative to heat-inactivated FVT and increased the ratio between the bacterial phyla *Bacteroidetes* and *Firmicutes*, which was lowered by the antibiotic treatment [23•].

FVT can be an effective tool to modulate the microbiota. However, this raises the question of which viruses are necessary or sufficient for the therapeutic action of FVT.

Figure 1

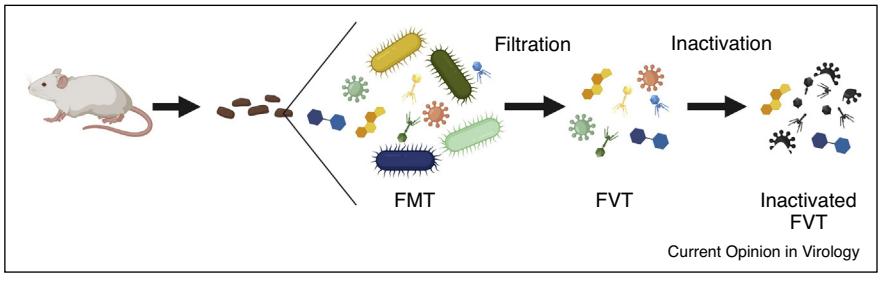

Faecal microbial and viral transplantation.
Faecal Microbial Transplantation (FMT) is the procedure used to transfer the faecal microbiota of an individual to himself or to another individual. It is used to correct dysbiosis and has proven to be effective to treat recurrent infections from *Clostridioides difficile* [49]. Faecal Viral Transplantation (FVT) is a similar approach that includes an additional filtration step during the preparatory procedure. This method is aimed at eliminating intestinal bacteria while keeping only viruses and small molecules. It is sometimes also referred to as sterile Faecal Filtrate Transfer (FFT). FVT can be exposed to UV treatment or heat shock to inactivate viruses and determine if the effect of the FVT is due to viral activity or other small metabolites. Conversely, the effect of small molecules can be eliminated by a supplementary filtration step that will retain viral particles while excluding other small compounds. FVT has shown similar efficacy as FMT in treating *C. difficile* infection in a small clinical assay with 5 patients [50] while alleviating potential secondary effects such as the implantation of pathogenic bacteria. FVT is used in animal models to decipher the importance of the virome in the mechanisms governing physiology and pathology, as described in section 'Modifying the microbiota of animal models in virome studies'.

Mechanisms underlying interactions with the virome

The virome, bacteriome, and animal host coexist. Animal models reunite all three actors of this tripartite interaction and allow its study in a controlled environment by separating the myriad of parameters affecting its development (Figure 2).

Virome–host interactions

The virome can affect the host by infecting it or by stimulating its immune system, either directly or via the bacteriome. Animal models offer the possibility to study the mechanisms behind such interactions. The advantages include the possibility of using genetic engineering to decipher the molecular mechanisms at play *in vivo* [24••] and measuring gene expression of various host cells by RNA sequencing [19].

Phages can also interact directly with the mammalian host. Sweere *et al.* found that a temperate filamentous phage of *Pseudomonas aeruginosa* can impair the murine immune system in a wound-infection model by activating the TLR3 pathway and inhibiting the production of TNF and phagocytosis, thus facilitating infection by its bacterial host [24••]. In addition, phages infecting the genera *Lactobacillus*, *Escherichia*, and *Bacteroides*, as well as the phage DNA, triggered a specific inflammatory response in dendritic cells by stimulating the INFγ response via TLR9 and exacerbated the inflammation in a DSS-induced colitis in wild-type but not IFNγ$^{-/-}$ or TLR9$^{-/-}$ mice [25]. A recent article demonstrated that a prophage integrated into *Enterococcus hirae* interacts with the class I major histocompatibility complex and enhances the efficacy of anti-tumour immune treatment in mice bearing this bacteria, confirming the hypothesis resulting from metagenomic studies in human patients with a differential response to treatment [26•]. Overall, these studies show that the prokaryotic virome can directly interact with the host immune system. [24••,26•].

Figure 2

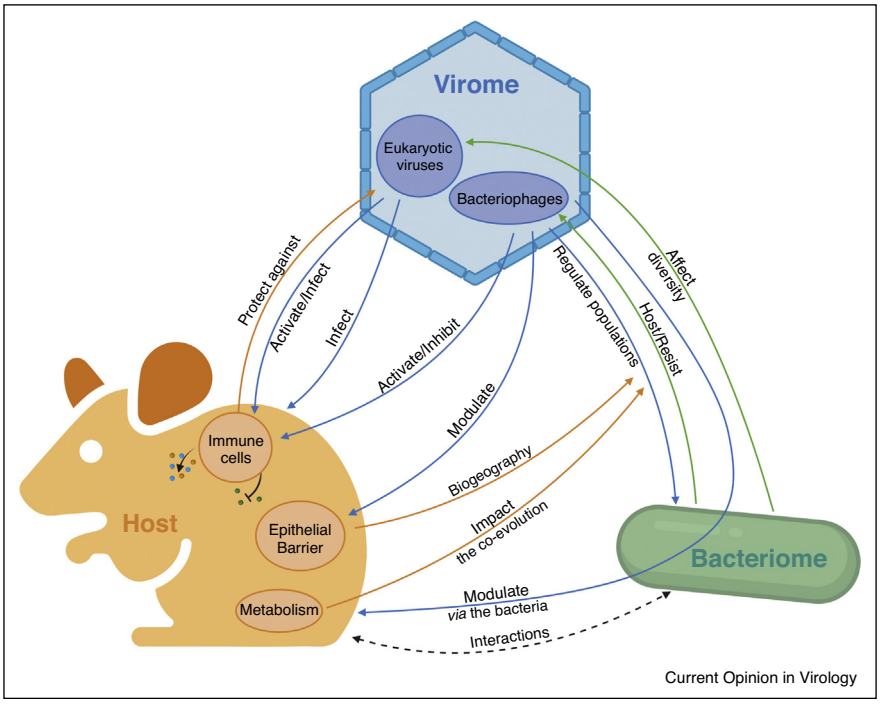

Virome, bacteriome, host: three actors and a myriad of interactions.
Schematic representation of the interactions between the viral, the bacterial compartments and the host. Most of the studies on the microbiota have focused on the bacteria–host interactions as reviewed by Ahern and Maloy [51] (dashed arrow). Viruses (blue arrows) have a strong connection to bacteria (green arrows): both populations regulate each other, directly (e.g. by phage predation or mutualism) or indirectly (via the immune system of the host). In turn, the virome can shift the metabolome by modulating bacterial populations and indirectly impacting the barrier and immunity (production cytokine is shown as coloured circles) of the host [31]. Antibiotic treatments can alter the alpha diversity of eukaryotic viruses, demonstrating that bacteria can also affect the diversity of eukaryotic viruses. The host (orange arrows) is interacting with eukaryotic and prokaryotic viruses that modulate its immune landscape and the epithelial barrier. The host offers a particular environment for phage–bacteria interactions and modulates their populations by secreting small regulatory molecules or by its spatial heterogeneity affecting their interactions. All displayed connections were drawn from studies in animal models, as described in this review.

Virome–bacteria interactions

The interactions between phages and bacteria *in vivo* have already been reviewed [27–30]. Here, we will focus on a few examples that illustrate the value of animal models in these studies.

Phages can directly modulate the gut microbiota by infecting their bacterial hosts, as well as indirectly, by modulating the diversity of bacterial populations. The addition of four phages, specific to a set of bacteria, profoundly shaped the microbiota of a gnotobiotic mouse model composed of 10 bacterial strains (either phage–hosts or not) coupled with shifts in secreted bacterial metabolites [31].

The host can affect both the virome and the bacteriome. Lourenço *et al.* demonstrated that the spatial heterogeneity of the gut creates refuges that protect bacteria against phage infection in a gnotobiotic mouse model [32••]. However, Green *et al.* [33] showed that specific phages can have a strong affinity for glycans, enhancing their effectiveness in the mucus layer. Thus, phage–bacteria interactions vary greatly between phage studies depending on the specificity of the phages, making it difficult to draw general conclusions.

De Sordi *et al.* characterised the phenomenon of 'host jump' (change of host) occurring in the murine gut. In this study, the diversity of the microbiota favoured the selection of genetic modifications that allowed phage infection of an originally resistant host strain via adaptation to intermediate intestinal hosts. This study shows the importance of the complexity of the environment in phage–bacteria interactions that can be modelled in animals [34].

Conversely, bacteria can modulate the virome. Depletion of the bacterial community with antibiotics in a rhesus monkey model was shown to reduce the alpha diversity and altered the virome composition of both phages and eukaryotic viruses (Box 2). The authors proposed a mechanism in which metabolites produced by the bacteria could shift, inhibit, or promote replication of the viruses [35].

Most of this work relies on reductionist approaches using defined couples of phages and bacteria that can be monitored within intestinal microbiota of different complexity. The necessity of simple model is partly driven by the fact that predicting the bacterial hosts of gut phages is a challenging task in natural communities. However, new advances in experimental and computational approaches show promise in tackling these limitations. As an example, meta3C, derived from the chromosome conformation capture method (3C), was used in mice microbiomes to assign putative bacterial hosts to specific phages using the physical proximity between their genomes [36].

Box 2 Roles of the eukaryotic virome in animal models

SPF mice have a low abundance of eukaryotic viruses. When detected, the most represented are DNA viruses of families *Phycodnaviridae* and *Mimiviridae* [7•,43] or the RNA viruses of the *Astroviridae* family [5]. However, viral annotation might be a limiting step in these analysis since two studies detected high amounts of giant *Mimiviridae* (with capsid of approximately 0.7 μm in diameter) that should have been excluded by filtration at 0.45 and 0.22 μm [7•].

Like for phages, the proportions of intestinal eukaryotic viruses are impacted by the diet, as shown by HFD-fed mice showing significant relative increase in the most abundant intestinal families [7•]. Eukaryotic viruses also do interact with the immune system of the host. Dallari *et al.* systematically assessed the immune response to six viruses belonging to different enteric families. The authors found that these viruses have an immunomodulatory properties independent of their capacity to induce gastroenteritis [44]. In another study, an intestinal murine astrovirus could confer protection from norovirus and rotavirus infections by complementing the animal immunodeficiency via the stimulation of IFN-λ-mediated signalling in epithelial cells [45••]. Here, the authors identify the active viral component by metagenomic comparison of active and inactive FVT in transferring protection to viral pathogens. Viral immunomodulation can also alter the physiopathology of bacterial infections. Both murine norovirus and astrovirus were shown to confer protection from to pathogenic *E. coli* in the gastrointestinal tract [46,47]. Conversely, mice treated with antibiotics are less susceptible to poliovirus infection, suggesting a facilitating role of bacteria in the infection process [48]. Eukaryotic viruses are less abundant than phages in the microbiota, but their influence on the host and its immune system is major. Whether a connection exists between the immune response elicited by eukaryotic viruses and the diversity of phage populations is still unexplored territory.

Animal models offer the possibility to unravel the complex relationships in which each population influences the other two. They reunite all three actors, viruses, bacteria, and the host, and each can be specifically modified to aid in the deciphering of this tripartite association (Figure 2). Models with a controlled microbiota, also called gnotobiotic models, facilitate the study of the virome using a simpler, characterised microbial environment.

Non mouse models

Although mice are the most widely used laboratory animals, other mammals are also suitable for the study of the intestinal microbiota. Macaques are genetically closely related to humans and are therefore a pertinent model to study parameters that influence the human virome. Cynomolgus macaques have recently been used to analyse the effect of aging on the gut virome [37]. Aging is already known to have an effect on the bacteriome [38], however, the consequences of aging on the composition of the virome are mostly unknown. The macaque virome has been found to be dominated by phages and alpha diversity is not significantly altered with aging. However, the viral species change with age, which was also shown to be the case for the KEGG pathways present in the virome, suggesting a role for the virome in regulating metabolism

[37]. The bacteriome and virome thus appear to be linked and to evolve together as the animals age.

Zhao *et al.* characterised the enteric virome of rhesus macaques with chronic diarrhoea [39]. They found the virome to be dominated by phages of the Caudovirales order and *Microviridae* family, much like the intestinal virome of mice and humans, as also confirmed in a second study [35]. They also used biogeographical analysis, to find that the rectal virome is similar to the one of the colon but distinct to the virome of the ileum. A recent study also confirmed the distinction in virome composition between the large and the small intestine in rhesus monkey and pigs with a higher phage diversity in the lumen and predominance of eukaryotic viruses in mucosal samples [40]. Recently, the faecal, oral, blood, and skin virome of laboratory rabbits were described leading to the identification of a novel polyomavirus [41]. Finally, swine models have also been used for virome studies. For example, FVT was shown to protect preterm pigs against necrotising enterocolitis [42].

Overall, these results show that different animals have a similar virome structure, with the presence of key eukaryotic viruses and quantitative domination by phages. However, further and more detailed characterisation of the components is required for a better understanding their differences and roles.

Conclusions

The virome has been increasingly linked to health and disease. Although animal models have been spearheading new discoveries in this field, the study of their virome is still in its infancy. As for humans, phages are the most abundant component of the animal virome and new mechanisms of their physiological roles remain to be characterised in relation to their direct effect on the host and indirect effect as a modulator of bacterial populations. Further studies, taking advantage of the flexibility of animal models, are required to investigate the interactions of the virome with both other elements of the microbiome and the host. In addition, future research needs to tackle the issue of determining the active actors in the microbiota in physiology and pathophysiology. The challenge lies in dissociating the actions of viruses from those of bacteria and between individual viruses, with the objective of identifying key players in human health.

Conflict of interest statement

Nothing declared.

Acknowledgements

LC is funded by a PhD fellowship from the Ministère de l'Enseignement Supérieur et de la Recherche, France, Ecole Doctorale 394. QLB is funded by École Doctorale FIRE - Programme Bettencourt. LD receives fundings from ANR-20-CE92-0048, and LDS receives fundings from the Agence Nationale de la Recerche (ANR) and the Societé Nationale Française de Gastro-Entérologie (SNFGE). Figures were created with Biorender.com.

References and recommended reading

Papers of particular interest, published within the period of review, have been highlighted as:

- • of special interest
- •• of outstanding interest

1. Matijašić M, Meštrović T, Paljetak HČ, Perić M, Barešić A, Verbanac D: **Gut microbiota beyond bacteria-mycobiome, virome, archaeome, and eukaryotic parasites in IBD**. *Int J Mol Sci* 2020, **21**:E2668.

2. Marine R, McCarren C, Vorrasane V, Nasko D, Crowgey E, Polson SW, Wommack KE: **Caught in the middle with multiple displacement amplification: the myth of pooling for avoiding multiple displacement amplification bias in a metagenome**. *Microbiome* 2014, **2**:3.

3. Manrique P, Dills M, Young MJ: **The human gut phage community and its implications for health and disease**. *Viruses* 2017, **9**:E141.

4. Kernbauer E, Ding Y, Cadwell K: **An enteric virus can replace the beneficial function of commensal bacteria**. *Nature* 2014, **516**:94-98.

5. Rosshart SP, Herz J, Vassallo BG, Hunter A, Wall MK, Badger JH, McCulloch JA, Anastasakis DG, Sarshad AA, Leonardi I *et al.*: **Laboratory mice born to wild mice have natural microbiota and model human immune responses**. *Science* 2019, **365**.

6. • Rasmussen TS, de Vries L, Kot W, Hansen LH, Castro-Mejía JL, Vogensen FK, Hansen AK, Nielsen DS: **Mouse vendor influence on the bacterial and viral gut composition exceeds the effect of diet**. *Viruses* 2019, **11**:E435

This study underlines the important influence of the origin of the mice on the virome composition, which should be taken into account when conceiving animal studies.

7. • Schulfer A, Santiago-Rodriguez TM, Ly M, Borin JM, Chopyk J, Blaser MJ, Pride DT: **Fecal viral community responses to high-fat diet in mice**. *mSphere [date unknown]* 2021, **5** e00833-19

This article is a necessary step towards the comprehension of the fundamental parameters related to diet influencing the virome composition.

8. Liang G, Bushman FD: **The human virome: assembly, composition and host interactions**. *Nat Rev Microbiol* 2021, **19**:514-527 http://dx.doi.org/10.1038/s41579-021-00536-5.

9. Sausset R, Petit MA, Gaboriau-Routhiau V, De Paepe M: **New insights into intestinal phages**. *Mucosal Immunol* 2020, **13**:205-215.

10. Franklin CL, Ericsson AC: **Microbiota and reproducibility of rodent models**. *Lab Anim* 2017, **46**:114-122.

11. Vujkovic-Cvijin I, Sklar J, Jiang L, Natarajan L, Knight R, Belkaid Y: **Host variables confound gut microbiota studies of human disease**. *Nature* 2020, **587**:448-454.

12. Bisanz JE, Upadhyay V, Turnbaugh JA, Ly K, Turnbaugh PJ: **Meta-analysis reveals reproducible gut microbiome alterations in response to a high-fat diet**. *Cell Host Microbe* 2019, **26**:265-272.e4.

13. Bäckhed F, Manchester JK, Semenkovich CF, Gordon JI: **Mechanisms underlying the resistance to diet-induced obesity in germ-free mice**. *Proc Natl Acad Sci U S A* 2007, **104**:979-984.

14. Clooney AG, Sutton TDS, Shkoporov AN, Holohan RK, Daly KM, O'Regan O, Ryan FJ, Draper LA, Plevy SE, Ross RP *et al.*: **Whole-virome analysis sheds light on viral dark matter in inflammatory bowel disease**. *Cell Host Microbe* 2019, **26**:764-778.e5.

15. Mangalea MR, Paez-Espino D, Kieft K, Chatterjee A, Chriswell ME, Seifert JA, Feser ML, Demoruelle MK, Sakatos A, Anantharaman K *et al.*: **Individuals at risk for rheumatoid arthritis harbor differential intestinal bacteriophage communities with distinct metabolic potential**. *Cell Host Microbe* 2021, **29**:726-739.e5.

16. Khan Mirzaei M, Khan MAA, Ghosh P, Taranu ZE, Taguer M, Ru J, Chowdhury R, Kabir MM, Deng L, Mondal D *et al.*:

Bacteriophages isolated from stunted children can regulate gut bacterial communities in an age-specific manner. *Cell Host Microbe* 2020, **27**:199-212.e5.

17. Seth RK, Maqsood R, Mondal A, Bose D, Kimono D, Holland LA, Janulewicz Lloyd P, Klimas N, Horner RD, Sullivan K *et al.*: **Gut DNA virome diversity and its association with host bacteria regulate inflammatory phenotype and neuronal immunotoxicity in experimental gulf war illness**. *Viruses* 2019, **11**:E968.

18. Cryan JF, O'Riordan KJ, Cowan CSM, Sandhu KV, Bastiaanssen TFS, Boehme M, Codagnone MG, Cussotto S, Fulling C, Golubeva AV *et al.*: **The microbiota-gut-brain axis**. *Physiol Rev* 2019, **99**:1877-2013.

19. Cao J, Wang C, Zhang Y, Lei G, Xu K, Zhao N, Lu J, Meng F, Yu L, Yan J *et al.*: **Integrated gut virome and bacteriome dynamics in COVID-19 patients**. *Gut Microbes* 2021, **13**:1-21.

20. • Rasmussen TS, Mentzel CMJ, Kot W, Castro-Mejía JL, Zuffa S, Swann JR, Hansen LH, Vogensen FK, Hansen AK, Nielsen DS: **Faecal virome transplantation decreases symptoms of type 2 diabetes and obesity in a murine model**. *Gut* 2020, **69**:2122-2130

This work is a well-designed study investigating the differences between FVT and FMT, and their importance for the clinical outcome.

21. Lin DM, Koskella B, Ritz NL, Lin D, Carroll-Portillo A, Lin HC: **Transplanting fecal virus-like particles reduces high-fat diet-induced small intestinal bacterial overgrowth in mice**. *Front Cell Infect Microbiol* 2019, **9**:348.

22. Wilson BC, Vatanen T, Cutfield WS, O'Sullivan JM: **The super-donor phenomenon in fecal microbiota transplantation**. *Front Cell Infect Microbiol* 2019, **9**:2.

23. • Draper LA, Ryan FJ, Dalmasso M, Casey PG, McCann A, Velayudhan V, Ross RP, Hill C: **Autochthonous faecal viral transfer (FVT) impacts the murine microbiome after antibiotic perturbation**. *BMC Biol* 2020, **18**:173

This article includes a novel temporal aspect to the study of microbiome with FVT treatment allowing the study of the evolution of the microbiome after an FVT.

24. •• Sweere JM, Belleghem JDV, Ishak H, Bach MS, Popescu M, Sunkari V, Kaber G, Manasherob R, Suh GA, Cao X *et al.*: **Bacteriophage trigger antiviral immunity and prevent clearance of bacterial infection**. *Science* 2019, **363**

This article is a great example of a phage interacting directly with the animal host immune system.

25. Gogokhia L, Buhrke K, Bell R, Hoffman B, Brown DG, Hanke-Gogokhia C, Ajami NJ, Wong MC, Ghazaryan A, Valentine JF *et al.*: **Expansion of bacteriophages is linked to aggravated intestinal inflammation and colitis**. *Cell Host Microbe* 2019, **25**:285-299.e8.

26. • Fluckiger A, Daillère R, Sassi M, Sixt BS, Liu P, Loos F, Richard C, Rabu C, Alou MT, Goubet A-G *et al.*: **Cross-reactivity between tumor MHC class I-restricted antigens and an enterococcal bacteriophage**. *Science* 2020, **369**:936-942

This work highlights the mechanisms behind the interactions between a phage and the immune system, influencing the outcome of cancer treatments.

27. Guerin E, Hill C: **Shining light on human gut bacteriophages**. *Front Cell Infect Microbiol* 2020, **10**:481.

28. Blazanin M, Turner PE: **Community context matters for bacteria-phage ecology and evolution**. *ISME J* 2021 http://dx.doi.org/10.1038/s41396-021-01012-x. online ahead of print.

29. Dahlman S, Avellaneda-Franco L, Barr JJ: **Phages to shape the gut microbiota?** *Curr Opin Biotechnol* 2021, **68**:89-95.

30. Shkoporov AN, Hill C: **Bacteriophages of the human gut: the "Known Unknown" of the microbiome**. *Cell Host Microbe* 2019, **25**:195-209.

31. Hsu BB, Gibson TE, Yeliseyev V, Liu Q, Lyon L, Bry L, Silver PA, Gerber GK: **Dynamic modulation of the gut microbiota and metabolome by bacteriophages in a mouse model**. *Cell Host Microbe* 2019, **25**:803-814.e5.

32. •• Lourenço M, Chaffringeon L, Lamy-Besnier Q, Pédron T, Campagne P, Eberl C, Bérard M, Stecher B, Debarbieux L, De Sordi L: **The spatial heterogeneity of the gut limits predation and fosters coexistence of bacteria and bacteriophages**. *Cell Host Microbe* 2020, **28**:390-401.e5

This well-designed work illustrates the difference between *in vitro* and *in vivo* dynamics of phages and bacterial populations and highlights the importance of the spatial heterogeneity of the gut in such interactions.

33. Green SI, Gu Liu C, Yu X, Gibson S, Salmen W, Rajan A, Carter HE, Clark JR, Song X, Ramig RF *et al.*: **Targeting of mammalian glycans enhances phage predation in the gastrointestinal tract**. *mBio [date unknown]* 2021, **12** e03474-20.

34. De Sordi L, Khanna V, Debarbieux L: **The gut microbiota facilitates drifts in the genetic diversity and infectivity of bacterial viruses**. *Cell Host Microbe* 2017, **22**:801-808.e3.

35. Li H, Li H, Wang J, Guo L, Fan H, Zheng H, Yang Z, Huang X, Chu M, Yang F *et al.*: **The altered gut virome community in rhesus monkeys is correlated with the gut bacterial microbiome and associated metabolites**. *Virol J* 2019, **16**:105.

36. Marbouty M, Baudry L, Cournac A, Koszul R: **Scaffolding bacterial genomes and probing host-virus interactions in gut microbiome by proximity ligation (chromosome capture) assay**. *Sci Adv* 2017, **3**:e1602105.

37. Tan X, Chai T, Duan J, Wu J, Zhang H, Li Y, Huang Y, Hu X, Zheng P, Song J *et al.*: **Dynamic changes occur in the DNA gut virome of female cynomolgus macaques during aging**. *Microbiologyopen* 2021, **10**:e1186.

38. Biagi E, Nylund L, Candela M, Ostan R, Bucci L, Pini E, Nikkïla J, Monti D, Satokari R, Franceschi C *et al.*: **Through ageing, and beyond: gut microbiota and inflammatory status in seniors and centenarians**. *PLoS One* 2010, **5**:e10667.

39. Zhao G, Droit L, Gilbert MH, Schiro FR, Didier PJ, Si X, Paredes A, Handley SA, Virgin HW, Bohm RP *et al.*: **Virome biogeography in the lower gastrointestinal tract of rhesus macaques with chronic diarrhea**. *Virology* 2019, **527**:77-88.

40. Shkoporov A, Stockdale S, Lavelle A, Kondova I, Hueston C, Upadrasta A, Khokhlova E, Kamp I van der, Ouwerling B, Draper L *et al.*: **Viral biogeography of gastrointestinal tract and parenchymal organs in two representative species of mammals.** 2021, DOI: https://doi.org/10.21203/rs.3.rs-803286/v1.

41. Xiao Y, Wang H, Feng L, Pan J, Chen Z, Wang H, Yang S, Shen Q, Wang X, Shan T *et al.*: **Fecal, oral, blood and skin virome of laboratory rabbits**. *Arch Virol* 2020, **165**:2847-2856.

42. Brunse A, Deng L, Pan X, Hui Y, Castro-Mejía JL, Kot W, Nguyen DN, Secher JB-M, Nielsen DS, Thymann T: **Fecal filtrate transplantation protects against necrotizing enterocolitis**. *ISME J* 2021 http://dx.doi.org/10.1038/s41396-021-01107-5. online ahead of print.

43. Rasmussen TS, Jakobsen RR, Castro-Mejía JL, Kot W, Thomsen AR, Vogensen FK, Nielsen DS, Hansen AK: **Inter-vendor variance of enteric eukaryotic DNA viruses in specific pathogen free C57BL/6N mice**. *Res Vet Sci* 2021, **136**:1-5.

44. Dallari S, Heaney T, Rosas-Villegas A, Neil JA, Wong S-Y, Brown JJ, Urbanek K, Herrmann C, Depledge DP, Dermody TS *et al.*: **Enteric viruses evoke broad host immune responses resembling those elicited by the bacterial microbiome**. *Cell Host Microbe* 2021, **29**:1014-1029.e8.

45. •• Ingle H, Lee S, Ai T, Orvedahl A, Rodgers R, Zhao G, Sullender M, Peterson ST, Locke M, Liu T-C *et al.*: **Viral complementation of immunodeficiency confers protection against enteric pathogens via interferon-λ**. *Nat Microbiol* 2019, **4**:1120-1128

This article investigates with success the active element of an FVT and shows that only one virus was sufficient for its effectiveness in conferring protection against norovirus and rotavirus infections.

46. Neil JA, Matsuzawa-Ishimoto Y, Kernbauer-Hölzl E, Schuster SL, Sota S, Venzon M, Dallari S, Galvao Neto A, Hine A, Hudesman D *et al.*: **IFN-I and IL-22 mediate protective effects of intestinal viral infection**. *Nat Microbiol* 2019, **4**:1737-1749.

47. Cortez V, Boyd DF, Crawford JC, Sharp B, Livingston B, Rowe HM, Davis A, Alsallaq R, Robinson CG, Vogel P *et al.*: **Astrovirus**

infects actively secreting goblet cells and alters the gut mucus barrier. *Nat Commun* 2020, **11**:2097.

48. Kuss SK, Best GT, Etheredge CA, Pruijssers AJ, Frierson JM, Hooper LV, Dermody TS, Pfeiffer JK: **Intestinal microbiota promote enteric virus replication and systemic pathogenesis**. *Science* 2011, **334**:249-252.

49. Bakken JS, Borody T, Brandt LJ, Brill JV, Demarco DC, Franzos MA, Kelly C, Khoruts A, Louie T, Martinelli LP *et al.*: **Treating *Clostridium difficile* infection with fecal microbiota transplantation**. *Clin Gastroenterol Hepatol Off Clin Pract J Am Gastroenterol Assoc* 2011, **9**:1044-1049.

50. Ott SJ, Waetzig GH, Rehman A, Moltzau-Anderson J, Bharti R, Grasis JA, Cassidy L, Tholey A, Fickenscher H, Seegert D *et al.*: **Efficacy of sterile fecal filtrate transfer for treating patients with *Clostridium difficile* infection**. *Gastroenterology* 2017, **152**:799-811.e7.

51. Ahern PP, Maloy KJ: **Understanding immune-microbiota interactions in the intestine**. *Immunology* 2020, **159**:4-14.

Références

1. File:Digestive system diagram edit.svg - Wikipedia [Internet]. [cité 2 mai 2022]. Disponible sur: https://commons.wikimedia.org/wiki/File:Digestive_system_diagram_edit.svg

2. Allaire JM, Crowley SM, Law HT, Chang SY, Ko HJ, Vallance BA. The Intestinal Epithelium: Central Coordinator of Mucosal Immunity. Trends Immunol. sept 2018;39(9):677-96.

3. Bellafante E, Morgano A, Salvatore L, Murzilli S, Di Tullio G, D'Orazio A, et al. PGC-1β promotes enterocyte lifespan and tumorigenesis in the intestine. Proceedings of the National Academy of Sciences. 21 oct 2014;111(42):E4523-31.

4. Sternini C, Anselmi L, Rozengurt E. Enteroendocrine cells: a site of « taste » in gastrointestinal chemosensing. Curr Opin Endocrinol Diabetes Obes. févr 2008;15(1):73-8.

5. Corr SC, Gahan CCGM, Hill C. M-cells: origin, morphology and role in mucosal immunity and microbial pathogenesis. FEMS Immunology & Medical Microbiology. 1 janv 2008;52(1):2-12.

6. Gribble FM, Reimann F. Function and mechanisms of enteroendocrine cells and gut hormones in metabolism. Nat Rev Endocrinol. avr 2019;15(4):226-37.

7. Sarkar A, Ye A, Singh H. On the role of bile salts in the digestion of emulsified lipids. Food Hydrocolloids. 1 oct 2016;60:77-84.

8. Schonewille M, de Boer JF, Groen AK. Bile salts in control of lipid metabolism. Current Opinion in Lipidology. juin 2016;27(3):295-301.

9. Ridlon JM, Wolf PG, Gaskins HR. Taurocholic acid metabolism by gut microbes and colon cancer. Gut Microbes. 3 mai 2016;7(3):201-15.

10. Gribble FM, Reimann F. Enteroendocrine Cells: Chemosensors in the Intestinal Epithelium. Annu Rev Physiol. 2016;78:277-99.

11. Barrett KE, Ganong WF. Ganong's review of medical physiology. New York; London: McGraw-Hill Medical ; McGraw-Hill [distributor; 2012.

12. Li T, Chiang JYL. Bile Acid Signaling in Liver Metabolism and Diseases. Journal of Lipids. 3 oct 2011;2012:e754067.

13. Li J, Dawson PA. Animal models to study bile acid metabolism. Biochim Biophys Acta Mol Basis Dis. 1 mai 2019;1865(5):895-911.

14. Takahashi S, Fukami T, Masuo Y, Brocker CN, Xie C, Krausz KW, et al. Cyp2c70 is responsible for the species difference in bile acid metabolism between mice and humans. J Lipid Res. déc 2016;57(12):2130-7.

15. Studer N, Desharnais L, Beutler M, Brugiroux S, Terrazos MA, Menin L, et al. Functional Intestinal Bile Acid 7α-Dehydroxylation by Clostridium scindens Associated with Protection from Clostridium difficile Infection in a Gnotobiotic Mouse Model. Front Cell Infect Microbiol. 2016;6:191.

16. Song Z, Cai Y, Lao X, Wang X, Lin X, Cui Y, et al. Taxonomic profiling and populational patterns of bacterial bile salt hydrolase (BSH) genes based on worldwide human gut microbiome. Microbiome. 23 janv 2019;7(1):9.

17. Hofmann AF. The enterohepatic circulation of bile acids in mammals: form and functions. Front Biosci (Landmark Ed). 1 janv 2009;14:2584-98.

18. Guzior DV, Quinn RA. Review: microbial transformations of human bile acids. Microbiome. 14 juin 2021;9(1):140.

19. Ridlon JM, Harris SC, Bhowmik S, Kang DJ, Hylemon PB. Consequences of bile salt biotransformations by intestinal bacteria. Gut Microbes. 2 janv 2016;7(1):22-39.

20. Ridlon JM, Hylemon PB. Identification and characterization of two bile acid coenzyme A transferases from Clostridium scindens, a bile acid 7α-dehydroxylating intestinal bacterium. Journal of Lipid Research. 1 janv 2012;53(1):66-76.

21. Lepercq P, Gérard P, Béguet F, Raibaud P, Grill JP, Relano P, et al. Epimerization of chenodeoxycholic acid to ursodeoxycholic acid by Clostridium baratii isolated from human feces. FEMS Microbiology Letters. 1 juin 2004;235(1):65-72.

22. Lee JY, Arai H, Nakamura Y, Fukiya S, Wada M, Yokota A. Contribution of the 7β-hydroxysteroid dehydrogenase from Ruminococcus gnavus N53 to ursodeoxycholic acid formation in the human colon. J Lipid Res. nov 2013;54(11):3062-9.

23. Doden HL, Wolf PG, Gaskins HR, Anantharaman K, Alves JMP, Ridlon JM. Completion of the gut microbial epi-bile acid pathway. Gut Microbes. 2021;13(1):1907271.

24. Mythen SM, Devendran S, Méndez-García C, Cann I, Ridlon JM. Targeted Synthesis and Characterization of a Gene Cluster Encoding NAD(P)H-Dependent 3α-, 3β-, and 12α-Hydroxysteroid Dehydrogenases from Eggerthella CAG:298, a Gut Metagenomic Sequence. Applied and Environmental Microbiology [Internet]. 12 janv 2018 [cité 26 janv 2022]; Disponible sur: https://journals.asm.org/doi/abs/10.1128/AEM.02475-17

25. Ridlon JM, Bajaj JS. The human gut sterolbiome: bile acid-microbiome endocrine aspects and therapeutics. Acta Pharmaceutica Sinica B. 1 mars 2015;5(2):99-105.

26. Lopez CA, Miller BM, Rivera-Chávez F, Velazquez EM, Byndloss MX, Chávez-Arroyo A, et al. Virulence factors enhance Citrobacter rodentium expansion through aerobic respiration. Science. 16 sept 2016;353(6305):1249-53.

27. Atuma C, Strugala V, Allen A, Holm L. The adherent gastrointestinal mucus gel layer: thickness and physical state in vivo. Am J Physiol Gastrointest Liver Physiol. mai 2001;280(5):G922-929.

28. Furter M, Sellin ME, Hansson GC, Hardt WD. Mucus Architecture and Near-Surface Swimming Affect Distinct Salmonella Typhimurium Infection Patterns along the Murine Intestinal Tract. Cell Reports. 28 mai 2019;27(9):2665-2678.e3.

29. Goll R, van Beelen Granlund A. Intestinal barrier homeostasis in inflammatory bowel disease. Scand J Gastroenterol. janv 2015;50(1):3-12.

30. Johansson MEV, Phillipson M, Petersson J, Velcich A, Holm L, Hansson GC. The inner of the two Muc2 mucin-dependent mucus layers in colon is devoid of bacteria. Proceedings of the National Academy of Sciences. 30 sept 2008;105(39):15064-9.

31. Odenwald MA, Turner JR. The intestinal epithelial barrier: a therapeutic target? Nat Rev Gastroenterol Hepatol. janv 2017;14(1):9-21.

32. Edelblum KL, Turner JR. The tight junction in inflammatory disease: communication breakdown. Curr Opin Pharmacol. déc 2009;9(6):715-20.

33. Jauregi-Miguel A. Chapter Four - The tight junction and the epithelial barrier in coeliac disease. In: Castellanos-Rubio A, Galluzzi L, éditeurs. International Review of Cell and Molecular Biology [Internet]. Academic Press; 2021 [cité 14 avr 2022]. p. 105-32. (Immunopathology of Celiac Disease; vol. 358). Disponible sur: https://www.sciencedirect.com/science/article/pii/S1937644820301027

34. Anderson JM, Van Itallie CM. Physiology and function of the tight junction. Cold Spring Harb Perspect Biol. août 2009;1(2):a002584.

35. O'Neil DA, Porter EM, Elewaut D, Anderson GM, Eckmann L, Ganz T, et al. Expression and regulation of the human beta-defensins hBD-1 and hBD-2 in intestinal epithelium. J Immunol. 15 déc 1999;163(12):6718-24.

36. Chromek M, Arvidsson I, Karpman D. The Antimicrobial Peptide Cathelicidin Protects Mice from Escherichia coli O157:H7-Mediated Disease. PLOS ONE. 15 oct 2012;7(10):e46476.

37. Iimura M, Gallo RL, Hase K, Miyamoto Y, Eckmann L, Kagnoff MF. Cathelicidin Mediates Innate Intestinal Defense against Colonization with Epithelial Adherent Bacterial Pathogens. The Journal of Immunology. 15 avr 2005;174(8):4901-7.

38. Mukherjee S, Zheng H, Derebe MG, Callenberg KM, Partch CL, Rollins D, et al. Antibacterial membrane attack by a pore-forming intestinal C-type lectin. Nature. janv 2014;505(7481):103-7.

39. Stelter C, Käppeli R, König C, Krah A, Hardt WD, Stecher B, et al. Salmonella-Induced Mucosal Lectin RegIIIβ Kills Competing Gut Microbiota. PLOS ONE. 9 juin 2011;6(6):e20749.

40. Vaishnava S, Yamamoto M, Severson KM, Ruhn KA, Yu X, Koren O, et al. The Antibacterial Lectin RegIIIγ Promotes the Spatial Segregation of Microbiota and Host in the Intestine. Science. 14 oct 2011;334(6053):255-8.

41. Zheng Y, Valdez PA, Danilenko DM, Hu Y, Sa SM, Gong Q, et al. Interleukin-22 mediates early host defense against attaching and effacing bacterial pathogens. Nat Med. mars 2008;14(3):282-9.

42. Qu XD, Lehrer RI. Secretory Phospholipase A2 Is the Principal Bactericide for Staphylococci and Other Gram-Positive Bacteria in Human Tears. Infection and Immunity. juin 1998;66(6):2791-7.

43. Margulieux KR, Fox JW, Nakamoto RK, Hughes MA. CXCL10 Acts as a Bifunctional Antimicrobial Molecule against Bacillus anthracis. mBio. 2016;7(3):e00334-16.

44. Schutte KM, Fisher DJ, Burdick MD, Mehrad B, Mathers AJ, Mann BJ, et al. Escherichia coli pyruvate dehydrogenase complex is an important component of CXCL10-mediated antimicrobial activity. Infection and Immunity. 2015;84(1):320-8.

45. Diaz-Ochoa VE, Jellbauer S, Klaus S, Raffatellu M. Transition metal ions at the crossroads of mucosal immunity and microbial pathogenesis. Frontiers in Cellular and Infection Microbiology. 2014;4(JAN).

46. Cassat JE, Skaar EP. Iron in Infection and Immunity. Cell Host & Microbe. 15 mai 2013;13(5):509-19.

47. Flo TH, Smith KD, Sato S, Rodriguez DJ, Holmes MA, Strong RK, et al. Lipocalin 2 mediates an innate immune response to bacterial infection by sequestrating iron. Nature. déc 2004;432(7019):917-21.

48. Raffatellu M, Santos RL, Verhoeven DE, George MD, Wilson RP, Winter SE, et al. Simian immunodeficiency virus–induced mucosal interleukin-17 deficiency promotes Salmonella dissemination from the gut. Nat Med. avr 2008;14(4):421-8.

49. Raffatellu M, George MD, Akiyama Y, Hornsby MJ, Nuccio SP, Paixao TA, et al. Lipocalin-2 Resistance Confers an Advantage to Salmonella enterica Serotype Typhimurium for Growth and Survival in the Inflamed Intestine. Cell Host & Microbe. 21 mai 2009;5(5):476-86.

50. Kuhn KA, Pedraza I, Demoruelle MK. Mucosal immune responses to microbiota in the development of autoimmune disease. Rheum Dis Clin North Am. nov 2014;40(4):711-25.

51. Coquant G. Impact de la 3-oxo-c12 : 2, MOLECULE DU QUORUM SENSING, SUR L'INFLAMMATION ET L'ECOSYSTEME INTESTINAL [Internet] [These en préparation]. Sorbonne université; 2018 [cité 2 mai 2022]. Disponible sur: http://www.theses.fr/s267052

52. Murphy K Weaver, Casey, Janeway C. Janeway's immunobiology. 2017.

53. Fan S, Liao Y, Lian Y, Jiang G, Jiang L, Dong C, et al. Role of innate lymphoid cells and dendritic cells in intradermal immunization of the enterovirus antigen. npj Vaccines. 27 mars 2019;4(1):1-11.

54. Zenewicz LA, Yancopoulos GD, Valenzuela DM, Murphy AJ, Stevens S, Flavell RA. Innate and adaptive interleukin-22 protects mice from inflammatory bowel disease. Immunity. 19 déc 2008;29(6):947-57.

55. Brown EM, Sadarangani M, Finlay BB. The role of the immune system in governing host-microbe interactions in the intestine. Nat Immunol. juill 2013;14(7):660-7.

56. Ahluwalia B, Magnusson MK, Öhman L. Mucosal immune system of the gastrointestinal tract: maintaining balance between the good and the bad. Scandinavian Journal of Gastroenterology. 2 nov 2017;52(11):1185-93.

57. Fiorucci S, Carino A, Baldoni M, Santucci L, Costanzi E, Graziosi L, et al. Bile Acid Signaling in Inflammatory Bowel Diseases. Digestive Diseases and Sciences. 1 mars 2021;66:1-20.

58. Katsuma S, Hirasawa A, Tsujimoto G. Bile acids promote glucagon-like peptide-1 secretion through TGR5 in a murine enteroendocrine cell line STC-1. Biochem Biophys Res Commun. 1 avr 2005;329(1):386-90.

59. Fiorucci S, Biagioli M, Zampella A, Distrutti E. Bile Acids Activated Receptors Regulate Innate Immunity. Front Immunol. 2018;9:1853.

60. Carino A, Biagioli M, Marchianò S, Fiorucci C, Zampella A, Monti MC, et al. Ursodeoxycholic acid is a GPBAR1 agonist and resets liver/intestinal FXR signaling in a model of diet-induced dysbiosis and NASH. Biochim Biophys Acta Mol Cell Biol Lipids. oct 2019;1864(10):1422-37.

61. Staudinger JL, Goodwin B, Jones SA, Hawkins-Brown D, MacKenzie KI, LaTour A, et al. The nuclear receptor PXR is a lithocholic acid sensor that protects against liver toxicity. Proceedings of the National Academy of Sciences of the United States of America. 13 mars 2001;98(6):3369-74.

62. Moore LB, Maglich JM, McKee DD, Wisely B, Willson TM, Kliewer SA, et al. Pregnane X receptor (PXR), constitutive androstane receptor (CAR), and benzoate X receptor (BXR) define three pharmacologically distinct classes of nuclear receptors. Mol Endocrinol. mai 2002;16(5):977-86.

63. Makishima M, Lu TT, Xie W, Whitfield GK, Domoto H, Evans RM, et al. Vitamin D receptor as an intestinal bile acid sensor. Science. 17 mai 2002;296(5571):1313-6.

64. Nagahashi M, Takabe K, Liu R, Peng K, Wang X, Wang Y, et al. Conjugated Bile Acid Activated S1P Receptor 2 Is a Key Regulator of Sphingosine Kinase 2 and Hepatic Gene Expression. Hepatology. avr 2015;61(4):1216-26.

65. Hang S, Paik D, Yao L, Kim E, Trinath J, Lu J, et al. Bile acid metabolites control TH17 and Treg cell differentiation. Nature. déc 2019;576(7785):143-8.

66. Tanaka H, Makino Y, Miura T, Hirano F, Okamoto K, Komura K, et al. Ligand-independent activation of the glucocorticoid receptor by ursodeoxycholic acid. Repression of IFN-gamma-induced MHC class II gene expression via a glucocorticoid receptor-dependent pathway. J Immunol. 15 févr 1996;156(4):1601-8.

67. Duboc H, Rajca S, Rainteau D, Benarous D, Maubert MA, Quervain E, et al. Connecting dysbiosis, bile-acid dysmetabolism and gut inflammation in inflammatory bowel diseases. Gut. avr 2013;62(4):531-9.

68. Sinha SR, Haileselassie Y, Nguyen LP, Tropini C, Wang M, Becker LS, et al. Dysbiosis-Induced Secondary Bile Acid Deficiency Promotes Intestinal Inflammation. Cell Host & Microbe. 8 avr 2020;27(4):659-670.e5.

69. Campbell C, McKenney PT, Konstantinovsky D, Isaeva OI, Schizas M, Verter J, et al. Bacterial metabolism of bile acids promotes generation of peripheral regulatory T cells. Nature. mai 2020;581(7809):475-9.

70. Song X, Sun X, Oh SF, Wu M, Zhang Y, Zheng W, et al. Microbial bile acid metabolites modulate gut RORγ+ regulatory T cell homeostasis. Nature. janv 2020;577(7790):410-5.

71. Sorrentino G, Perino A, Yildiz E, El Alam G, Bou Sleiman M, Gioiello A, et al. Bile Acids Signal via TGR5 to Activate Intestinal Stem Cells and Epithelial Regeneration. Gastroenterology. sept 2020;159(3):956-968.e8.

72. Xu M, Cen M, Shen Y, Zhu Y, Cheng F, Tang L, et al. Deoxycholic Acid-Induced Gut Dysbiosis Disrupts Bile Acid Enterohepatic Circulation and Promotes Intestinal Inflammation. Dig Dis Sci. 1 févr 2021;66(2):568-76.

73. Ward JBJ, Lajczak NK, Kelly OB, O'Dwyer AM, Giddam AK, Ní Gabhann J, et al. Ursodeoxycholic acid and lithocholic acid exert anti-inflammatory actions in the colon. Am J Physiol Gastrointest Liver Physiol. 1 juin 2017;312(6):G550-8.

74. Zhang H, Xu H, Zhang C, Tang Q, Bi F. Ursodeoxycholic acid suppresses the malignant progression of colorectal cancer through TGR5-YAP axis. Cell Death Discov. 7 août 2021;7(1):207.

75. Lloyd-Price J, Arze C, Ananthakrishnan AN, Schirmer M, Avila-Pacheco J, Poon TW, et al. Multi-omics of the gut microbial ecosystem in inflammatory bowel diseases. Nature. mai 2019;569(7758):655-62.

76. Thormann J, Steinberg H. Friedrich Theodor von Frerichs (1819–1885). J Neurol. 1 janv 2014;261(1):248-9.

77. Friedmann HC. Escherich and Escherichia. In: Advances in Applied Microbiology [Internet]. Academic Press; 2006 [cité 21 janv 2022]. p. 133-96. Disponible sur: https://www.sciencedirect.com/science/article/pii/S0065216406600051

78. Krienitz W. Ueber das Auftreten von Spirochäten verschiedener Form im Mageninhalt bei Carcinoma ventriculi. 1 mai 1906 [cité 6 oct 2021]; Disponible sur: https://zenodo.org/record/2035372

79. Buckley MJ, O'Morain CA. Helicobacter biology--discovery. Br Med Bull. 1998;54(1):7-16.

80. Marshall B, Warren JR. UNIDENTIFIED CURVED BACILLI IN THE STOMACH OF PATIENTS WITH GASTRITIS AND PEPTIC ULCERATION. The Lancet. 16 juin 1984;323(8390):1311-5.

81. Marshall BJ, Armstrong JA, McGechie DB, Glancy RJ. Attempt to fulfil Koch's postulates for pyloric Campylobacter. Med J Aust. 15 avr 1985;142(8):436-9.

82. Woese CR. Bacterial evolution. Microbiol Rev. juin 1987;51(2):221-71.

83. Lloyd-Price J, Mahurkar A, Rahnavard G, Crabtree J, Orvis J, Hall AB, et al. Strains, functions and dynamics in the expanded Human Microbiome Project. Nature. oct 2017;550(7674):61-6.

84. O'Hara AM, Shanahan F. The gut flora as a forgotten organ. EMBO Rep. juill 2006;7(7):688-93.

85. Patterson E, Ryan PM, Cryan JF, Dinan TG, Ross RP, Fitzgerald GF, et al. Gut microbiota, obesity and diabetes. Postgrad Med J. mai 2016;92(1087):286-300.

86. Tomasello G, Mazzola M, Leone A, Sinagra E, Zummo G, Farina F, et al. Nutrition, oxidative stress and intestinal dysbiosis: Influence of diet on gut microbiota in inflammatory bowel diseases. Biomed Pap Med Fac Univ Palacky Olomouc Czech Repub. déc 2016;160(4):461-6.

87. Sears CL, Garrett WS. Microbes, Microbiota, and Colon Cancer. Cell Host & Microbe. 12 mars 2014;15(3):317-28.

88. Gurung M, Li Z, You H, Rodrigues R, Jump DB, Morgun A, et al. Role of gut microbiota in type 2 diabetes pathophysiology. EBioMedicine. janv 2020;51:102590.

89. Shkoporov AN, Hill C. Bacteriophages of the Human Gut: The « Known Unknown » of the Microbiome. Cell Host Microbe. 13 févr 2019;25(2):195-209.

90. Kim JY, Whon TW, Lim MY, Kim YB, Kim N, Kwon MS, et al. The human gut archaeome: identification of diverse haloarchaea in Korean subjects. Microbiome. 4 août 2020;8(1):114.

91. Mueller NT, Bakacs E, Combellick J, Grigoryan Z, Dominguez-Bello MG. The infant microbiome development: mom matters. Trends Mol Med. févr 2015;21(2):109-17.

92. Jost T, Lacroix C, Braegger CP, Rochat F, Chassard C. Vertical mother-neonate transfer of maternal gut bacteria via breastfeeding. Environ Microbiol. sept 2014;16(9):2891-904.

93. Dominguez-Bello MG, Costello EK, Contreras M, Magris M, Hidalgo G, Fierer N, et al. Delivery mode shapes the acquisition and structure of the initial microbiota across multiple body habitats in newborns. PNAS. 29 juin 2010;107(26):11971-5.

94. Tanaka S, Kobayashi T, Songjinda P, Tateyama A, Tsubouchi M, Kiyohara C, et al. Influence of antibiotic exposure in the early postnatal period on the development of intestinal microbiota. FEMS immunology and medical microbiology. 2009;

95. Jauréguy F, Carton M, Panel P, Foucaud P, Butel MJ, Doucet-Populaire F. Effects of intrapartum penicillin prophylaxis on intestinal bacterial colonization in infants. J Clin Microbiol. nov 2004;42(11):5184-8.

96. Knol J, Scholtens P, Kafka C, Steenbakkers J, Gro S, Helm K, et al. Colon microflora in infants fed formula with galacto- and fructo-oligosaccharides: more like breast-fed infants. J Pediatr Gastroenterol Nutr. janv 2005;40(1):36-42.

97. Milani C, Duranti S, Bottacini F, Casey E, Turroni F, Mahony J, et al. The First Microbial Colonizers of the Human Gut: Composition, Activities, and Health Implications of the Infant Gut Microbiota. Microbiol Mol Biol Rev. déc 2017;81(4):e00036-17.

98. Yatsunenko T, Rey FE, Manary MJ, Trehan I, Dominguez-Bello MG, Contreras M, et al. Human gut microbiome viewed across age and geography. Nature. juin 2012;486(7402):222-7.

99. Koenig JE, Spor A, Scalfone N, Fricker AD, Stombaugh J, Knight R, et al. Succession of microbial consortia in the developing infant gut microbiome. Proc Natl Acad Sci U S A. 15 mars 2011;108 Suppl 1:4578-85.

100. King CH, Desai H, Sylvetsky AC, LoTempio J, Ayanyan S, Carrie J, et al. Baseline human gut microbiota profile in healthy people and standard reporting template. PLOS ONE. 11 sept 2019;14(9):e0206484.

101. Mirzaei MK, Maurice CF. Ménage à trois in the human gut: interactions between host, bacteria and phages. Nat Rev Microbiol. juill 2017;15(7):397-408.

102. Rinninella E, Raoul P, Cintoni M, Franceschi F, Miggiano GAD, Gasbarrini A, et al. What is the Healthy Gut Microbiota Composition? A Changing Ecosystem across Age, Environment, Diet, and Diseases. Microorganisms. 10 janv 2019;7(1):E14.

103. Zmora N, Suez J, Elinav E. You are what you eat: diet, health and the gut microbiota. Nat Rev Gastroenterol Hepatol. janv 2019;16(1):35-56.

104. Xie H, Guo R, Zhong H, Feng Q, Lan Z, Qin B, et al. Shotgun Metagenomics of 250 Adult Twins Reveals Genetic and Environmental Impacts on the Gut Microbiome. Cell Syst. 21 déc 2016;3(6):572-584.e3.

105. Donaldson GP, Lee SM, Mazmanian SK. Gut biogeography of the bacterial microbiota. Nat Rev Microbiol. janv 2016;14(1):20-32.

106. Johansson MEV, Larsson JMH, Hansson GC. The two mucus layers of colon are organized by the MUC2 mucin, whereas the outer layer is a legislator of host-microbial interactions. Proc Natl Acad Sci U S A. 15 mars 2011;108 Suppl 1:4659-65.

107. Rowland I, Gibson G, Heinken A, Scott K, Swann J, Thiele I, et al. Gut microbiota functions: metabolism of nutrients and other food components. Eur J Nutr. févr 2018;57(1):1-24.

108. Duncan SH, Holtrop G, Lobley GE, Calder AG, Stewart CS, Flint HJ. Contribution of acetate to butyrate formation by human faecal bacteria. Br J Nutr. juin 2004;91(6):915-23.

109. Gantois I, Ducatelle R, Pasmans F, Haesebrouck F, Hautefort I, Thompson A, et al. Butyrate specifically down-regulates salmonella pathogenicity island 1 gene expression. Appl Environ Microbiol. janv 2006;72(1):946-9.

110. Fukuda S, Toh H, Hase K, Oshima K, Nakanishi Y, Yoshimura K, et al. Bifidobacteria can protect from enteropathogenic infection through production of acetate. Nature. janv 2011;469(7331):543-7.

111. De Vadder F, Kovatcheva-Datchary P, Goncalves D, Vinera J, Zitoun C, Duchampt A, et al. Microbiota-generated metabolites promote metabolic benefits via gut-brain neural circuits. Cell. 16 janv 2014;156(1-2):84-96.

112. Frost G, Sleeth ML, Sahuri-Arisoylu M, Lizarbe B, Cerdan S, Brody L, et al. The short-chain fatty acid acetate reduces appetite via a central homeostatic mechanism. Nat Commun. 29 avr 2014;5(1):3611.

113. Lavelle A, Sokol H. Gut microbiota-derived metabolites as key actors in inflammatory bowel disease. Nat Rev Gastroenterol Hepatol. avr 2020;17(4):223-37.

114. Gustafsson BE, Daft FS, Mcdaniel EG, Smith JC, Fitzgerald RJ. Effects of vitamin K-active compounds and intestinal microorganisms in vitamin K-deficient germfree rats. J Nutr. déc 1962;78(4):461-8.

115. Frick PG, Riedler G, Brögli H. Dose response and minimal daily requirement for vitamin K in man. Journal of Applied Physiology. 1 sept 1967;23(3):387-9.

116. Magnúsdóttir S, Ravcheev D, de Crécy-Lagard V, Thiele I. Systematic genome assessment of B-vitamin biosynthesis suggests co-operation among gut microbes. Frontiers in Genetics [Internet]. 2015 [cité 21 janv 2022];6. Disponible sur: https://www.frontiersin.org/article/10.3389/fgene.2015.00148

117. Cario E, Gerken G, Podolsky DK. Toll-like receptor 2 controls mucosal inflammation by regulating epithelial barrier function. Gastroenterology. avr 2007;132(4):1359-74.

118. Hooper LV, Wong MH, Thelin A, Hansson L, Falk PG, Gordon JI. Molecular analysis of commensal host-microbial relationships in the intestine. Science. 2 févr 2001;291(5505):881-4.

119. Stappenbeck TS, Hooper LV, Gordon JI. Developmental regulation of intestinal angiogenesis by indigenous microbes via Paneth cells. Proc Natl Acad Sci U S A. 26 nov 2002;99(24):15451-5.

120. Ahmad S, Wang B, Walker MD, Tran HKR, Stogios PJ, Savchenko A, et al. An interbacterial toxin inhibits target cell growth by synthesizing (p)ppApp. Nature. nov 2019;575(7784):674-8.

121. Russell AB, Wexler AG, Harding BN, Whitney JC, Bohn AJ, Goo YA, et al. A Type VI Secretion-Related Pathway in Bacteroidetes Mediates Interbacterial Antagonism. Cell Host & Microbe. août 2014;16(2):227-36.

122. Wang T, Si M, Song Y, Zhu W, Gao F, Wang Y, et al. Type VI Secretion System Transports Zn2+ to Combat Multiple Stresses and Host Immunity. PLoS Pathog. juill 2015;11(7):e1005020.

123. Coyne MJ, Comstock LE. Type VI Secretion Systems and the Gut Microbiota. Microbiol Spectr. mars 2019;7(2).

124. Wood TE, Aksoy E, Hachani A. From Welfare to Warfare: The Arbitration of Host-Microbiota Interplay by the Type VI Secretion System. Frontiers in Cellular and Infection Microbiology [Internet]. 2020 [cité 14 avr 2022];10. Disponible sur: https://www.frontiersin.org/article/10.3389/fcimb.2020.587948

125. Brugiroux S, Beutler M, Pfann C, Garzetti D, Ruscheweyh HJ, Ring D, et al. Genome-guided design of a defined mouse microbiota that confers colonization resistance against Salmonella enterica serovar Typhimurium. Nat Microbiol. févr 2017;2(2):16215.

126. Keeney KM, Yurist-Doutsch S, Arrieta MC, Finlay BB. Effects of antibiotics on human microbiota and subsequent disease. Annu Rev Microbiol. 2014;68:217-35.

127. Al Nabhani Z, Dulauroy S, Marques R, Cousu C, Al Bounny S, Déjardin F, et al. A Weaning Reaction to Microbiota Is Required for Resistance to Immunopathologies in the Adult. Immunity. 21 mai 2019;50(5):1276-1288.e5.

128. Yang W, Yu T, Huang X, Bilotta AJ, Xu L, Lu Y, et al. Intestinal microbiota-derived short-chain fatty acids regulation of immune cell IL-22 production and gut immunity. Nat Commun. 8 sept 2020;11(1):4457.

129. Isobe J, Maeda S, Obata Y, Iizuka K, Nakamura Y, Fujimura Y, et al. Commensal-bacteria-derived butyrate promotes the T-cell-independent IgA response in the colon. Int Immunol. 12 avr 2020;32(4):243-58.

130. Spencer SP, Fragiadakis GK, Sonnenburg JL. Pursuing Human-Relevant Gut Microbiota-Immune Interactions. Immunity. 20 août 2019;51(2):225-39.

131. Tan HE, Sisti AC, Jin H, Vignovich M, Villavicencio M, Tsang KS, et al. The gut–brain axis mediates sugar preference. Nature. avr 2020;580(7804):511-6.

132. Strandwitz P. Neurotransmitter modulation by the gut microbiota. Brain Res. 15 août 2018;1693(Pt B):128-33.

133. Silva YP, Bernardi A, Frozza RL. The Role of Short-Chain Fatty Acids From Gut Microbiota in Gut-Brain Communication. Frontiers in Endocrinology [Internet]. 2020 [cité 21 janv 2022];11. Disponible sur: https://www.frontiersin.org/article/10.3389/fendo.2020.00025

134. Doifode T, Giridharan VV, Generoso JS, Bhatti G, Collodel A, Schulz PE, et al. The impact of the microbiota-gut-brain axis on Alzheimer's disease pathophysiology. Pharmacol Res. févr 2021;164:105314.

135. Caputi V, Giron MC. Microbiome-Gut-Brain Axis and Toll-Like Receptors in Parkinson's Disease. Int J Mol Sci. 6 juin 2018;19(6):E1689.

136. Kanji S, Fonseka TM, Marshe VS, Sriretnakumar V, Hahn MK, Müller DJ. The microbiome-gut-brain axis: implications for schizophrenia and antipsychotic induced weight gain. Eur Arch Psychiatry Clin Neurosci. févr 2018;268(1):3-15.

137. Zimmermann M, Zimmermann-Kogadeeva M, Wegmann R, Goodman AL. Mapping human microbiome drug metabolism by gut bacteria and their genes. Nature. juin 2019;570(7762):462-7.

138. Wallace BD, Wang H, Lane KT, Scott JE, Orans J, Koo JS, et al. Alleviating cancer drug toxicity by inhibiting a bacterial enzyme. Science. 5 nov 2010;330(6005):831-5.

139. Des produits Kinder rappelés par Ferrero pour suspicion de présence de salmonelles. Le Monde.fr [Internet]. 5 avr 2022 [cité 26 avr 2022]; Disponible sur: https://www.lemonde.fr/economie/article/2022/04/05/ferrero-rappelle-des-produits-kinder-pour-suspicion-de-presence-de-salmonelles_6120635_3234.html

140. Bactérie « E. coli » : rappel massif de pizzas surgelées Buitoni, un « lien possible » avec des cas graves de contamination. Le Monde.fr [Internet]. 18 mars 2022 [cité 2 mai 2022]; Disponible sur: https://www.lemonde.fr/societe/article/2022/03/18/bacterie-e-coli-rappel-massif-de-pizzas-surgelees-buitoni-lien-possible-avec-des-cas-graves_6118186_3224.html

141. Diarrhoeal disease [Internet]. [cité 16 avr 2022]. Disponible sur: https://www.who.int/news-room/fact-sheets/detail/diarrhoeal-disease

142. Leimbach A, Hacker J, Dobrindt U. E. coli as an all-rounder: the thin line between commensalism and pathogenicity. Curr Top Microbiol Immunol. 2013;358:3-32.

143. Tenaillon O, Skurnik D, Picard B, Denamur E. The population genetics of commensal Escherichia coli. Nat Rev Microbiol. mars 2010;8(3):207-17.

144. Kaper JB, Nataro JP, Mobley HLT. Pathogenic Escherichia coli. Nat Rev Microbiol. févr 2004;2(2):123-40.

145. Khalil RKS, Skinner C, Patfield S, He X. Phage-mediated Shiga toxin (Stx) horizontal gene transfer and expression in non-Shiga toxigenic Enterobacter and Escherichia coli strains. Pathogens and Disease. 1 juill 2016;74(5):ftw037.

146. Darfeuille-Michaud A. Adherent-invasive Escherichia coli: a putative new E. coli pathotype associated with Crohn's disease. Int J Med Microbiol. sept 2002;292(3-4):185-93.

147. Itoh K, Matsui T, Tsuji K, Mitsuoka T, Ueda K. Genetic control in the susceptibility of germfree inbred mice to infection by Escherichia coli O115a,c:K(B). Infect Immun. 1 avr 1988;56(4):930-5.

148. Mullineaux-Sanders C, Sanchez-Garrido J, Hopkins EGD, Shenoy AR, Barry R, Frankel G. Citrobacter rodentium–host–microbiota interactions: immunity, bioenergetics and metabolism. Nat Rev Microbiol. nov 2019;17(11):701-15.

149. Papapietro O, Teatero S, Thanabalasuriar A, Yuki KE, Diez E, Zhu L, et al. R-spondin 2 signalling mediates susceptibility to fatal infectious diarrhoea. Nat Commun. 2013;4:1898.

150. Wiles S, Clare S, Harker J, Huett A, Young D, Dougan G, et al. Organ specificity, colonization and clearance dynamics in vivo following oral challenges with the murine pathogen Citrobacter rodentium. Cell Microbiol. oct 2004;6(10):963-72.

151. Garmendia J, Frankel G, Crepin VF. Enteropathogenic and Enterohemorrhagic Escherichia coli Infections: Translocation, Translocation, Translocation. Infect Immun. mai 2005;73(5):2573-85.

152. Yang J, Tauschek M, Hart E, Hartland EL, Robins-Browne RM. Virulence regulation in Citrobacter rodentium: the art of timing. Microb Biotechnol. mai 2010;3(3):259-68.

153. Alsharif G, Ahmad S, Islam MS, Shah R, Busby SJ, Krachler AM. Host attachment and fluid shear are integrated into a mechanical signal regulating virulence in Escherichia coli O157:H7. Proceedings of the National Academy of Sciences. 28 avr 2015;112(17):5503-8.

154. Nakanishi N, Tashiro K, Kuhara S, Hayashi T, Sugimoto N, Tobe T. Regulation of virulence by butyrate sensing in enterohaemorrhagic Escherichia coli. Microbiology (Reading). févr 2009;155(Pt 2):521-30.

155. Umanski T, Rosenshine I, Friedberg D. Thermoregulated expression of virulence genes in enteropathogenic Escherichia coli. Microbiology (Reading). sept 2002;148(Pt 9):2735-44.

156. Hart E, Yang J, Tauschek M, Kelly M, Wakefield MJ, Frankel G, et al. RegA, an AraC-Like Protein, Is a Global Transcriptional Regulator That Controls Virulence Gene Expression in Citrobacter rodentium. Infection and Immunity. nov 2008;76(11):5247-56.

157. Moreira CG, Russell R, Mishra AA, Narayanan S, Ritchie JM, Waldor MK, et al. Bacterial Adrenergic Sensors Regulate Virulence of Enteric Pathogens in the Gut. mBio. 7 juin 2016;7(3):e00826-16.

158. Pifer R, Russell RM, Kumar A, Curtis MM, Sperandio V. Redox, amino acid, and fatty acid metabolism intersect with bacterial virulence in the gut. Proceedings of the National Academy of Sciences of the United States of America. 6 nov 2018;115(45):E10712-9.

159. Yang B, Feng L, Wang F, Wang L. Enterohemorrhagic Escherichia coli senses low biotin status in the large intestine for colonization and infection. Nat Commun. 20 mars 2015;6(1):6592.

160. Cepeda-Molero M, Berger CN, Walsham ADS, Ellis SJ, Wemyss-Holden S, Schüller S, et al. Attaching and effacing (A/E) lesion formation by enteropathogenic E. coli on human intestinal mucosa is dependent on non-LEE effectors. PLOS Pathogens. 30 oct 2017;13(10):e1006706.

161. Simmons CP, Clare S, Ghaem-Maghami M, Uren TK, Rankin J, Huett A, et al. Central role for B lymphocytes and CD4+ T cells in immunity to infection by the attaching and effacing pathogen Citrobacter rodentium. Infect Immun. sept 2003;71(9):5077-86.

162. Kamada N, Kim YG, Sham HP, Vallance BA, Puente JL, Martens EC, et al. Regulated virulence controls the ability of a pathogen to compete with the gut microbiota. Science. 8 juin 2012;336(6086):1325-9.

163. Ver Heul A, Planer J, Kau AL. The Human Microbiota and Asthma. Clin Rev Allergy Immunol. déc 2019;57(3):350-63.

164. Hughes HK, Rose D, Ashwood P. The Gut Microbiota and Dysbiosis in Autism Spectrum Disorders. Curr Neurol Neurosci Rep. 24 sept 2018;18(11):81.

165. Angelucci F, Cechova K, Amlerova J, Hort J. Antibiotics, gut microbiota, and Alzheimer's disease. Journal of Neuroinflammation. 22 mai 2019;16(1):108.

166. Glassner KL, Abraham BP, Quigley EMM. The microbiome and inflammatory bowel disease. Journal of Allergy and Clinical Immunology. 1 janv 2020;145(1):16-27.

167. Maloy KJ, Powrie F. Intestinal homeostasis and its breakdown in inflammatory bowel disease. Nature. 15 juin 2011;474(7351):298-306.

168. Palmela C, Chevarin C, Xu Z, Torres J, Sevrin G, Hirten R, et al. Adherent-invasive Escherichia coli in inflammatory bowel disease. Gut. mars 2018;67(3):574-87.

169. Manichanh C, Borruel N, Casellas F, Guarner F. The gut microbiota in IBD. Nat Rev Gastroenterol Hepatol. oct 2012;9(10):599-608.

170. Frank DN, St. Amand AL, Feldman RA, Boedeker EC, Harpaz N, Pace NR. Molecular-phylogenetic characterization of microbial community imbalances in human inflammatory bowel diseases. Proc Natl Acad Sci U S A. 21 août 2007;104(34):13780-5.

171. Walker AW, Sanderson JD, Churcher C, Parkes GC, Hudspith BN, Rayment N, et al. High-throughput clone library analysis of the mucosa-associated microbiota reveals dysbiosis and differences between inflamed and non-inflamed regions of the intestine in inflammatory bowel disease. BMC Microbiol. 10 janv 2011;11:7.

172. Quévrain E, Maubert MA, Michon C, Chain F, Marquant R, Tailhades J, et al. Identification of an anti-inflammatory protein from Faecalibacterium prausnitzii, a commensal bacterium deficient in Crohn's disease. Gut. mars 2016;65(3):415-25.

173. Nishida A, Inoue R, Inatomi O, Bamba S, Naito Y, Andoh A. Gut microbiota in the pathogenesis of inflammatory bowel disease. Clin J Gastroenterol. févr 2018;11(1):1-10.

174. Michielan A, D'Incà R. Intestinal Permeability in Inflammatory Bowel Disease: Pathogenesis, Clinical Evaluation, and Therapy of Leaky Gut. Mediators Inflamm. 2015;2015:628157.

175. Caro I, Boulenc X, Rousset M, Meunier V, Bourrié M, Julian B, et al. Characterisation of a newly isolated Caco-2 clone (TC-7), as a model of transport processes and biotransformation of drugs. International Journal of Pharmaceutics. 28 mars 1995;116(2):147-58.

176. Gómez DP, Boudreau F. Organoids and Their Use in Modeling Gut Epithelial Cell Lineage Differentiation and Barrier Properties During Intestinal Diseases. Frontiers in Cell and Developmental Biology [Internet]. 2021 [cité 26 avr 2022];9. Disponible sur: https://www.frontiersin.org/article/10.3389/fcell.2021.732137

177. Jung Kim H, Huh D, Hamilton G, E. Ingber D. Human gut-on-a-chip inhabited by microbial flora that experiences intestinal peristalsis-like motions and flow. Lab on a Chip. 2012;12(12):2165-74.

178. Van de Wiele T, Van den Abbeele P, Ossieur W, Possemiers S, Marzorati M. The Simulator of the Human Intestinal Microbial Ecosystem (SHIME®). In: Verhoeckx K, Cotter P, López-Expósito I, Kleiveland C, Lea T, Mackie A, et al., éditeurs. The Impact of Food Bioactives on Health: in vitro and ex vivo models [Internet]. Cham (CH): Springer; 2015 [cité 15 avr 2022]. Disponible sur: http://www.ncbi.nlm.nih.gov/books/NBK500150/

179. Treuting PM, Dintzis SM. 12 - Lower Gastrointestinal Tract. In: Treuting PM, Dintzis SM, éditeurs. Comparative Anatomy and Histology [Internet]. San Diego: Academic Press; 2012 [cité 15 avr 2022]. p. 177-92. Disponible sur: https://www.sciencedirect.com/science/article/pii/B9780123813619000123

180. Rasmussen TS, de Vries L, Kot W, Hansen LH, Castro-Mejía JL, Vogensen FK, et al. Mouse Vendor Influence on the Bacterial and Viral Gut Composition Exceeds the Effect of Diet. Viruses. 13 mai 2019;11(5):E435.

181. Nguyen TLA, Vieira-Silva S, Liston A, Raes J. How informative is the mouse for human gut microbiota research? Dis Model Mech. janv 2015;8(1):1-16.

182. Franklin CL, Ericsson AC. Microbiota and reproducibility of rodent models. Lab Anim (NY). 22 mars 2017;46(4):114-22.

183. Schaedler RW, Dubs R, Costello R. ASSOCIATION OF GERMFREE MICE WITH BACTERIA ISOLATED FROM NORMAL MICE. J Exp Med. 1 juill 1965;122:77-82.

184. Macpherson AJ, McCoy KD. Standardised animal models of host microbial mutualism. Mucosal Immunol. mai 2015;8(3):476-86.

185. d'Herelle F. On an invisible microbe antagonistic to dysentery bacilli. CR Acad Sci. 1917;165:373-5.

186. Twort FW. An Investigation on the Nature of Ultra-Microscopic Viruses. 1 déc 1915 [cité 2 févr 2022]; Disponible sur: https://zenodo.org/record/2380119

187. Abedon ST, Thomas-Abedon C, Thomas A, Mazure H. Bacteriophage prehistory: Is or is not Hankin, 1896, a phage reference? Bacteriophage. mai 2011;1(3):174-8.

188. D'Herelle F. On an invisible microbe antagonistic toward dysenteric bacilli: brief note by Mr. F. D'Herelle, presented by Mr. Roux. 1917. Res Microbiol. sept 2007;158(7):553-4.

189. Summers WC. The strange history of phage therapy. Bacteriophage. 1 avr 2012;2(2):130-3.

190. Ackermann HW. Ruska H. Visualization of bacteriophage lysis in the hypermicroscope. Naturwissenschaften1940; 28:45–6. Bacteriophage. 1 juill 2011;1(4):183-5.

191. Cisek AA, Dąbrowska I, Gregorczyk KP, Wyżewski Z. Phage Therapy in Bacterial Infections Treatment: One Hundred Years After the Discovery of Bacteriophages. Curr Microbiol. févr 2017;74(2):277-83.

192. Kutateladze M. Experience of the Eliava Institute in bacteriophage therapy. Virol Sin. févr 2015;30(1):80-1.

193. Hershey AD, Chase M. INDEPENDENT FUNCTIONS OF VIRAL PROTEIN AND NUCLEIC ACID IN GROWTH OF BACTERIOPHAGE. J Gen Physiol. 20 sept 1952;36(1):39-56.

194. Jinek M, Chylinski K, Fonfara I, Hauer M, Doudna JA, Charpentier E. A Programmable Dual-RNA–Guided DNA Endonuclease in Adaptive Bacterial Immunity. Science [Internet]. 17 août 2012 [cité 2 févr 2022]; Disponible sur: https://www.science.org/doi/abs/10.1126/science.1225829

195. O'Neill J. Tackling drug-resistant infections globally: final report and recommendations [Internet]. Government of the United Kingdom; 2016 mai [cité 2 févr 2022]. Disponible sur: https://apo.org.au/node/63983

196. Zinsstag J, Schelling E, Waltner-Toews D, Tanner M. From « one medicine » to « one health » and systemic approaches to health and well-being. Prev Vet Med. 1 sept 2011;101(3-4):148-56.

197. Weinbauer MG. Ecology of prokaryotic viruses. FEMS Microbiology Reviews. 1 mai 2004;28(2):127-81.

198. Suttle CA. Viruses in the sea. Nature. 15 sept 2005;437(7057):356-61.

199. Breitbart M, Bonnain C, Malki K, Sawaya NA. Phage puppet masters of the marine microbial realm. Nat Microbiol. juill 2018;3(7):754-66.

200. Ackermann HW. Phage classification and characterization. Methods Mol Biol. 2009;501:127-40.

201. Gontier M. Les bactériophages, de leur découverte à leurs utilisations [Internet]. 2021. Disponible sur: https://planet-vie.ens.fr/thematiques/microbiologie/virologie/les-bacteriophages-de-leur-decouverte-a-leurs-utilisations

202. Bolduc B, Jang HB, Doulcier G, You ZQ, Roux S, Sullivan MB. vConTACT: an iVirus tool to classify double-stranded DNA viruses that infect Archaea and Bacteria. PeerJ. 3 mai 2017;5:e3243.

203. Bin Jang H, Bolduc B, Zablocki O, Kuhn JH, Roux S, Adriaenssens EM, et al. Taxonomic assignment of uncultivated prokaryotic virus genomes is enabled by gene-sharing networks. Nat Biotechnol. juin 2019;37(6):632-9.

204. Low SJ, Džunková M, Chaumeil PA, Parks DH, Hugenholtz P. Evaluation of a concatenated protein phylogeny for classification of tailed double-stranded DNA viruses belonging to the order Caudovirales. Nat Microbiol. août 2019;4(8):1306-15.

205. Walker PJ, Siddell SG, Lefkowitz EJ, Mushegian AR, Adriaenssens EM, Alfenas-Zerbini P, et al. Changes to virus taxonomy and to the International Code of Virus Classification and

Nomenclature ratified by the International Committee on Taxonomy of Viruses (2021). Arch Virol. 1 sept 2021;166(9):2633-48.

206. Calendar R. The bacteriophages. New York: Oxford University Press; 2006.

207. Stone E, Campbell K, Grant I, McAuliffe O. Understanding and Exploiting Phage–Host Interactions. Viruses. 18 juin 2019;11(6):567.

208. Schiettekatte O, Vincent AT, Malosse C, Lechat P, Chamot-Rooke J, Veyrier FJ, et al. Characterization of LE3 and LE4, the only lytic phages known to infect the spirochete Leptospira. Sci Rep. 6 août 2018;8(1):11781.

209. Oppenheim AB, Kobiler O, Stavans J, Court DL, Adhya S. Switches in bacteriophage lambda development. Annu Rev Genet. 2005;39:409-29.

210. Zeng L, Skinner SO, Zong C, Sippy J, Feiss M, Golding I. Decision making at a subcellular level determines the outcome of bacteriophage infection. Cell. 14 mai 2010;141(4):682-91.

211. Erez Z, Steinberger-Levy I, Shamir M, Doron S, Stokar-Avihail A, Peleg Y, et al. Communication between viruses guides lysis-lysogeny decisions. Nature. 26 janv 2017;541(7638):488-93.

212. Susskind MM, Wright A, Botstein D. Superinfection exclusion by P22 prophage in lysogens of Salmonella typhimurium: IV. Genetics and physiology of sieB exclusion. Virology. 1 déc 1974;62(2):367-84.

213. Bobay LM, Touchon M, Rocha EPC. Manipulating or Superseding Host Recombination Functions: A Dilemma That Shapes Phage Evolvability. PLOS Genetics. 26 sept 2013;9(9):e1003825.

214. Cenens W, Makumi A, Mebrhatu MT, Lavigne R, Aertsen A. Phage-host interactions during pseudolysogeny: Lessons from the Pid/dgo interaction. Bacteriophage. 1 janv 2013;3(1):e25029.

215. Hobbs Z, Abedon ST. Diversity of phage infection types and associated terminology: the problem with « Lytic or lysogenic ». FEMS Microbiol Lett. avr 2016;363(7):fnw047.

216. Kulikov EE, Golomidova AK, Prokhorov NS, Ivanov PA, Letarov AV. High-throughput LPS profiling as a tool for revealing of bacteriophage infection strategies. Sci Rep. 27 févr 2019;9(1):2958.

217. Riede I, Eschbach ML. Evidence that TraT interacts with OmpA of Escherichia coli. FEBS Lett. 15 sept 1986;205(2):241-5.

218. Manning AJ, Kuehn MJ. Contribution of bacterial outer membrane vesicles to innate bacterial defense. BMC Microbiol. 1 déc 2011;11:258.

219. Mangalea MR, Duerkop BA. Fitness Trade-Offs Resulting from Bacteriophage Resistance Potentiate Synergistic Antibacterial Strategies. Infect Immun. 22 juin 2020;88(7):e00926-19.

220. Bernheim A, Sorek R. The pan-immune system of bacteria: antiviral defence as a community resource. Nat Rev Microbiol. févr 2020;18(2):113-9.

221. Wang L, Chen S, Xu T, Taghizadeh K, Wishnok JS, Zhou X, et al. Phosphorothioation of DNA in bacteria by dnd genes. Nat Chem Biol. nov 2007;3(11):709-10.

222. Oliveira PH, Touchon M, Rocha EPC. The interplay of restriction-modification systems with mobile genetic elements and their prokaryotic hosts. Nucleic Acids Res. 2014;42(16):10618-31.

223. Hille F, Richter H, Wong SP, Bratovič M, Ressel S, Charpentier E. The Biology of CRISPR-Cas: Backward and Forward. Cell. 8 mars 2018;172(6):1239-59.

224. Makarova KS, Wolf YI, Alkhnbashi OS, Costa F, Shah SA, Saunders SJ, et al. An updated evolutionary classification of CRISPR-Cas systems. Nat Rev Microbiol. nov 2015;13(11):722-36.

225. Koonin EV, Makarova KS, Wolf YI. Evolutionary Genomics of Defense Systems in Archaea and Bacteria. Annu Rev Microbiol. 8 sept 2017;71:233-61.

226. Makarova KS, Wolf YI, Koonin EV. Comparative genomics of defense systems in archaea and bacteria. Nucleic Acids Res. avr 2013;41(8):4360-77.

227. Kaufmann G. Anticodon nucleases. Trends Biochem Sci. févr 2000;25(2):70-4.

228. Cohen D, Melamed S, Millman A, Shulman G, Oppenheimer-Shaanan Y, Kacen A, et al. Cyclic GMP–AMP signalling protects bacteria against viral infection. Nature. oct 2019;574(7780):691-5.

229. Kronheim S, Daniel-Ivad M, Duan Z, Hwang S, Wong AI, Mantel I, et al. A chemical defence against phage infection. Nature. déc 2018;564(7735):283-6.

230. Fillol-Salom A, Martínez-Rubio R, Abdulrahman RF, Chen J, Davies R, Penadés JR. Phage-inducible chromosomal islands are ubiquitous within the bacterial universe. ISME J. sept 2018;12(9):2114-28.

231. Martínez-Rubio R, Quiles-Puchalt N, Martí M, Humphrey S, Ram G, Smyth D, et al. Phage-inducible islands in the Gram-positive cocci. ISME J. avr 2017;11(4):1029-42.

232. Doron S, Melamed S, Ofir G, Leavitt A, Lopatina A, Keren M, et al. Systematic discovery of antiphage defense systems in the microbial pangenome. Science. 2 mars 2018;359(6379):eaar4120.

233. Chapman-McQuiston E, Wu XL. Stochastic receptor expression allows sensitive bacteria to evade phage attack. Part II: theoretical analyses. Biophys J. juin 2008;94(11):4537-48.

234. Bull JJ, Vegge CS, Schmerer M, Chaudhry WN, Levin BR. Phenotypic Resistance and the Dynamics of Bacterial Escape from Phage Control. PLOS ONE. 17 avr 2014;9(4):e94690.

235. Porter NT, Hryckowian AJ, Merrill BD, Fuentes JJ, Gardner JO, Glowacki RWP, et al. Phase-variable capsular polysaccharides and lipoproteins modify bacteriophage susceptibility in Bacteroides thetaiotaomicron. Nat Microbiol. sept 2020;5(9):1170-81.

236. Cayrou C, Barratt NA, Ketley JM, Bayliss CD. Phase Variation During Host Colonization and Invasion by Campylobacter jejuni and Other Campylobacter Species. Front Microbiol. 2021;12:705139.

237. Shkoporov AN, Khokhlova EV, Stephens N, Hueston C, Seymour S, Hryckowian AJ, et al. Long-term persistence of crAss-like phage crAss001 is associated with phase variation in Bacteroides intestinalis. BMC Biology. 18 août 2021;19(1):163.

238. Meyer JR, Dobias DT, Weitz JS, Barrick JE, Quick RT, Lenski RE. Repeatability and contingency in the evolution of a key innovation in phage lambda. Science. 27 janv 2012;335(6067):428-32.

239. Bair CL, Black LW. A type IV modification dependent restriction nuclease that targets glucosylated hydroxymethyl cytosine modified DNAs. J Mol Biol. 23 févr 2007;366(3):768-78.

240. Walkinshaw MD, Taylor P, Sturrock SS, Atanasiu C, Berge T, Henderson RM, et al. Structure of Ocr from bacteriophage T7, a protein that mimics B-form DNA. Mol Cell. janv 2002;9(1):187-94.

241. Mendoza SD, Nieweglowska ES, Govindarajan S, Leon LM, Berry JD, Tiwari A, et al. A bacteriophage nucleus-like compartment shields DNA from CRISPR nucleases. Nature. janv 2020;577(7789):244-8.

242. Bondy-Denomy J, Garcia B, Strum S, Du M, Rollins MF, Hidalgo-Reyes Y, et al. Multiple mechanisms for CRISPR–Cas inhibition by anti-CRISPR proteins. Nature. oct 2015;526(7571):136-9.

243. Sanjuán R, Domingo-Calap P. Mechanisms of viral mutation. Cell Mol Life Sci. déc 2016;73(23):4433-48.

244. Hendrix RW, Smith MC, Burns RN, Ford ME, Hatfull GF. Evolutionary relationships among diverse bacteriophages and prophages: all the world's a phage. Proc Natl Acad Sci U S A. 2 mars 1999;96(5):2192-7.

245. Maslov S, Sneppen K. Population cycles and species diversity in dynamic Kill-the-Winner model of microbial ecosystems. Sci Rep. 4 janv 2017;7(1):39642.

246. Suttle CA. Marine viruses — major players in the global ecosystem. Nat Rev Microbiol. oct 2007;5(10):801-12.

247. Paul JH, Sullivan MB, Segall AM, Rohwer F. Marine phage genomics. Comp Biochem Physiol B Biochem Mol Biol. déc 2002;133(4):463-76.

248. Sillankorva S, Oliveira R, Vieira MJ, Sutherland I, Azeredo J. Pseudomonas fluorescens infection by bacteriophage ΦS1: the influence of temperature, host growth phase and media. FEMS Microbiology Letters. 1 déc 2004;241(1):13-20.

249. Steinhoff U. Who controls the crowd? New findings and old questions about the intestinal microflora. Immunol Lett. 15 juin 2005;99(1):12-6.

250. Denou E, Berger B, Barretto C, Panoff JM, Arigoni F, Brüssow H. Gene Expression of Commensal Lactobacillus johnsonii Strain NCC533 during In Vitro Growth and in the Murine Gut. J Bacteriol. nov 2007;189(22):8109-19.

251. Maura D, Morello E, du Merle L, Bomme P, Le Bouguénec C, Debarbieux L. Intestinal colonization by enteroaggregative Escherichia coli supports long-term bacteriophage replication in mice. Environmental Microbiology. 2012;14(8):1844-54.

252. Galtier M, De Sordi L, Sivignon A, de Vallée A, Maura D, Neut C, et al. Bacteriophages Targeting Adherent Invasive Escherichia coli Strains as a Promising New Treatment for Crohn's Disease. J Crohns Colitis. 1 juill 2017;11(7):840-7.

253. Weiss M, Denou E, Bruttin A, Serra-Moreno R, Dillmann ML, Brüssow H. In vivo replication of T4 and T7 bacteriophages in germ-free mice colonized with Escherichia coli. Virology. 10 oct 2009;393(1):16-23.

254. De Sordi L, Khanna V, Debarbieux L. The Gut Microbiota Facilitates Drifts in the Genetic Diversity and Infectivity of Bacterial Viruses. Cell Host & Microbe. 13 déc 2017;22(6):801-808.e3.

255. Breitbart M, Hewson I, Felts B, Mahaffy JM, Nulton J, Salamon P, et al. Metagenomic Analyses of an Uncultured Viral Community from Human Feces. Journal of Bacteriology. 15 oct 2003;185(20):6220-3.

256. Breitbart M, Haynes M, Kelley S, Angly F, Edwards RA, Felts B, et al. Viral diversity and dynamics in an infant gut. Res Microbiol. juin 2008;159(5):367-73.

257. Dutilh BE, Cassman N, McNair K, Sanchez SE, Silva GGZ, Boling L, et al. A highly abundant bacteriophage discovered in the unknown sequences of human faecal metagenomes. Nat Commun. 24 juill 2014;5(1):4498.

258. Guerin E, Shkoporov A, Stockdale SR, Clooney AG, Ryan FJ, Sutton TDS, et al. Biology and Taxonomy of crAss-like Bacteriophages, the Most Abundant Virus in the Human Gut. Cell Host Microbe. 14 nov 2018;24(5):653-664.e6.

259. Liang G, Bushman FD. The human virome: assembly, composition and host interactions. Nat Rev Microbiol. 30 mars 2021;1-14.

260. Minot S, Sinha R, Chen J, Li H, Keilbaugh SA, Wu GD, et al. The human gut virome: inter-individual variation and dynamic response to diet. Genome Res. oct 2011;21(10):1616-25.

261. Manrique P, Bolduc B, Walk ST, van der Oost J, de Vos WM, Young MJ. Healthy human gut phageome. Proceedings of the National Academy of Sciences. 13 sept 2016;113(37):10400-5.

262. Clooney AG, Sutton TDS, Shkoporov AN, Holohan RK, Daly KM, O'Regan O, et al. Whole-Virome Analysis Sheds Light on Viral Dark Matter in Inflammatory Bowel Disease. Cell Host Microbe. 11 déc 2019;26(6):764-778.e5.

263. Chaffringeon L, Lamy-Besnier Q, Debarbieux L, De Sordi L. The intestinal virome: lessons from animal models. Current Opinion in Virology. 1 déc 2021;51:141-8.

Résultats

Objectifs de thèse

Cette thèse a pour objectif de comprendre les interactions entre les différents partenaires du microbiote intestinal dans un contexte physiologique ou pathologique. Les résultats sont organisés selon deux axes principaux. Tous les travaux sont présentés sous forme d'article, publié ou non.

Le premier est centré sur l'étude des interactions entre bactériophages virulent et bactéries dans l'intestin. Dans une première étude, nous avons étudié les différences transcriptomiques de souche la *Escherichia coli* dans différents environnements, *in vitro* et *in vivo* dans l'intestin de souris. Nous avons alors pu identifier plusieurs gènes pouvant impacter les interactions bactériophages-bactéries. Nous avons démontré expérimentalement que ces gènes modulaient le cycle infectieux de bactériophages. Confirmant ainsi que l'environnement intestinal modifiait l'expression génétique bactérienne qui à son tour influençait la susceptibilité des bactéries aux bactériophages.

Dans une seconde étude, nous avons colonisé des souris avec une souche de *E. coli* puis ajouté un cocktail de trois bactériophages ciblant cette souche. Nous avons observé une baisse transitoire de la colonisation puis une coexistence entre les bactériophages et les bactéries sans émergence de clones résistants. La répartition hétérogène des bactériophages et des bactéries entre les parties mucosale et luminale nous ont conduit à proposer un modèle « source-puits » expliquant cette cohabitation. Ces résultats ont été confirmé avec une seconde souche de *E. coli* ciblé cette fois par un unique bactériophage.

Le second axe se concentre sur les effets des acides biliaires issu du métabolisme bactérien sur l'inflammation. Pour cela, l'élaboration d'un modèle *in vivo* a été nécessaire. Des souris OMM^{12} disposant d'un microbiote contrôlé ne métabolisant pas les acides biliaires, ont été colonisé par l'entéropathogène murin *Citrobacter rodentium*. Une fois le modèle caractérisé, nous avons ajouté de l'UDCA dans la nourriture des souris OMM^{12} infectées par *C. rodentium*. Nous avons alors observé que l'UDCA inhibait la production d'IL-22, une cytokine clé de la réponse inflammatoire contre *C. rodentium*.

Enfin, un objectif qui n'a pas pu être atteint concerne la possibilité de combiner l'action anti-inflammatoire de l'UDCA et l'action antibactérienne des bactériophages. L'intérêt de cet objectif à la lumière des résultats acquis est abordé dans la discussion.

I – Caractériser les interactions entre bactéries et bactériophages dans l'intestin

A) L'environnement intestinal régule l'expression des gènes bactériens qui modifient la susceptibilité aux bactériophages

Un des modèles utilisés au laboratoire pour étudier les interactions bactériophages-bactéries dans l'intestin est constitué de la souche *Escherichia coli* 55989, une souche entéroaggrégative et de trois bactériophages, CLB_P1 un podoviridae, CLB_P2 un myoviridae et CLB_P3 un siphoviridae. *In vitro* ces bactériophages entrainent une baisse rapide de la densité optique d'une culture de *E. coli* 55989 avec apparition de clones résistant quelques heures plus tard pour CLB_P1 et CLB_P3 mais pas CLB_P2. *In vivo*, l'addition du cocktail des trois bactériophages virulents dans l'eau de boissons de souris conventionnelles colonisées par *E. coli* ne provoque qu'une réduction transitoire de la quantité de 55989 dans les fèces. En revanche les bactériophages restent abondants pendant au moins deux semaines, témoignant d'une multiplication *in situ*, ainsi que d'une coexistence entre ces deux populations antagonistes (1). Ces données nous ont conduits à envisager une étude transcriptomique de la souche 55989.

Nous avons comparé trois environnements différents: *in vitro* en phase stationnaire et exponentielle et *in vivo* dans le colon. Nous avons alors identifié des gènes différentiellement exprimés dans de nombreuses voies métaboliques. Parmi ceux-ci nous nous sommes intéressés à quatre gènes (*bss*R, *fli*A, *lsr*C et *rfa*L) pouvant impacter le cycle infectieux d'un bactériophage. Nous avons ensuite confirmé expérimentalement que chacun de ces gènes modulaient les interactions bactériophages-bactéries pour au moins un des trois bactériophages. Nous avons ainsi démontré que la croissance de la bactérie dans le tube digestif modifiait l'expression de gènes qui à son tour influençait la susceptibilité des bactéries aux bactériophages.

Ce travail a été initié par Marta Lourenço, une ancienne doctorante qui a soutenu sa thèse en avril 2019. J'ai effectué tous les tests phénotypiques sur les biofilms ainsi que les analyses statistiques et figures correspondantes. J'ai également participé à la rédaction du manuscrit.

1. Maura D, Morello E, du Merle L, Bomme P, Le Bouguénec C, Debarbieux L. Intestinal colonization by enteroaggregative Escherichia coli supports long-term bacteriophage replication in mice. Environmental Microbiology. 2012;14(8):1844-54.

Article

Cell Host & Microbe

The gut environment regulates bacterial gene expression which modulates susceptibility to bacteriophage infection

Graphical abstract

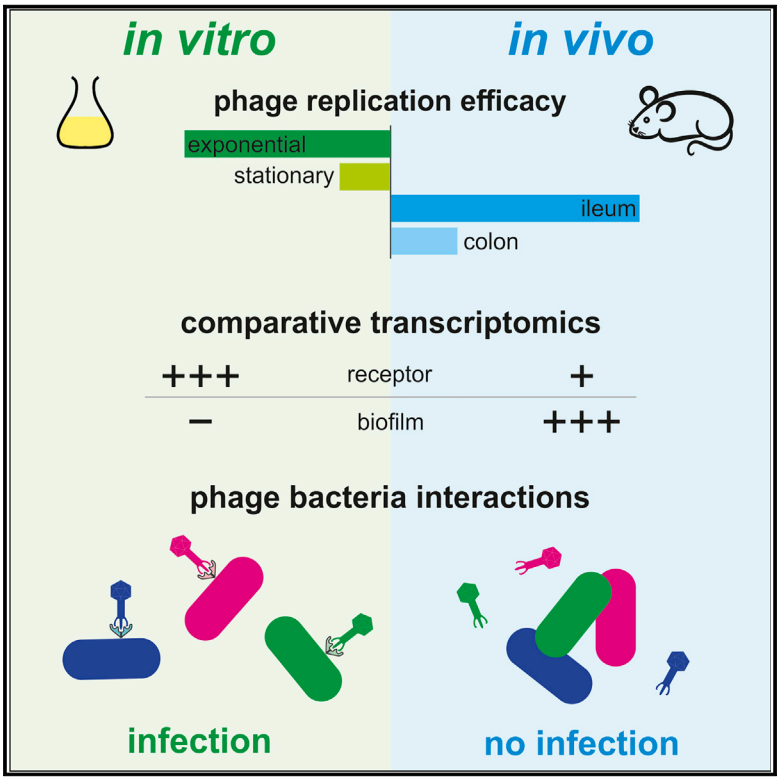

Authors

Marta Lourenço,
Lorenzo Chaffringeon,
Quentin Lamy-Besnier, ...,
Marion Bérard, Luisa De Sordi,
Laurent Debarbieux

Correspondence

laurent.debarbieux@pasteur.fr

In brief

The intestinal microbiota harbor a broad diversity of bacteriophages and bacteria that stably coexist. Lourenço et al. show that gene expression regulation of enteroaggregative *Escherichia coli* in the mammalian gut modifies its susceptibility to bacteriophages. Escaping bacteriophage predation without the selection of mutations provides opportunities for long-term coexistence.

Highlights

- Bacteriophage infection is variable along the gastrointestinal tract
- Stationary and intestinal growth reduce flagellum expression and increase biofilms
- Downregulation of bacterial receptors in the gut controls bacteriophage infection
- Bacteria can escape bacteriophage predation without dedicated defense systems

Lourenço et al., 2022, Cell Host & Microbe *30*, 556–569
April 13, 2022
https://doi.org/10.1016/j.chom.2022.03.014

CellPress

CellPress

Cell Host & Microbe

Article

The gut environment regulates bacterial gene expression which modulates susceptibility to bacteriophage infection

Marta Lourenço,[1,2,9] Lorenzo Chaffringeon,[1,3,4] Quentin Lamy-Besnier,[1] Marie Titécat,[1,5] Thierry Pédron,[1] Odile Sismeiro,[6] Rachel Legendre,[6,7] Hugo Varet,[6,7] Jean-Yves Coppée,[6] Marion Bérard,[8] Luisa De Sordi,[1,3,4] and Laurent Debarbieux[1,10,*]

[1]Institut Pasteur, Université Paris Cité, CNRS UMR 6047, Bacteriophage Bacterium Host, 75015 Paris, France
[2]Sorbonne Université, Collège Doctoral, 75005 Paris, France
[3]Sorbonne Université, INSERM, Centre de Recherche St Antoine, UMRS_938, Paris, France
[4]Paris Center for Microbiome Medicine (PaCeMM) FHU, AP-HP, Paris, Ile-de-France, France
[5]Université de Lille, INSERM, CHU Lille, U1286-INFINITE-Institute for Translational Research in Inflammation, 59000 Lille, France
[6]Transcriptome and EpiGenome Platform, Biomics, Center for Technological Resources and Research (C2RT), Institut Pasteur, Université Paris Cité, 75015 Paris, France
[7]Bioinformatics and Biostatistics Hub, Department of Computational Biology, Institut Pasteur, Université Paris Cité, 75015 Paris, France
[8]Institut Pasteur, Université Paris Cité, DT, Animalerie Centrale, Centre de Gnotobiologie, 75724 Paris, France
[9]Present address: Institut Pasteur, Université Paris Cité, Department of Global Health, 75015 Paris, France
[10]Lead contact
*Correspondence: laurent.debarbieux@pasteur.fr
https://doi.org/10.1016/j.chom.2022.03.014

SUMMARY

Abundance and diversity of bacteria and their viral predators, bacteriophages (phages), in the digestive tract are associated with human health. Particularly intriguing is the long-term coexistence of these two antagonistic populations. We performed genome-wide RNA sequencing on a human enteroaggregative *Escherichia coli* isolate to identify genes differentially expressed between *in vitro* conditions and in murine intestines. We experimentally demonstrated that four of these differentially expressed genes modified the interactions between *E. coli* and three virulent phages by either increasing or decreasing its susceptibility/resistance pattern and also by interfering with biofilm formation. Therefore, the regulation of bacterial genes expression during the colonization of the digestive tract influences the coexistence of phages and bacteria, highlighting the intricacy of tripartite relationships between phages, bacteria, and the animal host in intestinal homeostasis.

INTRODUCTION

The microbiota of the mammalian gut include bacteria and their viral predators, bacteriophages (phages). In healthy individuals, these two antagonistic populations generally remain stable over time, but variations in their density and diversity have been associated with several human diseases or disorders (Gregory et al., 2020; Manrique et al., 2017; Mirzaei and Maurice, 2017; Shkoporov et al., 2019; Zuo et al., 2020). The long-term coexistence of populations of phages and bacteria *in vivo* probably results from a combination of mechanisms deployed by each of the three partners: phages, bacteria, and the host (Kirsch et al., 2021; Mirzaei and Maurice, 2017).

Multiple molecular mechanisms regulate the dynamics of phage-bacterium interactions. These include mutations of the genes encoding phage receptors to prevent attachment, restriction-modification enzymes, and CRISPR systems to degrade phage genomes, mutations of genes encoding proteins essential for phage infection and replication, abortive infection, and superinfection exclusion systems (Labrie et al., 2010). Genome data mining has recently identified a growing number of bacterial genes involved in phage-defense systems experimentally tested only *in vitro* (Bernheim and Sorek, 2020; Millman et al., 2020; Rousset et al., 2021). In addition, other mechanisms, such as phenotypic resistance, a reversible state providing bacteria with temporary resistance to phages (Bull et al., 2014; Chapman-McQuiston and Wu, 2008; Levin et al., 2013), and leaky resistance (Chaudhry et al., 2018), have been proposed as means of prolonging the coexistence of phages and bacteria in microcosms *in vitro*. Moreover, abiotic (temperature, oxygen, and nutrients) and biotic (microbial and mammalian cells) factors have been shown to influence phage-bacterium interactions in both *in vitro* and *in vivo* environments (Alseth et al., 2019; Golec et al., 2014; Hadas et al., 1997; Labedan, 1984; Lourenço et al., 2020; Scanlan et al., 2019; Sillankorva et al., 2004). However, the relevance and preponderance of these mechanisms in the mammalian gut remain poorly explored (Cornuault et al., 2020; De Sordi et al., 2019).

Bacteria modulate gene expression during their establishment in the digestive tract of mammals. Whether and how this could affect their susceptibility to phages remain unknown. However, there have been several observations indicating that phages with a similar efficacy *in vitro* behave differently in the gastrointestinal tract of mice (Maura and Debarbieux, 2012; Weiss et al., 2009). Likewise, we showed that phage replication in homogenized intestinal sections from colonized mice (*ex vivo*) is different not only from that *in vitro* but also between different gut sections (Galtier et al., 2017; Lourenço et al., 2020; Maura et al., 2012a). These findings suggest that the gut environment modulates phage-bacterium interactions.

Here, we aimed to identify bacterial genes for which regulation within the digestive tract modifies bacterial susceptibility to phages. We performed a genome-wide transcriptomic analysis comparing *in vitro* and *in vivo* conditions for the *Escherichia coli* strain 55989. This strain is an enteroaggregative O104:H4 clinical isolate (EAEC pathotype frequently associated with traveler's diarrhea) (Lääveri et al., 2021) that is known to form biofilms and that carries a pAA plasmid encoding virulence determinants (Touchon et al., 2009). We previously isolated and characterized three virulent phages (*Podoviridae* CLB_P1, *Myoviridae* CLB_P2, and *Siphoviridae* CLB_P3) infecting strain 55989 (Maura et al., 2012b). Associated in a cocktail, these three phages rapidly decreased the intestinal load of strain 55989 colonizing the gut of conventional mice (Maura et al., 2012a) before to promote a long-term coexistence with this strain (Maura et al., 2012b).

We identified chromosome- and plasmid-encoded genes differentially expressed by the *E. coli* strain 55989 during gut colonization, encoding proteins with functions relating to iron acquisition, aerobic and anaerobic respiration, sugar metabolism, motility, adhesion, aggregation, biofilm regulation, and lipopolysaccharide (LPS) biosynthesis. We studied four of these genes (*bssR*, *fliA*, *lsrC*, and *rfaL*), encoding proteins with functions expected to affect phage-bacterium interactions. Using a combination of phenotypic assays, we experimentally confirmed that each of these four genes modulated phage-bacterium interactions for at least one of the phages. This study reveals a molecular mechanism, i.e., the modification of bacterial gene expression by the gut environment, which influences the susceptibility of bacteria to phages, thereby contributing to the coexistence of these two antagonistic populations.

RESULTS

The efficacy of phage replication on *E. coli* cells grown *in vitro* differs from homogenized *E. coli*-colonized gut samples

We previously tested individually the ability of phages CLB_P1, CLB_P2, and CLB_P3 to establish a long-term coexistence with the strain 55989 colonizing conventional mice. Each of these phages behave differently. Phage CLB_P2 lasted over 4 weeks, whereas CLP_P3 and CLB_P1 fell below the threshold of detection after 11 and 4 days, respectively (Maura and Debarbieux, 2012). These data, together with *in vitro* and *ex vivo* phage replication assays performed on 55989 cells (Maura et al., 2012a), supported the hypothesis that the regulation of bacterial genes may influence phage-bacteria interactions. To test this hypothesis, we aimed to perform *in vivo* transcriptomics on samples from monocolonized mice (axenic mice colonized only with strain 55989). First, we assessed the individual phage replication on 55989 cells recovered from homogenized gut sections (ileum and colon) of monocolonized mice, as well as on 55989 cells collected from liquid medium during the exponential and stationary growth phases (Figure 1). As a control, we tested the stability of the three phages in absence of strain 55989 and found that during the assay (5 h), the number of phages decreased by about 1-log in LB and gut samples from axenic mice (Figure 1, left). We also evaluated the behavior of exponential and stationary grown 55989 cells when added to gut homogenates from axenic mice during 5 h. We found that exponentially grown cells were capable of growing by about 2-log in both ileum and colon sections, whereas stationary grown cells could not (Figure 1, right).

The three phages displayed an amplification of three to four orders of magnitude relative to the initial phage dose on exponentially growing 55989 cells (Figure 1, central). In sharp contrast, the level of phages CLB_P1 and CLB_P3 that was recovered after incubation with the cells collected during the stationary growth phase was several orders of magnitude lower than that during the initial dose, showing that these phages did not amplify, whereas phage CLB_P2 displayed a moderately impaired amplification (two orders of magnitude lower compared with the exponential growth condition) (Figure 1, central part). The strong reduction of the amount of recovered phage CLB_P1 upon incubation with stationary cells suggests that it binds to cells but is unable to infect them. A similar situation was previously reported for phage T7 that was exposed to *E. coli* cells lacking *flhDC* and overexpressing curli in biofilms (Vidakovic et al., 2018). Perhaps, the inability of phage CLB_P1 to persist in the murine gut could be linked to its inability to infect 55989 cells colonizing the gut of mice.

On homogenized ileal samples from monocolonized mice, the three phages amplified to a similar degree in cells collected during exponential growth. On colon samples from monocolonized mice, CLB_P2 and CLB_P3 amplification were similar to that on ileal samples, but the amplification of CLB_P1 was strongly reduced by 4-log (Figure 1, central part). These data are consistent with a previous assessment of the amplification of these phages in intestinal sections collected from conventional mice colonized with strain 55989, demonstrating that the presence of other microbes is not involved in the differences observed between *in vitro* and *ex vivo* conditions (Maura et al., 2012a). Therefore, the replication of each of the three phages was differentially affected by the growth of strain 55989 in different environments. Since the regulation of gene expression is a hallmark of the adaptation of bacteria to changing environments, we next looked for relationships between bacterial gene expression and phage-bacterium interactions.

E. coli strain 55989 experiences metabolic shifts during gut colonization

For identification of the set of genes from strain 55989 specifically expressed in the gut, we compared the genome-wide pool of mRNAs extracted in three sets of growth conditions: (1) *in vitro* exponential growth (OD_{600nm} = 0.5; "exponential" samples n = 4), (2) *in vitro* stationary growth (equivalent OD_{600nm} = 5; "stationary" samples n = 4), and (3) *in vivo* growth in the colon

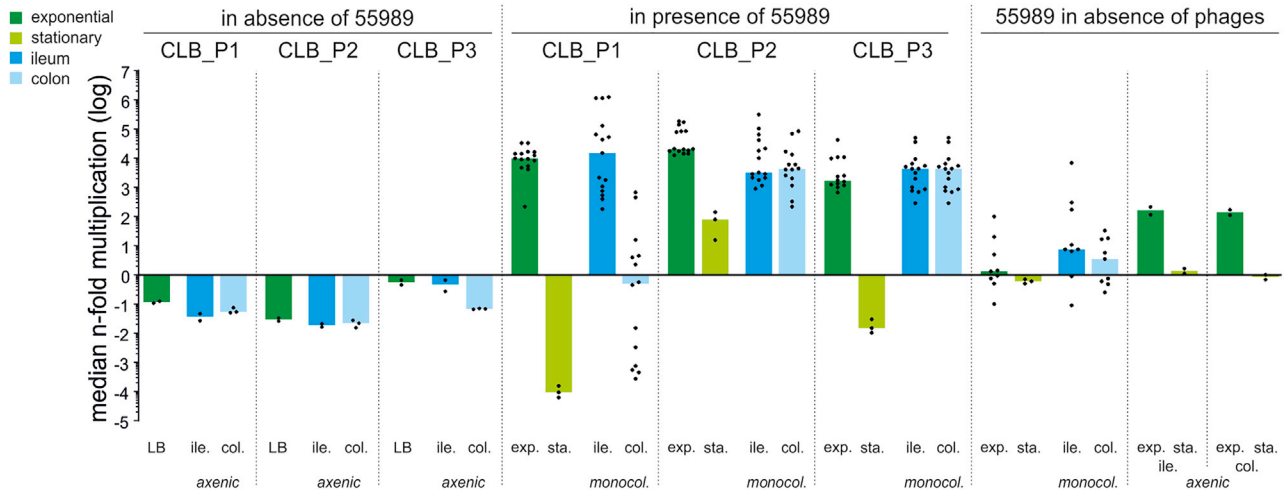

Figure 1. The replication of phages CLB_P1, CLB_P2, and CLB_P3 on strain 55989 is affected by growth conditions *in vitro* and *ex vivo*

Phages CLB_P1, CLB_P2, or CLB_P3 were added to LB (green) or to homogenized gut sections (ile, ileum, dark blue; col, colon, light blue) from axenic mice and incubated for 5 h before quantification (left part). The amplification of phages (CLB_P1, CLB_P2, and CLB_P3, each added at an MOI of ~0.01) is reported after 5 h of incubation with strain 55989 (central part) in the indicated conditions: exponentially growing cells (exp, dark green; OD_{600nm} = 0.5); cells in stationary phase (sta, light green; equivalent OD_{600nm} = 5); homogenized gut sections from monocolonized mice (ile, ileum, dark blue; col, colon, light blue). 55989 cells collected from exponential or stationary growth conditions were incubated with homogenized gut sections from axenic mice for 5 h, and their density was reported (right part). Median n-fold multiplication is shown relative to the initial number of plaque-forming units (PFUs) or colony-forming units (CFUs). n = 2–5 biological replicates with 1–3 technical replicates.

of monocolonized mice ("colon" samples n = 4; see STAR Methods). A principal component analysis (PCA) showed that the three conditions were very different, and within each condition, the replicates were very similar, resulting in a remarkable differentiation and supporting further analysis (Figure 2A). Interestingly, the global gene expression pattern of colon samples was more similar to exponential samples than to stationary samples (Figure 2B). We then compared the transcriptomes of the colon with exponential and stationary samples separately to identify the set of genes differentially expressed between these sets of conditions (Figure 2C). Next, we cross-checked genes from these comparisons with the differentially expressed genes between exponential and stationary samples to remove those in common and identify genes that were differentially expressed during the growth of strain 55989 in the colon. We obtained a list of 156 overexpressed and 53 underexpressed genes, the functions of which were determined using a Gene Ontology analysis (http://geneontology.org/) and the EcoCyc database (Keseler et al., 2011; Tables S1 and S2).

A large proportion of the functions of genes overexpressed in the colon concerned sugar metabolism and transport (Figure 3A; Table S1A). The most significantly overexpressed gene, *ompG*, encodes a specific porin involved in carbohydrate transport (Fajardo et al., 1998). Several carbohydrate pathways (sucrose, gluconate, glucurate, galactarate, and galactonate) were overexpressed, consistent with previous reports of *E. coli* adaptation to the gut environment (Conway and Cohen, 2015; Fabich et al., 2008; Lourenço et al., 2016). We also found that the genes involved in carnitine metabolism (*fixA*, *fixB*, *fixC*, and *caiT*), were overexpressed. Furthermore, genes involved in the utilization of ethanolamine (*eutN*, *eutG*, *eutJ*, and *eutP*) were overexpressed.

As expected, we observed differential expression for genes involved in the transition from aerobic to anaerobic environments. Together with the genes involved in carnitine metabolism, the *frdBCD* genes encoding the fumarate reductase and *fumB*, encoding a fumarase, were all found to be overexpressed, as previously reported (Condon and Weiner, 1988; Meadows and Wargo, 2015; Woods and Guest, 1987). Conversely, the full operon *cyoABCDE*, encoding the subunits of the cytochrome bo terminal oxidase and haem O synthase, was strongly underexpressed, which is a hallmark of decreased oxygen availability (Figure 3B; Table S1B; Cotter et al., 1990). The second most significantly underexpressed set of genes was related to iron acquisition and included enterobactin biosynthesis and export genes (*entC*, *entS*, *fepD*, and *fhuD*), together with *fecI*, *yncD*, and *yncE* genes, all of which encode proteins with functions relating to iron transport. These observations not only validated our approach to identify bacterial genes whose expression could affect phage-bacteria interactions in the gut but also highlighted a number of specific features putatively involved in the intestinal colonization process of this enteroaggregative *E. coli* strain and that require further investigations.

Plasmid-encoded virulence determinants are upregulated during *E. coli* growth in the gut

The EAEC strain 55989 carries a plasmid (p55989) from the pAA family (Croxen and Finlay, 2010) that harbors several genes encoding factors involved in adhesion to epithelial cells (Boll et al., 2017; Weintraub, 2007). In our analysis of *in vivo* differentially expressed plasmid-encoded genes, we identified seven overexpressed genes, four of them with functions relating to adhesion (*agg3B*, *agg3C, agg3D*, and *p55989_0069*) (Figure S1; Table S1C), consistent with the phenotype of EAEC strains,

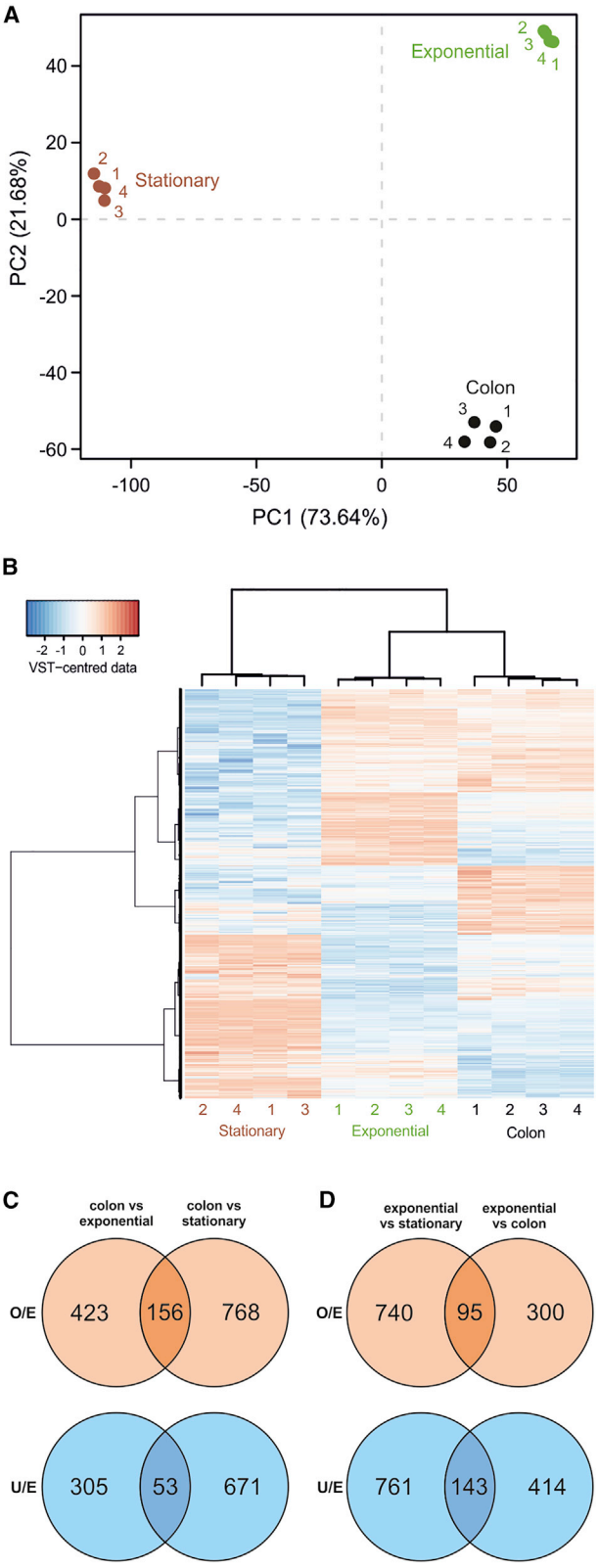

Figure 2. The mRNA content of *E. coli* cells growing in the gut is different from that of cells grown *in vitro*

(A) Cells of *E. coli* strain 55989 were collected from *in vitro* cultures (LB medium, 37°C with shaking) at an OD_{600nm} of 0.5 (exponential, n = 4) and an equivalent OD_{600nm} of 5 (stationary, n = 4) or from *in vivo* tissues (colon of monocolonized mice, n = 4), and their mRNA was extracted, sequenced, and subjected to principal component analysis (biological variability was the main source of variance).

(B) Heatmap and dendrogram obtained for VST-transformed data for sequenced mRNAs from the samples analyzed in (A) (see STAR Methods).

(C) Numbers of overexpressed (O/E) and underexpressed (U/E) genes from pairwise comparisons between colon and either exponential or stationary phase samples.

(D) Numbers of overexpressed (O/E) and underexpressed (U/E) genes from pairwise comparisons between exponential and either stationary or colon samples.

which form aggregates at the surface of intestinal cells. We also found two plasmid genes encoding putative transposases to be overexpressed, consistent with the mechanisms involved in the genetic adaptation of *E. coli* cells to the gut environment (Barroso-Batista et al., 2014; Lourenço et al., 2016). Regarding other mobile genetic elements, the *in silico* analysis of the genome of strain 55989 revealed that it contains seven intact prophage regions, one incomplete and one questionable (see STAR Methods). None of these regions were differentially expressed in our RNA-seq data.

Comparative transcriptomic analysis highlights bacterial genes related to phage infection

Since phage replication is altered in both stationary phase and colon compared with exponential phase samples (Figure 1), we analyzed the above transcriptomics dataset by performing pairwise comparisons between exponential phase with either colon or stationary phase samples to identify genes potentially linked to these changes in phage replication. Then, we removed genes differentially expressed between colon and stationary phase samples (see STAR Methods; Figure 2D). In total, 238 genes (73 overexpressed and 143 underexpressed) were identified, and about 50% of them have no known function (Tables S1D and S1E, respectively). The underexpressed genes (Table S1E) with known functions included genes involved in the biosynthetic pathway for flagella (including *fliA*) and LPS (including *rfaL*), both of which act as cell wall receptors for phages (Choi et al., 2013; Feugeas et al., 2016; Shin et al., 2012). All genes encoding proteins involved in the flagellum apparatus were indeed underexpressed, suggesting that phages relying on this structure for entry would less efficiently infect strain 55989 in both stationary phase and colonic samples. None of the overexpressed genes with known functions were previously associated with phage infection (Table S1D). However, the most significantly overexpressed gene, *bssR*, has been implicated in biofilm formation, and another two genes (*lsrC* and *ego*) are involved in the import of autoinducer-2, a quorum sensing molecule. Interestingly, the function of these genes is related to bacterial community lifestyle and could possibly affect phage-bacterium interactions as previously shown for *Vibrio cholerae* (Hoque et al., 2016; Pires et al., 2021). Therefore, we experimentally tested the contribution of these four genes (*bssR*, *fliA*, *lsrC*, and *rfaL*) to the infectivity of each of the three phages.

The impact on phage-bacterium interactions of the two underexpressed genes— *fliA*, the master regulator of flagellum assembly (Helmann and Chamberlin, 1987) and *rfaL* (also known as *waaL*), which encodes the O-antigen ligase (Klena et al.,

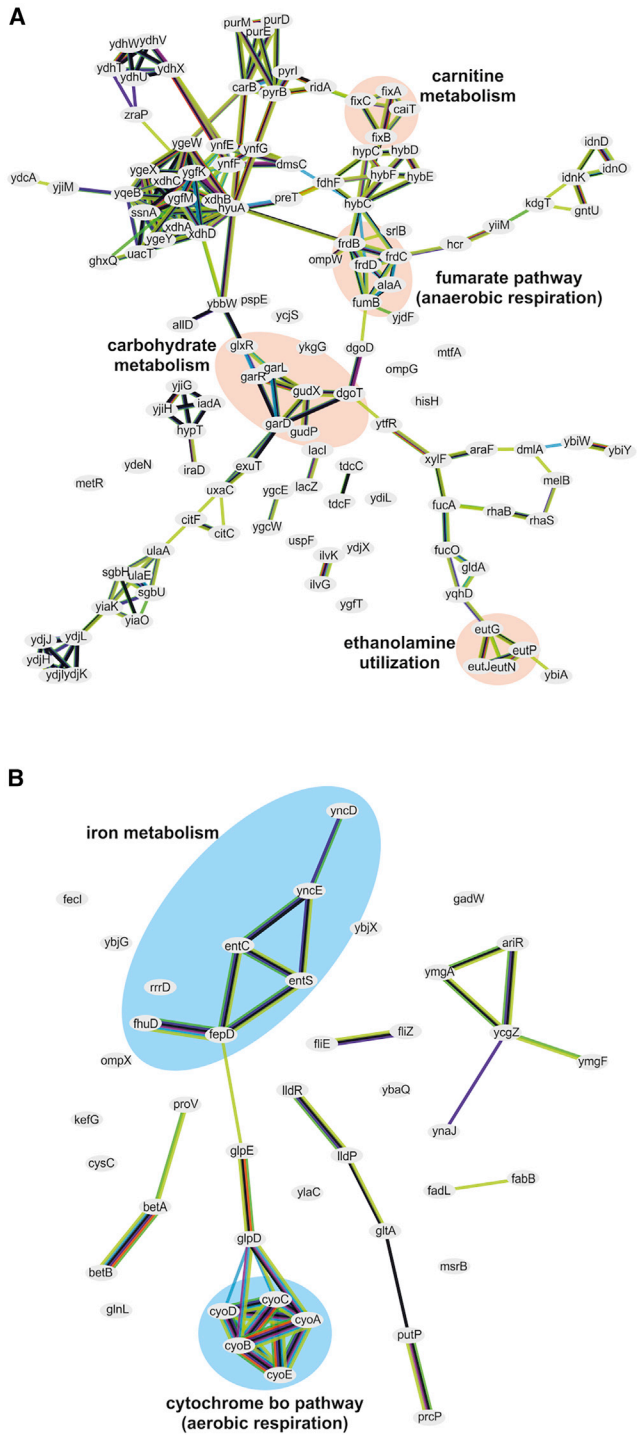

Figure 3. The growth of *E. coli* strain 55989 in the colon involves the activation of carbohydrate metabolism and a decrease in aerobic respiration

(A and B) A network analysis was performed, based on translated protein-protein interactions, with the STRING webserver (string-db.org) using strain MG1655 as template on genes overexpressed (A) and underexpressed (B) in the colon of monocolonized mice relative to cells in the stationary and exponential growth phases. The full list of genes analyzed is available in Tables S1 and S2. The large closed circles (orange for overexpressed and blue for underexpressed genes) correspond to pathways indicated in bold and discussed in the text.

1992)— was assessed using 55989 strains in which either gene was deleted (55989Δ*fliA* and 55989Δ*rfaL*). To investigate the role of the two overexpressed genes, namely, *bssR*, which encodes a global transcriptional regulator involved in biofilm formation (Domka et al., 2006), and *lsrC*, which encodes a subunit of the autoinducer-2 membrane transporter (Xavier and Bassler, 2005), we introduced a plasmid carrying either of these genes into strain 55989 under the control of an isopropyl β-D-1-thiogalactopyranoside (IPTG)-inducible promoter.

The lack of *rfaL* decreases the susceptibility of strain 55989 to phage CLB_P1

We first assessed the efficiency of plating (EOP) of phage CLB_P1 and found that it dropped by 3-log ($2.10 \times 10^{-3} \pm 3.11 \times 10^{-4}$) on the 55989Δ*rfaL* strain but remained unchanged in the 55989Δ*fliA* strain (1.19 ± 0.28), as well as in the strain 55989, overexpressing either *bssR* (1.08 ± 0.33) or *lsrC* (1.18 ± 0.45) genes. The growth and lysis of cells over time in liquid medium following exposure to phage CLB_P1 confirmed these results with notably the lack of lysis of the 55989Δ*rfaL* strain (Figures 4A and 4B). As *rfaL* encodes the O-antigen ligase, we hypothesized that the O-antigen could act as a receptor for this phage. In fact, phage CLB_P1 could not bind to the 55989Δ*rfaL* strain compared with either the WT or the 55989Δ*fliA* strain (Figures 4C–4E). Moreover, cell aggregation by a O104 serotype specific antibody was prevented when 55989 cells were incubated with phage CLB_P1 but not with another unrelated phage, showing that phage CLB_P1 recognizes the O-antigen part of the LPS as a receptor (Figure 4F). We then evaluated the impact of phage CLB_P1 when added to 24-h-old biofilms formed by either 55989Δ*fliA*, 55989Δ*rfaL*, 55989-p*bssR*, or 55989-p*lsrC* strains (Figure S2). The overexpression of either *bssR* or *lsrC* genes had no significant effect on the amount of biofilm produced compared with the strain 55989 carrying the empty plasmid between 24 and 48 h in absence or presence of phage CLB_P1 as assessed by crystal violet quantification (Figure S2A; Tables S2A and S2B). Likewise, the amount of CFUs recovered at 48 h from the corresponding experiments did not reveal any significant differences (Figure S2B; Tables S2A and S2B). We obtained similar results with 55989Δ*fliA* and 55989Δ*rfaL* strains (Figures S2C and S2D; Tables S2A and S2B). In conclusion, these data show that the downregulation of *rfaL* when 55989 cells inhabit the colon of mice likely impairs their infection by phage CLB_P1, which by itself does not affect biofilm formation.

Phage CLB_P2 infection is insensitive to the lack of *rfaL* or *fliA* genes, as well as the overexpression of *bssR* or *lsrC* genes

Neither the EOP of CLB_P2 (Table S2C) nor the lysis of 55989Δ*fliA* or 55989Δ*rfaL* strains nor the lysis of 55989 cells carrying the plasmids p*bssR* or p*lsrC* was affected in comparison with their corresponding control strains (WT and p*empty*), showing that none of these genes interfere with CLB_P2 infection in these growth conditions (Figures 5A and 5B). Unexpectedly, the presence of CLB_P2 significantly increased the amount of biofilm when either *bssR* ($p = 0.0029$) or *lsrC* ($p = 0.0007$) was IPTG-induced in comparison with the control strain (Figure 5C; Table S2A). This was not correlated to the changes of CFUs in

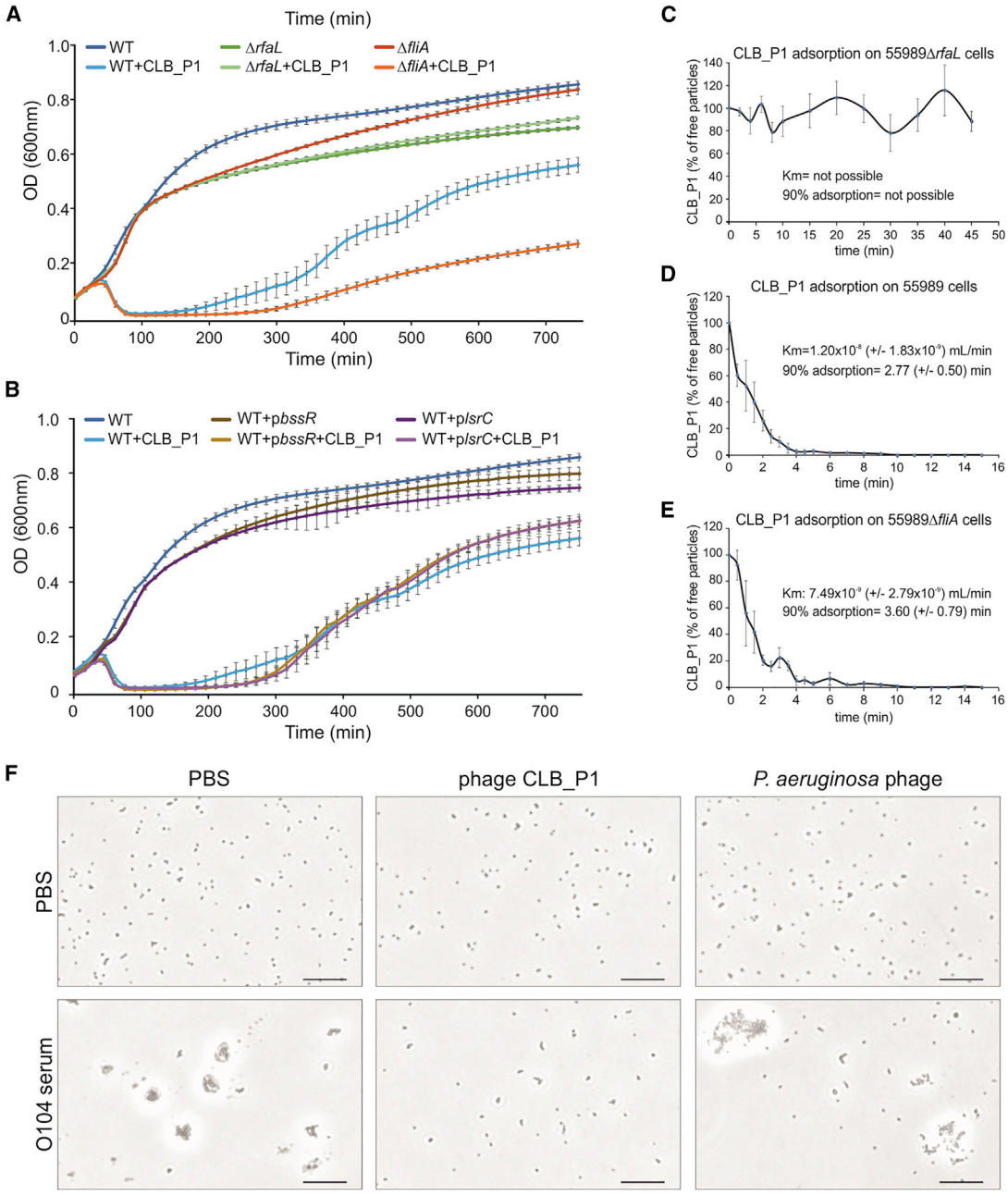

Figure 4. Phage CLB_P1 does not infect 55989Δ*rfaL* cells and recognizes the O104-antigen moiety of the LPS

(A) Growth curves in LB of the *E. coli* strains 55989 (WT), 55989Δ*rfaL*, and 55989Δ*fliA* (supplemented with kanamycin for Δ*rfaL* and Δ*fliA* strains) in the presence and absence of phage CLB_P1, added at $t = 0$, at an MOI of 0.01 (n = 2–3 for each set of conditions). Error = standard error of the mean.

(B) Growth curves in LB of *E. coli* strain 55989 (WT), WT + pbssR (supplemented with 0.05 mM IPTG) and WT + plsrC (supplemented with 0.01 mM IPTG) in presence or absence of phage CLB_P1 added at $t = 0$ and a MOI of 0.01 (n = 2–3 for each condition). Errors = standard error of the mean.

(C–E) The adsorption of phage CLB_P1 on strains 55989Δ*rfaL* (C), 55989 (D), and 55989Δ*fliA* (E) was evaluated according to standard procedures (see STAR Methods). Adsorption constants and adsorption kinetics (90% of phages bound) were calculated by applying an exponential decay function to the corresponding data.

(F) Microscopic observations of 55989 cells (1×10^7 CFU) mixed with either PBS or phage CLB_P1 (2.5×10^7 PFU) or a *Pseudomonas aeruginosa* phage (2.5×10^7 PFU) during 10 min, followed by the addition of either O104 anti-serum or PBS. Scale bars, 20 μm.

the overexpressing strains compared with the control (Figure 5D; Table S2B). We even noticed that the presence of CLB_P2 led to a significant reduction of the level of CFUs of all strains compared with its absence (p = 0.005 and below) (Figure 5D; Table S2B). This moderate drop of 1- to 2-logs of CFUs indicates that some phage CLB_P2 infected cells embedded in the biofilm

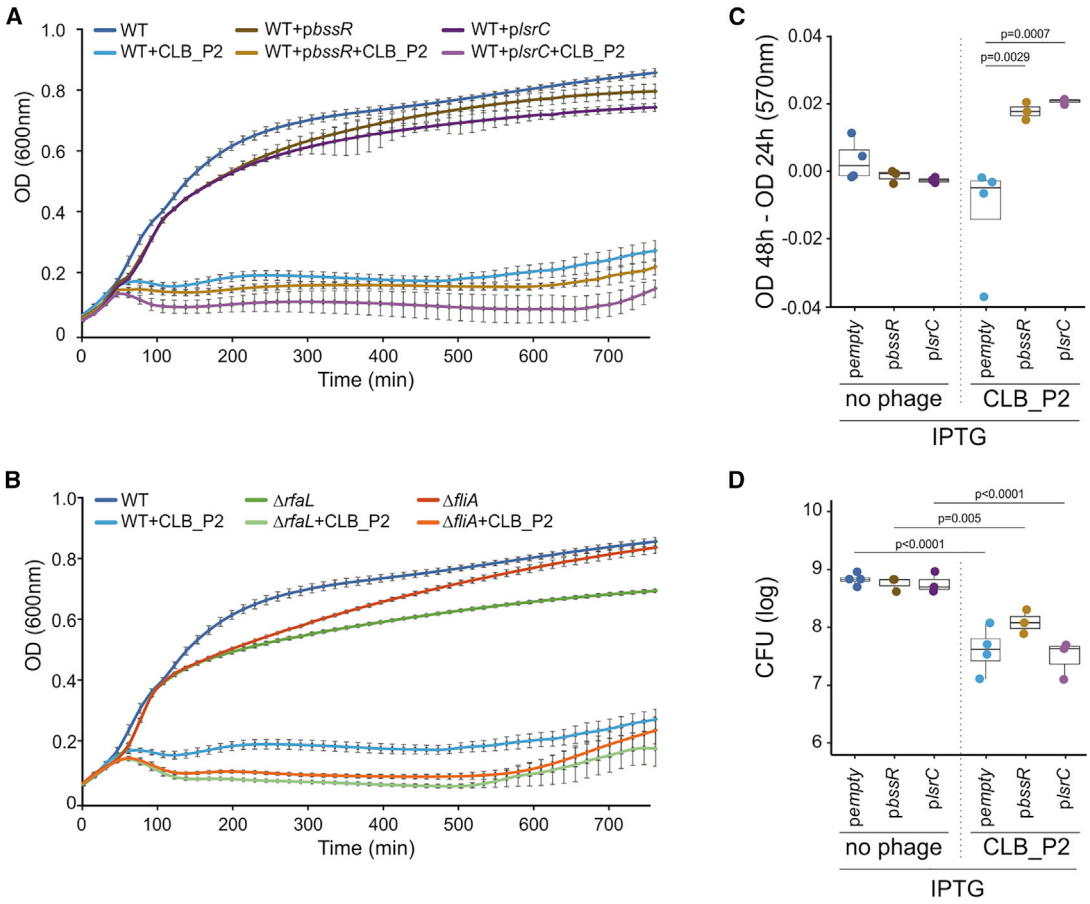

Figure 5. Phage CLB_P2 increases the formation of biofilms in 55989 cells overexpressing either *bssR* or *lsrC* genes

(A) Growth curves in LB of *E. coli* strain 55989 (WT), WT + pbssR (supplemented with 0.05 mM IPTG) and WT + plsrC (supplemented with 0.01 mM IPTG) in presence or absence of phage CLB_P2 added at t = 0 and a MOI of 0.01 (n = 2–3 for each condition). Errors = standard error of the mean.

(B) Growth curves in LB of the *E. coli* strains 55989 (WT), 55989Δ*rfaL*, and 55989Δ*fliA* (supplemented with kanamycin for Δ*rfaL* and Δ*fliA* strains), in the presence and absence of phage CLB_P2, added at t=0, at an MOI of 0.01 (n = 2–3 for each set of conditions). Error = standard error of the mean.

(C) Biofilm formation, reported as variations of OD_{570nm} recorded at 48 h relative to 24 h for the indicated *E. coli* strains in the presence or absence of phage CLB_P2 added at 24 h (1×10^7 PFU/mL) and IPTG at 0.05 mM for empty and *bssR* plasmids or 0.01 mM for the *lsrC* plasmid, as well as kanamycin; n = 3–4 independent experiments. The boxes indicate the interquartile range, the horizontal bars correspond to the median and the vertical bars indicated the minimum and maximum values (within 1.5 interquartile intervals), p = p value of the Tukey post hoc tests (Table S2A).

(D) Number of CFU resuspended from biofilms recovered from microplates setup in parallel to those used for biofilm quantification shown in (C) (see STAR Methods).

matrix. We hypothesize that this phage displays some affinity to the biofilm matrix, which leads to carry over some particles during the washing steps before the cells are resuspended and mixed with this residual phage population. This was further supported by the data obtained from biofilm assays performed with 55989Δ*fliA* or 55989Δ*rfaL* strains and their plasmid-complemented counterparts. For all of these strains, phage CLB_P2 did not change the amount of biofilms produced, but its presence led again to a significant reduction of the level of CFUs recovered (Figures S3A and S3B; Tables S2A and S2B). Therefore, none of the four candidate genes were affecting the capacity of phage CLB_P2 to infect 55989 cells, but we uncovered that the presence of CLB_P2 increases biofilm formation by the cells overexpressing genes related to community lifestyle, perhaps as a defense response against this phage.

Phage CLB_P3 strongly promotes biofilm formation of 55989Δ*fliA* and 55989Δ*rfaL* strains

The EOP of phage CLB_P3 (Table S2C) on strain 55989Δ*rfaL* was slightly higher compared with the control, whereas it remained unchanged for the strains 55989Δ*fliA*, 55989p*bssR*, and 55989p*lsrC*. The lysis kinetics of strain 55989Δ*rfaL* by CLB_P3 was not affected during early time points in contrast to late time points compared with all the other strains tested that were not different from their respective controls (WT and p*empty*) (Figures 6A and 6B). We then observed that the presence of CLB_P3 significantly increased the amount of biofilm formed by both the 55989Δ*fliA* ($p = 0.0040$) and 55989Δ*rfaL* ($p < 0.0001$) strains (Figure 6C; Table S2B). Particularly surprising was the amount of biofilm formed by the 55989Δ*rfaL* strain that increased by a factor of 5 on the OD scale compared with the highest values observed in all the other conditions tested

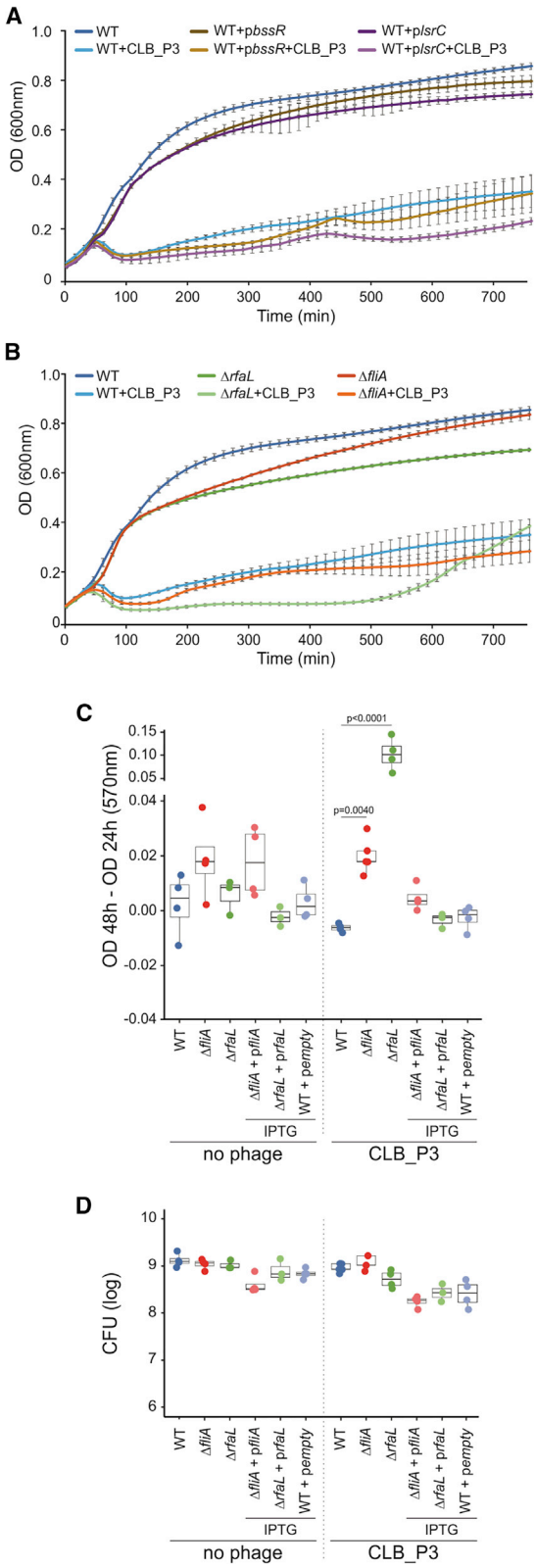

Figure 6. Phage CLB_P3 increases biofilms formation in 55989 cells deleted for either *fliA* or *rfaL* genes

(A) Growth curves in LB of *E. coli* strain 55989 (WT), WT + pbssR (supplemented with 0.05 mM IPTG), and WT + plsrC (supplemented with 0.01 mM IPTG) in presence or absence of phage CLB_P3 added at $t = 0$ and a MOI of 0.01 (n = 2–3 for each condition). Errors = standard error of the mean.

(B) Growth curves in LB of the *E. coli* strains 55989 (WT), 55989Δ*rfaL*, and 55989Δ*fliA* (supplemented with kanamycin for Δ*rfaL* and Δ*fliA* strains) in the presence and absence of phage CLB_P3, added at $t = 0$, at an MOI of 0.01 (n = 2–3 for each set of conditions). Errors = standard error of the mean.

(C) Biofilm formation, reported as change in OD_{570nm} at 48 h relative to 24 h for the indicated *E. coli* strains in the presence or absence of phage CLB_P3 added at 24 h (1×10^7 PFU/mL); n = 3–4 independent experiments. When necessary, IPTG was added at 0.05 mM. The boxes represent the interquartile range; the horizontal bars represent the median; and the vertical bars represent the minimum and maximum values (within 1.5 interquartile intervals), p = p value for post hoc Tukey tests (Table S2A).

(D) Number of CFU resuspended from biofilms recovered from microplates setup in parallel with those used to quantify biofilms shown in (C) (see STAR Methods).

(0.1 versus 0.02). When trans-complemented with a plasmid expressing either *fliA* or *rfaL*, the corresponding defective strains formed as much biofilm as the wild-type strain (Figure 6C). This large increase in biofilms was not correlated to an increase in CFUs (Figure 6D; Table S2C). Moreover, adsorption assays of phage CLB_P3 revealed that its affinity to each of the 55989Δ*fliA* and the 55989Δ*rfaL* strains was nearly 1-log lower compared with the wild-type strain, excluding the hypothesis that a stronger binding of this phage elicits an elevated biofilm formation (Figure S4). In contrast, no significant impact of phage CLB_P3 was observed on the amount of biofilms formed by strains overexpressing either *bssR* or *lsrC* (Figure S5A; Table S2A). Nevertheless, the amount of CFUs recovered from 55989 p*lsrC* biofilms exposed to CLB_P3 was significantly higher compared with the corresponding control cells (p = 0.0016), a result that is the opposite of those obtained with phage CLB_P2 (Figure S5B; Table S2B). Here, we found that cells that are lacking either *fliA* or *rfaL* gene strongly increase biofilm formation only in presence of phage CLB_P3, perhaps eliciting a phage-defense system.

The replication of phage CLB_P1 is abolished in the ileum of 55989Δ*rfaL*-colonized mice

The two strongest phenotypes associated with the four gene candidates were observed with phage CLB_P1 that is severely impaired in infecting 55989Δ*rfaL* cells and phage CLB_P3 that strongly promotes biofilm formation of both 55989Δ*fliA* and 55989Δ*rfaL* cells. We then asked to what extent these phenotypes would translate into modifications of phage-bacteria interactions in the mouse gut. For this, we tested the *ex vivo* replication of the three phages (CLB_P2 serving as a control phage) in intestinal organs from 55989Δ*fliA*- and 55989Δ*rfaL*-colonized mice. As expected, we found that the amplification of phage CLB_P1 is strongly affected on ileal and colonic homogenates from 55989Δ*rfaL*-colonized mice compared with phages CLB_P2 and CLB_P3 (Figure 7). These data demonstrate that a 3-log reduction of the EOP observed *in vitro* translates into a weak replication in organ homogenates, preventing the further *in vivo* evaluation of phage CLB_P1. The results obtained with homogenates from 55989Δ*fliA*-colonized mice were not dissimilar to those obtained from wild-type-colonized mice for the three phages (Figure 1), showing that this gene has no impact on phage infection in organs (Figure 7). Therefore, the increased biofilm formation promoted by the presence of CLB_P3 during

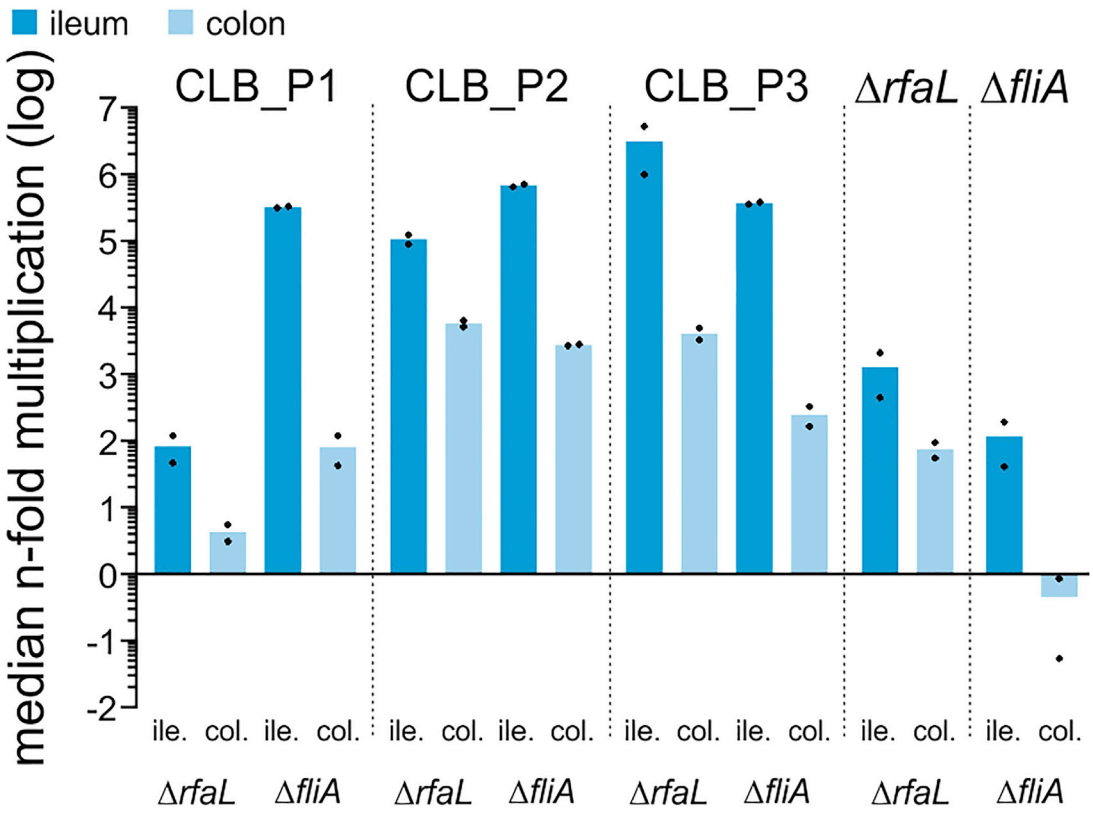

Figure 7. Phage CLB_P1 cannot replicate on intestinal homogenates of 55989Δ*rfaL*-colonized mice

Amplification (n = 2 biological replicates) of phages (CLB_P1, CLB_P2, and CLB_P3, each added at an MOI of ~0.01) after 5 h of incubation with either strain 55989Δ*rfaL* or 55989Δ*fliA* from homogenized gut sections from either 55989Δ*rfaL*- or 55989Δ*fliA*-monocolonized mice (ile, ileum, dark blue; col, colon, light blue). The median n-fold multiplication is shown relative to the initial number of PFUs or CFUs.

the *in vitro* assays does not translate into an impaired phage infection in organs. Nevertheless, during this assay, we observed that the number of CFUs of the 55989Δ*fliA* strain did not increase in the colon compared with the ileal samples. This suggests that some genes under *fliA* regulation may be required for optimal growth in this gut section. This could also explain the trend of a lower amplification in colon compared with ileal sections observed with the three phages.

DISCUSSION

Bacteria and virulent phages coexist over time in the digestive tract of mammals, raising questions about the predator-prey dynamics of these two antagonistic populations (Lourenço et al., 2020; Mirzaei and Maurice, 2017). Here, we investigated whether the regulation of bacterial gene expression occurring during their colonization of the gut environment affects their susceptibility to phages (Lourenço et al., 2018). We performed a genome-wide transcriptomic analysis of the *E. coli* strain 55989, an enteroaggregative pathogenic strain for which we had already characterized three virulent phages, CLB_P1, CLB_P2, and CLB_P3.

Comparisons of the transcriptomics data from colon samples with exponentially and stationary grown cells revealed the differential expression of several genes. In addition to expected genes related to anaerobic growth, as well as sugar metabolism and transport in the gut, we identified some genes related to host adaptation. For instance, the overexpression of *ompG* implies the activation of the transcriptional regulator *ycjW* (Luhachack et al., 2019), which in turn, also regulates the production of H_2S, which has been shown to protect pathogens against the host immune response (Toliver-Kinsky et al., 2019). We also report the overexpression of genes involved in the metabolism of carnitine and ethanolamine, which are compounds derived from the host cells membrane. Both are known to play roles in the gut microbiota, with carnitine being used for osmoprotection or as a source of nutrients (Meadows and Wargo, 2015), whereas ethanolamine has been previously shown to be used by enteroaggregative *E. coli* for improving its ability to outcompete commensal *E. coli* (Bertin et al., 2011). Among the underexpressed genes, we found several iron acquisition systems, including enterobactin. This counterintuitive observation—since it is well established that iron acquisition systems are required for gut colonization (Deriu et al., 2013)—must be counterbalanced by the diversity of multiple iron acquisition systems identified in *E. coli* genomes, some of which, such as Feo, are expressed in anaerobic conditions (Lau et al., 2016). Moreover, *fumB*, the expression of which decreases in conditions of iron limitation, was found to be overexpressed in the colon, suggesting that iron supply was not a limiting factor in our experimental conditions (Figure 3A; Table S1A). In addition, the analysis of the

55989 plasmid-encoded genes identified four overexpressed genes with functions related to adhesion. Together with the concomitant overexpression of *uspF* (Table S1A) and underexpression of *ompX* (Table S1B), both of which are located on the chromosome, these observations support that bacterial motility is reduced in the colon (Nachin et al., 2005; Otto et al., 2001). Beyond the specificities linked to this particular enteropathogenic strain of *E. coli*, which would deserve further investigations, our data are congruent with similar studies using comparative transcriptomics between *in vitro* and *in vivo* conditions for intestinal bacteria (Denou et al., 2007).

The untargeted approach (whole intestinal sections) used for this work has some limitations despite its success for identifying genes involved in phage susceptibility. For instance, the transcriptomic profiles were treated as belonging to a single homogeneous bacterial population, whereas bacteria within an intestinal section actually face different physiological conditions (Li et al., 2015). Moreover, about 50% of the candidate genes that were identified had no predicted functions. Some may then encode proteins involved in phage-bacterium interactions, warranting additional studies to determine their mode of action.

We showed that four of the genes that were identified from transcriptomic comparisons alter the interactions of strain 55989 with at least one of the three phages, CLB_P1, CLB_P2, or CLB_P3. When overexpressed or deleted, these genes led to phenotypes that could be related to a global response protecting cells against phages. However, the elicited response was specific to each of the three phages (only 55989Δ*rfaL* cells for CLB_P1, both 55989p*bssR* and 55989p*lsrC* cells for CLB_P2, and both 55989Δ*fliA* and 55989Δ*rfaL* cells for CLB_P3), highlighting the complexity of predicting the *in vivo* efficacy of phages from *in vitro* experiments.

In *E. coli*, LPS is one of the receptors most frequently used by phages (Hantke, 2020). However, as K12 strains (the most frequently used in laboratories) do not synthesize O-antigen (Liu and Reeves, 1994), *rfaL* (the gene encoding the O-antigen ligase) has not previously been identified as a gene involved in phage infection, including a recent systematic study (Maffei et al., 2021). Here, we demonstrated that phage CLB_P1 recognizes the O104 antigen as a receptor, consistent with its host range toward the ECOR collection (Maura et al., 2012b). Interestingly, the lack of *rfaL* does not completely abolish the capacity of phage CLB_P1 to form plaques on the 55989Δ*rfaL* lawns, suggesting that CLB_P1 recognizes a secondary receptor. However, neither in liquid broth with agitation nor in gut homogenates, this secondary receptor was sufficient to allow phage CLB_P1 infection. Therefore, the low rates of replication of phage CLB_P1 on cells in the stationary phase or in colon samples (Figure 1) can be attributed to the underexpression of *rfaL* that is identified during the comparative analysis of transcriptomics data. More broadly, when considering application in humans, our data suggest that a phage that displays a 3-log reduction of the EOP on a clinical isolate would likely be inefficient *in vivo*.

The strong stimulation of biofilm formation by the CLB_P3 phage in the 55989Δ*fliA* and 55989Δ*rfaL* strains was both striking and puzzling, as the functions of these genes are unrelated to each other. Furthermore, these two strains remained as susceptible to CLB_P3 as the WT on both solid and liquid media. It is therefore tempting to speculate that the presence of CLB_P3 led to an increase in the production of an extracellular polysaccharide matrix in these two mutant strains but not in the wild type, perhaps as a defense against phage CLB_P3. Since *fliA* is a sigma factor, we hypothesize that its absence unlocks a genetic regulation that is otherwise inactive, only in the presence of phage CLB_P3 but not of CLB_P1 or CLB_P2. As the lack of *rfaL* affects the structure of the LPS, we hypothesize that the presence of CLB_P3, but not of CLB_P1 or CLB_P2, uncovers a bacterial receptor not involved in phage infection but instead in a signaling process promoting matrix production, perhaps as a phage-defense system. Interestingly, these two hypotheses are not exclusive.

The presence of phage CLB_P2 increased the formation of biofilms by the strains overexpressing either *bssR* or *lsrC* with similar amplitude. Again, it is tempting to suggest that the increase in biofilm formation is linked to the induction of a phage-defense mechanism, as exopolysaccharide production has been shown to protect cells from phage infection in many bacterial species (Darch et al., 2017; de Sousa et al., 2020; Radke and Siegel, 1971). It is worth noting that the presence of CLB_P2, compared with its absence, resulted in the recovery of significantly fewer cells from biofilm for all strains tested. This observation suggests that CLB_P2 may be the most potent of the three phages at killing cells embedded in biofilms. Alternatively, this phage may have a loose affinity for the biofilm matrix (Barr et al., 2013) and decrease the number of CFUs at the plating step instead of within the biofilm.

The phenotypes observed with the four genes converged to lower bacterial susceptibility to phages, in other words increasing phage resistance in both the presence (*in vitro*) and absence (*in vivo*) of phages. This suggests that bacteria become less susceptible to phages when they colonize the gut. Here, the formation of biofilms at the surface of epithelial cells could be invoked as a phage-defense response that could have a negative impact on health when such biofilms are linked to virulence as for the enteroaggregative strain 55989. Moreover, gene regulation entails a lesser fitness cost than loss-of-function due to genetic mutations, which may be crucial to ensure persistence within a fluctuating environment, including the competition between bacteria.

Experiments in animals with a cocktail of these three phages, or other phage cocktails, have shown that despite the initial reduction of bacterial levels in the gut, coexistence of phages with their hosts is rapidly established (Hsu et al., 2019; Maura et al., 2012b). This coexistence is supported by multiple overlapping mechanisms, including the regulation of bacterial gene expression as shown here (Javaudin et al., 2021; Lourenço et al., 2018). Aligning the composition of phage cocktails to the environmental conditions in which they are to be used may be the best option for optimizing phage applications. In addition, repeated phage applications, prescribed similar to a standard anti-microbial drug, might result in more effective treatments by preventing the establishment of coexistence.

In conclusion, tripartite interactions occur between phages, bacteria, and the host, all of which influence each other. The mammalian gut environment and its response to bacterial colonization affects bacterial gene expression, which in turn, influences phage infection. Conversely, phage variants may be

selected to improve efficacy against established bacterial clones by adaptation (De Sordi et al., 2017; Mathieu et al., 2020), potentially inducing a response in the bacteria (De Sordi et al., 2019) affecting their relationship with the host (intestinal epithelial and immune cells) (Diard et al., 2017; Sausset et al., 2020). Globally, the balance between these equilibria governs gut homeostasis and health.

STAR★METHODS

Detailed methods are provided in the online version of this paper and include the following:

- KEY RESOURCES TABLE
- RESOURCE AVAILABILITY
  - Lead contact
  - Materials availability
  - Data and code availability
- EXPERIMENTAL MODELS AND SUBJECT DETAILS
  - Ethics statement
  - Phages and bacterial strains
- METHODS DETAILS
  - *Ex vivo* assay
  - Transcriptomics
  - Data analysis
  - Phage efficiency of plating (EOP) test
  - Adsorption assays and phage growth
  - Biofilm formation and quantification
  - Agglutination assay
- QUANTIFICATION AND STATISTICAL ANALYSIS

SUPPLEMENTAL INFORMATION

Supplemental information can be found online at https://doi.org/10.1016/j.chom.2022.03.014.

ACKNOWLEDGMENTS

We thank Jorge Moura de Sousa for writing the customized R script for the pairwise comparisons between lists of genes from the different samples and for critically reading the manuscript. We thank Dwayne Roach and Anne Chevallereau for valuable discussions. We thank the Genetics of Biofilms team (Jean-Marc Ghigo) of Institut Pasteur and in particular Anne-Aurélie Lopes for training on the biofilm assays and Christophe Beloin for access to the ASKA plasmids collection. We thank the members of the Centre for Gnotobiology Platform of the Institut Pasteur (Thierry Angélique, Eddie Maranghi, Martine Jacob, Jérome Toutain, and Marisa Gabriela Lopez Dieguez) for their help with the animal work. M.L. is funded as part of the Pasteur-Paris University (PPU) International PhD Program. M.L. is funded by Institut Carnot Pasteur Maladies Infectieuses (ANR 11-CARN 017-01). L.D.S. is funded by a Roux-Cantarini Fellowship from the Institut Pasteur (Paris, France). L.C. is funded by a PhD Fellowship from the Ministère de l'Enseignement Supérieur et de la Recherche, France, École Doctorale 394. Q.L.-B. is funded by École Doctorale FIRE - Programme Bettencourt. M.T. received a fellowship from Fondation DigestScience (Lille, France). The transcriptome and epigenome Platform is part of the France Génomique consortium (ANR10-NBS-09-08).

AUTHOR CONTRIBUTIONS

Conceptualization and methodology, L.D., L.D.S., and M.L.; investigations, L.C., M.L., M.T., O.S., Q.L.-B., and T.P.; formal analysis, J.-Y.C., R.L., M.L., and H.V.; resources, M.B.; supervision and funding acquisition, L.D.; writing—original draft, M.L. and L.D.; writing—review and editing, L.C., L.D., L.D.S., Q.L.-B., M.L., and T.P.

DECLARATION OF INTERESTS

The authors declare no competing interests.

Received: June 22, 2021
Revised: January 14, 2022
Accepted: March 10, 2022
Published: April 13, 2022

REFERENCES

Alseth, E.O., Pursey, E., Luján, A.M., McLeod, I., Rollie, C., and Westra, E.R. (2019). Bacterial biodiversity drives the evolution of CRISPR-based phage resistance. Nature *574*, 549–552. https://doi.org/10.1038/s41586-019-1662-9.

Anders, S., and Huber, W. (2010). Differential expression analysis for sequence count data. Genome Biol. *11*, R106. https://doi.org/10.1186/gb-2010-11-10-r106.

Arndt, D., Grant, J.R., Marcu, A., Sajed, T., Pon, A., Liang, Y., and Wishart, D.S. (2016). PHASTER: a better, faster version of the PHAST phage search tool. Nucleic Acids Res. *44*, W16–W21. https://doi.org/10.1093/nar/gkw387.

Ashburner, M., Ball, C.A., Blake, J.A., Botstein, D., Butler, H., Cherry, J.M., Davis, A.P., Dolinsk, i, K., Dwight, S.S., and Eppig, J.T.. (2000). Gene ontology: tool for the unification of biology. The Gene Ontology Consortium. Nat. Genet. *1*, 25–29. https://doi.org/10.1038/75556.

Aziz, R.K., Bartels, D., Best, A.A., DeJongh, M., Disz, T., Edwards, R.A., Formsma, K., Gerdes, S., Glass, E.M., Kubal, M., et al. (2008). The RAST Server: rapid annotations using subsystems technology. BMC Genomics *9*, 75. https://doi.org/10.1186/1471-2164-9-75.

Barr, J.J., Auro, R., Furlan, M., Whiteson, K.L., Erb, M.L., Pogliano, J., Stotland, A., Wolkowicz, R., Cutting, A.S., Doran, K.S., et al. (2013). Bacteriophage adhering to mucus provide a non-host-derived immunity. Proc. Natl. Acad. Sci. U. S. A. *110*, 10771–10776. https://doi.org/10.1073/pnas.1305923110.

Barroso-Batista, J., Sousa, A., Lourenço, M., Bergman, M.L., Sobral, D., Demengeot, J., Xavier, K.B., and Gordo, I. (2014). The first steps of adaptation of *Escherichia coli* to the gut are dominated by soft sweeps. PLoS Genet. *10*, e1004182. https://doi.org/10.1371/journal.pgen.1004182.

Bates, D., Mächler, M., Bolker, B., and Walker, S. (2015). Fitting linear mixed-effects models using lme4. J. Stat. Softw. *67*, 1–48. https://doi.org/10.18637/jss.v067.i01.

Bernheim, A., and Sorek, R. (2020). The pan-immune system of bacteria: antiviral defence as a community resource. Nat. Rev. Microbiol. *18*, 113–119. https://doi.org/10.1038/s41579-019-0278-2.

Bertin, Y., Girardeau, J.P., Chaucheyras-Durand, F., Lyan, B., Pujos-Guillot, E., Harel, J., and Martin, C. (2011). Enterohaemorrhagic *Escherichia coli* gains a competitive advantage by using ethanolamine as a nitrogen source in the bovine intestinal content. Environ. Microbiol. *13*, 365–377. https://doi.org/10.1111/j.1462-2920.2010.02334.x.

Boll, E.J., Ayala-Lujan, J., Szabady, R.L., Louissaint, C., Smith, R.Z., Krogfelt, K.A., Nataro, J.P., Ruiz-Perez, F., and McCormick, B.A. (2017). Enteroaggregative *Escherichia coli* adherence fimbriae drive inflammatory cell recruitment via interactions with epithelial MUC1. mBio *8*, e00717. https://doi.org/10.1128/mBio.00717-17.

Bull, J.J., Vegge, C.S., Schmerer, M., Chaudhry, W.N., and Levin, B.R. (2014). Phenotypic resistance and the dynamics of bacterial escape from phage control. PLoS One *9*, e94690. https://doi.org/10.1371/journal.pone.0094690.

Chapman-McQuiston, E., and Wu, X.L. (2008). Stochastic receptor expression allows sensitive bacteria to evade phage attack. Part I: experiments. Biophys. J. *94*, 4525–4536. https://doi.org/10.1529/biophysj.107.120212.

Chaudhry, W.N., Pleška, M., Shah, N.N., Weiss, H., McCall, I.C., Meyer, J.R., Gupta, A., Guet, C.C., and Levin, B.R. (2018). Leaky resistance and the conditions for the existence of lytic bacteriophage. PLoS Biol. *16*, e2005971. https://doi.org/10.1371/journal.pbio.2005971.

Chaveroche, M.K., Ghigo, J.M., and d'Enfert, C. (2000). A rapid method for efficient gene replacement in the filamentous fungus Aspergillus nidulans. Nucleic Acids Res. *28*, E97. https://doi.org/10.1093/nar/28.22.e97.

Chevallereau, A., Blasdel, B.G., De Smet, J., Monot, M., Zimmermann, M., Kogadeeva, M., Sauer, U., Jorth, P., Whiteley, M., Debarbieux, L., and Lavigne, R. (2016). Next-generation "-omics" approaches reveal a massive alteration of host RNA metabolism during bacteriophage infection of *Pseudomonas aeruginosa*. PLoS Genet. *12*, e1006134. https://doi.org/10.1371/journal.pgen.1006134.

Choi, Y., Shin, H., Lee, J.H., and Ryu, S. (2013). Identification and characterization of a novel flagellum-dependent Salmonella-infecting bacteriophage. iEPS5. Appl. Environ. Microbiol. *79*, 4829–4837. https://doi.org/10.1128/AEM.00706-13.

Condon, C., and Weiner, J.H. (1988). Fumarate reductase of *Escherichia coli*: an investigation of function and assembly using *in vivo* complementation. Mol. Microbiol. *2*, 43–52. https://doi.org/10.1111/j.1365-2958.1988.tb00005.x.

Conway, T., and Cohen, P.S. (2015). Commensal and pathogenic *Escherichia coli* metabolism in the gut. Microbiol. Spec. *3*. https://doi.org/10.1128/microbiolspec.MBP-0006-2014.

Cornuault, J.K., Moncaut, E., Loux, V., Mathieu, A., Sokol, H., Petit, M.A., and De Paepe, M. (2020). The enemy from within: a prophage of Roseburia intestinalis systematically turns lytic in the mouse gut, driving bacterial adaptation by CRISPR spacer acquisition. ISME J. *14*, 771–787. https://doi.org/10.1038/s41396-019-0566-x.

Cotter, P.A., Chepuri, V., Gennis, R.B., and Gunsalus, R.P. (1990). Cytochrome o (cyoABCDE) and d (cydAB) oxidase gene expression in *Escherichia coli* is regulated by oxygen, pH, and the fnr gene product. J. Bacteriol. *172*, 6333–6338. https://doi.org/10.1128/jb.172.11.6333-6338.1990.

Croxen, M.A., and Finlay, B.B. (2010). Molecular mechanisms of *Escherichia coli* pathogenicity. Nat. Rev. Microbiol. *8*, 26–38. https://doi.org/10.1038/nrmicro2265.

Darch, S.E., Kragh, K.N., Abbott, E.A., Bjarnsholt, T., Bull, J.J., and Whiteley, M. (2017). Phage inhibit pathogen dissemination by targeting bacterial migrants in a chronic infection model. mBio *8*. e00240–e00217. https://doi.org/10.1128/mBio.00240-17.

De Sordi, L., Khanna, V., and Debarbieux, L. (2017). The gut microbiota facilitates drifts in the genetic diversity and infectivity of bacterial viruses. Cell Host Microbe *22*, 801–808.e3. https://doi.org/10.1016/j.chom.2017.10.010.

De Sordi, L., Lourenço, M., and Debarbieux, L. (2019). I will survive": a tale of bacteriophage-bacteria coevolution in the gut. Gut Microbes *10*, 92–99. https://doi.org/10.1080/19490976.2018.1474322.

de Sousa, J.A.M., Buffet, A., Haudiquet, M., Rocha, E.P.C., and Rendueles, O. (2020). Modular prophage interactions driven by capsule serotype select for capsule loss under phage predation. ISME J. *14*, 2980–2996. https://doi.org/10.1038/s41396-020-0726-z.

Denou, E., Berger, B., Barretto, C., Panoff, J.M., Arigoni, F., and Brüssow, H. (2007). Gene expression of commensal Lactobacillus johnsonii strain NCC533 during *in vitro* growth and in the murine gut. J. Bacteriol. *189*, 8109–8119. https://doi.org/10.1128/JB.00991-07.

Deriu, E., Liu, J.Z., Pezeshki, M., Edwards, R.A., Ochoa, R.J., Contreras, H., Libby, S.J., Fang, F.C., and Raffatellu, M. (2013). Probiotic bacteria reduce *Salmonella* typhimurium intestinal colonization by competing for iron. Cell Host Microbe *14*, 26–37. https://doi.org/10.1016/j.chom.2013.06.007.

Diard, M., Bakkeren, E., Cornuault, J.K., Moor, K., Hausmann, A., Sellin, M.E., Loverdo, C., Aertsen, A., Ackermann, M., De Paepe, M., et al. (2017). Inflammation boosts bacteriophage transfer between Salmonella spp. Science *355*, 1211–1215. https://doi.org/10.1126/science.aaf8451.

Domka, J., Lee, J., and Wood, T.K. (2006). YliH (BssR) and YceP (BssS) regulate *Escherichia coli* K-12 biofilm formation by influencing cell signaling. Appl. Environ. Microbiol. *72*, 2449–2459. https://doi.org/10.1128/AEM.72.4.2449-2459.2006.

Fabich, A.J., Jones, S.A., Chowdhury, F.Z., Cernosek, A., Anderson, A., Smalley, D., McHargue, J.W., Hightower, G.A., Smith, J.T., Autieri, S.M., et al. (2008). Comparison of carbon nutrition for pathogenic and commensal *Escherichia coli* strains in the mouse intestine. Infect. Immun. *76*, 1143–1152. https://doi.org/10.1128/IAI.01386-07.

Fajardo, D.A., Cheung, J., Ito, C., Sugawara, E., Nikaido, H., and Misra, R. (1998). Biochemistry and regulation of a novel *Escherichia coli* K-12 porin protein, OmpG, which produces unusually large channels. J. Bacteriol. *180*, 4452–4459. https://doi.org/10.1128/JB.180.17.4452-4459.1998.

Feugeas, J.P., Tourret, J., Launay, A., Bouvet, O., Hoede, C., Denamur, E., and Tenaillon, O. (2016). Links between transcription, environmental adaptation and gene variability in *Escherichia coli*: correlations between gene expression and gene variability reflect growth efficiencies. Mol. Biol. Evol. *33*, 2515–2529. https://doi.org/10.1093/molbev/msw105.

Fox, J., and Weisberg, S. (2018). An R Companion to Applied Regression (SAGE Publications).

Galtier, M., De Sordi, L., Sivignon, A., de Vallée, A., Maura, D., Neut, C., Rahmouni, O., Wannerberger, K., Darfeuille-Michaud, A., Desreumaux, P., et al. (2017). Bacteriophages targeting adherent invasive *Escherichia coli* Strains as a promising new treatment for Crohn's disease. J. Crohns Colitis *11*, 840–847. https://doi.org/10.1093/ecco-jcc/jjw224.

Gentleman, R.C., Carey, V.J., Bates, D.M., Bolstad, B., Dettling, M., Dudoit, S., Ellis, B., Gautier, L., Ge, Y., Gentry, J., et al. (2004). Bioconductor: open software development for computational biology and bioinformatics. Genome Biol. *5*, R80. https://doi.org/10.1186/gb-2004-5-10-r80.

Golec, P., Karczewska-Golec, J., Łoś, M., and Węgrzyn, G. (2014). Bacteriophage T4 can produce progeny virions in extremely slowly growing *Escherichia coli* host: comparison of a mathematical model with the experimental data. FEMS Microbiol. Lett. *351*, 156–161. https://doi.org/10.1111/1574-6968.12372.

Gregory, A.C., Zablocki, O., Zayed, A.A., Howell, A., Bolduc, B., and Sullivan, M.B. (2020). The gut Virome database reveals age-dependent patterns of Virome diversity in the human gut. Cell Host Microbe *28*, 724–740.e8. https://doi.org/10.1016/j.chom.2020.08.003.

Hadas, H., Einav, M., Fishov, I., and Zaritsky, A. (1997). Bacteriophage T4 development depends on the physiology of its host *Escherichia coli*. Microbiol. Reading Engl. *143*, 179–185. https://doi.org/10.1099/00221287-143-1-179.

Hantke, K. (2020). Compilation of *Escherichia coli* K-12 outer membrane phage receptors - their function and some historical remarks. FEMS Microbiol. Lett. *367*. https://doi.org/10.1093/femsle/fnaa013.

Helmann, J.D., and Chamberlin, M.J. (1987). DNA sequence analysis suggests that expression of flagellar and chemotaxis genes in *Escherichia coli* and *Salmonella* typhimurium is controlled by an alternative sigma factor. Proc. Natl. Acad. Sci. USA *84*, 6422–6424. https://doi.org/10.1073/pnas.84.18.6422.

Henry, M., Lavigne, R., and Debarbieux, L. (2013). Predicting in vivo efficacy of therapeutic bacteriophages used to treat pulmonary infections. Antimicrob. Agents Chemother. *57*, 5961–5968. https://doi.org/10.1128/AAC.01596-13.

Hoque, M.M., Naser, I.B., Bari, S.M., Zhu, J., Mekalanos, J.J., and Faruque, S.M. (2016). Quorum regulated resistance of Vibrio cholerae against environmental bacteriophages. Sci. Rep. *6*, 37956. https://doi.org/10.1038/srep37956.

Hsu, B.B., Gibson, T.E., Yeliseyev, V., Liu, Q., Lyon, L., Bry, L., Silver, P.A., and Gerber, G.K. (2019). Dynamic modulation of the gut microbiota and metabolome by bacteriophages in a mouse model. Cell Host Microbe *25*, 803–814.e5. https://doi.org/10.1016/j.chom.2019.05.001.

Javaudin, F., Latour, C., Debarbieux, L., and Lamy-Besnier, Q. (2021). Intestinal bacteriophage therapy: looking for optimal efficacy. Clin. Microbiol. Rev. *34*, e0013621. https://doi.org/10.1128/CMR.00136-21.

Keseler, I.M., Collado-Vides, J., Santos-Zavaleta, A., Peralta-Gil, M., Gama-Castro, S., Muñiz-Rascado, L., Bonavides-Martinez, C., Paley, S., Krummenacker, M., Altman, T., et al. (2011). EcoCyc: a comprehensive database of *Escherichia coli* biology. Nucleic Acids Res. *39*, D583–D590. https://doi.org/10.1093/nar/gkq1143.

Kirsch, J.M., Brzozowski, R.S., Faith, D., Round, J.L., Secor, P.R., and Duerkop, B.A. (2021). Bacteriophage-bacteria interactions in the gut: From

invertebrates to mammals. Annu. Rev. Virol. *8*, 95–113. https://doi.org/10.1146/annurev-virology-091919-101238.

Kitagawa, M., Ara, T., Arifuzzaman, M., Ioka-Nakamichi, T., Inamoto, E., Toyonaga, H., and Mori, H. (2005). Complete set of ORF clones of *Escherichia coli* ASKA library (a complete set of *E. coli* K-12 ORF archive): unique resources for biological research. DNA Res. *12*, 291–299. https://doi.org/10.1093/dnares/dsi012.

Klena, J.D., Ashford, R.S., 2nd, and Schnaitman, C.A. (1992). Role of *Escherichia coli* K-12 rfa genes and the rfp gene of Shigella dysenteriae 1 in generation of lipopolysaccharide core heterogeneity and attachment of O antigen. J. Bacteriol. *174*, 7297–7307. https://doi.org/10.1128/jb.174.22.7297-7307.1992.

Kuznetsova, A., Brockhoff, P.B., and Christensen, R.H.B. (2017). lmerTest package: tests in linear mixed effects models. J. Stat. Software *82*, 1–26. https://doi.org/10.18637/jss.v082.i13.

Lääveri, T., Antikainen, J., Mero, S., Pakkanen, S.H., Kirveskari, J., Roivainen, M., and Kantele, A. (2021). Bacterial, viral and parasitic pathogens analysed by qPCR: findings from a prospective study of travellers' diarrhoea. Travel Med. Infect. Dis. *40*, 101957. https://doi.org/10.1016/j.tmaid.2020.101957.

Labedan, B. (1984). Requirement for a fluid host cell membrane in injection of coliphage T5 DNA. J. Virol. *49*, 273–275. https://doi.org/10.1128/JVI.49.1.273-275.1984.

Labrie, S.J., Samson, J.E., and Moineau, S. (2010). Bacteriophage resistance mechanisms. Nat. Rev. Microbiol. *8*, 317–327. https://doi.org/10.1038/nrmicro2315.

Lau, C.K., Krewulak, K.D., and Vogel, H.J. (2016). Bacterial ferrous iron transport: the Feo system. FEMS Microbiol. Rev. *40*, 273–298. https://doi.org/10.1093/femsre/fuv049.

Lenth, R.V. (2016). Least-Squares Means: the R package lsmeans. J. Stat. Softw. *69*, 1–33. https://doi.org/10.18637/jss.v069.i01.

Levin, B.R., Moineau, S., Bushman, M., and Barrangou, R. (2013). The population and evolutionary dynamics of phage and bacteria with CRISPR-mediated immunity. PLoS Genet. *9*, e1003312. https://doi.org/10.1371/journal.pgen.1003312.

Li, H., Limenitakis, J.P., Fuhrer, T., Geuking, M.B., Lawson, M.A., Wyss, M., Brugiroux, S., Keller, I., Macpherson, J.A., Rupp, S., et al. (2015). The outer mucus layer hosts a distinct intestinal microbial niche. Nat. Commun. *6*, 8292. https://doi.org/10.1038/ncomms9292.

Li, H., Handsaker, B., Wysoker, A., Fennell, T., Ruan, J., Homer, N., Marth, G., Abecasis, G., and Durbin, R.; 1000 Genome Project Data Processing Subgroup (2009). The Sequence Alignment/Map format and SAMtools. Bioinformatics *25*, 2078–2079. https://doi.org/10.1093/bioinformatics/btp352.

Liu, D., and Reeves, P.R. (1994). *Escherichia coli* K12 regains its O antigen. Microbiology (Reading) *140*, 49–57. https://doi.org/10.1099/13500872-140-1-49.

Lourenço, M., Chaffringeon, L., Lamy-Besnier, Q., Pédron, T., Campagne, P., Eberl, C., Bérard, M., Stecher, B., Debarbieux, L., and De Sordi, L. (2020). The spatial heterogeneity of the gut limits predation and fosters coexistence of bacteria and bacteriophages. Cell Host Microbe *28*, 390–401.e5. https://doi.org/10.1016/j.chom.2020.06.002.

Lourenço, M., De Sordi, L., and Debarbieux, L. (2018). The diversity of bacterial lifestyles hampers bacteriophage tenacity. Viruses *10*, 327. https://doi.org/10.3390/v10060327.

Lourenço, M., Ramiro, R.S., Güleresi, D., Barroso-Batista, J., Xavier, K.B., Gordo, I., and Sousa, A. (2016). A mutational hotspot and strong selection contribute to the order of mutations selected for during *Escherichia coli* adaptation to the gut. PLoS Genet. *12*, e1006420. https://doi.org/10.1371/journal.pgen.1006420.

Love, M.I., Huber, W., and Anders, S. (2014). Moderated estimation of fold change and dispersion for RNA-seq data with DESeq2. Genome Biol. *15*, 550. https://doi.org/10.1186/s13059-014-0550-8.

Luhachack, L., Rasouly, A., Shamovsky, I., and Nudler, E. (2019). Transcription factor YcjW controls the emergency H(2)S production in *E. coli*. Nat. Commun. *10*, 2868. https://doi.org/10.1038/s41467-019-10785-x.

Maffei, E., Shaidullina, A., Burkolter, M., Heyer, Y., Estermann, F., Druelle, V., Sauer, P., Willi, L., Michaelis, S., Hilbi, H., et al. (2021). Systematic exploration of *Escherichia coli* phage-host interactions with the BASEL phage collection. PLoS Biol. *19*, e3001424. https://doi.org/10.1371/journal.pbio.3001424.

Manrique, P., Dills, M., and Young, M.J. (2017). The human gut phage community and its implications for health and disease. Viruses *9*, 141. https://doi.org/10.3390/v9060141.

Martin, M. (2011). Cutadapt removes adapter sequences from high-throughput sequencing reads. EMBnet. j. *17*, 3. https://doi.org/10.14806/ej.17.1.200.

Mathieu, A., Dion, M., Deng, L., Tremblay, D., Moncaut, E., Shah, S.A., Stokholm, J., Krogfelt, K.A., Schjørring, S., Bisgaard, H., et al. (2020). Virulent coliphages in 1-year-old children fecal samples are fewer, but more infectious than temperate coliphages. Nat. Commun. *11*, 378. https://doi.org/10.1038/s41467-019-14042-z.

Maura, D., and Debarbieux, L. (2012). On the interactions between virulent bacteriophages and bacteria in the gut. Bacteriophage *2*, 229–233. https://doi.org/10.4161/bact.23557.

Maura, D., Galtier, M., Le Bouguénec, C., and Debarbieux, L. (2012a). Virulent bacteriophages can target O104:H4 enteroaggregative *Escherichia coli* in the mouse intestine. Antimicrob. Agents Chemother. *56*, 6235–6242. https://doi.org/10.1128/AAC.00602-12.

Maura, D., Morello, E., du Merle, L., Bomme, P., Le Bouguénec, C., and Debarbieux, L. (2012b). Intestinal colonization by enteroaggregative *Escherichia coli* supports long-term bacteriophage replication in mice. Environ. Microbiol. *14*, 1844–1854. https://doi.org/10.1111/j.1462-2920.2011.02644.x.

Meadows, J.A., and Wargo, M.J. (2015). Carnitine in bacterial physiology and metabolism. Microbiol. Reading Engl. *161*, 1161–1174. https://doi.org/10.1099/mic.0.000080.

Millman, A., Bernheim, A., Stokar-Avihail, A., Fedorenko, T., Voichek, M., Leavitt, A., Oppenheimer-Shaanan, Y., and Sorek, R. (2020). Bacterial retrons function in anti-phage defense. Cell *183*, 1551–1561.e12. https://doi.org/10.1016/j.cell.2020.09.065.

Mirzaei, M.K., and Maurice, C.F. (2017). Ménage à trois in the human gut: interactions between host, bacteria and phages. Nat. Rev. Microbiol. *15*, 397–408. https://doi.org/10.1038/nrmicro.2017.30.

Mossoro, C., Glaziou, P., Yassibanda, S., Lan, N.T., Bekondi, C., Minssart, P., Bernier, C., Le Bouguénec, C., and Germani, Y. (2002). Chronic diarrhea, hemorrhagic colitis, and hemolytic-uremic syndrome associated with HEp-2 adherent *Escherichia coli* in adults infected with human immunodeficiency virus in Bangui, Central African Republic. J. Clin. Microbiol. *40*, 3086–3088. https://doi.org/10.1128/JCM.40.8.3086-3088.2002.

Nachin, L., Nannmark, U., and Nyström, T. (2005). Differential roles of the universal stress proteins of *Escherichia coli* in oxidative stress resistance, adhesion, and motility. J. Bacteriol. *187*, 6265–6272. https://doi.org/10.1128/JB.187.18.6265-6272.2005.

Otto, K., Norbeck, J., Larsson, T., Karlsson, K.A., and Hermansson, M. (2001). Adhesion of type 1-fimbriated *Escherichia coli* to abiotic surfaces leads to altered composition of outer membrane proteins. J. Bacteriol. *183*, 2445–2453. https://doi.org/10.1128/JB.183.8.2445-2453.2001.

Pires, D.P., Melo, L.D.R., and Azeredo, J. (2021). Understanding the complex phage-host interactions in biofilm communities. Annu. Rev. Virol. *8*, 73–94. https://doi.org/10.1146/annurev-virology-091919-074222.

R Core Team (2020). R: A language and environment for statistical computing (Vienna, Austria: R Foundation for Statistical Computing). https://www.R-project.org/.

Radke, K.L., and Siegel, E.C. (1971). Mutation preventing capsular polysaccharide synthesis in *Escherichia coli* K-12 and its effect on bacteriophage resistance. J. Bacteriol. *106*, 432–437. https://doi.org/10.1128/jb.106.2.432-437.1971.

Rousset, F., Dowding, J., Bernheim, A., Rocha, E.P.C., and Bikard, D. (2021). Prophage-encoded hotspots of bacterial immune systems. Preprint at bioRxiv. https://doi.org/10.1101/2021.01.21.427644.

Sausset, R., Petit, M.A., Gaboriau-Routhiau, V., and De Paepe, M. (2020). New insights into intestinal phages. Mucosal Immunol. *13*, 205–215. https://doi.org/10.1038/s41385-019-0250-5.

Scanlan, J.G., Hall, A.R., and Scanlan, P.D. (2019). Impact of bile salts on coevolutionary dynamics between the gut bacterium *Escherichia coli* and its lytic phage PP01. Infect. Genet. Evol. *73*, 425–432. https://doi.org/10.1016/j.meegid.2019.05.021.

Shin, H., Lee, J.H., Kim, H., Choi, Y., Heu, S., and Ryu, S. (2012). Receptor diversity and host interaction of bacteriophages infecting Salmonella enterica serovar Typhimurium. PLoS One *7*, e43392. https://doi.org/10.1371/journal.pone.0043392.

Shkoporov, A.N., Clooney, A.G., Sutton, T.D.S., Ryan, F.J., Daly, K.M., Nolan, J.A., McDonnell, S.A., Khokhlova, E.V., Draper, L.A., Forde, A., et al. (2019). The human gut Virome is highly diverse, stable, and individual specific. Cell Host Microbe *26*, 527–541.e5. https://doi.org/10.1016/j.chom.2019.09.009.

Sillankorva, S., Oliveira, R., Vieira, M.J., Sutherland, I., and Azeredo, J. (2004). Pseudomonas fluorescens infection by bacteriophage PhiS1: the influence of temperature, host growth phase and media. FEMS Microbiol. Lett. *241*, 13–20. https://doi.org/10.1016/j.femsle.2004.06.058.

Szklarczyk, D., Gable, A.L., Lyon, D., Junge, A., Wyder, S., Huerta-Cepas, J., Simonovic, M., Doncheva, N.T., Morris, J.H., Bork, P., et al. (2019). STRING v11: protein-protein association networks with increased coverage, supporting functional discovery in genome-wide experimental datasets. Nucleic Acids Res. *47*, D607–D613. https://doi.org/10.1093/nar/gky1131.

Toliver-Kinsky, T., Cui, W., Törö, G., Lee, S.J., Shatalin, K., Nudler, E., and Szabo, C. (2019). H(2)S, a bacterial defense mechanism against the host immune response. Infect. Immun. *87*. e00272–e00218. https://doi.org/10.1128/IAI.00272-18.

Touchon, M., Hoede, C., Tenaillon, O., Barbe, V., Baeriswyl, S., Bidet, P., Bingen, E., Bonacorsi, S., Bouchier, C., Bouvet, O., et al. (2009). Organised genome dynamics in the *Escherichia coli* species results in highly diverse adaptive paths. PLoS Genet. *5*, e1000344. https://doi.org/10.1371/journal.pgen.1000344.

Varet, H., Brillet-Guéguen, L., Coppée, J.Y., and Dillies, M.A. (2016). SARTools: a DESeq2- and EdgeR-based R pipeline for comprehensive differential analysis of RNA-seq data. PLoS ONE *11*, e0157022. https://doi.org/10.1371/journal.pone.0157022.

Vidakovic, L., Singh, P.K., Hartmann, R., Nadell, C.D., and Drescher, K. (2018). Dynamic biofilm architecture confers individual and collective mechanisms of viral protection. Nat. Microbiol. *3*, 26–31. https://doi.org/10.1038/s41564-017-0050-1.

Weintraub, A. (2007). Enteroaggregative *Escherichia coli*: epidemiology, virulence and detection. J. Med. Microbiol. *56*, 4–8. https://doi.org/10.1099/jmm.0.46930-0.

Weiss, M., Denou, E., Bruttin, A., Serra-Moreno, R., Dillmann, M.L., and Brüssow, H. (2009). *In vivo* replication of T4 and T7 bacteriophages in germ-free mice colonized with *Escherichia coli*. Virology *393*, 16–23. https://doi.org/10.1016/j.virol.2009.07.020.

Woods, S.A., and Guest, J.R. (1987). Differential roles of the *Escherichia coli* fumarases and fnr-dependent expression of fumarase B and aspartase. FEMS Microbiol. Lett. *48*, 219–224. https://doi.org/10.1111/j.1574-6968.1987.tb02545.x.

Xavier, K.B., and Bassler, B.L. (2005). Regulation of uptake and processing of the quorum-sensing autoinducer AI-2 in *Escherichia coli*. J. Bacteriol. *187*, 238–248. https://doi.org/10.1128/JB.187.1.238-248.2005.

Zuo, T., Sun, Y., Wan, Y., Yeoh, Y.K., Zhang, F., Cheung, C.P., Chen, N., Luo, J., Wang, W., Sung, J.J.Y., et al. (2020). Human-gut-DNA Virome variations across geography, ethnicity, and urbanization. Cell Host Microbe *28*, 741–751.e4. https://doi.org/10.1016/j.chom.2020.08.005.

STAR★METHODS

KEY RESOURCES TABLE

REAGENT or RESOURCE	SOURCE	IDENTIFIER
Antibodies		
rabbit monoclonal antibody anti E. coli O104	SSI diagnostica	Cat#45840
Bacterial and Virus Strains		
Escherichia coli Strain 55989	Mossoro et al., 2002	CRBIP14.5
Escherichia coli Strain 55989Δ*fliA*	This manuscript	N/A
Escherichia coli Strain 55989p*bssR*	This manuscript	N/A
Escherichia coli Strain 55989p*lsrC*	This manuscript	N/A
Escherichia coli Strain 55989Δ*rfaL*	This manuscript	N/A
Escherichia coli Strain MG1655	This manuscript	N/A
ASKA collection	Kitagawa et al., 2005	N/A
Bacteriophage CLB_P1	Maura et al., 2012b	Genbank: KC109329.1
Bacteriophage CLB_P2	Maura et al., 2012b	Genbank: OL770107
Bacteriophage CLB_P3	Maura et al., 2012b	Genbank: OL770108
Bacteriophage PAK_P3	Henry et al., 2013	Genbank: NC_022970.1
Chemicals, Peptides, and Recombinant Proteins		
Drigalski	CONDA	Cat# 1344
LB Lennox broth or agar	Difco	Cat# 240230 and 240110
Streptomycin	Sigma-Aldrich	Cat# S6501
Kanamycin	Sigma-Aldrich	Cat# K1637
Chloramphenicol	Sigma-Aldrich	Cat# C0378
TRIzol	Sigma-Aldrich	Cat# T-9424
Chloroform	N/A	Cat# 288306
Crystal violet	Sigma-Aldrich	Cat# V5265
Critical commercial assays		
RNeasy mini kit	Qiagen	Cat# 74104
on-column RNAse-free DNAse	Qiagen	Cat# 79254
Ribo-Zero rRNA depletion kit	Illumina	Cat# 20040525
TruSeq Stranded RNA LT prep kit	Illumina	Cat# 20020596
"Quant-It" assay kit	Invitrogen	Cat# Q33232
Deposited Data		
Bacteriophage CLB_P1	This manuscript	Genbank: KC109329.1
Bacteriophage CLB_P2	This manuscript	Genbank: OL770107
Bacteriophage CLB_P3	This manuscript	Genbank: OL770108
RNA-seq data from Ec55989 Colon 1 (Col1) sample	This manuscript	GEO: GSM5047178
RNA-seq data from Ec55989 Colon 2 (Col2) sample	This manuscript	GEO: GSM5047179
RNA-seq data from Ec55989 Colon 3 (Col3) sample	This manuscript	GEO: GSM5047180
RNA-seq data from Ec55989 Colon 4 (Col4) sample	This manuscript	GEO: GSM5047181
RNA-seq data from Ec55989 Exponential 1 (Exp1) sample	This manuscript	GEO: GSM5047182
RNA-seq data from Ec55989 Exponential 2 (Exp2) sample	This manuscript	GEO: GSM5047183
RNA-seq data from Ec55989 Exponential 3 (Exp3) sample	This manuscript	GEO: GSM5047184
RNA-seq data from Ec55989 Exponential 4 (Exp4) sample	This manuscript	GEO: GSM5047185
RNA-seq data from Ec55989 Stationary 1 (Sta1) sample	This manuscript	GEO: GSM5047186
RNA-seq data from Ec55989 Stationary 2 (Sta2) sample	This manuscript	GEO: GSM5047187
RNA-seq data from Ec55989 Stationary 3 (Sta3) sample	This manuscript	GEO: GSM5047188
RNA-seq data from Ec55989 Stationary 4 (Sta4) sample	This manuscript	GEO: GSM5047189

(*Continued on next page*)

Continued

REAGENT or RESOURCE	SOURCE	IDENTIFIER
Experimental Models: Organisms/Strains		
C3H axenic mice	Institut Pasteur	N/A
Oligonucleotides		
rfaL_bf_F (3-step PCR *rfaL* gene deletion and insertion of kanR – up) : 5'- ATCACGGTTTATGGACCAAC -3'	This manuscript	N/A
rfaL_bf_R_kan (3-step PCR *rfaL* gene deletion and insertion of kanR – up) : 5'-gtgagctatgagaaagcgcc CTTATCTCCGATGTCAACTT -3'	This manuscript	N/A
rfaL_bf_F_kan (3-step PCR *rfaL* gene deletion and insertion of kanR – down) : 5'- aaacaaataggggttcc gcgAAAATAAAAAAGGCTGCATA -3'	This manuscript	N/A
rfaL_af_R (3-step PCR *rfaL* gene deletion and insertion of kanR – down) : 5'- GCAAAGCAAG GTCAGGACTT -3'	This manuscript	N/A
fliA_bf_F (3-step PCR *fliA* gene deletion and insertion of kanR – up) : 5'- TAAGAACTCCTGGTAGTCA -3'	This manuscript	N/A
fliA_bf_kan_R2 (3-step PCR *fliA* gene deletion and insertion of kanR – up) : 5'- gtgagctatgag aaagcgccCGTCAGTAAATGCCGCACT -3'	This manuscript	N/A
fliA_bf_kan_F (3-step PCR *fliA* gene deletion and insertion of kanR – down) : 5'- aaacaaat aggggttccgcgGATAAACAGCCCTGCGTTAT -3'	This manuscript	N/A
fliA_bf_R (3-step PCR *fliA* gene deletion and insertion of kanR – down) : 5'- AACCTGCCT GACCCCGCTA -3'	This manuscript	N/A
KanF (kanamycin resistance cassete Forward) : 5'- GGCGCTTTCTCATAGCTCAC -3'	This manuscript	N/A
KanR (kanamycin resistance cassete Reverse) : 5'- CGCGGAACCCCTATTTGTTT -3'	This manuscript	N/A
Software and Algorithms		
FastQC	Brabraham Bioinformatics	RRID: SCR_005539
cutadapt	Martin, 2011	RRID: SCR_011841
RAST	Aziz et al., 2008	RRID: SCR_014806
Bowtie	Li et al., 2009	RRID: SCR_005476
Subread (featureCounts)	Gentleman et al., 2004	RRID: SCR_009803
R	R Core Team, 2020	RRID: SCR_001905
DESeq2 package	Anders and Huber, 2010; Love et al., 2014	RRID: SCR_015687
SARTools package	Varet et al., 2016	RRID: SCR_016533
Geneontology	Ashburner et al., 2000	(http://geneontology.org/).
EcoCyc database	Keseler et al., 2011	RRID: SCR_002433
STRING webserver	Szklarczyk et al., 2019	RRID: SCR_005223
PHASTER (PHAge Search Tool - Enhanced Release)	Arndt et al., 2016	https://phaster.ca/
lme4 package	Bates et al., 2015	RRID: SCR_015654
lmerTest package	Kuznetsova et al., 2017	RRID: SCR_015656
car package	Fox and Weisberg, 2018	https://cran.r-project.org/web/packages/car/
lsmeans R package	Lenth, 2016	https://cran.r-project.org/web/packages/lsmeans/index.html

RESOURCE AVAILABILITY

Lead contact

Further information and requests for resources and reagents should be directed to and will be fulfilled by the lead contact, Laurent Debarbieux (laurent.debarbieux@pasteur.fr).

Materials availability

The bacterial strains 55989Δ*rfaL* and 55989Δ*fliA* as well as phages are available from the lead contact upon completion of a Materials Transfer Agreement (MTA).

Data and code availability

RNA-Seq data have been deposited at GEO and are publicly available as of the date of publication. Accession numbers are listed in the key resources table.

This paper does not report original code.

Any additional information required to reanalyze the data reported in this paper is available from the lead contact upon request.

EXPERIMENTAL MODELS AND SUBJECT DETAILS

Ethics statement

C3H axenic mice (seven to nine weeks old) reared at Institut Pasteur (Paris, France) were housed in an animal facility in accordance with Institut Pasteur guidelines and European recommendations. Food and drinking water were provided *ad libitum*. Protocols were approved by the veterinary staff of the Institut Pasteur animal facility (Ref.#18.271) and the National Ethics Committee (APAFIS#26874-2020081309052574 v1). We used 17 mice (2 males and 15 female) for this study.

Phages and bacterial strains

The *Escherichia coli* strain 55989 was previously described (Mossoro et al., 2002) and other strains are listed in the key resources table.

Phages CLB_P1 (KC109329.1), CLB_P2 (OL770107) and CLB_P3 (OL770108) have been described elsewhere (Maura et al., 2012b). The 55989 mutants were obtained by a three-step PCR in which each gene (*rfaL and fliA*) was disrupted by the insertion of a kanamycin resistance marker gene by lambda Red-mediated homologous recombination (Chaveroche et al., 2000). Primers used for this study are listed in key resources table. ASKA plasmids (chloramphenicol resistant) were used for the overexpression of *bssR* and lsrC and the complementation of 55989Δ*rfaL* and 55989Δ*fliA* strains (Kitagawa et al., 2005).

Strains were routinely cultured in lysogeny broth (LB Lennox - BD), or on LB Lennox agar (BD) or Drigalski agar (lactose agar with bromothymol blue and crystal violet- CONDA) plates, at 37C. When required for selection, streptomycin (100 μg/mL) or kanamycin (100 μg/mL) or chloramphenicol (30 μg/ml) (Sigma) was added.

METHODS DETAILS

Ex vivo assay

C3H axenic mice received 200 μL of PBS or strains 55989 or 55989Δ*fliA* or 55989Δ*rfaL* (10^7 CFU prepared from an overnight culture in LB at 37°C) in sterile sucrose sodium bicarbonate solution (20% sucrose and 2.6% sodium bicarbonate, pH 8) by oral gavage. Three days later, they were killed, and intestinal sections (ileum and colon) were collected and weighed. PBS was added to each sample (1.75 mL for ileum and colon) before homogenisation (Oligo-Macs, Miltenyi Biotec). We dispensed 140 μL of each homogenized sample into the wells of a 96-well plate and 10 μL of each individual phage was added, to reach an MOI of 1 x 10^{-2}, and the plate was incubated at 37°C. A fraction of the homogenized samples was also serially diluted in PBS and plated on Drigalski medium for the counting of *E. coli* colonies at *t*=0. Following five hours of incubation, samples were serially diluted in PBS and plated on Drigalski medium and on LB agar plates overlaid with strain 55989. Both sets of plates were incubated at 37°C overnight. The same procedure was followed for *in vitro* assays with bacteria collected during the exponential (OD_{600nm}=0.5) or stationary (24 h; equivalent OD_{600nm}=5) growth phases, at 37°C, with shaking. These cells were also incubated during 5 h with homogenized gut samples from axenic mice as a control of experiments performed with samples from monocolonized mice.

Transcriptomics

Strain 55989 was grown overnight at 37°C with shaking (n=4 replicates). Cultures were diluted in fresh medium and incubated until they reached an OD_{600nm} of about 0.5, at which point, half the volume was collected for RNA extraction, the other half being maintained at 37°C, with shaking, up to 24 h at which time point they reached an equivalent OD_{600nm} of 5, corresponding to stationary phase. RNA was extracted by centrifuging the cells and incubating them with TRIzol (Sigma T-9424) for lysis.

For intestinal samples, axenic mice received 200 μL of strain 55989 (10^7 CFU prepared from an overnight culture in LB at 37°C) in sterile sucrose sodium bicarbonate solution (20% sucrose and 2.6% sodium bicarbonate, pH 8) by oral gavage. Three days later, the mice were killed, and intestinal sections were collected and immediately frozen in liquid nitrogen (ileum and colon). TRIzol was then added to the frozen samples, which were homogenized (Oligo-Macs, Miltenyi Biotec). Total RNA from both *in vitro* and *in vivo* samples was purified by standard organic extraction (phenol/chloroform) followed by ethanol precipitation. It was then treated with the RNeasy mini kit (Qiagen) for final purification, and the remaining genomic DNA was removed with an on-column RNAse-free DNAse set protocol (Qiagen). RNA integrity was assessed with the Bioanalyser system (Agilent) and RNA integrity number (RIN) and ribosomal ratio (23S/16S) were determined. We obtained rRNA-depleted RNA with the Ribo-Zero rRNA depletion kit for eukaryotic and prokaryotic RNA (Illumina). Libraries were prepared with the TruSeq Stranded RNA LT prep kit (Illumina), with final validation

on the Bioanalyser system. Final DNA quantification was performed with sensitive fluorescence-based quantification assays ("Quant-It" assay kit and a QuBit fluorometer, Invitrogen). Librairies were then normalised to a concentration of 2 nM and multiplexed. The samples were then denatured at a concentration of 1 nM with 0.1 N NaOH at room temperature, and were finally diluted to 9.5 pM for loading onto the sequencing flowcell. Sequencing was performed on an Illumina HiSeq 2500 machine, producing 65 bp single-reads. A mean of 266 M and 2 M of reads was obtained for colonic and *in vitro* samples, respectively.

Data analysis

After sequencing, we performed a first quality check with fastQC (https://www.bioinformatics.babraham.ac.uk/projects/fastqc/), and then cleaned up the reads with cutadapt (Martin, 2011). Bowtie was used for read alignment and files were transformed into BAM and SAM formats with samtools software (Li et al., 2009). Finally, reads were counted with featureCounts and the statistical analysis was performed with R software (https://www.r-project.org/) (Gentleman et al., 2004) packages including DESeq2 (Anders and Huber, 2010; Love et al., 2014) and the SARTools package (Varet et al., 2016). Normalisation and differential analysis were performed with the DESeq2 model and package. This report comes with additional tab-delimited text files containing lists of differentially expressed features. A gene ontology analysis was performed on the lists of under- and overexpressed genes (http://geneontology.org/). Gene functions were verified with the EcoCyc database (Keseler et al., 2011). A comparative analysis was performed with a customised R script performing all possible pairwise comparisons between the gene lists for the different samples. A variance stabilizing transformation (VST) representation of the data was obtained with the DESeq2 package (Love et al., 2014). Protein-protein association networks were generated with the STRING webserver (https://string-db.org/network/) using the MG1655 strain as a template (Szklarczyk et al., 2019). Putative prophages in the *E. coli* 55989 genome were identified using PHASTER (PHAge Search Tool - Enhanced Release) (Arndt et al., 2016) and are listed below.

prediction	start	end	size (kb)
questionable	821138	866847	45.7
intact	1093207	1140290	45.0
incomplete	1408037	1417268	9.2
intact	1420060	1456075	36.0
intact	1758317	1808332	50.0
intact	2141235	2180631	39.3
intact	2664274	2710113	45.8
intact	3339788	3384869	45.0
intact	4784434	4810665	26.2

Phage efficiency of plating (EOP) test

The efficiency of plating (EOP) was calculated (ratio of the number of plaques formed by the phage on each strain tested to the number of plaques formed on the host strain 55989) for each phage. Three independent replicates were performed using bacterial cultures grown to an OD_{600nm} of approximately 0.2 and spread on LB plates onto which phage dilutions were spotted. Plates were incubated at 37°C overnight.

Adsorption assays and phage growth

Three independent adsorption assays were performed for each phage, in accordance with a previously described protocol (Chevallereau et al., 2016). Data were approximated with an exponential decay function and adsorption times were defined as the time required to reach a threshold of 10% non-adsorbed phage particles. Phage growth and bacterial lysis were assessed by diluting an overnight culture of each strain in LB broth and culturing the cells to an OD_{600nm} of 0.2. We then dispensed 140 μL of this culture into each of the wells of a 96-well plate (Microtest 96 plates, Falcon). We added 10 μL of sterile phage lysate diluted in PBS to obtain a multiplicity of infection (MOI) of 1×10^{-2} to each well. Plates were incubated in a microplate reader at 37°C, with shaking 30 s before the automatic recording of OD_{600nm} at 15-minute intervals over a period of 20 h (GloMax®-Multi Detection System, Promega, USA).

Biofilm formation and quantification

Overnight bacterial cultures were diluted 1:100 in LB medium with, when required, chloramphenicol or kanamycin, and dispensed into UV-sterilised 96-well PVC microplates. The wells located at the edge of the microplates were filled with 200 μL water to prevent evaporation during incubation in a static chamber, at 37°C, for 24 h and 48 h. Two microplates were used after 24 h, for biofilm staining and CFU counts. Biofilm staining was performed by adding 125 μL of 1% crystal violet (V5265; Sigma-Aldrich) to wells previously washed twice with water. After 15 min of staining, the crystal violet solution was removed by flicking, and biofilms were washed three times with water. For CFU counts, aggregates were homogenized within the wells by repeated pipetting and serial dilutions were

plated on LB agar plates. For the other eight microplates, the LB medium was removed at 24 h by pipetting. Two microplates were filled with LB and incubated for a further 24 h and the treated as described above for the 24 h time point. A similar pair of microplates was filled with one of the three phages ($2x10^6$ PFU in 200 μL in LB) and incubated for a further 24 h. These microplates were treated as described above for the 24 h time point. Stained microplates were left to dry overnight under a hood and the crystal violet was then resuspended in a 1:4 acetone:ethanol mixture, for the reading of absorbance at 570 nm (Tecan Infinite M200 PRO). For each microplate, we measured the OD for five technical replicates (five wells), and three to five independent experiments were performed for each strain.

Agglutination assay

The O104 immun-serum (Monospecific O Rabbit antiserum, réf #45840, lot O104L11H11, SSI Diagnostica) was used as recommended by the provider. Briefly, a volume of 700 μL of a stationary phase liquid culture of strain 55989 grown in LB at 37°C under agitation was centrifuged 10 min at 5.000g and after discarding the supernatant, the pellet was resuspended in 700 μL of PBS. This sample was heated during 80 min at 99°C and then cooled to room temperature as recommended. Then 5 μL ($1x10^7$ CFU) of this sample was introduce in different wells of a 96-well plates (Microtest 96 plates, Falcon). Then either 5 μL of PBS, or phage CLB_P1 (2.5×10^7 PFU) or phage PAK_P3 (2.5×10^7 PFU). After 10 min at room temperature either 10 μL of PBS or O104 immun-serum was added and the plate was incubated 1 h at 37°C. Next, a drop (5 μL) of each condition was put on a glass slide and covered with a cover slip for direct examination under a phase contrast microscope (Olympus IX81). Pictures were taken at X20 magnification.

QUANTIFICATION AND STATISTICAL ANALYSIS

Quantification and statistical analysis of the transcriptomics data are reported in the corresponding STAR Methods section and in the Table S1.

For the growth curves of bacterial strains (n=2 to 3 for each condition) error bars represent standard error of the mean (SEM) as indicate in the legends of Figures 4, 5, and 6. Statistical analysis on the number of bacteria and the OD_{570nm} generated by the biofilm experiments were carried out using the lme4, lmerTest and car packages of R (Bates et al., 2015; Fox and Weisberg, 2018; Kuznetsova et al., 2017). CFU were log_{10}-transformed prior to analysis. Linear mixed-models were used to account for random experimental effects (i.e. the effect of the plate and experiments). Prior analysis, normality was assessed with a QQ-plot. Overall effects were assessed with Analysis of Variance (ANOVA) and post-hoc Tukey's comparisons and were performed using the lsmeans R package (Lenth, 2016). $p < 0.05$ was considered statistically significant. The results of the comparisons are recapitulated in Tables S2A and S2B.

Cell Host & Microbe, Volume *30*

Supplemental information

The gut environment regulates bacterial gene expression which modulates susceptibility to bacteriophage infection

Marta Lourenço, Lorenzo Chaffringeon, Quentin Lamy-Besnier, Marie Titécat, Thierry Pédron, Odile Sismeiro, Rachel Legendre, Hugo Varet, Jean-Yves Coppée, Marion Bérard, Luisa De Sordi, and Laurent Debarbieux

Figure S1 related to main Figure 2. Differentially expressed genes encoded by plasmid p55989

Plasmid-encoded genes overexpressed (orange) in the colon of mice relative to cells cultured *in vitro* to the exponential and stationary growth phases. Only genes with a Log_2-fold change >2 and adjusted p-value ≤ 0.05 are represented on the plasmid map.

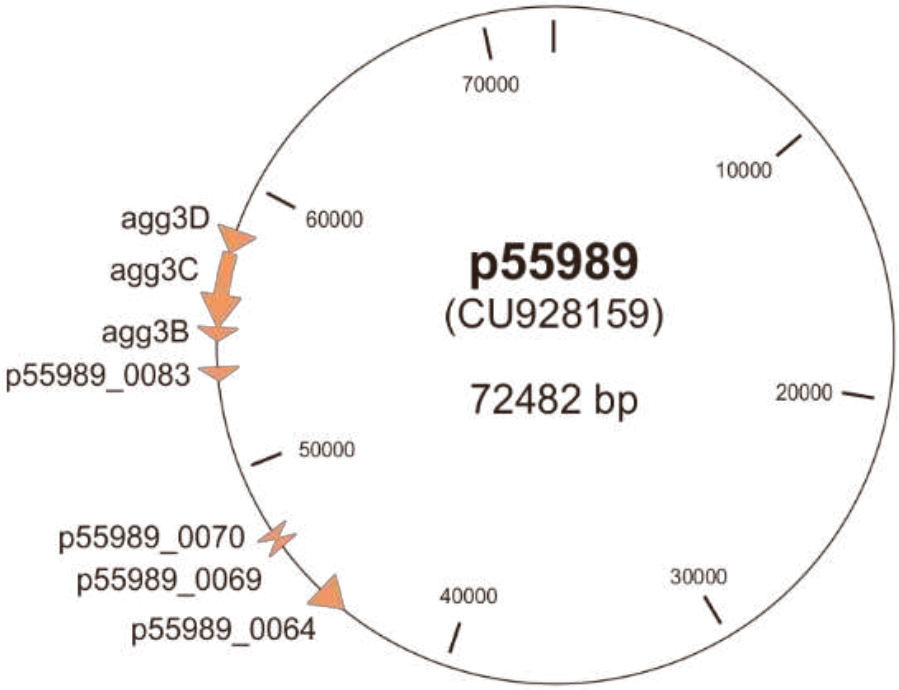

Figure S2 related to main Figure 4. Phage CLB_P1 has no impact on biofilm formation

A. Biofilm formation, reported as variations of OD_{570nm} recorded at 48 h relative to 24 h for the indicated *E. coli* strains in the presence or absence of phage CLB_P1 added at 24 h ($1x10^7$ PFU/mL) and IPTG at 0.05 mM for empty and *bssR* plasmids or 0.01 mM for the *lsrC* plasmid, as well as kanamycin; *n*=3 to 4 independent experiments. The boxes indicate the interquartile range; the horizontal bars correspond to the median and the vertical bars indicated the minimum and maximum values (within 1.5 interquartile intervals), *p*=*p*-value of the Tukey post-hoc tests (Table S6).

B. Number of CFU resuspended from biofilms recovered from microplates set up in parallel to those used for biofilm quantification shown in panel C (see methods).

C. Biofilm formation, reported as change in OD_{570nm} at 48 h relative to 24 h for the indicated *E. coli* strains in the presence or absence of phage CLB_P1 added at 24 h ($1x10^7$ PFU/mL); *n*=3 to 4 independent experiments. When necessary IPTG was added at 0.05 mM. The boxes represents the interquartile range; the horizontal bars represent the median and the vertical bars represent the minimum and maximum values (within 1.5 interquartile intervals), *p*=*p*-value for post hoc Tukey tests (Table S6).

D. Number of CFU resuspended from biofilms recovered from microplates set up in parallel with those used to quantify biofilms shown in panel C (see methods).

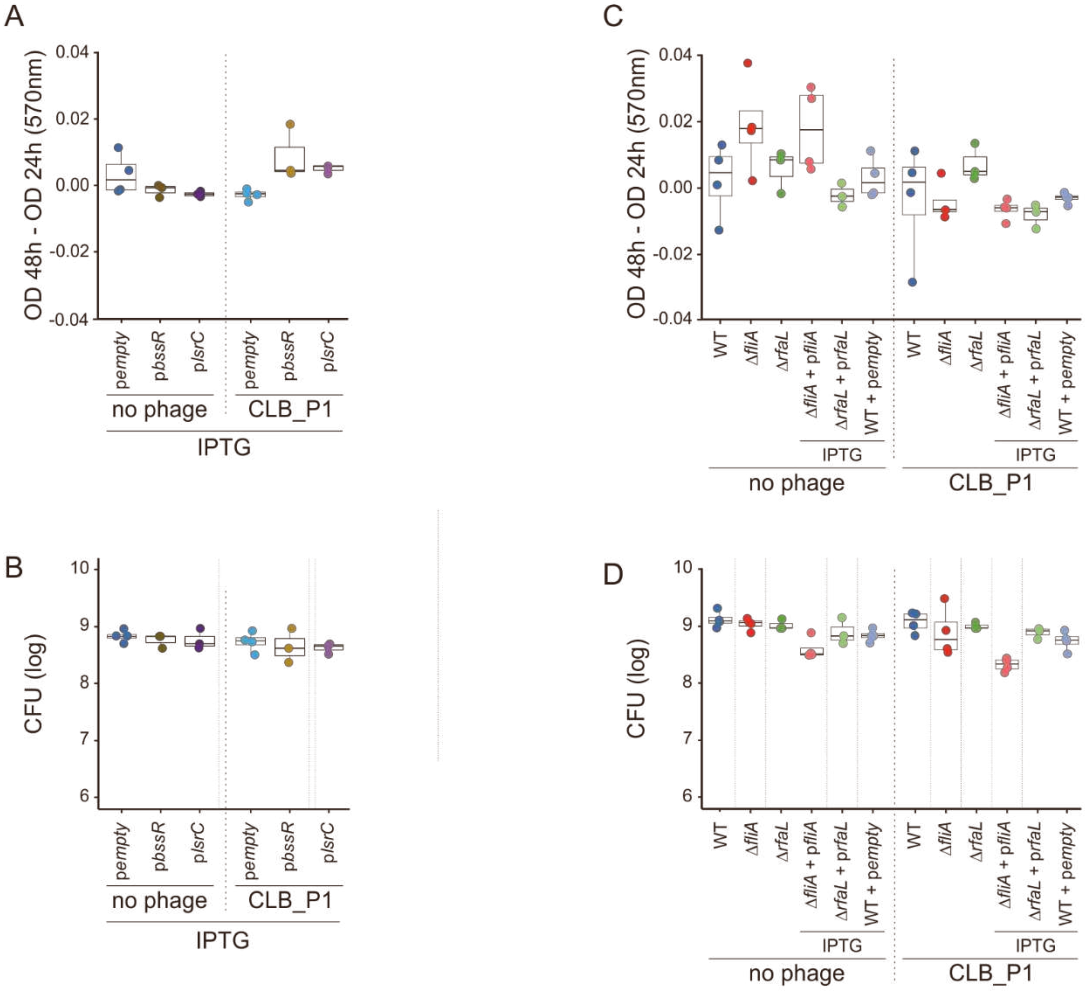

Figure S3 related to main Figure 5. Phage CLB_P2 does not alter biofilm formation of 55989Δ*fliA* or 55989Δ*rfaL* strains

A. Biofilm formation, reported as change in OD_{570nm} at 48 h relative to 24 h for the indicated *E. coli* strains in the presence or absence of phage CLB_P2 added at 24 h ($1x10^7$ PFU/mL); *n*=3 to 5 independent experiments. When necessary IPTG was added at 0.05 mM. The boxes represent the interquartile range; the horizontal bars represent the median and the vertical bars represent the minimum and maximum values (within 1.5 interquartile intervals), *p*=*p*-value for post hoc Tukey tests (Table S6).

B. Number of CFU resuspended from biofilms recovered from microplates set up in parallel with those used to quantify biofilms shown in panel C (see methods).

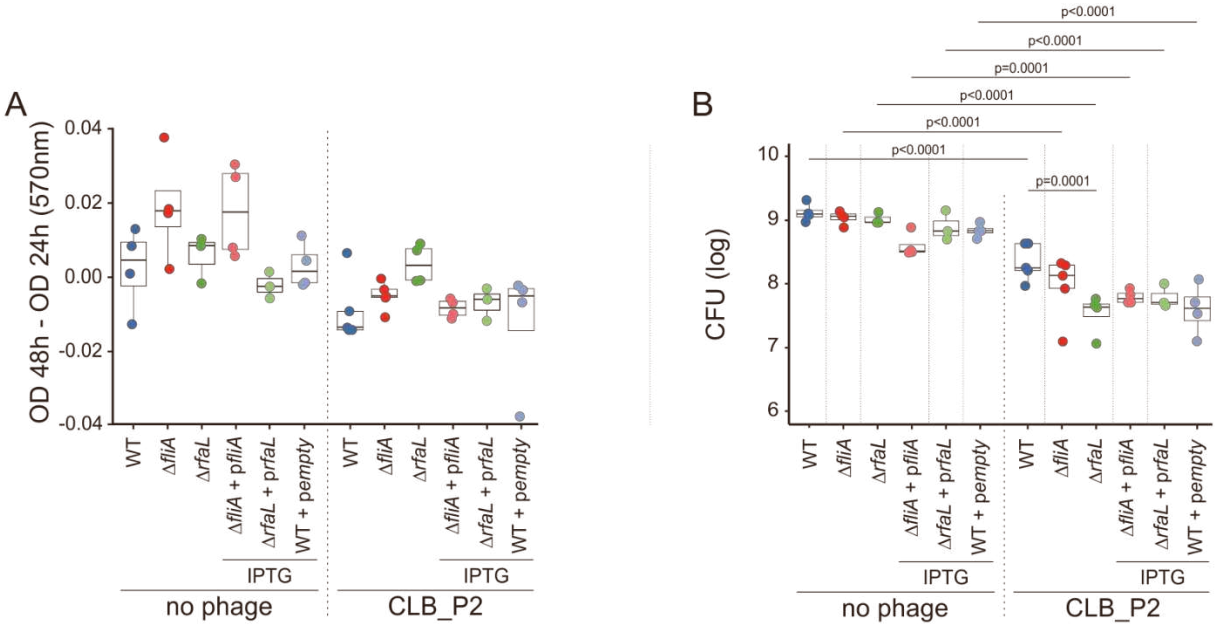

Figure S4 related to main Figure 6. Adsorption of phages CLB_P2 and CLB_P3 on 55989, 55989Δ*rfaL* and 55989Δ*fliA* cells.

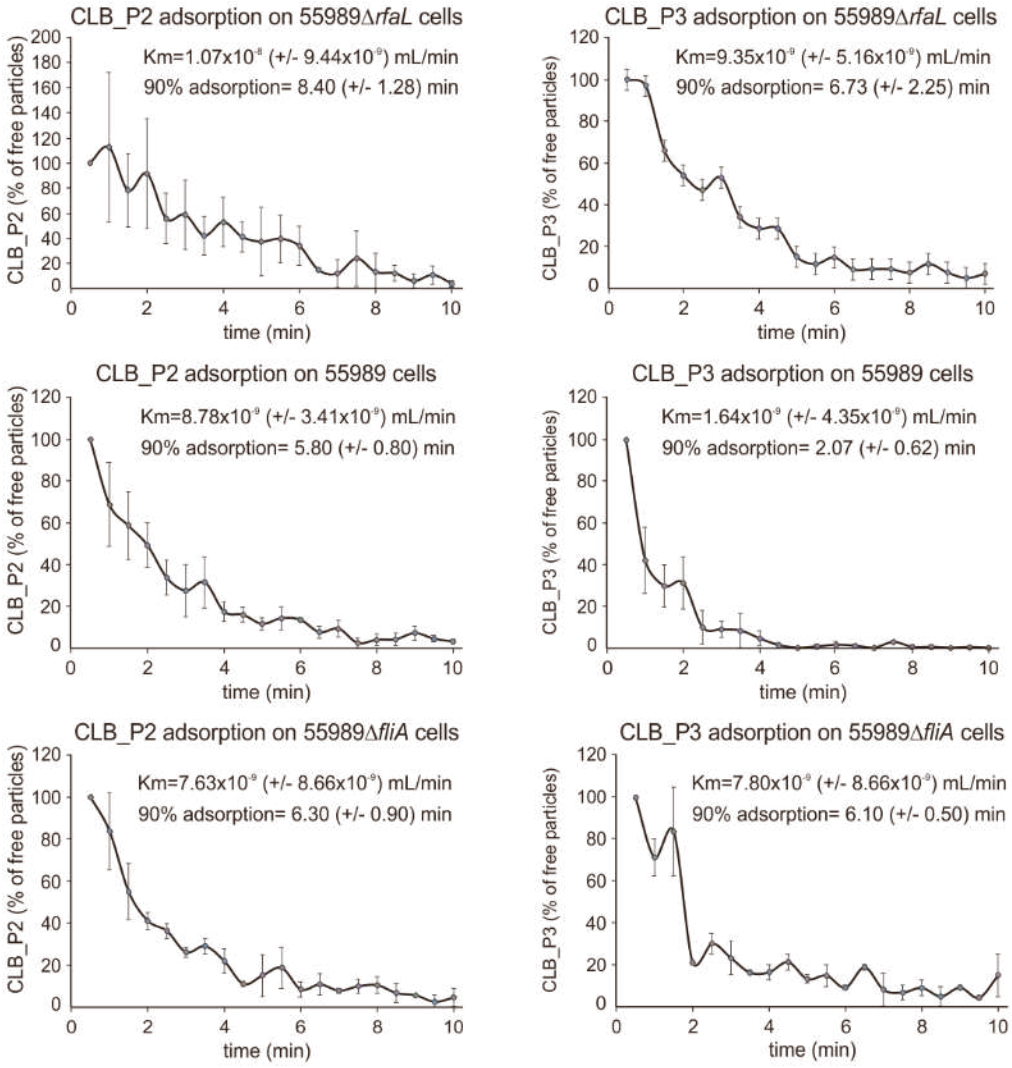

Figure S5 related to main Figure 6. Phage CLB_P3 has no impact on biofilm formation of 55989 cells overexpressing either *bssR* or *lsrC* genes

A. Biofilm formation, reported as variations of OD_{570nm} recorded at 48 h relative to 24 h for the indicated *E. coli* strains in the presence or absence of phage CLB_P3 added at 24 h ($1x10^7$ PFU/mL) and IPTG at 0.05 mM for empty and *bssR* plasmids or 0.01 mM for the *lsrC* plasmid, as well as kanamycin; *n*=3 to 4 independent experiments. The boxes indicate the interquartile range; the horizontal bars correspond to the median and the vertical bars indicated the minimum and maximum values (within 1.5 interquartile intervals), *p*=*p*-value of the Tukey post-hoc tests (Table S6).

B. Number of CFU resuspended from biofilms recovered from microplates set up in parallel to those used for biofilm quantification shown in panel C (see methods).

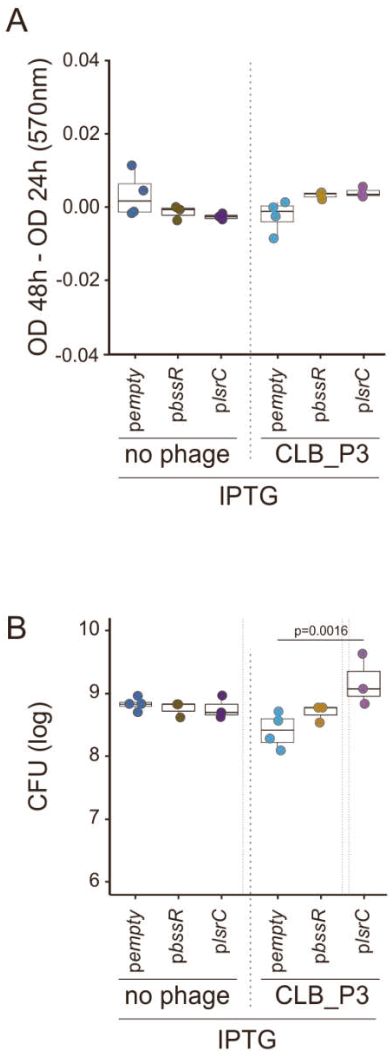

B) L'hétérogénéité spatiale de l'intestin limite la prédation et favorise la coexistence des bactéries et des bactériophages

Afin de poursuivre l'étude sur la coexistence entre bactériophages et bactéries dans l'intestin, nous avons utilisé un modèle murin disposant d'un microbiote caractérisé et stable, le modèle OMM[12]. Ces animaux ont été colonisé avec deux souches de *Escherichia coli*: *E. coli* Mt1B1, une souche bactérienne commensale murine ainsi que *E. coli* 55989 utilisée dans l'étude précédente. Dans un premier temps, nous avons vérifié que le phénotype de coexistence entre bactériophages et bactéries était reproduit avec ces deux souches chez ces souris.

Pour ceci nous avons utilisé un cocktail de trois bactériophages ciblant la souche *E. coli* Mt1B1 et le bactériophage CLB_P2 ciblant la souche *E. coli* 55989. Dans les deux cas, la coexistence a été vérifiée. De plus, aucun clone résistant à leurs bactériophages respectifs n'a été détecté. Nous avons cependant fait l'observation que le ratio de bactériophages sur bactéries était significativement diminué dans les muqueuses, par comparaison avec la lumière intestinale. Ces observations sont en accord avec le modèle écologique « source-puits » dans lequel l'hétérogénéité spatiale crée des niches où les bactéries peuvent se multiplier sans être en contact avec des bactériophages. Ainsi, lorsque ces bactéries diffusent dans le lumen certaines d'entre elles permettent aux bactériophages de se multiplier. *In fine*, la coexistence entre ces deux populations antagonistes peut se mettre en place sans émergence de clone résistant.

Ce travail a également été initié par Marta Lourenço, une ancienne doctorante qui a soutenu sa thèse en avril 2019. J'ai pu y prendre part en participant à toutes les expériences incluant la souche E. coli 55989, lors de l'analyse statistiques des résultats, la réalisation de figures et la rédaction de l'article

Article

Cell Host & Microbe

The Spatial Heterogeneity of the Gut Limits Predation and Fosters Coexistence of Bacteria and Bacteriophages

Graphical Abstract

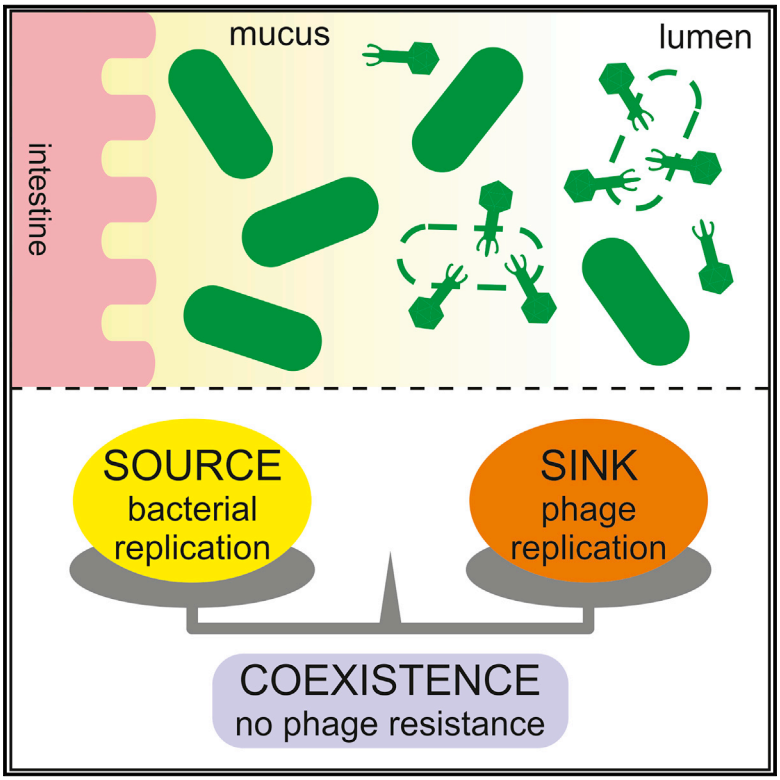

Authors

Marta Lourenço,
Lorenzo Chaffringeon,
Quentin Lamy-Besnier, ...,
Bärbel Stecher, Laurent Debarbieux,
Luisa De Sordi

Correspondence

laurent.debarbieux@pasteur.fr (L.D.),
luisa.de_sordi@
sorbonne-universite.fr (L.D.S.)

In Brief

In the gut microbiota of mammals, the long-term coexistence of antagonistic populations of bacteriophages and bacteria remains unresolved. Lourenço et al. show that the uneven spatial distribution of bacteriophages in the gut creates bacterial refuges, which may hinder the overall efficacy of phage therapy targeting intestinal pathogens.

Highlights

- Bacteriophage/bacteria coexistence is reproduced in murine gut with synthetic microbiota
- Bacteriophage resistant clones are not detected over time throughout the gut
- Coexistence is not linked to off-target bacteriophage amplification
- Spatial distribution and source-sink dynamics support phage-bacteria coexistence

Lourenço et al., 2020, Cell Host & Microbe *28*, 390–401
September 9, 2020
https://doi.org/10.1016/j.chom.2020.06.002

CellPress

CellPress

Cell Host & Microbe

Article

The Spatial Heterogeneity of the Gut Limits Predation and Fosters Coexistence of Bacteria and Bacteriophages

Marta Lourenço,[1,2] Lorenzo Chaffringeon,[1,3] Quentin Lamy-Besnier,[1,4] Thierry Pédron,[1] Pascal Campagne,[5] Claudia Eberl,[6] Marion Bérard,[7] Bärbel Stecher,[6,8] Laurent Debarbieux,[1,9,*] and Luisa De Sordi[1,3,*]

[1]Bacteriophage, Bacterium, Host Laboratory, Department of Microbiology, Institut Pasteur, Paris 75015, France
[2]Sorbonne Université, Collège Doctoral, Paris 75005, France
[3]Sorbonne Université, Centre de Recherche St Antoine, INSERM UMRS_938, Paris, France
[4]Université Paris Descartes, Paris, France
[5]Bioinformatics and Biostatistics Hub, Institut Pasteur, Paris 75015, France
[6]Max von Pettenkofer Institute of Hygiene and Medical Microbiology, Faculty of Medicine, Ludwig Maximilian University of Munich, Munich, Germany
[7]Institut Pasteur, DTPS, Animalerie Centrale, Centre de Gnotobiologie, Paris 75724, France
[8]German Center for Infection Research (DZIF), Partner Site Munich, Munich, Germany
[9]Lead Contact
*Correspondence: laurent.debarbieux@pasteur.fr (L.D.), luisa.de_sordi@sorbonne-universite.fr (L.D.S.)
https://doi.org/10.1016/j.chom.2020.06.002

SUMMARY

The ecological dynamics underlying the coexistence between antagonistic populations of bacteria and their viruses, bacteriophages (phages), in the mammalian gut microbiota remain poorly understood. We challenged a murine synthetic bacterial community with phages to study the factors allowing phages-bacteria coexistence. Coexistence was not dependent on the development of phage-resistant clones nor on the ability of phages to extend their host range. Instead, our data suggest that phage-inaccessible sites in the mucosa serve as a spatial refuge for bacteria. From there, bacteria disseminate in the gut lumen where they are predated by luminal phages fostering the presence of intestinal phage populations. The heterogeneous biogeography of microbes contributes to the long-term coexistence of phages with phage-susceptible bacteria. This observation could explain the persistence of intestinal phages in humans as well as the low efficiency of oral phage therapy against enteric pathogens in animal models and clinical trials.

INTRODUCTION

The mammalian gut is a highly complex and structured organ lined by a variety of eukaryotic cell types that serve the establishment of a mutualistic relationship between the host and different enteric microbes, including viruses. Bacteriophages (phages) are the most abundant viruses residing in the gut, but their precise role in shaping the microbiome remains unclear (Manrique et al., 2017). Changes in the viral and bacterial communities of the gut are increasingly reported to be associated with pathological conditions in humans, including diabetes, inflammatory bowel diseases, and colorectal cancer (Hannigan et al., 2018b; Manrique et al., 2017; Zhao et al., 2017). Although fluctuations in the viral communities have been reported in a recent longitudinal study in humans, a large proportion of individual-specific viral contigs remain detectable over time (months to years), suggesting that individuals possess their own viral fingerprint (Manrique et al., 2016; Shkoporov et al., 2019). However, it remains understudied how phages and their corresponding bacterial targets persist together in the gut.

Using phage-bacterial model systems, dynamics of the coexistence of predators and preys have been the subject of theoretical and experimental studies, mostly performed *in vitro* and *in silico* (Betts et al., 2014; Brockhurst et al., 2006; Hannigan et al., 2018a; Lenski and Levin, 1985; Weitz et al., 2013). In the mammalian gut, the interaction of phages and bacteria has been explored in mice and pigs (Galtier et al., 2016; Looft et al., 2014; Maura et al., 2012a, 2012b; Reyes et al., 2013; Weiss et al., 2009; Yen et al., 2017), while human data are derived from metagenomics studies (Manrique et al., 2017; Shkoporov et al., 2019) and few clinical trials of phage therapy (Sarker and Brüssow, 2016).

Studies in mice have shown that virulent phages have a limited effect on the targeted bacterial populations within the gut (Bhandare et al., 2019; Galtier et al., 2017; Maura et al., 2012a; Weiss et al., 2009). Nevertheless, both phage and bacterial populations could persist in the gut of animals for several weeks (Maura and Debarbieux, 2012; Maura et al., 2012b). Likewise, a large randomized phage therapy trial targeting *Escherichia coli* diarrhea in Bangladeshi children showed no

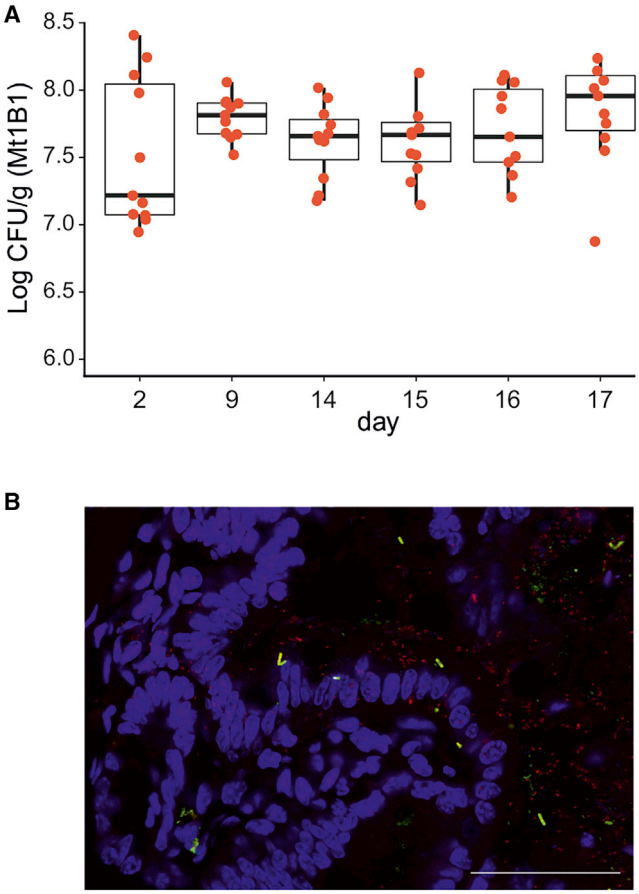

Figure 1. The *E. coli* Strain Mt1B1 Stably Colonizes the Gut of the OMM^{12} Mice

(A) Fecal levels of the *E. coli* strain Mt1B1 at the indicated time points for each OMM^{12} mouse (n = 11) receiving a single dose of 10^8 CFU by oral gavage at d0. Red dots, individual values; horizontal bar, median; box, 25th–75th quantiles, vertical bars, min and max values (within 1.5 × interquartile interval).

(B) Localization by FISH of the strain Mt1B1 in the ileal section of Mt1B1-colonized OMM^{12} mice. Intestinal cells (nuclei) were stained with DAPI (purple), Mt1B1 (red + green = yellow), and Eubacteria (red) were stained with specific FISH probes. A representative image from a group of four mice is presented. Scale bar, 50 μm. See also Figure S1.

evidence for *in vivo* amplification of oral phages in the gut despite their persistence (Sarker et al., 2016). A similar situation was described in the human gut where the crAssphage coexists with its highly abundant Bacteriodetes bacterial host (Guerin et al., 2018; Shkoporov et al., 2018; Yutin et al., 2018). Three recent studies showed that administration of virulent phages can also strongly impact the intestinal colonization of their targeted bacteria and nevertheless, still support long-term coexistence (Duan et al., 2019; Gogokhia et al., 2019; Hsu et al., 2019). The experimental settings of these studies could account for differences in the amplitude of the impact, notably because of the use of axenic mice, characterized by an immature immune system, and thus, unstable colonization of bacteria of human origin. Moreover, the limited number of phages and bacteria couples that have been studied in the gut environment does not allow yet drawing conclusions on the type and prominence of factors that influence phage-bacterium interactions.

Since phages are proposed as a treatment for the major public health threat of antibiotic-resistant bacterial infections (Roach and Debarbieux, 2017) as well as means to precisely engineer the intestinal microbiota, further insight into the variety of phage-bacterium interactions and their coexistence in the mammalian gut are deeply needed (Brüssow, 2017). Several factors were shown or proposed to be involved in this coexistence, such as (1) arms race dynamics with resistance development to phage infection and viral counter-resistance, (2) the inherent or evolved ability of the phage to infect multiple hosts, and (3) the distribution of these two antagonistic populations into distinct spatial structures (Brockhurst et al., 2006; De Sorti et al., 2017; Doron et al., 2018; Heilmann et al., 2012; Hilborn, 1975; Labrie et al., 2010). In this report, we investigated the contribution of these factors using the synthetic oligo-mouse-microbiota comprising 12 distinct strains (OMM^{12}) (Brugiroux et al., 2016).

This animal model allows following defined pairs of phages and bacteria in the gut without the need of antibiotic treatments as a confounding factor commonly used to study enteric pathogens in murine models (Croswell et al., 2009). In addition, it provides more realistic conditions than mono-colonized mice that lack aspects of competitive and synergistic interspecies interactions of microbes (Weiss et al., 2009). We established stable colonization of two *E. coli* strains in gnotobiotic OMM^{12} mice and studied the population dynamics of these strains in the presence of virulent phages. We found that phages were less abundant in the mucosal part of the gut compared with *E. coli* levels. Our data are in agreement with the ecological theory of source-sink dynamics (Holt, 1985), providing an explanation for the lack for phage-resistant mutant selection and the limited efficacy of virulent phages in reducing intestinal bacterial loads.

RESULTS

E. coli Commensal Strain Mt1B1 Colonizes the Gut of OMM^{12} Mice

Mice harboring the OMM^{12} consortium (*Acutalibacter muris*, *Akkermansia muciniphila*, *Bacteroides caecimuris*, *Bifidobacterium longum subsp animalis*, *Blautia coccoides*, *Clostridium clostridioforme*, *Clostridium innocuum*, *Enterococcus faecalis*, *Flavonifractor plautii*, *Lactobacillus reuteri*, *Muribaculum intestinale*, and *Turicimonas muris*) were exposed to the murine *E. coli* commensal strain Mt1B1 to test its capacity to establish in this synthetic community. Mice became colonized with this strain within 2 to 3 days. The fecal levels of strain Mt1B1 remained stable over a period of 2 weeks (Figure 1A). Mice did not exhibit signs of discomfort or change in feces consistency. Twelve days after inoculation of strain Mt1B1, intestinal sections (ileum and colon) were examined, and the location of strain Mt1B1 was determined by fluorescence *in situ* hybridization (FISH) (Figures 1B and S1). Strain Mt1B1 was found in all sections of the gut, including the ileum, consistent with the location from which it was isolated (mucosa from the ileum of conventional laboratory mice) (Garzetti et al., 2018; Lagkouvardos et al., 2016).

Table 1. Main Characteristics of Mt1B1 Phages P3, P10, and P17

	Mt1B1_P3	Mt1B1_P10	Mt1B1_P17
Family	*Podoviridae*	*Podoviridae*	*Myoviridae*
Subfamily	*Autographivirinae*	*Autographivirinae*	unclassified
Genus	Teseptimavirus	Zindervirus	unclassified
Genome size (kb)	40.3	45.4	151.2
Number of predicted ORFs	47	54	284
Genes unknown function (%)	40.4	64.3	94.7
Affinity constant ($mL.min^{-1}$)	$5.26 \times 10^{-10} \pm 2.8 \times 10^{-10}$	$4.60 \times 10^{-10} \pm 2.15 \times 10^{-10}$	$1.83 \times 10^{-10} \pm 5.60 \times 10^{-11}$
Adsorption of 90% of phage (min)	2.8 ± 0.14	2.03 ± 0.19	5.53 ± 1.28

Selected Virulent Phages Replicate Only on Strain Mt1B1 in the Gut Environment of OMM^{12} Mice

We isolated several phages infecting strain Mt1B1 from the environment and selected three (Mt1B1_P3, Mt1B1_P10, and Mt1B1_P17) with different characteristics (host range, adsorption and lysis kinetics, and genomic content) (Figure S2; Tables 1, S1, S2, and S3). Both, Podoviridae P3 and P10 are close to *E. coli* phages K1F and K1E, respectively, which are capsule-specific phages. Myoviridae P17 is closely related to *E. coli* phages phAPEC8 and ESCO13. Like ESCO13 and by contrast to phAPEC8, Mt1B1_P17 does not carry an endo-N-acetylneuraminidase gene involved in the degradation of the K1 capsule and, therefore, is most likely not capsule specific (Trotereau et al., 2017). In liquid broth phages P3 and P10 displayed similar infection kinetics patterns on strain Mt1B1, with rapid lysis followed by a moderate bacterial regrowth at 1.5 h. In contrast, phage P17 halted the growth of strain Mt1B1 for several hours and slow bacterial regrowth resumed only after more than 10 h (Figure 2A). When used in combination, these three phages caused rapid lysis of strain Mt1B1 followed by very slow regrowth (Figure 2A). Then, we assessed the capacity of each phage to replicate in gut sections collected from Mt1B1-colonized OMM^{12} mice in an *ex vivo* assay previously used to reveal the activities of phages along different gut sections (Galtier et al., 2017; Maura et al., 2012a). We collected samples of the ileum and colon from Mt1B1-colonized OMM^{12} mice. We then separated out the mucosal and luminal parts of the ileum and colonic tissues. We compared the replication of the three phages in these samples *ex vivo* with their replication on Mt1B1 planktonic cultures, at both exponential and stationary growth phases. All three phages displayed similar patterns with efficient replication in all tested gut sections and in exponential growth phase liquid culture, whereas no amplification was observed in cells at stationary phase (Figure 2B). As strain Mt1B1 did not multiply in the stationary growth phase (gray bars in Figure 2B), we concluded that Mt1B1 cell growth is necessary for amplification of these three phages.

Next, we evaluated the transit time of Mt1B1 phages at 6, 24, 48, and 72 h in axenic mice that received a single oral dose (6×10^7 plaque-forming unit [PFU]) of a mixture of the three phages (equal amounts of each phage). The fecal level of Mt1B1 phages was below the threshold at 6 h, maximum at 24 h and then decreased at 48 h and finally reached the limit of detection at 72 h (Figure 3A). In gut sections, we found that the level of phages at 6 h reached 10^6, 10^4, and 10^3 PFU/g in the luminal part of the ileum, the mucosal part of the ileum, and the luminal part of the colon, respectively, whereas it remained undetected in the mucosal part of the colon. At 24 h the level of phages in the ileum dropped, whereas it increased in the colon, and at 48 h it was barely detectable in the ileum while only present in the luminal part of the colon. At 72 h the level of phages was below the threshold of detection in all gut sections tested (Figure 3B). Then, we performed a similar experiment in OMM^{12} mice, not inoculated with strain Mt1B1, by taking samples at 24 and 48 h post-gavage (same dose as above). Phage levels in feces were slightly lower than those observed in axenic mice. We could detect phages only in the luminal part of the colon at both 24 and 48 h post-gavage as anticipated from experiments with axenic mice (Figure 3C). These findings indicate that none of the Mt1B1 phages amplified *in vivo* on any of the 12 strains ruling out a possible off-target amplification. These data are in agreement with previous results on phage safety from human volunteers and from conventional mice not colonized with the targeted bacteria (Bruttin and Brüssow, 2005; Maura et al., 2012b; Weiss et al., 2009).

In Vivo Infection of Mt1B1-Colonized OMM^{12} Mice by a Phage Cocktail

We next investigated how Mt1B1-colonized OMM^{12} mice responded to an identical single oral dose of the three phages (6×10^7 PFU). The fecal levels of phages and bacteria were monitored at short (4 and 6 h post-oral dose) and long (during 2 weeks) periods of time (Figure S3A). At all time points but one (day 18 [d18]) following phage administration, levels of Mt1B1 in the phage group were lower than in the control group, despite remaining within one-log of variation and not reaching significance. Within the two weeks of observation phage levels fluctuated within 2 logs (Figure S3B). Nevertheless, phage:bacteria ratios remained stable (less than 1 log variation) over time (Figure S3C). These data show that a single dose of these three phages is sufficient to initiate their long-term replication in Mt1B1-colonized OMM^{12} mice indicating that this animal model is suitable to study the coexistence of phages and bacteria in the gut.

Afterward, we asked whether repeating the phages administration during three consecutive days could disturb this coexistence between phages and strain Mt1B1. Such a setting mimics a phage therapy treatment targeting bacterial pathogens residing in the human gut (Corbellino et al., 2020). In two independent experiments, we observed a

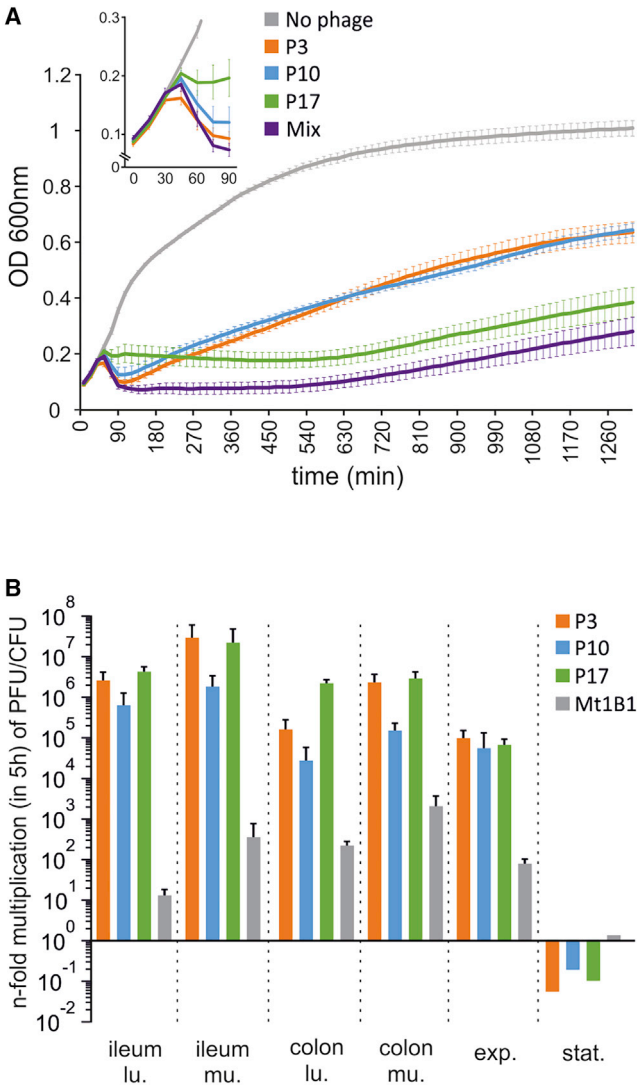

Figure 2. Mt1B1 Phages P3, P10, and P17 Infect Strain Mt1B1 Both *In Vitro* and *Ex Vivo*

(A) Growth curves for strain Mt1B1 (n = 3 for each condition) measured via OD_{600nm} reading in liquid broth in the absence (gray) or presence of phage P3 (orange), P10 (blue), or P17 (green), or of a cocktail of these three phages (purple; equal proportions of each) added at t = 0 at multiplicity of infection (MOI) of 1×10^{-2}. The inset shows an enlargement for early time points. (Error bars represent standard error of the mean, SEM)

(B) Amplification over 5 h (n = 3 biological replicates) of individual phages (P3, orange; P10, blue; P17, green; each at an MOI of 1×10^{-2}) and Mt1B1 cells (gray) in indicated homogenized gut sections (lu, luminal; mu, mucosal) from Mt1B1-colonized OMM^{12} mice (*ex vivo*) and flasks with Mt1B1 cells in exponential (exp.) (OD_{600nm} = 0.5) or stationary (stat.; 24 h) growth phases (*in vitro*). N-fold multiplication relative to the initial number of phages added at t = 0, which was approximately 100-fold lower than the amount of Mt1B1 cells, is shown. The n-fold multiplication of strain Mt1B1 was calculated by plating samples before and after the 5-h incubation (means with standard deviation).

small but significant decrease in the fecal levels of strain Mt1B1 when comparing phage-treated and control groups (d15, p = 0.0001; d16, p = 0.002; d17, p = 0.023) (Figure 4A; Table S4). Despite this significant impact, phage levels and phage:bacteria ratios remained stable (within 1-log) (Figures 4B and 4C) and were comparable to data obtained with a single dose of phages showing that the three consecutive phage administrations did not destabilize phage-bacteria coexistence (Figure S3).

Phage Replication Does Not Trigger Shifts in the OMM^{12} Bacterial Community

We next assessed the stability of the gut microbiota of both phage-treated (n = 6) and non-treated (n = 5) mice groups by two methods, 16S rRNA specific qPCR (Brugiroux et al., 2016) and 16S amplicon sequencing. This quantification was performed at d0 (before colonization with strain Mt1B1), d14 (before the gavage with the three phages), and d17 (1 day after the third phages gavage), and both methods showed similar results (Figure S4). Changes in the bacterial community (qPCR data) were analyzed by performing a between-class principal component analysis (PCA), taking into account days, cages, and phage inoculation. Results identified daily fluctuations as the main source of the observed variations regardless of the presence or absence of phages (Figure 4D; Table S5). This finding is also consistent with the passive transit of these phages in OMM^{12} devoid of *E. coli* strain Mt1B1 (Figure 3C). Therefore, the replication of phages observed in Mt1B1-colonized OMM^{12} mice result exclusively from their capacity to infect strain Mt1B1 in the gut environment, confirming the lack of a possible off-target amplification to support phage coexistence.

Maintenance of Bacterial Populations Is Not Caused by the Emergence of Phage-Resistant Clones

Next, we tested whether the emergence of phage-resistant clones could explain how bacteria can coexist with phages. A total of 280 isolated fecal clones of strain Mt1B1 from 13 mice exposed to the three phages cocktail (from both short and long-term colonization) were susceptible to each of the three phages. We also tested for the emergence of phage-resistant clones from several gut sections (luminal and mucosal parts from ileum and colon). Again, all of these clones (n = 800) were susceptible to each of the three phages. Thus, phage resistance development does not explain the maintenance of susceptible bacterial populations in presence of phages.

Heterogeneous Spatial Localization of Bacteria in the Gut Can Explain Phage-Bacteria Coexistence

In the absence of evidence for off-target phage amplification on heterologous bacteria and a lack of support for the emergence of phage-resistant bacteria, we wondered whether the spatial heterogeneity of the mammalian gut might create niches where bacteria remain protected against phage predation (Heilmann et al., 2012). We tested this hypothesis by examining luminal and mucosal parts from ileum and colon sections from Mt1B1-colonized OMM^{12} mice exposed or not to phages. Compared with Mt1B1 titers in control mice, phage cocktail application was associated with small but significant Mt1B1 titer decreases in both, the luminal and mucosal parts of the ileum and the mucosal part of the colon (Figure 4E; Table S4). This indicates that these regions harbor Mt1B1 cells susceptible to phage infection. We observed an average of 2-log and 1-log lower phage titers in the mucosal compared with the luminal parts of the ileum and colon, respectively (Figure 4F). Consequently, in mucosal

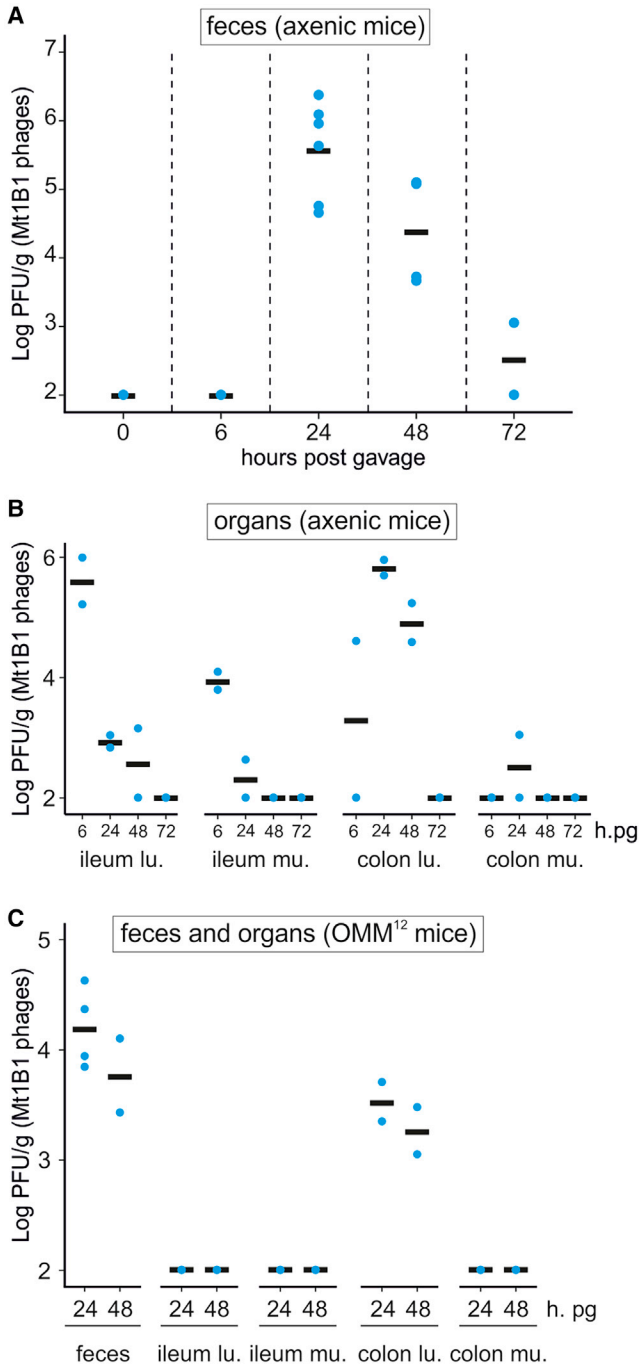

Figure 3. Passive Phage Transit in Axenic and OMM^{12} Mice

Axenic (n = 8) and OMM^{12} (n = 4) mice received a single dose of the three Mt1B1 phages (3 × 10^7 PFU; phages mixed in equal proportions). Phage titers were determined in fecal pellets and intestinal sections at indicated time points. Dots represent individual data and horizontal bars represent the average.

(A) Fecal phage titers from axenic mice.

(B) Phage titers in organs from axenic mice.

(C) Phage titers from OMM^{12} mice feces and organs.

parts we found a parallel reduction of the density of both phages and bacteria. However, phage:bacteria ratios revealed a significant (p = 0.006) lower relative abundance of phages in the mucosal part of the ileum suggesting that at this location some Mt1B1 bacteria might not be exposed to phages (Figure 4G; Table S4). We concluded that a heterogeneous spatial localization of strain Mt1B1 in the ileum reduces accessibility to phages by providing phage-free refuges.

Coexistence of a Single Phage (CLB_P2) with Its Targeted Bacterium (*E. coli* Strain 55989) Is Also Explained by Spatial Refuges

To challenge and strengthen the causal role of spatial localization of bacteria in their coexistence with virulent phages, we investigated the behavior of the Myoviridae phage CLB_P2 infecting the human pathobiont enteroaggregative *E. coli* strain 55989. This phage was previously shown to efficiently infect strain 55989 in gut sections and to coexist with it over 3 weeks (Maura and Debarbieux, 2012; Maura et al., 2012b). First, we showed that strain 55989 colonizes the gut of OMM^{12} mice (Figure S5A) as previously reported in conventional mice (Maura et al., 2012b) and did likewise not result in any sign of intestinal disease. Second, when 55989-colonized OMM^{12} mice received a single oral dose of phage CLB_P2 (1 × 10^8 PFU) we observed that fecal levels of strain 55989 in presence or absence of phage CLB_P2 were similar around 10^8 CFU/g and the phage titers remained stable around 10^7 PFU/g (Figures 5A and 5B), showing that this model reproduces conditions for stable phage:bacteria ratios (Figure 5C). No significant difference in the fecal levels of strain 55989 was observed on individual days between phage CLB_P2-treated and control groups (Table S6). However, the ANOVA comparison between these two groups, when including the 3 days, reached significance (p = 0.0268) (Table S7). Third, we examined the luminal and mucosal parts of both ileum and colon from 55989-colonized OMM^{12} mice 3 days after the administration of the single dose of phage CLB_P2. In all sections, but the mucosal part of the colon, the level of strain 55989 was significantly lower in the phage CLB_P2 group than in the control group (Figure 5D; Table S6). Phage CLB_P2 levels were similar in all sections except in the mucosal part of the ileum in which it was about 2-log lower (Figure 5E). Phage CLB_P2:strain 55959 ratios in gut sections indicate a significant difference between luminal and mucosal parts of the ileum, whereas no such difference was observed in the colon (Figure 5F; Table S6). Fourth, we tested 165 and 822 colonies isolated from feces and gut sections, respectively, for their susceptibility to phage CLB_P2 and found that they were all susceptible, showing that development of phage resistance to a single phage could not explain the maintenance of susceptible bacterial populations in presence of this phage (Figure S5B). In addition, we determined the frequency of phage-resistant clones in fecal pellets from 55989-colonized OMM12 mice that received either phage CLB_P2 or PBS and found that they were at the same range for both groups and equivalent to the frequency obtained with a fresh culture of strain 55989 (Table S7).

To support further our conclusions, we quantified the abundance of strain 55989 in unwashed gut sections using immunohistochemistry (Figures 6A and S6). We found no difference in the abundance of strain 55989 in the mucosal parts of both ileal

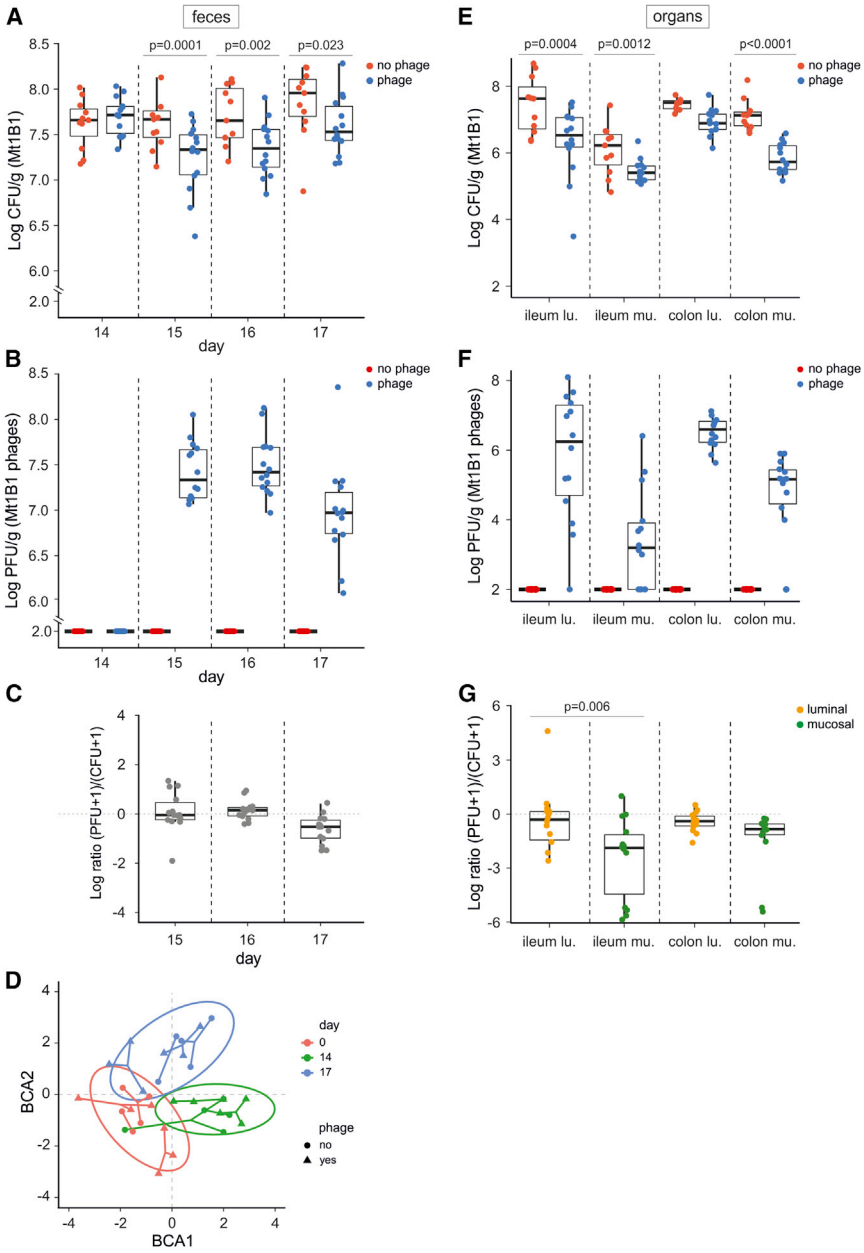

Figure 4. Virulent Mt1B1 Phages Do Not Affect the Microbiota Composition of the OMM^{12} Mice and Display an Heterogeneous Repartition in Gut Sections Supporting Their Coexistence with Strain Mt1B1

Mt1B1-colonized OMM^{12} mice (n = 25) received at d14, d15, and d16 PBS (red, n = 11) or the three Mt1B1 phages P3, P10, and P17 together (blue, n = 14; 6 × 10^7 PFU per dose made of the same amount of each phage) by oral gavage.

(A) Levels of *E. coli* strain Mt1B1 in the feces.

(B) Titers of Mt1B1 phages in the fecal samples reported in (A).

(C) Phage:bacteria ratios for fecal samples collected on d15, d16, and d17.

(D) Between-group PCA (BCA, axes 1 and 2) for the 16S rRNA qPCR data for mice receiving PBS (n = 5, filled circle) or the phage cocktail (n = 6, filled triangle) by oral gavage at the indicated time points (see the colors indicated) for 10 bacteria from the fecal microbiota of OMM^{12} mice (strains YL2 and KB18 were not detected). On d17 mice were sacrificed and gut section analyzed.

(E) Levels of the *E.coli* strain Mt1B1 in indicated gut sections (lu, luminal; mu, mucosal).

(F) Titers of Mt1B1 phages in the samples reported in (E).

(G) Phage:bacteria ratios for the indicated gut sections reported in (E and F).

Dots, individual values; horizontal bar, median; box, 25th–75th quantiles, vertical bars, min and max values (within 1.5 × interquartile interval). See also Tables S4 and S5.

and colonic sections from phage CLB_P2-treated mice compared with controls, which is in agreement with the presence of bacterial refuges on the mucosal parts of the gut (Figure 6B; Table S8). In the luminal parts of both ileum and colonic sections the abundance of strain 55989 (quantified by fluorescence intensity) was not different between the two conditions, while a significant difference was reached when comparing colony-forming unit (CFU) data (Figure 5D). This underlines the difficulty to compare indirect (microscopy) with direct (plating) quantifications. To conclude, the lower abundance of phages in the mucosal parts of the ileum provides opportunities for bacteria to reside in phage-free niches thus escaping phage predation. Taken together, data from two independent models (Mt1B1- and 55989-colonized OMM^{12} mice) using different phages show that the biogeography of bacteria participates to the coexistence of phages and phage-susceptible bacteria in the gut.

DISCUSSION

The intestinal microbiota of mammals is relatively stable over time in healthy subjects while it contains large antagonistic populations of bacteria and phages. The mechanisms that underlie this apparently peaceful coexistence are unknown. Several hypotheses can be drawn from years of *in vitro* studies of isolated systems (one phage/one bacterium) or more recently from environmental studies (Buckling and Rainey, 2002; Fortuna et al., 2019; Horne, 1970; Laanto et al., 2017; Meyer et al., 2016). However, none of them has yet been tested in a relevant intestinal environment. Using a gnotobiotic mouse model, two *E. coli* strains, and four different virulent phages, we showed that the emergence of phage-resistant bacteria and the possibility to infect off-target bacteria can be excluded as major factors supporting coexistence. Instead, we found that the spatial distribution of phages and bacteria along the radial axis of the gut fits the classical ecological theory of source-sink dynamics (Holt, 1985). Our data suggest that refuges for bacteria in the mucosal layer serve

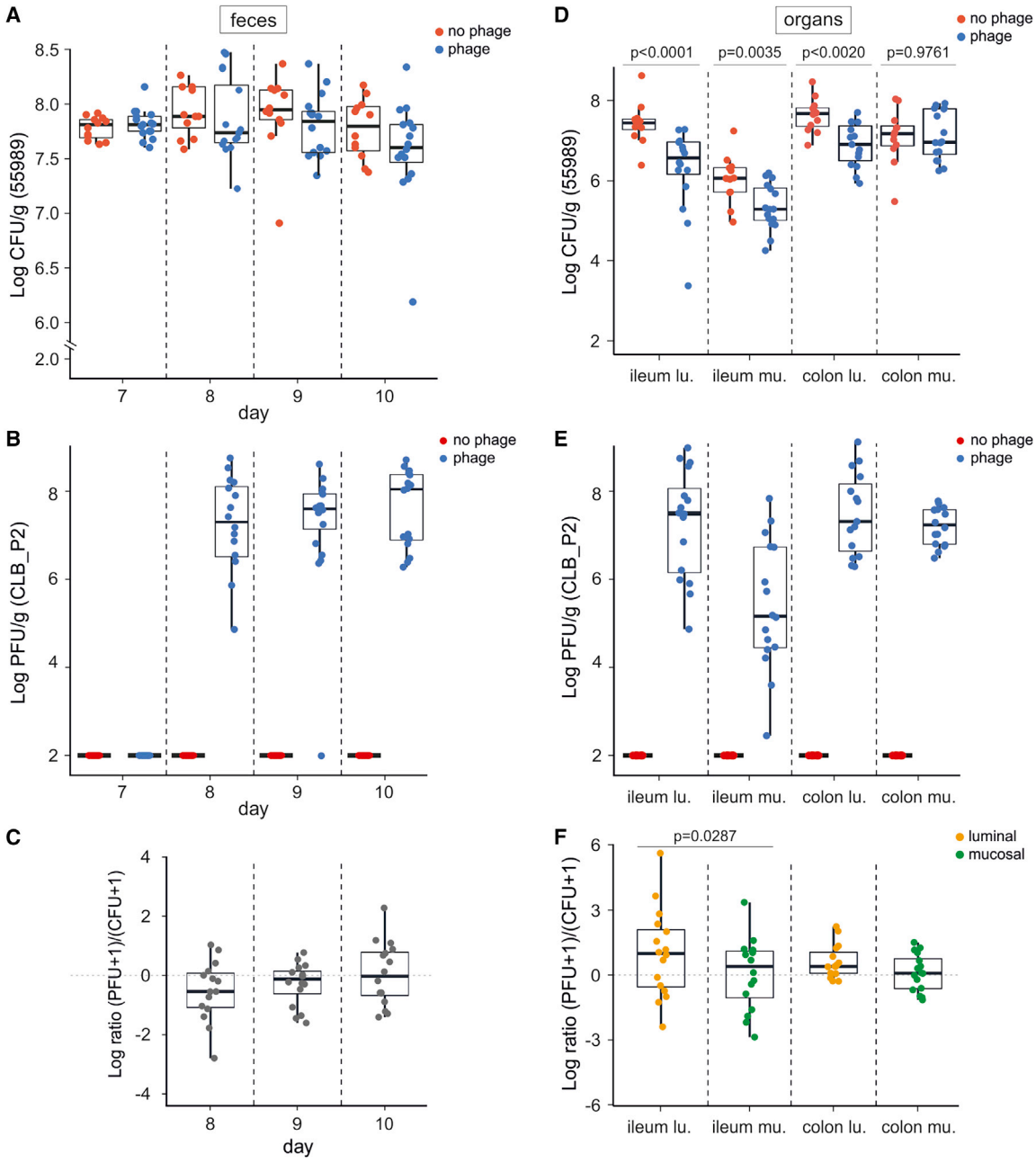

Figure 5. Spatial Heterogeneity of the *E. coli* Strain 55989 in the Gut Sections Participates to the Coexistence with Virulent Phage CLB_P2

OMM[12] mice (n = 28) were colonized with the *E. coli* strain 55989 during 7 days before receiving a single administration of PBS (red, n = 12) or phage CLB_P2 (blue, n = 16; 1 × 10^8 PFU) by oral gavage.

(A) Levels of the *E. coli* strain 55989 in the feces.

(B) Phage CLB_P2 titers from the fecal samples reported in (A).

(C) Phage:bacteria ratios for fecal samples collected on d8, d9, and d10. On d10 mice were sacrificed and gut section analyzed.

(D) Levels of the *E. coli* strain 55989 in indicated gut sections

(E) Titers of phage CLB_P2 in the samples reported in (D).

(F) Phage:bacteria ratios for the indicated gut sections reported in (D and E).

Dots, individual values; horizontal bar, median; box, 25th–75th quantiles, vertical bars, min and max values (within 1.5 × interquartile interval). See also Table S6.

as a source, with the lumen acting as a sink in which the phages can infect their target. As phages do not exert a major direct selective pressure on the source, the bacteria reaching the gut lumen remain susceptible enabling the phages to maintain their density in the lumen over time (Figure 6C). This different luminal-mucosal distribution of phages was significant in ileal but not in

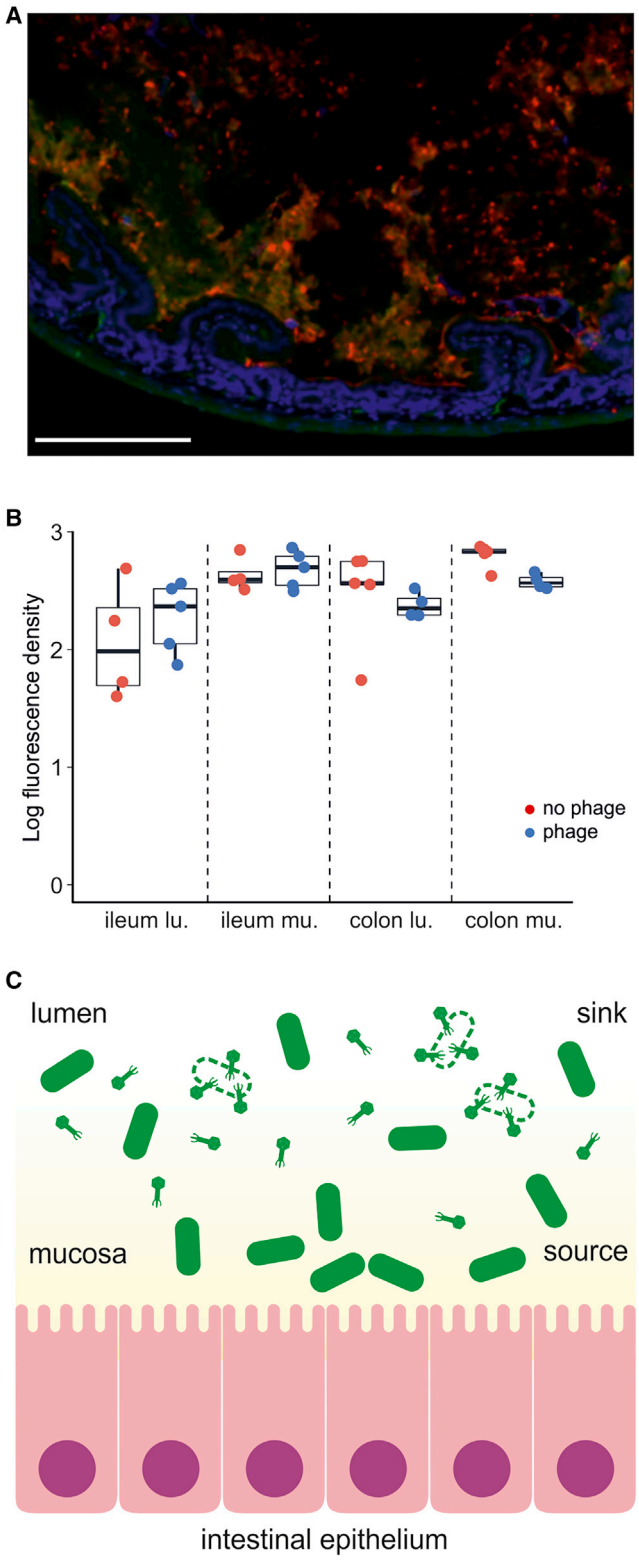

Figure 6. Source-Sink Dynamics Support the Coexistence of Virulent Phages and Bacteria in the Gut

(A) Representative photograph (scale bar, 200 μm) of immunofluorescence staining of strain 55989 (red) and mucus (green) in unwashed ileum section with nuclei of epithelial cells stained with DAPI (blue).

(B) Quantification of the red fluorescence per pixel in mucosal and luminal parts of ileal and colonic sections from 55989-colonized OMM^{12} mice at d10 (n = 4 to 5). Dots, individual values; horizontal bar, median; box, 25th–75th quantiles, vertical bars, min/max values (within 1.5 × interquartile interval).

(C) Schematic representation of the source-sink dynamics between virulent phage and bacteria populations in the gut. Bacteria located close to the mucosal layer (in yellow) form refuges that phages cannot reached. Bacteria located in the intestinal lumen are killed (dotted lines) by phages that can persist through the gut. Bacteria and phage populations coexist without the strong selection of phage-resistant bacteria.

colonic sections. This might not be the case in the human colon that displays organizational differences compared with mice colon, the latter being essentially filled with structured fecal pellets in which phage-bacteria interactions are likely to be less intense (Nguyen et al., 2015).

In phage-bacteria interaction studies, the prey-predator dynamics have been classically studied through the prism of phage-resistant bacteria and counter resistant phages. Recently, an *in vitro* study has proposed the model named "leaky resistance" to explain the maintenance of virulent phages by the high rate of transitions between phage-resistant and phage-susceptible bacteria within the populations (Chaudhry et al., 2018; Silveira and Rohwer, 2016). However, we failed to isolate phage-resistant bacteria within the entire gut during this work performed with two couples of phages and bacteria. This suggests that phage-resistant bacteria may, *in vivo*, either carry a high cost or have a low selective value in both single and repeated phage application (Gómez and Buckling, 2011; Koskella et al., 2012). Coupled with the concept of costly phage resistance mutations, our results are in agreement with observations from *in silico* individual-based stochastic spatial models, which showed that structured environments can create spatial refuges that lead to coexistence between bacteria and phages without the emergence of resistant clones (Heilmann et al., 2012; Sousa and Rocha, 2019).

The lower abundance of phages in the mucosal parts could be triggered by the reduced bacterial density compared with luminal parts, according to a density-dependent phenomenon that was previously observed in several *in vitro* structured environments (Eriksen et al., 2018). This density-dependent phenomenon was linked to the "proliferation threshold", which proposes that a minimum number of bacteria is needed for phages to initiate infection and amplify (Payne et al., 2000; Wiggins and Alexander, 1985). Note that the source-sink and the "proliferation threshold" hypotheses are not mutually exclusive to support the presence of bacterial refuges driving the long-term coexistence of phages and susceptible bacteria. We propose that the gut displays a mucosal-luminal gradient of phage density exposing bacterial populations to different phage concentrations (Figure 6C). Such a gradient can explain the persistence for months and years of phage populations in human fecal samples without major variations of the microbiota composition.

Nevertheless, the heterogeneous spatial distribution of bacteria in the gut does not exclude other factors or processes that could also participate to the long-term coexistence of phage with susceptible bacteria. Some of these processes were not directly tackled in this study like the influence of

abiotic factors (Lourenço et al., 2018; Scanlan et al., 2019). In particular, phenotypic resistance that is described as the ability of bacteria to oscillate between phage-susceptible and phage-resistant cells could be involved in some of our observations. This phenotypic resistance is led by environmental or cellular stochasticity that modulate the expression of genes, for example those encoding for phage receptors (Bull et al., 2014; Chapman-McQuiston and Wu, 2008). Phage diffusion may be limited by mucins and other glycoproteins, lipids, and DNA molecules (Johansson et al., 2011; Qi et al., 2017). Immunoglobulin motifs in structural phage proteins were also shown to favor phage binding to mucus (Barr et al., 2013). However, only ORF118 of phage Mt1B1_P17 possesses such a motif (identified by a specific *in silico* search) homologous to the bacterial immunoglobin (Ig)-like domain (Big_2) (bit score = 29.5, individual E value = 5.1×10^{-9} and conditional E value = 2.8×10^{-11}) (Fraser et al., 2006). The absence of such motifs in three out of the four phages and in particular in CLB_P2 is consistent with our *in vivo* observation that these phages are less abundant in the mucosal parts of gut sections.

Our data show that the gnotobiotic OMM^{12} model is particularly well suited to study the mechanisms involved in phage-bacteria dynamics in the gut. OMM^{12} community establishes a long-term stable composition over several mouse generations and can be used as platform to flexibly incorporate additional bacterial strains (Brugiroux et al., 2016; Herp et al., 2019; Studer et al., 2016). Interestingly, Hsu and colleagues recently reported the use of similar synthetic microbiota models to study phage-bacteria interactions with two major differences. First, axenic mice were inoculated with bacterial strains during 2 weeks before the inoculation of phages, compared with stably colonized OMM^{12} mice. Second, the 10 bacterial strains chosen are from human origin, instead of mouse origin for OMM^{12}, and may rapidly undergo genetic adaptation to the mouse environment (Barroso-Batista et al., 2014; Lourenço et al., 2016). Despite these differences, both mouse models confirm that the inoculation of virulent phages in the gut generally leads to the coexistence of phages and bacteria. Hsu et al. found that *Enterococcus faecalis* phage-resistant mutants increased over time and that the microbial community structure was affected. Here, we could not detect any of these two events. In addition, they found that some phages have strong impact on abundance of cognate host bacteria, while such impact was not previously observed in several mouse models (Maura et al., 2012a; Weiss et al., 2009). This suggests that different phage-bacteria couples may exhibit distinct eco-evolutionary dynamics, increasing the complexity of studying these interactions in natural environments (Shkoporov and Hill, 2019). A recent example of such complexity was reported when studying the *in vivo* prophage induction of *Roseburia intestinalis*, a dominant bacterium of the human gut, which leads to the coexistence of phages and bacteria with the selection of CRISPR-mediated bacterial resistance along with hypervirulent phage variants (Cornuault et al., 2019).

Deciphering the dynamics of phage-bacteria interactions in the gut is required to develop efficient phage-guided therapeutic strategies and ultimately obtain firm clinical evidences that are still lacking for intestinal infections (Brüssow, 2017; Duan et al., 2019; Sarker et al., 2016). A recent case report showed that the *in vitro* isolation of a single virulent phage, used to target a multidrug resistant strain of *Klebsiella pneumoniae*, led to the eradication of this pathogen from the patient's gut (Corbellino et al., 2020). While lacking mechanistic insights, this work confirms the medical potential of phages to selectively target bacteria residing in the gut.

STAR★METHODS

Detailed methods are provided in the online version of this paper and include the following:

- KEY RESOURCES TABLE
- RESOURCE AVAILABILITY
  - Lead Contact
  - Materials Availability
  - Data and Code Availability
- EXPERIMENTAL MODEL AND SUBJECT DETAILS
  - Microorganisms
  - Animals and Ethics
- METHOD DETAILS
  - Phage Isolation
  - Host Range Tests
  - Adsorption Assays and Phage Growth
  - Phage Genomes Sequencing and Analysis
  - Search for Ig-like Domains on Phage Genomes
  - *Ex Vivo* Phage Replication Assay
  - Passive Phages Transit in Axenic and OMM^{12} Mice
  - Murine Model of *E. coli* Colonization
  - Identification of Resistant Clones
  - Histological Analysis by FISH and Immunochemistry
  - OMM^{12} Community Composition
- QUANTIFICATION AND STATISTICAL ANALYSIS

SUPPLEMENTAL INFORMATION

Supplemental Information can be found online at https://doi.org/10.1016/j.chom.2020.06.002.

ACKNOWLEDGMENTS

We thank Harald Brüssow for critically reading the manuscript and Jorge Moura de Sousa for valuable discussion and opinion on early versions of the manuscript. We thank Dwayne Roach and Anne Chevallereau for valuable discussions. We thank Sean Benler for kindly sharing the comprehensive HMM database of Ig-like domains identified on Pfam database. We thank the members of the Centre for Gnotobiology Platform of the Institut Pasteur (Thierry Angélique, Eddie Maranghi, Martine Jacob, and Marisa Gabriela Lopez Dieguez) for their help with the animal work. We thank Cédric Fund for 16S libraries and sequencing from the Biomics Platform, C2RT, Institut Pasteur, Paris, France, supported by France Génomique (ANR-10-INBS-09-09) and IBISA. M.L. is part of the Pasteur - Paris University (PPU) International PhD Program. M.L. is funded by Institut Carnot Pasteur Maladie Infectieuse (ANR 11-CARN 017-01). L.D.S. is funded by a Roux-Cantarini fellowship from the Institut Pasteur (Paris, France). L.C. is funded by a PhD fellowships from the Ministère de l'Enseignement Supérieur et de la Recherche, France, École Doctorale n°394. Q.L.-B. is funded by École Doctorale FIRE - Program Bettencourt. B.S. is supported by the German Center of Infection Research (DZIF), the Center for Gastrointestinal Microbiome Research (CEGIMIR), the DFG, Germany, Priority

Programme SPP1656 (STE 1971/4-2 and STE 1971/6-1), and the Collaborative Research Center CRC 1371.

AUTHOR CONTRIBUTIONS

Conceptualization, L.D., L.D.S., and M.L.; Methodology, B.S., L.D., L.D.S., M.B., and M.L.; Investigation, C.E., L.C., L.D.S., M.L., Q.L.-B., and T.P.; Formal Analysis, L.C., M.L., and P.C.; Writing – Original Draft, L.D., L.D.S., and M.L.; Writing – Review & Editing, B.S., L.C., L.D., L.D.S., and M.L.; Funding Acquisition, B.S., L.D., and M.B.; Resources, B.S., M.B., L.D., and P.C.; Supervision, L.D. and L.D.S.

DECLARATION OF INTERESTS

The authors declare no competing interests.

Received: November 21, 2019
Revised: March 30, 2020
Accepted: June 2, 2020
Published: July 1, 2020

REFERENCES

Adriaenssens, E., and Brister, J.R. (2017). How to name and classify your phage: an informal guide. Viruses *9*, 70.

Aziz, R.K., Bartels, D., Best, A.A., DeJongh, M., Disz, T., Edwards, R.A., Formsma, K., Gerdes, S., Glass, E.M., Kubal, M., et al. (2008). The RAST Server: rapid annotations using subsystems technology. BMC Genomics *9*, 75.

Barr, J.J., Auro, R., Furlan, M., Whiteson, K.L., Erb, M.L., Pogliano, J., Stotland, A., Wolkowicz, R., Cutting, A.S., Doran, K.S., et al. (2013). Bacteriophage adhering to mucus provide a non-host-derived immunity. Proc. Natl. Acad. Sci. USA *110*, 10771–10776.

Barroso-Batista, J., Sousa, A., Lourenço, M., Bergman, M.L., Sobral, D., Demengeot, J., Xavier, K.B., and Gordo, I. (2014). The first steps of adaptation of Escherichia coli to the gut are dominated by soft sweeps. PLoS Genet. *10*, e1004182.

Bates, D., Machler, M., Bolker, B.M., and Walker, S.C. (2015). Fitting linear mixed-effects models using lme4. J. Stat. Softw. *67*, 1–48.

Betts, A., Kaltz, O., and Hochberg, M.E. (2014). Contrasted coevolutionary dynamics between a bacterial pathogen and its bacteriophages. Proc. Natl. Acad. Sci. USA *111*, 11109–11114.

Bhandare, S., Colom, J., Baig, A., Ritchie, J.M., Bukhari, H., Shah, M.A., Sarkar, B.L., Su, J., Wren, B., Barrow, P., and Atterbury, R.J. (2019). Reviving phage therapy for the treatment of cholera. J. Infect. Dis. *219*, 786–794.

Brockhurst, M.A., Buckling, A., and Rainey, P.B. (2006). Spatial heterogeneity and the stability of host-parasite coexistence. J. Evol. Biol. *19*, 374–379.

Brugiroux, S., Beutler, M., Pfann, C., Garzetti, D., Ruscheweyh, H.J., Ring, D., Diehl, M., Herp, S., Lötscher, Y., Hussain, S., et al. (2016). Genome-guided design of a defined mouse microbiota that confers colonization resistance against Salmonella enterica serovar Typhimurium. Nat. Microbiol. *2*, 16215.

Brüssow, H. (2017). Phage therapy for the treatment of human intestinal bacterial infections: soon to be a reality? Expert Rev. Gastroenterol. Hepatol. *11*, 785–788.

Bruttin, A., and Brüssow, H. (2005). Human volunteers receiving Escherichia coli phage T4 orally: a safety test of phage therapy. Antimicrob. Agents Chemother. *49*, 2874–2878.

Buckling, A., and Rainey, P.B. (2002). Antagonistic coevolution between a bacterium and a bacteriophage. Proc. Biol. Sci. *269*, 931–936.

Bull, J.J., Vegge, C.S., Schmerer, M., Chaudhry, W.N., and Levin, B.R. (2014). Phenotypic resistance and the dynamics of bacterial escape from phage control. PLoS One *9*, e94690.

Chapman-McQuiston, E., and Wu, X.L. (2008). Stochastic receptor expression allows sensitive bacteria to evade phage attack. Part I: experiments. Biophys. J. *94*, 4525–4536.

Chaudhry, W.N., Pleška, M., Shah, N.N., Weiss, H., McCall, I.C., Meyer, J.R., Gupta, A., Guet, C.C., and Levin, B.R. (2018). Leaky resistance and the conditions for the existence of lytic bacteriophage. PLoS Biol. *16*, e2005971.

Chevallereau, A., Blasdel, B.G., De Smet, J., Monot, M., Zimmermann, M., Kogadeeva, M., Sauer, U., Jorth, P., Whiteley, M., Debarbieux, L., and Lavigne, R. (2016). Next-generation "-omics" approaches reveal a massive alteration of host RNA metabolism during bacteriophage infection of Pseudomonas aeruginosa. PLoS Genet. *12*, e1006134.

Corbellino, M., Kieffer, N., Kutateladze, M., Balarjishvili, N., Leshkasheli, L., Askilashvili, L., Tsertsvadze, G., Rimoldi, S.G., Nizharadze, D., Hoyle, N., et al. (2020). Eradication of a multi-drug resistant, carbapenemase-producing Klebsiella pneumoniae isolate following oral and intra-rectal therapy with a custom-made, lytic bacteriophage preparation. Clin. Infect. Dis. *70*, 1998–2001.

Cornuault, J.K., Moncaut, E., Loux, V., Mathieu, A., Sokol, H., Petit, M.-A., and Paepe, M.D. (2019). The enemy from within: a prophage of Roseburia intestinalis systematically turns lytic in the mouse gut, driving bacterial adaptation by CRISPR spacer acquisition. bioRxiv. https://doi.org/10.1101/575076v1.

Croswell, A., Amir, E., Teggatz, P., Barman, M., and Salzman, N.H. (2009). Prolonged impact of antibiotics on intestinal microbial ecology and susceptibility to enteric Salmonella infection. Infect. Immun. *77*, 2741–2753.

De Sorti, L., Khanna, V., and Debarbieux, L. (2017). The Gut Microbiota Facilitates Drifts in the Genetic Diversity and Infectivity of Bacterial Viruses. Cell Host Microbe. *22*, 801–808.

Doron, S., Melamed, S., Ofir, G., Leavitt, A., Lopatina, A., Keren, M., Amitai, G., and Sorek, R. (2018). Systematic discovery of antiphage defense systems in the microbial pangenome. Science *359*, eaar4120.

Dray, S., and Dufour, A. (2007). The ade4 package: implementing the duality diagram for ecologists. J. Stat. Softw. *22*, 1–20.

Duan, Y., Llorente, C., Lang, S., Brandl, K., Chu, H., Jiang, L., White, R.C., Clarke, T.H., Nguyen, K., Torralba, M., et al. (2019). Bacteriophage targeting of gut bacterium attenuates alcoholic liver disease. Nature *575*, 505–511.

Eriksen, R.S., Svenningsen, S.L., Sneppen, K., and Mitarai, N. (2018). A growing microcolony can survive and support persistent propagation of virulent phages. Proc. Natl. Acad. Sci. USA *115*, 337–342.

Fortuna, M.A., Barbour, M.A., Zaman, L., Hall, A.R., Buckling, A., and Bascompte, J. (2019). Coevolutionary dynamics shape the structure of bacteria-phage infection networks. Evolution *73*, 1001–1011.

Fox, J., and Weisberg, S. (2019). An R Companion to Applied Regression, Second Edition (SAGE Publications).

Fraser, J.S., Yu, Z., Maxwell, K.L., and Davidson, A.R. (2006). Ig-like domains on bacteriophages: a tale of promiscuity and deceit. J. Mol. Biol. *359*, 496–507.

Galtier, M., De Sordi, L., Maura, D., Arachchi, H., Volant, S., Dillies, M.A., and Debarbieux, L. (2016). Bacteriophages to reduce gut carriage of antibiotic resistant uropathogens with low impact on microbiota composition. Environ. Microbiol. *18*, 2237–2245.

Galtier, M., De Sordi, L., Sivignon, A., de Vallée, A., Maura, D., Neut, C., Rahmouni, O., Wannerberger, K., Darfeuille-Michaud, A., Desreumaux, P., et al. (2017). Bacteriophages targeting adherent invasive Escherichia coli strains as a promising new treatment for Crohn's disease. J. Crohns Colitis *11*, 840–847.

Garneau, J.R., Depardieu, F., Fortier, L.C., Bikard, D., and Monot, M. (2017). PhageTerm: a tool for fast and accurate determination of phage termini and packaging mechanism using next-generation sequencing data. Sci. Rep. *7*, 8292.

Garzetti, D., Eberl, C., and Stecher, B. (2018). Complete genome sequencing of the mouse intestinal isolate Escherichia coli Mt1B1. Genome Announc. *6*, e00426–18.

Gogokhia, L., Buhrke, K., Bell, R., Hoffman, B., Brown, D.G., Hanke-Gogokhia, C., Ajami, N.J., Wong, M.C., Ghazaryan, A., Valentine, J.F., et al. (2019). Expansion of bacteriophages is linked to aggravated intestinal inflammation and colitis. Cell Host Microbe *25*, 285–299.e8.

Gómez, P., and Buckling, A. (2011). Bacteria-phage antagonistic coevolution in soil. Science *332*, 106–109.

Guerin, E., Shkoporov, A., Stockdale, S.R., Clooney, A.G., Ryan, F.J., Sutton, T.D.S., Draper, L.A., Gonzalez-Tortuero, E., Ross, R.P., and Hill, C. (2018). Biology and Taxonomy of crAss-like bacteriophages, the most abundant virus in the human gut. Cell Host Microbe *24*, 653–664.e6.

Hannigan, G.D., Duhaime, M.B., Koutra, D., and Schloss, P.D. (2018a). Biogeography and environmental conditions shape bacteriophage-bacteria networks across the human microbiome. PLoS Comput. Biol. *14*, e1006099.

Hannigan, G.D., Duhaime, M.B., Ruffin, M.T.t., Koumpouras, C.C., and Schloss, P.D. (2018b). Diagnostic potential and interactive dynamics of the colorectal cancer virome. mBio *9*, e02248-18.

Heilmann, S., Sneppen, K., and Krishna, S. (2012). Coexistence of phage and bacteria on the boundary of self-organized refuges. Proc. Natl. Acad. Sci. USA *109*, 12828–12833.

Henry, M., Lavigne, R., and Debarbieux, L. (2013). Predicting in vivo efficacy of therapeutic bacteriophages used to treat pulmonary infections. Antimicrob. Agents Chemother. *57*, 5961–5968.

Herp, S., Brugiroux, S., Garzetti, D., Ring, D., Jochum, L.M., Beutler, M., Eberl, C., Hussain, S., Walter, S., Gerlach, R.G., et al. (2019). Mucispirillum schaedleri antagonizes Salmonella virulence to protect mice against colitis. Cell Host Microbe *25*, 681–694.e8.

Hilborn, R. (1975). The effect of spatial heterogeneity on the persistence of predator-prey interactions. Theor. Popul. Biol. *8*, 346–355.

Holt, R.D. (1985). Population-dynamics in two-patch environments: some anomalous consequences of an optimal habitat distribution. Theor. Popul. Biol. *28*, 181–208.

Horne, M.T. (1970). Coevolution of Escherichia coli and bacteriophages in chemostat culture. Science *168*, 992–993.

Hsu, B.B., Gibson, T.E., Yeliseyev, V., Liu, Q., Lyon, L., Bry, L., Silver, P.A., and Gerber, G.K. (2019). Dynamic modulation of the gut microbiota and metabolome by bacteriophages in a mouse model. Cell Host Microbe *25*, 803–814.e5.

Johansson, M.E., Ambort, D., Pelaseyed, T., Schütte, A., Gustafsson, J.K., Ermund, A., Subramani, D.B., Holmén-Larsson, J.M., Thomsson, K.A., Bergström, J.H., et al. (2011). Composition and functional role of the mucus layers in the intestine. Cell. Mol. Life Sci. *68*, 3635–3641.

Koskella, B., Lin, D.M., Buckling, A., and Thompson, J.N. (2012). The costs of evolving resistance in heterogeneous parasite environments. Proc. Biol. Sci. *279*, 1896–1903.

Kuznetsova, A., Brockhoff, P.B., and Christensen, R.H.B. (2017). lmerTest package: tests in linear mixed effects models. J. Stat. Soft. *82*, 1–26.

Laanto, E., Hoikkala, V., Ravantti, J., and Sundberg, L.R. (2017). Long-term genomic coevolution of host-parasite interaction in the natural environment. Nat. Commun. *8*, 111.

Labrie, S.J., Samson, J.E., and Moineau, S. (2010). Bacteriophage resistance mechanisms. Nat. Rev. Microbiol. *8*, 317–327.

Lagkouvardos, I., Pukall, R., Abt, B., Foesel, B.U., Meier-Kolthoff, J.P., Kumar, N., Bresciani, A., Martínez, I., Just, S., Ziegler, C., et al. (2016). The mouse intestinal bacterial collection (miBC) provides host-specific insight into cultured diversity and functional potential of the gut microbiota. Nat. Microbiol. *1*, 16131.

Lenski, R.E., and Levin, B.R. (1985). Constraints on the coevolution of bacteria and virulent phage: a model, some experiments, and predictions for natural communities. The American Naturalist *125*, 585–602.

Lenth, R.V. (2016). Least-squares means: the R package lsmeans. J. Stat. Softw. *69*, 1–33.

Looft, T., Allen, H.K., Cantarel, B.L., Levine, U.Y., Bayles, D.O., Alt, D.P., Henrissat, B., and Stanton, T.B. (2014). Bacteria, phages and pigs: the effects of in-feed antibiotics on the microbiome at different gut locations. ISME J. *8*, 1566–1576.

Lourenço, M., De Sordi, L., and Debarbieux, L. (2018). The diversity of bacterial lifestyles hampers bacteriophage tenacity. Viruses *10*, 327.

Lourenço, M., Ramiro, R.S., Güleresi, D., Barroso-Batista, J., Xavier, K.B., Gordo, I., and Sousa, A. (2016). A mutational hotspot and strong selection contribute to the order of mutations selected for during Escherichia coli adaptation to the gut. PLoS Genet. *12*, e1006420.

Manrique, P., Bolduc, B., Walk, S.T., van der Oost, J., de Vos, W.M., and Young, M.J. (2016). Healthy human gut phageome. Proc. Natl. Acad. Sci. USA *113*, 10400–10405.

Manrique, P., Dills, M., and Young, M.J. (2017). The human gut phage community and its implications for health and disease. Viruses *9*, 141.

Maura, D., and Debarbieux, L. (2012). On the interactions between virulent bacteriophages and bacteria in the gut. Bacteriophage *2*, 229–233.

Maura, D., Galtier, M., Le Bouguénec, C., and Debarbieux, L. (2012a). Virulent bacteriophages can target O104:H4 enteroaggregative Escherichia coli in the mouse intestine. Antimicrob. Agents Chemother. *56*, 6235–6242.

Maura, D., Morello, E., du Merle, L., Bomme, P., Le Bouguénec, C., and Debarbieux, L. (2012b). Intestinal colonization by enteroaggregative Escherichia coli supports long-term bacteriophage replication in mice. Environ. Microbiol. *14*, 1844–1854.

Meyer, J.R., Dobias, D.T., Medina, S.J., Servilio, L., Gupta, A., and Lenski, R.E. (2016). Ecological speciation of bacteriophage lambda in allopatry and sympatry. Science *354*, 1301–1304.

Mossoro, C., Glaziou, P., Yassibanda, S., Lan, N.T.P., Bekondi, C., Minssart, P., Bernier, C., Le Bouguénec, C., and Germani, Y. (2002). Chronic Diarrhea, Hemorrhagic Colitis, and Hemolytic-Uremic Syndrome Associated With HEp-2 Adherent Escherichia Coli in Adults Infected With Human Immunodeficiency Virus in Bangui, Central African Republic. J Clin Microbiol. *40*, 3086–3088.

Nguyen, T.L., Vieira-Silva, S., Liston, A., and Raes, J. (2015). How informative is the mouse for human gut microbiota research? Dis. Model Mech. *8*, 1–16.

Payne, R.J., Phil, D., and Jansen, V.A. (2000). Phage therapy: the peculiar kinetics of self-replicating pharmaceuticals. Clin. Pharmacol. Ther. *68*, 225–230.

Pickard, D.J. (2009). Preparation of bacteriophage lysates and pure DNA. Methods Mol. Biol. *502*, 3–9.

Potter, S.C., Luciani, A., Eddy, S.R., Park, Y., Lopez, R., and Finn, R.D. (2018). HMMER web server: 2018 update. Nucleic Acids Res. *46*, W200–W204.

Qi, C., Li, Y., Yu, R.Q., Zhou, S.L., Wang, X.G., Le, G.W., Jin, Q.Z., Xiao, H., and Sun, J. (2017). Composition and immuno-stimulatory properties of extracellular DNA from mouse gut flora. World J. Gastroenterol. *23*, 7830–7839.

Quereda, J.J., Dussurget, O., Nahori, M.A., Ghozlane, A., Volant, S., Dillies, M.A., Regnault, B., Kennedy, S., Mondot, S., Villoing, B., et al. (2016). Bacteriocin from epidemic Listeria strains alters the host intestinal microbiota to favor infection. Proc. Natl. Acad. Sci. USA *113*, 5706–5711.

Reyes, A., Wu, M., McNulty, N.P., Rohwer, F.L., and Gordon, J.I. (2013). Gnotobiotic mouse model of phage-bacterial host dynamics in the human gut. Proc. Natl. Acad. Sci. USA *110*, 20236–20241.

Roach, D.R., and Debarbieux, L. (2017). Phage therapy: awakening a sleeping giant. Emerging Top. Life Sci. *1*, 93–103.

Sarker, S.A., and Brüssow, H. (2016). From bench to bed and back again: phage therapy of childhood Escherichia coli diarrhea. Ann. N. Y. Acad. Sci. *1372*, 42–52.

Sarker, S.A., Sultana, S., Reuteler, G., Moine, D., Descombes, P., Charton, F., Bourdin, G., McCallin, S., Ngom-Bru, C., Neville, T., et al. (2016). Oral phage therapy of acute bacterial diarrhea With two coliphage preparations: A randomized trial in children From Bangladesh. EBioMedicine *4*, 124–137.

Scanlan, J.G., Hall, A.R., and Scanlan, P.D. (2019). Impact of bile salts on coevolutionary dynamics between the gut bacterium Escherichia coli and its lytic phage PP01. Infect. Genet. Evol. *73*, 425–432.

Shkoporov, A.N., Clooney, A.G., Sutton, T.D.S., Ryan, F.J., Daly, K.M., Nolan, J.A., McDonnell, S.A., Khokhlova, E.V., Draper, L.A., Forde, A., et al. (2019). The human gut virome is highly diverse, stable, and individual specific. Cell Host Microbe *26*, 527–541.e5.

Shkoporov, A.N., and Hill, C. (2019). Bacteriophages of the human gut: the "known unknown" of the microbiome. Cell Host Microbe *25*, 195–209.

Shkoporov, A.N., Khokhlova, E.V., Fitzgerald, C.B., Stockdale, S.R., Draper, L.A., Ross, R.P., and Hill, C. (2018). ΦCrAss001 represents the most abundant bacteriophage family in the human gut and infects Bacteroides intestinalis. Nat. Commun. *9*, 4781.

Silveira, C.B., and Rohwer, F.L. (2016). Piggyback-the-Winner in host-associated microbial communities. NPJ Biofilms Microbiomes *2*, 16010.

Sousa, J.A.M., and Rocha, E.P.C. (2019). Environmental structure drives resistance to phages and antibiotics during phage therapy and to invading lysogens during colonisation. Sci. Rep. *9*, 3149.

Studer, N., Desharnais, L., Beutler, M., Brugiroux, S., Terrazos, M.A., Menin, L., Schürch, C.M., McCoy, K.D., Kuehne, S.A., Minton, N.P., et al. (2016). Functional intestinal bile acid 7alpha-dehydroxylation by Clostridium scindens associated with protection from Clostridium difficile infection in a Gnotobiotic mouse model. Front. Cell. Infect. Microbiol. *6*, 191.

Trotereau, A., Gonnet, M., Viardot, A., Lalmanach, A.C., Guabiraba, R., Chanteloup, N.K., and Schouler, C. (2017). Complete genome sequences of two Escherichia coli phages, vB_EcoM_ ESCO5 and vB_EcoM_ESCO13, which are related to phAPEC8. Genome Announc. *5*, e01337-16.

Weiss, M., Denou, E., Bruttin, A., Serra-Moreno, R., Dillmann, M.L., and Brüssow, H. (2009). In vivo replication of T4 and T7 bacteriophages in germ-free mice colonized with Escherichia coli. Virology *393*, 16–23.

Weitz, J.S., Poisot, T., Meyer, J.R., Flores, C.O., Valverde, S., Sullivan, M.B., and Hochberg, M.E. (2013). Phage-bacteria infection networks. Trends Microbiol. *21*, 82–91.

Wiggins, B.A., and Alexander, M. (1985). Minimum bacterial density for bacteriophage replication: implications for significance of bacteriophages in natural ecosystems. Appl. Environ. Microbiol. *49*, 19–23.

Yen, M., Cairns, L.S., and Camilli, A. (2017). A cocktail of three virulent bacteriophages prevents Vibrio cholerae infection in animal models. Nat. Commun. *8*, 14187.

Yu, Z., and Morrison, M. (2004). Improved extraction of PCR-quality community DNA from digesta and fecal samples. BioTechniques *36*, 808–812.

Yutin, N., Makarova, K.S., Gussow, A.B., Krupovic, M., Segall, A., Edwards, R.A., and Koonin, E.V. (2018). Discovery of an expansive bacteriophage family that includes the most abundant viruses from the human gut. Nat. Microbiol. *3*, 38–46.

Zhao, G., Vatanen, T., Droit, L., Park, A., Kostic, A.D., Poon, T.W., Vlamakis, H., Siljander, H., Härkönen, T., Hämäläinen, A.-M., et al. (2017). Intestinal virome changes precede autoimmunity in type I diabetes-susceptible children. Proc. Natl. Acad. Sci. USA *114*, E6166–E6175.

STAR★METHODS

KEY RESOURCES TABLE

REAGENT or RESOURCE	SOURCE	IDENTIFIER
Antibodies		
mouse monoclonal antibody anti Muc2-A488	Santa Cruz Biotechnology	Cat#sc-515032; RRID:AB_2815005
rabbit monoclonal antibody anti E. coli O104	SSI diagnostica	Cat#45840
fluorescence-labeled secondary antibodies anti-mouse-A488	Life Technologies	Cat#A11029; RRID:AB_2534088
fluorescence-labeled secondary antibodies anti-rabbit-A555	Life Technologies	Cat#A32732; RRID:AB_2633281
Bacterial and Virus Strains		
Escherichia coli Strain Mt1B1 (DSM-28618)	Garzetti et al., 2018	Genbank: NZ_CP028714.1
Escherichia coli Strain 55989 (CRBIP14.5)	Mossoro et al., 2002	Genbank: CU928145.2
Bacteriophage Mt1B1_P3	This manuscript	Genbank: MT496969
Bacteriophage Mt1B1_P10	This manuscript	Genbank: MT496971
Bacteriophage Mt1B1_P17	This manuscript	Genbank: MT496970
Bacteriophage CLB_P2	Maura et al., 2012b	CNCM: I-4675
Chemicals, Peptides, and Recombinant Proteins		
Drigalski	Bio-Rad	Cat#64664
SsoAdvancedTM Universal Probes Supermix	BioRad	Cat#1725280
Retrievagen A	BD BIOSCIENCES	Cat#550524
Protein Block Serum Free	DAKO	Cat#X0909
Deposited Data		
Bacteriophage Mt1B1_P3	This manuscript	Genbank: MT496969
Bacteriophage Mt1B1_P10	This manuscript	Genbank: MT496971
Bacteriophage Mt1B1_P17	This manuscript	Genbank: MT496970
Experimental Models: Organisms/Strains		
C57Bl/6J OMM^{12} mice	Institut Pasteur, LMU Munich	Brugiroux et al., 2016
C57Bl/6J axenic mice	Institut Pasteur	N/A
Oligonucleotides		
V3-V4 16S region forward primer: 5'-TCG TCGGCAGCGTCAGATGTGTATAAGAGACA GCCTACGGGNGGCWGCAG-3'	Illumina	N/A
V3-V4 16S region reverse primer: 5'-GTCTCGTGG GCTCGGAGATGTGTATAAGAGACAGGACTACH VGGGTATCTAATCC-3'	Illumina	N/A
FISH probe: Ent186-2xCy3: 5'-CCC CCW CTT TGG TCT TGC-3'	Brugiroux et al., 2016	N/A
FISH probe: Eub338I-2xCy5:(5'-GCT GCC TCC CGT AGG AGT-3'	Brugiroux et al., 2016	N/A
FISH probe: Eub338III-2xCy5: 5'-GCT GCC ACC CGT AGG TGT-3'	Brugiroux et al., 2016	N/A
Software and Algorithms		
FastQC	Brabraham Bioinformatics	v0.10.1, https://www.bioinformatics.babraham.ac.uk/projects/fastqc/
CLC Genomics	CLC Bio, Qiagen	v4.4.2
RAST	Aziz et al., 2008	v2.0, https://rast.nmpdr.org/
PhageTerm	Garneau et al., 2017	https://sourceforge.net/projects/phageterm/

(*Continued on next page*)

Continued

REAGENT or RESOURCE	SOURCE	IDENTIFIER
HMMER	Potter et al., 2018	https://www.ebi.ac.uk/Tools/hmmer/search/hmmscan
SHAMAN	Quereda et al., 2016	shaman.c3bi.pasteur.fr
R	R core team 2020	https://www.r-project.org/
lme4 R package	Bates et al., 2015	https://cran.r-project.org/web/packages/lme4/index.html
lmerTest R package	Kuznetsova et al., 2017	https://cran.r-project.org/web/packages/lmerTest/index.html
lsmeans R package	Lenth, 2016	https://cran.r-project.org/web/packages/lsmeans/index.html
car R package	Fox and Weisberg, 2019	https://cran.r-project.org/web/packages/car/index.html
ade4 R package	Dray and Dufour, 2007	https://cran.r-project.org/web/packages/ade4/index.html

RESOURCE AVAILABILITY

Lead Contact

Further information and requests for resources and reagents should be directed to and will be fulfilled by the Lead Contact, Laurent Debarbieux (laurent.debarbieux@pasteur.fr).

Materials Availability

This study did not generate new unique reagents

Data and Code Availability

The accession numbers for phage genomes reported in this paper will be accessible upon publication and are: Genbank: MT496969 for Mt1B1_P3, Genbank: MT496971 for Mt1B1_P10 and Genbank:MT496970 for Mt1B1_P17.

EXPERIMENTAL MODEL AND SUBJECT DETAILS

Microorganisms

Bacterial strains including Mt1B1 and 55989 are listed in Table S1. Bacteriophage CLB_P2 isolation and characterization is described on Maura et al. (Maura et al., 2012b).

Bacteriophage Mt1B1_P3, P10 and P17 were isolated and purified from sewage water, with an enrichment technique (explained in method details below) using *E. coli* strain Mt1B1. All phages used were amplified in exponential growing cultures of the respective host strain for approximately 4 h. Cell lysate supernatants containing amplified phages were 0.22 μm filter sterilized and stored at 4°C.

Strains were routinely cultured in lysogeny broth (LB), or on LB agar or Drigalski agar (Bio-Rad, Hercules, CA) plates, at 37°C.

Animals and Ethics

C57Bl/6J mice (seven to nine-week-old) OMM^{12} were bred at Institut Pasteur (Paris, France). A total of 72 OMM^{12} and 8 C57Bl/6J axenic healthy mice were used. For all the experiments littermates of the same sex (both females and males) were randomly assigned to experimental groups. Food and drinking water were provided ad libitum. All mice were housed in isocages and in an animal facility in accordance with Institut Pasteur guidelines and European recommendations. All animal experiments were approved by the committee on animal experimentation of the Institut Pasteur and by the French Ministry of Research.

METHOD DETAILS

Phage Isolation

First, sewage water from four locations was filtered at 0.45μm and mixed with an equal volume of 2X Luria- Bertani (LB) medium. Second, these four mixtures were inoculated with a fresh growing culture of Mt1B1 OD_{600nm} of 0.4 at 600nm, final dilution 1/200) and incubated on a shaker at 37°C overnight. The next day chloroform (1/10 vol./vol.) was added to the flasks and incubated at room temperature for one hour. Following centrifugation at 8000g for 10 min 1 mL of the supernatant was mixed with 1/10 vol./vol. of chloroform and centrifuged at 8000g for 5 min. A 100-fold dilution in TN buffer (10mM Tris HCl pH7.5, 100mM NaCl) of the aqueous phase was prepared. 10μL of the undiluted and diluted solutions were spread with an inoculation loop on the top of two separate LB agar plates and allowed to dry for 30 min under a safety cabinet. Subsequently, 1mL of an exponentially growing culture of

Mt1B1 was applied to fully cover each plate; the excess of liquid culture was removed and plates were incubated at 37°C overnight. The next day, individual plaques were picked and resuspended in tubes containing 200µl TN buffer. 1/10 vol/vol. chloroform was mixed and tubes were centrifuged at 8000g for 5 min. These steps of plaque purification were performed three times. Finally, 10µL of the last resuspended plaque were added to 1mL of a liquid culture of Mt1B1 (OD_{600nm} of 0.4 at 600nm) and incubated at 37°C in a shaker for 5 h. 1/10 vol./vol. of chloroform was mixed and after centrifugation at 8000g for 5min this stock was stored at 4°C and served as starting solution for large scale lysates (Henry et al., 2013).

Host Range Tests

Host range tests were performed as follows: 3µL of PBS-diluted phage solutions (0.2µm filtered sterilized crude lysates adjusted to 10^7 PFU/mL) were deposited side by side on the lawn of each tested bacterium on agar LB plates. Plates were incubated at 37°C overnight. Phages were grouped according to their host range and three representative phages (Mt1B1_P3, Mt1B1_P10 and Mt1B1_P17) of the main groups were chosen (Table S1).

Adsorption Assays and Phage Growth

Three independent adsorption assays were performed for each phage according to the protocol previously described (Chevallereau et al., 2016). Data were fitted using an exponential function and adsorption times were defined as the time required to reach a threshold of 10% of non-adsorbed phage particles. To record phage growth and bacteria lysis, an overnight culture of strain Mt1B1 was diluted in LB broth and grown to an OD_{600nm} of 0.2 from which 150µL were distributed into each of the wells of a 96-well plate (Microtest 96 plates, Falcon). 10 µL of sterile phage lysates diluted in PBS to obtain a multiplicity of infection (MOI) of 1 x 10^{-2} in each well. Plates were incubated in a microplate reader at 37°C, with a shaking step of 30sec before the automatic recording of OD_{600nm} every 15min over 20 h (Glomax MultiDetection System, Promega, USA).

Phage Genomes Sequencing and Analysis

Sterile phage lysates were treated by DNase (120 U) and RNase (240 µg/mL) and incubated for 30 min at 37°C before adding EDTA (20 mM). Lysates were treated with proteinase K (100 µg/mL) and SDS (0.5%) and incubated at 55°C for 30min. DNA was extracted by a phenol-chloroform protocol modified from Pickard (Pickard, 2009). Sequencing was performed using Illumina technology (Illumina Inc., San Diego, CA) MiSeq Nano with paired-end reads of 250bp. Quality of reads was visualised by FastQC v0.10.1 Brabraham Bioinformatics (http://www.bioinformatics.babraham.ac.uk/projects/fastqc/). Assembly was performed using a workflow implemented in Galaxy-Institut Pasteur using clc_assembler v4.4.2 and clc_mapper v4.4.2 (CLC Bio, Qiagen). Phage termini were determined by PhageTerm (Garneau et al., 2017) and annotations were performed by the RAST v2.0 server (Aziz et al., 2008). According to the nomenclature proposed for naming viruses (Adriaenssens and Brister, 2017), the full names for phages P3, P10 and P17 are vB_EcoP_Mt1B1_P3, vB_EcoP_Mt1B1_P10 and vB_EcoM_Mt1B1_P17, respectively. The Accession numbers for the phage genomes can be found on the Data and Code Availability section.

Search for Ig-like Domains on Phage Genomes

Protein sequences of the four phages were scanned for homologs on Pfam database using the HMMER website (Potter et al., 2018). The results were compared to a comprehensive HMM (Hidden Markov Models) database of Ig-like domains found on Pfam that was kindly provided by Dr. Sean Benler.

Ex Vivo Phage Replication Assay

Oligo-MM^{12} mice received 200µL of strain Mt1B1 (10^7 CFU prepared from an overnight culture in LB at 37°C) in sterile sucrose sodium bicarbonate solution (20% sucrose and 2.6% sodium bicarbonate, pH 8) by oral gavage and three days after were sacrificed to collect and weight intestinal sections (ileum and colon). PBS was added to each sample (1.75mL) before homogenization (gentleMacs Octo Dossociator, Milteny Biotec). A volume of 150µL of each homogenized gut sample was distributed in the wells of a 96-well plate and 10µL of each individual phage were added to reach an MOI of 1 x 10^{-2}, and the plate was incubated at 37°C. A fraction of the homogenized samples was also serially diluted in PBS and plated on Drigalski medium to count Mt1B1 colonies at t=0. Following five hours of incubation, samples were serially diluted in PBS and plated on Drigalski medium as well as on LB agar plates overlaid with strain Mt1B1. Both set of plates were incubated at 37°C overnight. The same procedure was followed for *in vitro* growth assays with bacteria taken during exponential (OD_{600nm} 0.5) or stationary (24 h) growth phase at 37°C with shaking.

Passive Phages Transit in Axenic and OMM^{12} Mice

Axenic (n=8 divided in 4 cages) or OMM^{12} (n=4 divided in 2 cages) mice were orally gavaged once by 200µL of a cocktail of Mt1B1 phages (1x10^7 PFU of each of the three phages) diluted in PBS. Fecal pellets were collected before phage gavage and at 6, 24, 48 and 72 h post-gavage for axenic mice and at 24 and 48 h post-gavage for OMM^{12} mice. Pellets were transferred in pre-weighted, sterile, 2mL tubes, weighted and resuspended in 1mL of PBS. Serial dilutions in PBS were performed and plated onto LB plates overlaid with strain Mt1B1 to assess phage titers. Two mice were sacrificed on each time point to collect intestinal sections, which were homogenized (as above) in PBS and then plated on LB plates overlaid with strain Mt1B1. The luminal part corresponds to the gut content that was recovered by squeezing the intestinal tube with the back of a scalpel, which was subsequently homogenized in 1mL of PBS. The

mucosal part corresponds to the remaining tissues (empty intestinal tube) that were washed in 10mL of PBS before being transferred into a new tube with 1.75mL of fresh PBS and then homogenized.

Murine Model of *E. coli* Colonization

The long-term coexistence experiment with strain Mt1B1 included 7 mice (5 that received phages and 2 that did not) and lasted 23 days. At day0 mice feces were collected prior to Mt1B1 administration by oral gavage (200 μL of bacteria resuspended in sodium bicarbonate buffer (see above)). Fecal pellets were transferred in pre-weighted, sterile, 2mL tubes, weighted and resuspended in 1mL of PBS. Serial dilutions in PBS were performed and plated onto Drigalski plates. The three phages ($2x10^7$ PFU of each phage in 200μL of PBS) were administered as a mixture once by oral gavage at day9. The level of phages was assessed from serial dilutions in PBS spotted on LB plates overlaid with strain Mt1B1.

Two shorter independent experiments with repeated phage administration were performed with 11 (6 with phages and 5 without divided in 4 cages) and 14 (8 with phages and 6 without divided in 4 cages) Mt1B1-colonized mice, respectively. At day0 mice feces were collected prior to Mt1B1 administration (as described above) by oral gavage. Fecal pellets were prepared as above. The three phages ($2x10^7$ PFU of each phage in 200μL of PBS) were administered altogether once by oral gavage at day14, 15 and 16. The level of phages was assessed as above. Each mouse was sacrificed at day17 to collect feces and intestinal sections, the latest being homogenized (as above) in PBS and all samples were plated on both Drigalski plates and LB plates overlaid with strain Mt1B1. Luminal and mucosal part of gut sections were recovered as described above.

For experiments with *E. coli* strain 55989 fecal samples were collected on days0, 1, 3, 7, 8, 9 and 10. On day0, after collecting fecal samples, oral gavage of *E. coli* strain 55989 was performed as described above for strain Mt1B1. At day7, after collecting fecal sample, 200μL of either phage CLB_P2 ($2x10^8$ PFU/mL) (16 mice divided in 6 cages) or PBS (12 mice divided in 5 cages) were administered to the mice by oral gavage (two independent experiments were performed). At day10, feces were collected before sacrifice and dissection of the mice and assessment of the levels of bacteria and phages as above.

Identification of Resistant Clones

For the experiments with Mt1B1-colonized OMM^{12} mice and the phage cocktail, 20 clones from each gut section from mice (n=8) exposed to the cocktail during three days and sacrificed at day17, as well as from fecal samples from mice (n=5) exposed to a single dose of the cocktail at days10, 16 and 24, were streaked vertically in LB agar plates and subsequently each of the three phages was horizontally streaked across. Plates were incubated at 37°C and phenotype was checked after 5h and overnight.

For the experiments using 55989-colonized OMM^{12} mice and phage CLB_P2, 75 to 94 isolated colonies per sample (gut sections and feces from n=8 mice sacrificed at day10) were randomly chosen by a robot (Qpix 420; Molecular Devices, Sunnyvale, USA) and cultured overnight in 150μL of LB in 96 well microplates. The next day, 10μL were added to a new plate filled with 140μL of LB and incubated at 37°C for 2 h. Then, 8μL of each clone were spotted on two separated LB agar plates and let dry for 20 min. Then, on one plate spots of 4μL of phage CLB_P2 (400 PFU) were spotted on top of each bacterial spot. On the second plate phage spots were 100 fold more concentrated (40,000 PFU). Susceptible clones are defined by the clearance of the bacterial spot at one or both phage concentrations (often full clearance was observed with 40,000 PFU and partial clearance with 400 PFU), while clones not affected by the phage at any concentration are defined as resistant. The frequency of phage-resistant clones in fecal samples from 55989-colonized OMM^{12} mice was assessed by plating $2.25x10^4$ to $3.42x10^5$ 55989 cells on Drigalski plates inundated with $3x10^7$ PFU of phage CLB_P2. The number of phage-resistant clones was recorded after overnight incubation at 37°C and compared to plates inundated with the same amount of phage CLB_P2 and on which $3.83x10^6$ cells from an exponential growing culture of strain 55989 was spread.

Histological Analysis by FISH and Immunochemistry

Fluorescence in situ hybridization was performed as previously described on intestinal samples from *E. coli* Mt1B1 colonized OMM^{12} mice bred at the LMU Munich where the fecal level of strain Mt1B1 reached 10^9 CFU/g (Brugiroux et al., 2016). Ileal and colonic tissues were fixed in 4% paraformaldehyde (4°C overnight), washed in 20% sucrose (4°C overnight), embedded in O.C.T (Sakura), and flash frozen in liquid nitrogen. FISH was performed on 7μm sections, using double 3′and 5′-labelled 16S rRNA targeted probes specific for Enterobacteriaceae (Ent186-2xCy3 (CCC CCW CTT TGG TCT TGC)) and Eubacteria (1:1 mix of Eub338I-2xCy5 (GCT GCC TCC CGT AGG AGT) and Eub338III-2xCy5 (GCT GCC ACC CGT AGG TGT)). 1μg/mL–1 4′,6-diamidino-2-phenylindole (Roth) was used for DNA staining. Images were recorded with a Leica TCS SP5 confocal microscope (Leica, Wetzlar).

For immunofluorescence staining unflushed ileal and colonic tissues from *E. coli* 55989-colonized OMM^{12} mice bred at Institut Pasteur were fixed in Carnoy (ethanol/chloroform/acetic acid 60:30:10) for mucus preservation, dehydrated, and embedded in paraffin according to the standard protocol. All the stainings were done on dewaxed 8μm sections. Antigen retrieval was performed with Retrievagen A (BD BIOSCIENCES) during 10min at 97°C, followed by 20min at room temperature. After blocking with Protein Block Serum Free (DAKO) during 15min at room temperature, immunofluorescence staining was performed using mouse monoclonal antibody anti Muc2-A488, 1/100 (Santa Cruz Biotechnology) and rabbit anti *E. coli* O104, 1/50 (SSI diagnostica) during 4 h at room temperature, then overnight at 4°C. After washings in PBS, the following fluorescence-labeled secondary antibodies were used: anti-mouse-A488, 1/200 (Life Technologies) and anti-rabbit-A555, 1/200 (Life Technologies) during 4.30 h at room temperature, and

nuclei stained with DAPI. Slides were examined under an Olympus IX81 microscope equipped with a charge-coupled device (CCD) camera, and red fluorescence (*E. coli* O104) per pixel was quantified with ImageJ software. An example of the different regions delimited for the quantifications is shown in Figure S6.

OMM^{12} Community Composition

From homogenized fecal samples, 500μL were centrifuged at 8.000g for 10min and the supernatant was removed. Pellets were diluted in 500μL of lysis buffer (500 mM NaCl, 50 mM Tris-HCl, pH 8.0, 50 mM EDTA, 4% sodium dodecyl sulfate (SDS) and incubated for 15min at 50°C (Yu and Morrison, 2004). Then, 100μL of lysozyme (25mg/ml) was added and samples were incubated at 37°C for 2 h. DNA extraction was performed using the Maxwell Cell tissue kit (Promega) and samples were frozen at -20°C until use. The primers, probes and qPCR protocol were used in conformity with previously described methods (Brugiroux et al., 2016) with the exception of the SsoAdvancedTM Universal Probes Supermix (BioRad). The qPCR reactions were performed in duplicate and in two independent runs using MasterCycler realplex4 from Eppendorf. Amplicon libraries targeting the V3-V4 16S region were amplified by PCR (25 cycles) using Illumina primers (forward primer: 5'-TCGTCGGCAGCGTCAGATGTGTATAAGAGACAGCC TACGGGNGGCWGCAG-3', reverse primer: 5'-GTCTCGTGGGCTCGGAGATGTGTATAAGAGACAGGACTACHVGGGTATC TAATCC-3') and then sequenced (Illumina MiSeq 2x300 bp). Sequences and statistical analyses were performed with SHAMAN (shaman.c3bi.pasteur.fr) (Quereda et al., 2016).

QUANTIFICATION AND STATISTICAL ANALYSIS

For the growth curves for strain Mt1B1 (n=3 for each condition) error bars represent standard error of the mean (SEM). The n-fold multiplication of strain Mt1B1 on the *ex vivo* experiment, represented on Figure 2 was calculated by plating samples before and after the 5 h incubation and the error bars represent means with standard deviation.

Statistical analysis on the number of bacteria and phages generated by the animal experiments were carried out using the lme4, lmerTest and car packages of R (Bates et al., 2015; Fox and Weisberg, 2019; Kuznetsova et al., 2017). Both cfu and PFU were $\log_{10}$-transformed prior to analysis. In each experiment, two groups of mice were considered, a group exposed to phages and an unexposed control group. The impact of phages could be assessed based on the abundance of phages (log-PFU). Given the non-linearity of responses, the day at which a measure was performed was considered as a categorical variable. Linear mixed-models were used to account for random experimental effects (i.e., individuals, experiments and cage effects).

Overall effects were assessed with Analysis of Variance (ANOVA) and post-hoc Tukey's comparisons and were performed using the lsmeans R package (Lenth, 2016). $p < 0.05$ was considered statistically significant.

16S-quantification data were analysed using multivariate analysis after standard normalization. A principal component analysis (PCA) was performed with the R package ade4 on the matrix of ΔCt values of 10 bacterial strains (strains YL2 and KB18 were not detected) (Dray and Dufour, 2007). In addition, a between-group PCA was done in order to assess experimental effects, based on 12 groups of observations: 3 days (0, 14, and 17) and 4 cages (2 exposed, 2 unexposed).

Cell Host & Microbe, Volume *28*

Supplemental Information

The Spatial Heterogeneity of the Gut Limits Predation and Fosters Coexistence of Bacteria and Bacteriophages

Marta Lourenço, Lorenzo Chaffringeon, Quentin Lamy-Besnier, Thierry Pédron, Pascal Campagne, Claudia Eberl, Marion Bérard, Bärbel Stecher, Laurent Debarbieux, and Luisa De Sordi

Supplemental material (Figure S1 to S6 and Table S1 to S8) linked to the article

Title

The spatial heterogeneity of the gut limits predation and fosters coexistence of bacteria and bacteriophages

Authors

Marta Lourenço[1,2], Lorenzo Chaffringeon[1,3], Quentin Lamy-Besnier[1,4], Thierry Pédron[1], Pascal Campagne[5], Claudia Eberl[6], Marion Bérard[7], Bärbel Stecher[6,8], Laurent Debarbieux[1*] and Luisa De Sordi[1,2*]

Affiliations

1 Department of Microbiology, Institut Pasteur, Paris F-75015 France.

2 Sorbonne Université, Collège Doctoral, F-75005 Paris, France

3 Sorbonne Université, Centre de Recherche Saint Antoine, INSERM UMRS_938, Paris, France

4 Université Paris Descartes, Paris, France

5 Bioinformatics and Biostatistics Hub, Institut Pasteur, Paris F-75015 France.

6 Max von Pettenkofer Institute of Hygiene and Medical Microbiology, Faculty of Medicine, LMU Munich, Munich, Germany

7 Institut Pasteur, DTPS, Animalerie Centrale, Centre de Gnotobiologie, 75724 Paris, France

8 German Center for Infection Research (DZIF), Partner Site Munich, Munich, Germany

Lead contact: laurent.debarbieux@pasteur.fr

Figure S1, related to Figure 1. Localization by FISH of the *E. coli* strain Mt1B1 in gut sections from Mt1B1-colonized OMM^{12} mice.

Intestinal cells (nuclei) were stained with DAPI, and Mt1B1 (red+green=yellow) and Eubacteria (red) were stained with specific FISH probes. Representative images from a group of five mice are presented. Scale bar, 50µm.

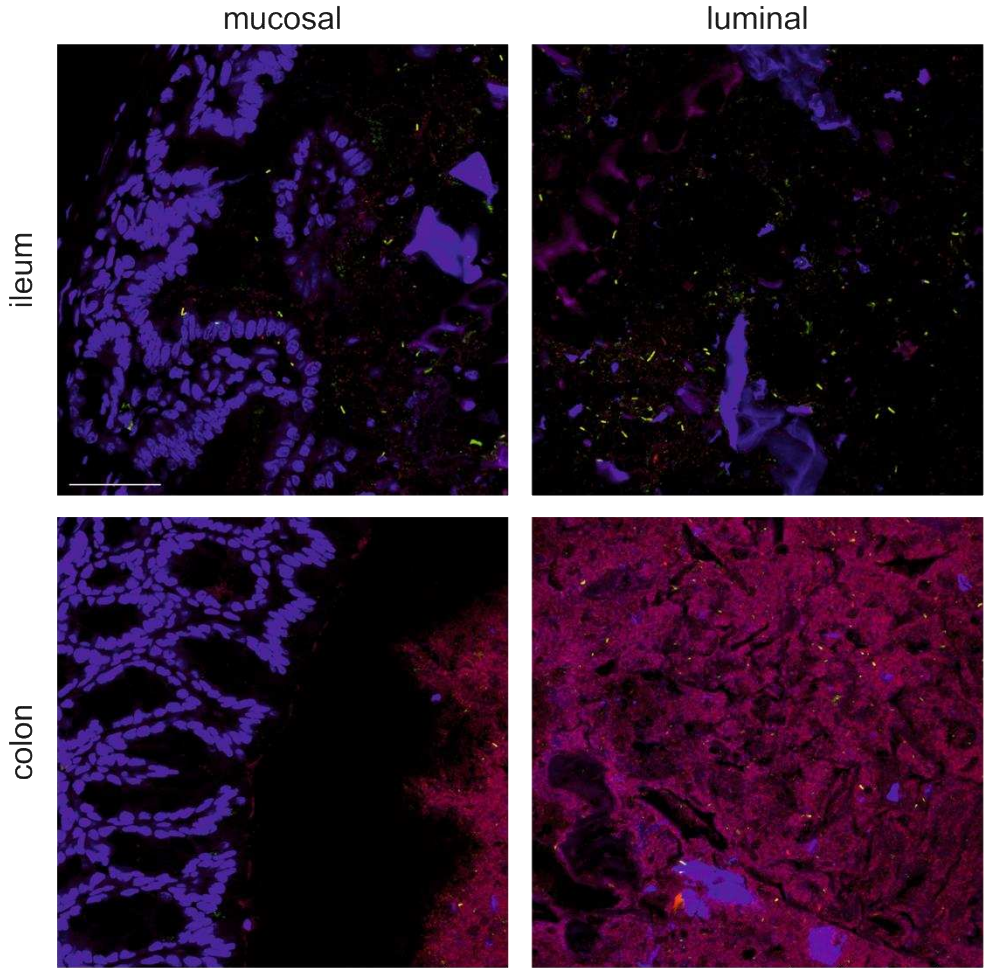

Figure S2, related to Table 1. Mt1B1 phages have different adsorption rates.

An exponentially growing culture of strain Mt1B1 in LB medium was infected separately by phages P3, P10 or P17 (MOI= 1 x 10^{-2}) and samples were collected over time for counting non-adsorbed phages. For phages P3 and P10, samples were taken every 30sec over a period of 10 minutes. For phage P17, sampling was performed every 30sec until 5min, and then every minute until 15min. The percentage of non-adsorbed phages is plotted against time (mean with standard deviations; n=3).

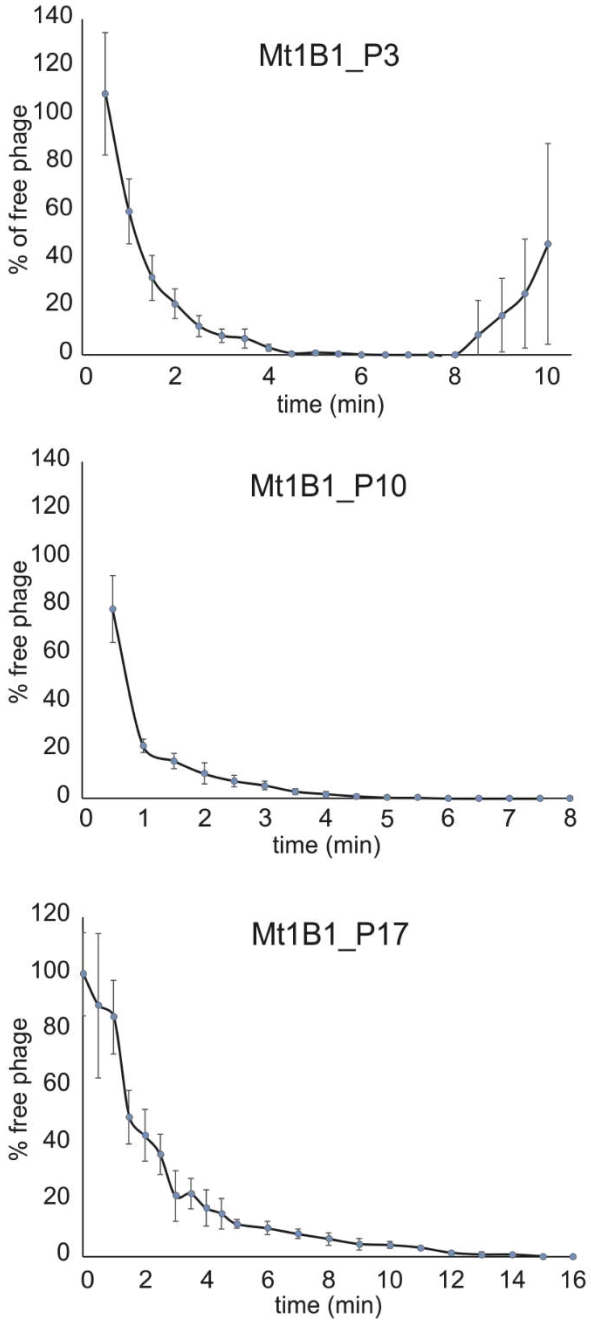

Figure S3, related to Figure 4. Mt1B1-colonized OMM^{12} mice provide *in vivo* conditions for the long-term coexistence of phage and bacteria in the mammalian gut.

OMM^{12} mice (n=7) were colonized during 14 days before a single administration of PBS (red, n=2) or the three phages P3, P10 and P17 together (blue, n=5; 6x10^{7} pfu per dose, consisting of equal proportions of each phage) by oral gavage on day9. **A.** Fecal titer of strain Mt1B1. **B.** Fecal titers of phages. **C.** Representation of the ratios phage:bacteria over time showing the stability of the coexistence. Dots, individual values; horizontal bar, median; box, 25th-75th quantiles, vertical bars, min/max values (within 1.5 x interquartile interval).

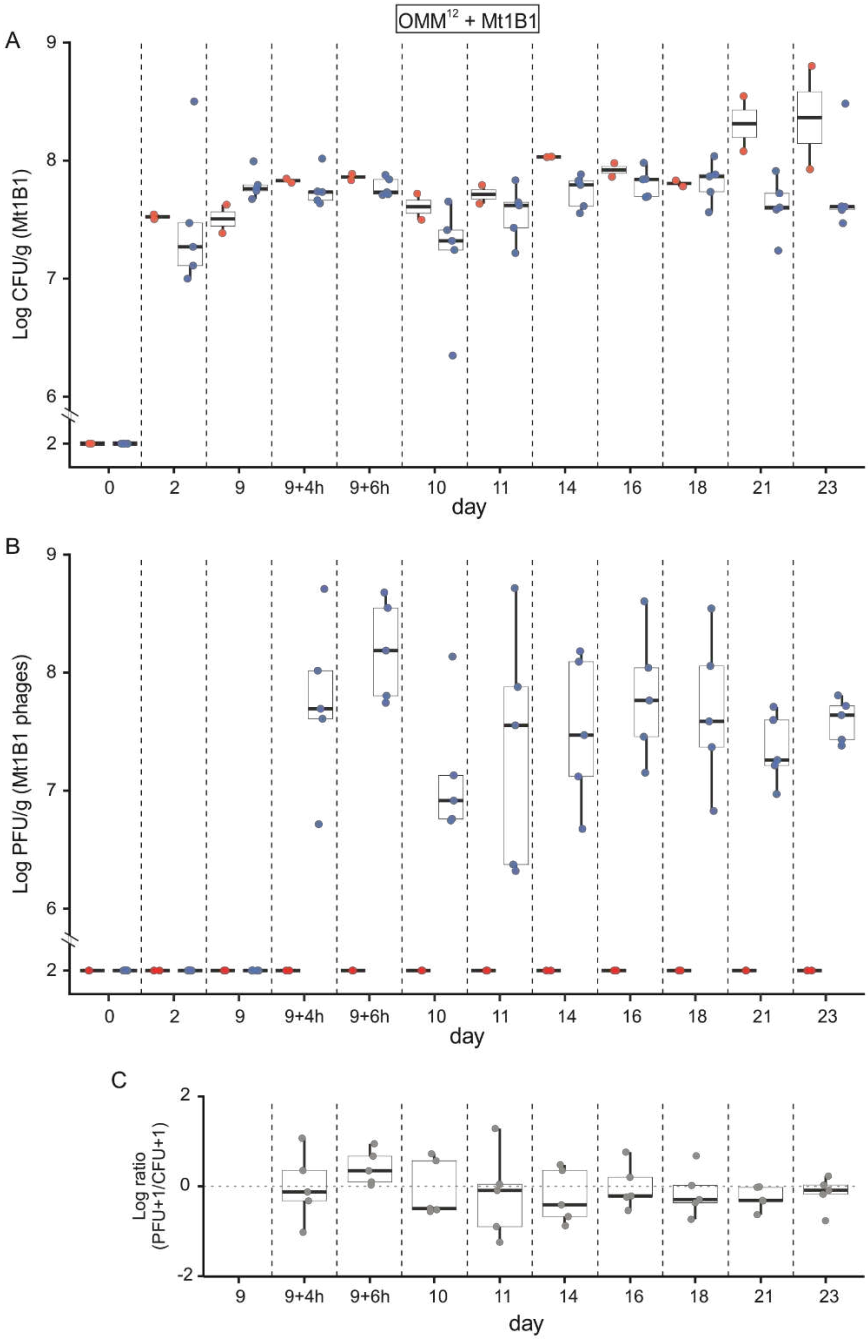

Figure S4, related to Figure 4D. Community composition of the OMM^{12} mice during Mt1B1 colonization and phage treatment.

Fecal pellets of OMM^{12} mice (n=11) were collected before Mt1B1 gavage (day0), after 14 days of colonization (day14) and after 3 repetitive phages (cocktail of three Mt1B1 phages, equal amount of each) administration (day17). DNA was extracted from pellets and the 16S rRNA content was quantified by qPCR (panel A). The same DNA samples were also subjected to 16S amplicon sequencing and results were compared day by day to qPCR quantifications (panel B).

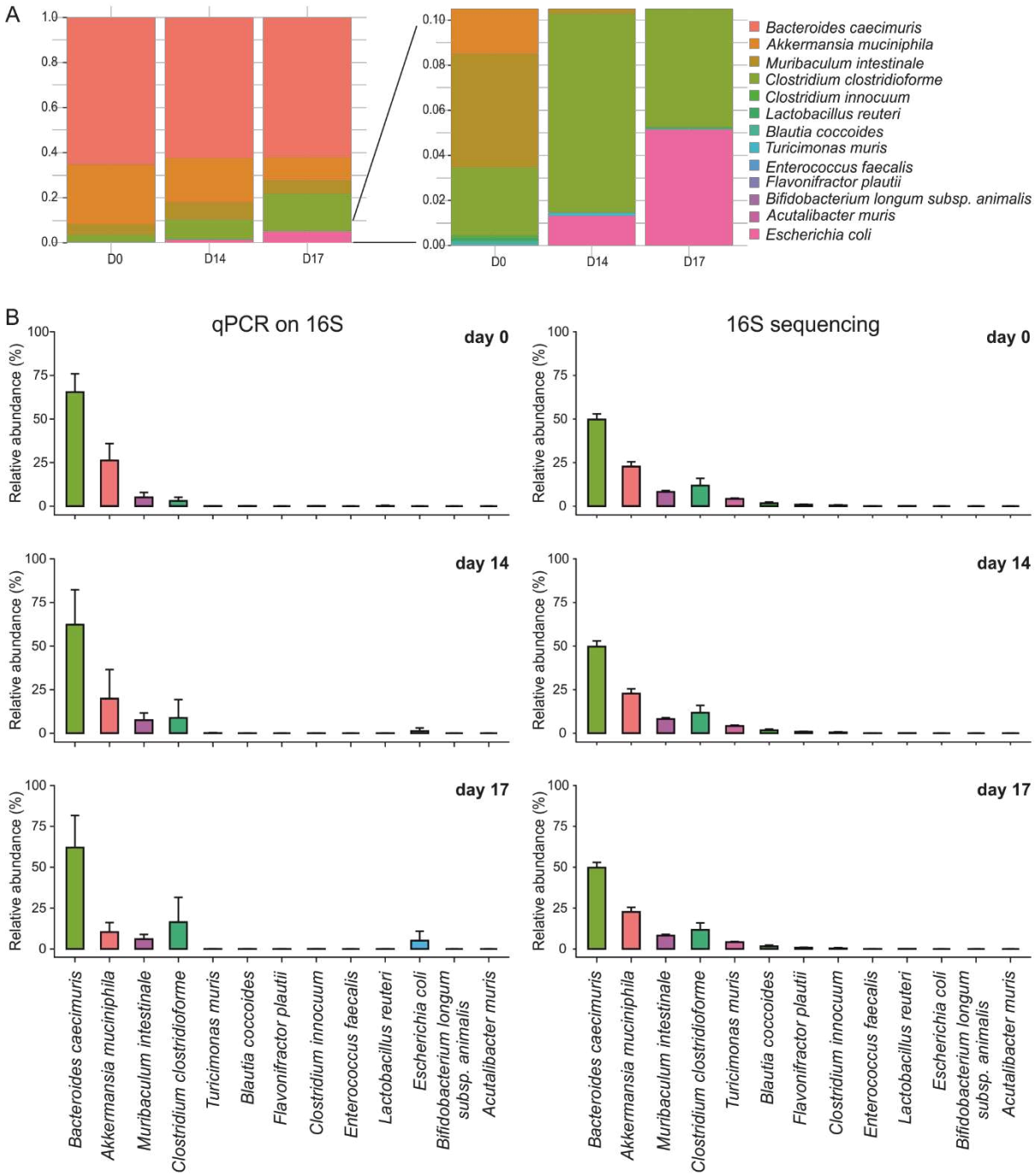

Figure S5, related to Figure 5. The *E. coli* strain 55989 can stably colonize the gut of OMM^{12} mice and does not become resistant to phage CLB_P2.

A. Fecal titers of *E. coli* strain 55989 at the indicated time points for each 55989-colonized OMM^{12} mouse (n=10) receiving a single dose of 10^8 cfu by oral gavage at day0. Red dots, individual values; horizontal bar, median; box, 25th-75th quantiles, vertical bars, min/max values (within 1.5 x interquartile interval).

B. Spots of 8 µL of 55989 clones grown in LB were placed on agar plates and dried under a safety cabinet for at least 20min before a second spot of 4µL of phage CLB_P2 containing 400 pfu (left side) or 40,000 pfu (right side) was placed on top of each bacterial spot. Plates were incubated overnight at 37°C and then scanned. Pictures shown are representative of tests performed along this study. R, correspond to a control strain that is resistant to CLB_P2, while S correspond to individual fecal clones isolated from 55989-colonized OMM^{12} mice treated with phage CLB_P2.

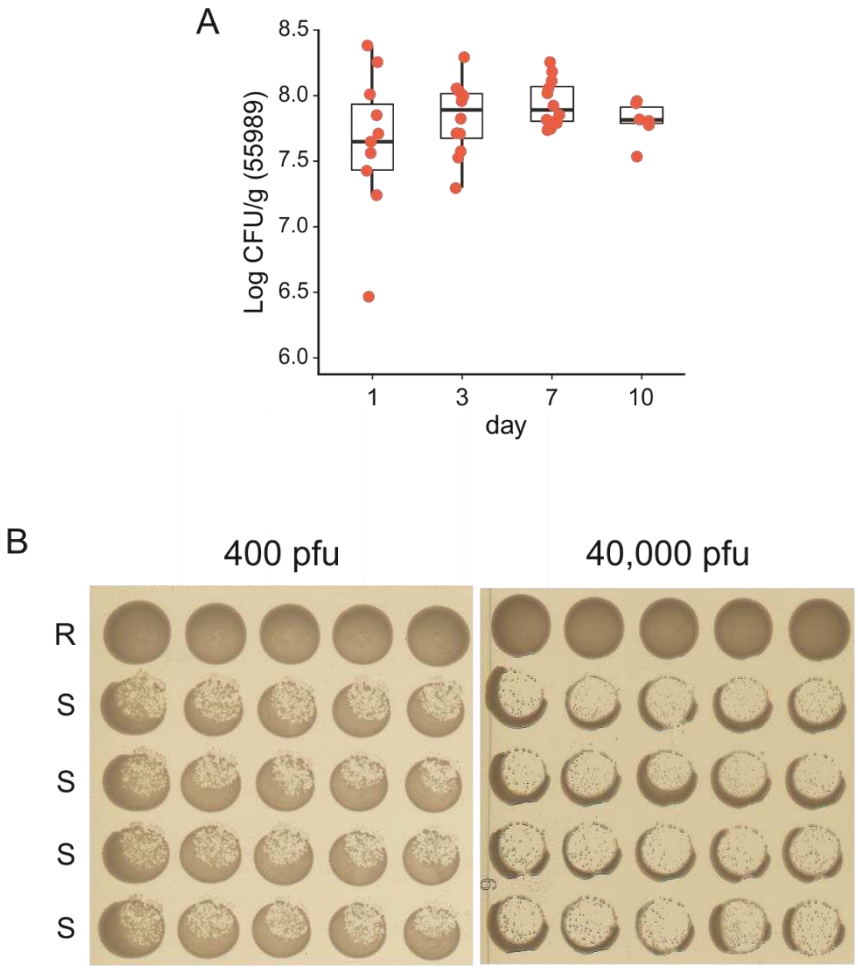

Figure S6, related to Figure 6. Regions of interest for red fluorescence quantification in ileal and colonic sections.

A. Ileum. Upper panel, representative photograph of immunofluorescence staining of *E. coli* strain 55989 (red) and mucus (green) in a whole unwashed ileum section (epithelial cells stained with DAPI, blue). Lower panel, the yellow lines defined the three regions used for the red fluorescence quantification. The red fluorescence mean per pixel from the background region was subtracted to the red fluorescence mean of the mucosal or luminal regions of the tissue.

B. Colon. Upper panel, representative photograph of immunofluorescence staining of *E. coli* strain 55989 (red) and mucus (green) in a whole unwashed colon section (epithelial cells stained with DAPI, blue). Lower panel, the yellow lines defined the three regions used for the red fluorescence quantification. The red fluorescence mean per pixel from the background region was subtracted to the red fluorescence mean of the mucosal or luminal regions of the tissue.

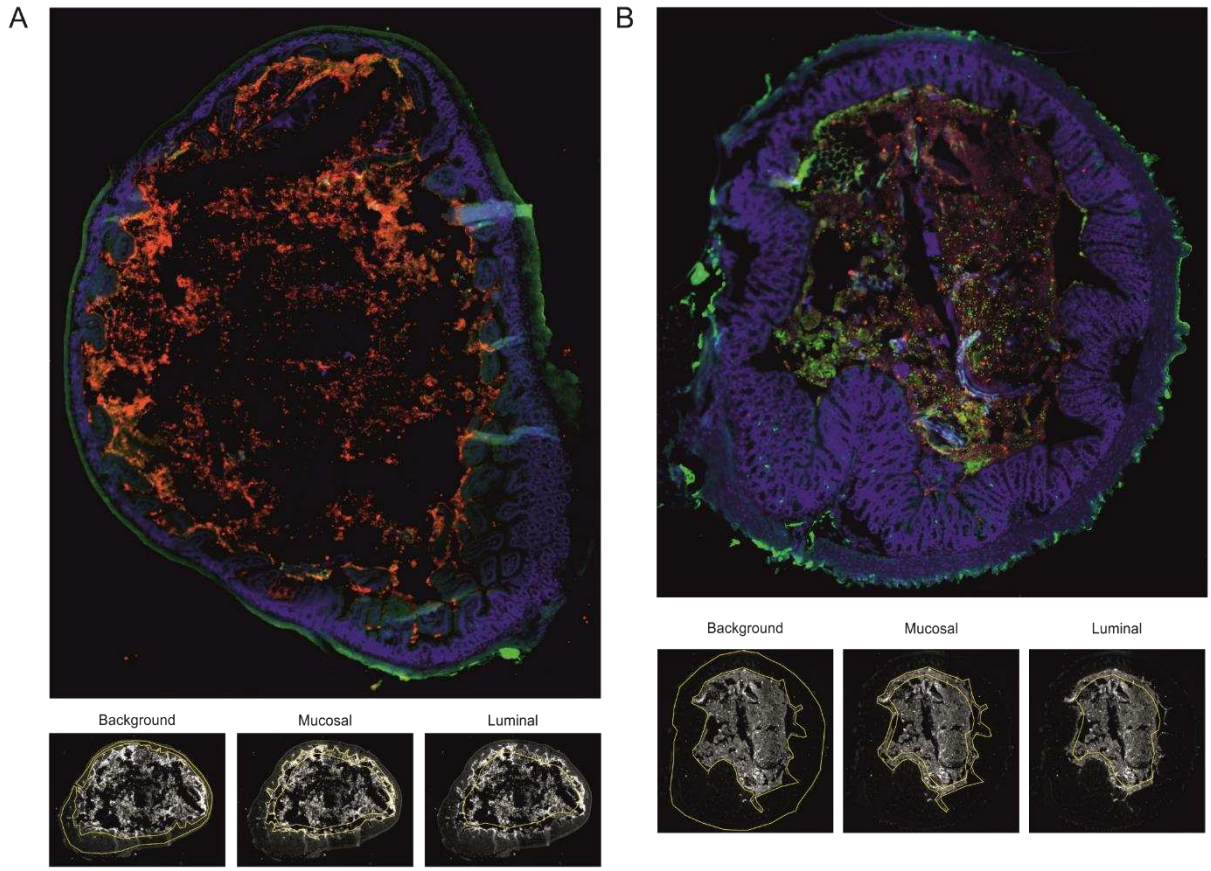

Supplemental Tables

Table S1, related to Table1. Host range of the 28 candidate phages isolated for strain Mt1B1.

Table S1. Host range of the 28 candidate phages isolated using strain Mt1B1

Phages / Strains	Mt1B1_P1	Mt1B1_P2	Mt1B1_P3	Mt1B1_P4	Mt1B1_P5	Mt1B1_P6	Mt1B1_P7	Mt1B1_P8	Mt1B1_P9	Mt1B1_P10	Mt1B1_P11	Mt1B1_P12	Mt1B1_P13	Mt1B1_P14	Mt1B1_P15	Mt1B1_P16	Mt1B1_P17	Mt1B1_P18	Mt1B1_P19	Mt1B1_P20	Mt1B1_P21	Mt1B1_P22	Mt1B1_P23	Mt1B1_P24	Mt1B1_P25	Mt1B1_P26	Mt1B1_P27	Mt1B1_P28	Reference
536	0	0	0	0	0	0	0	0	0	0	0	0	0	0	0	0	0	0	0	0	0	0	0	0	0	0	0	0	Brzuszkiewicz E et al ., 2006 (PMID:16912116)
7074	1	1	1	1	1	1	1	1	1	1	1	1	1	1	1	1	0	1	1	1	1	1	1	1	1	1	1	1	AIEC collection from University of Lille, France, via N. Barnich
55989	0	0	0	0	0	0	0	0	0	0	0	0	0	0	0	0	0	0	0	0	0	0	0	0	0	0	0	0	Mossoro et al ., 2002 (PMID:12149388)
AL505	1	0	0	0	0	0	0	0	0	1	0	1	1	0	0	0	0	0	0	0	0	0	0	0	0	0	0	0	Galtier et al ., 2016 (PMID:26971586)
BE	0	0	0	0	0	0	0	0	0	0	0	0	0	0	0	0	0	0	0	0	0	0	0	0	0	0	0	0	Laboratory collection, gift from H. Krisch
BW25113	0	0	0	0	0	0	0	0	0	0	0	0	0	0	0	0	0	0	0	0	0	0	0	0	0	0	0	0	Datsenko and Wanner, 2000 (PMID:10829079)
CR63	0	0	0	0	0	0	0	0	0	0	0	0	0	0	0	0	0	0	0	0	0	0	0	0	0	0	0	0	Laboratory collection, gift from H. Krisch
E22a	0	0	0	0	0	0	0	0	0	0	0	0	0	0	0	0	0	0	0	0	0	0	0	0	0	0	0	0	Camguilhem and Milon, 1989 (PMID:2656746)
ECOR 1	0	0	0	0	0	0	0	0	0	0	0	0	0	0	0	0	1	0	0	0	0	0	0	0	0	0	0	0	Ochman, H., and Selander, R.K. (1984) (PMID: 6363394)
ECOR 10	0	0	0	0	0	0	0	0	0	0	0	0	0	0	0	0	0	0	0	0	0	0	0	0	0	0	0	0	Ochman, H., and Selander, R.K. (1984) (PMID: 6363394)
ECOR 11	0	0	0	0	0	0	0	0	0	0	0	0	0	0	0	0	0	0	0	0	0	0	0	0	0	0	0	0	Ochman, H., and Selander, R.K. (1984) (PMID: 6363394)
ECOR 12	0	0	0	0	0	0	0	0	0	0	0	0	0	0	0	0	0	0	0	0	0	0	0	0	0	0	0	0	Ochman, H., and Selander, R.K. (1984) (PMID: 6363394)
ECOR 13	0	0	0	0	0	0	0	0	0	0	0	0	0	0	0	0	0	0	0	0	0	0	0	0	0	0	0	0	Ochman, H., and Selander, R.K. (1984) (PMID: 6363394)
ECOR 14	0	0	0	0	0	0	0	0	0	0	0	0	0	0	0	0	0	0	0	0	0	0	0	0	0	0	0	0	Ochman, H., and Selander, R.K. (1984) (PMID: 6363394)
ECOR 15	0	0	0	0	0	0	0	0	0	0	0	0	0	0	0	0	0	0	0	0	0	0	0	0	0	0	0	0	Ochman, H., and Selander, R.K. (1984) (PMID: 6363394)
ECOR 16	0	0	0	0	0	0	0	0	0	0	0	0	0	0	0	0	0	0	0	0	0	0	0	0	0	0	0	0	Ochman, H., and Selander, R.K. (1984) (PMID: 6363394)
ECOR 17	0	0	0	0	0	0	0	0	0	0	0	0	0	0	0	0	0	0	0	0	0	0	0	0	0	0	0	0	Ochman, H., and Selander, R.K. (1984) (PMID: 6363394)
ECOR 18	0	0	0	0	0	0	0	0	0	0	0	0	0	0	0	0	0	0	0	0	0	0	0	0	0	0	0	0	Ochman, H., and Selander, R.K. (1984) (PMID: 6363394)
ECOR 19	0	0	0	0	0	0	0	0	0	0	0	0	0	0	0	0	0	0	0	0	0	0	0	0	0	0	0	0	Ochman, H., and Selander, R.K. (1984) (PMID: 6363394)
ECOR 2	0	0	0	0	0	0	0	0	0	0	0	0	0	0	0	0	1	0	0	0	0	0	0	0	0	0	0	0	Ochman, H., and Selander, R.K. (1984) (PMID: 6363394)
ECOR 20	0	0	0	0	0	0	0	0	0	0	0	0	0	0	0	0	0	0	0	0	0	0	0	0	0	0	0	0	Ochman, H., and Selander, R.K. (1984) (PMID: 6363394)
ECOR 21	0	0	0	0	0	0	0	0	0	0	0	0	0	0	0	0	0	0	0	0	0	0	0	0	0	0	0	0	Ochman, H., and Selander, R.K. (1984) (PMID: 6363394)
ECOR 22	0	0	0	0	0	0	0	0	0	0	0	0	0	0	0	0	0	0	0	0	0	0	0	0	0	0	0	0	Ochman, H., and Selander, R.K. (1984) (PMID: 6363394)
ECOR 23	0	0	0	0	0	0	0	0	0	0	0	0	0	0	0	0	1	0	0	0	0	0	0	0	0	0	0	0	Ochman, H., and Selander, R.K. (1984) (PMID: 6363394)
ECOR 24	0	0	0	0	0	0	0	0	0	0	0	0	0	0	0	0	1	0	0	0	0	0	0	0	0	0	0	0	Ochman, H., and Selander, R.K. (1984) (PMID: 6363394)
ECOR 25	0	0	0	0	0	0	0	0	0	0	0	0	0	0	0	0	1	0	0	0	0	0	0	0	0	0	0	0	Ochman, H., and Selander, R.K. (1984) (PMID: 6363394)
ECOR 26	0	0	0	0	0	0	0	0	0	0	0	0	0	0	0	0	0	0	0	0	0	0	0	0	0	0	0	0	Ochman, H., and Selander, R.K. (1984) (PMID: 6363394)
ECOR 27	0	0	0	0	0	0	0	0	0	0	0	0	0	0	0	0	0	0	0	0	0	0	0	0	0	0	0	0	Ochman, H., and Selander, R.K. (1984) (PMID: 6363394)
ECOR 28	0	0	0	0	0	0	0	0	0	0	0	0	0	0	0	0	0	0	0	0	0	0	0	0	0	0	0	0	Ochman, H., and Selander, R.K. (1984) (PMID: 6363394)
ECOR 29	0	0	0	0	0	0	0	0	0	0	0	0	0	0	0	0	0	0	0	0	0	0	0	0	0	0	0	0	Ochman, H., and Selander, R.K. (1984) (PMID: 6363394)
ECOR 3	0	0	0	0	0	0	0	0	0	0	0	0	0	0	0	0	0	0	0	0	0	0	0	0	0	0	0	0	Ochman, H., and Selander, R.K. (1984) (PMID: 6363394)
ECOR 30	0	0	0	0	0	0	0	0	0	0	0	0	0	0	0	0	1	0	0	0	0	0	0	0	0	0	0	0	Ochman, H., and Selander, R.K. (1984) (PMID: 6363394)
ECOR 31	0	0	0	0	0	0	0	0	0	0	0	0	0	0	0	0	0	0	0	0	0	0	0	0	0	0	0	0	Ochman, H., and Selander, R.K. (1984) (PMID: 6363394)
ECOR 32	0	0	0	0	0	0	0	0	0	0	0	0	0	0	0	0	1	0	0	0	0	0	0	0	0	0	0	0	Ochman, H., and Selander, R.K. (1984) (PMID: 6363394)
ECOR 33	0	0	0	0	0	0	0	0	0	0	0	0	0	0	0	0	1	0	0	0	0	0	0	0	0	0	0	0	Ochman, H., and Selander, R.K. (1984) (PMID: 6363394)
ECOR 34	0	0	0	0	0	0	0	0	0	0	0	0	0	0	0	0	0	0	0	0	0	0	0	0	0	0	0	0	Ochman, H., and Selander, R.K. (1984) (PMID: 6363394)
ECOR 35	0	0	0	0	0	0	0	0	0	0	0	0	0	0	0	0	1	0	0	0	0	0	0	0	0	0	0	0	Ochman, H., and Selander, R.K. (1984) (PMID: 6363394)
ECOR 36	1	1	1	1	1	1	1	1	1	1	1	1	1	1	1	1	0	1	1	1	1	1	1	1	1	1	1	1	Ochman, H., and Selander, R.K. (1984) (PMID: 6363394)
ECOR 37	0	0	0	0	0	0	0	0	0	0	0	0	0	0	0	0	0	0	0	0	0	0	0	0	0	0	0	0	Ochman, H., and Selander, R.K. (1984) (PMID: 6363394)
ECOR 38	1	1	1	1	1	1	1	1	1	1	1	1	1	1	1	1	0	1	1	1	1	1	1	1	1	1	1	1	Ochman, H., and Selander, R.K. (1984) (PMID: 6363394)
ECOR 39	0	0	0	0	0	0	0	0	0	0	0	0	0	0	0	0	0	0	0	0	0	0	0	0	0	0	0	0	Ochman, H., and Selander, R.K. (1984) (PMID: 6363394)
ECOR 4	0	0	0	0	0	0	0	0	0	0	0	0	0	0	0	0	0	0	0	0	0	0	0	0	0	0	0	0	Ochman, H., and Selander, R.K. (1984) (PMID: 6363394)
ECOR 40	1	1	1	1	1	1	1	1	1	1	1	1	1	1	1	1	0	1	1	1	1	1	1	1	1	1	1	1	Ochman, H., and Selander, R.K. (1984) (PMID: 6363394)
ECOR 41	1	1	1	1	1	1	1	1	1	1	1	1	1	1	1	1	0	1	1	1	1	1	1	1	1	1	1	1	Ochman, H., and Selander, R.K. (1984) (PMID: 6363394)
ECOR 42	0	0	0	0	0	0	0	0	0	0	0	0	0	0	0	0	1	0	0	0	0	0	0	0	0	0	0	0	Ochman, H., and Selander, R.K. (1984) (PMID: 6363394)
ECOR 43	0	0	0	0	0	0	0	0	0	0	0	0	0	0	0	0	0	0	0	0	0	0	0	0	0	0	0	0	Ochman, H., and Selander, R.K. (1984) (PMID: 6363394)
ECOR 44	0	0	0	0	0	0	0	0	0	0	0	0	0	0	0	0	0	0	0	0	0	0	0	0	0	0	0	0	Ochman, H., and Selander, R.K. (1984) (PMID: 6363394)
ECOR 45	0	0	0	0	0	0	0	0	0	0	0	0	0	0	0	0	0	0	0	0	0	0	0	0	0	0	0	0	Ochman, H., and Selander, R.K. (1984) (PMID: 6363394)
ECOR 46	0	0	0	0	0	0	0	0	0	0	0	0	0	0	0	0	0	0	0	0	0	0	0	0	0	0	0	0	Ochman, H., and Selander, R.K. (1984) (PMID: 6363394)
ECOR 47	0	0	0	0	0	0	0	0	0	0	0	0	0	0	0	0	0	0	0	0	0	0	0	0	0	0	0	0	Ochman, H., and Selander, R.K. (1984) (PMID: 6363394)
ECOR 48	0	0	0	0	0	0	0	0	0	0	0	0	0	0	0	0	0	0	0	0	0	0	0	0	0	0	0	0	Ochman, H., and Selander, R.K. (1984) (PMID: 6363394)
ECOR 49	1	0	0	0	0	0	0	0	0	1	0	1	1	0	0	0	0	0	0	0	0	0	0	0	0	0	0	0	Ochman, H., and Selander, R.K. (1984) (PMID: 6363394)
ECOR 5	0	0	0	0	0	0	0	0	0	0	0	0	0	0	0	0	0	0	0	0	0	0	0	0	0	0	0	0	Ochman, H., and Selander, R.K. (1984) (PMID: 6363394)
ECOR 50	1	0	0	0	0	0	0	0	0	1	0	1	1	0	0	0	0	0	0	0	0	0	0	0	0	0	0	0	Ochman, H., and Selander, R.K. (1984) (PMID: 6363394)
ECOR 51	0	0	0	0	0	0	0	0	0	0	0	0	0	0	0	0	0	0	0	0	0	0	0	0	0	0	0	0	Ochman, H., and Selander, R.K. (1984) (PMID: 6363394)
ECOR 52	0	0	0	0	0	0	0	0	0	0	0	0	0	0	0	0	1	0	0	0	0	0	0	0	0	0	0	0	Ochman, H., and Selander, R.K. (1984) (PMID: 6363394)
ECOR 53	0	0	0	0	0	0	0	0	0	0	0	0	0	0	0	0	0	0	0	0	0	0	0	0	0	0	0	0	Ochman, H., and Selander, R.K. (1984) (PMID: 6363394)
ECOR 54	0	0	0	0	0	0	0	0	0	0	0	0	0	0	0	0	0	0	0	0	0	0	0	0	0	0	0	0	Ochman, H., and Selander, R.K. (1984) (PMID: 6363394)
ECOR 55	0	0	0	0	0	0	0	0	0	0	0	0	0	0	0	0	0	0	0	0	0	0	0	0	0	0	0	0	Ochman, H., and Selander, R.K. (1984) (PMID: 6363394)
ECOR 56	0	0	0	0	0	0	0	0	0	0	0	0	0	0	0	0	0	0	0	0	0	0	0	0	0	0	0	0	Ochman, H., and Selander, R.K. (1984) (PMID: 6363394)
ECOR 57	0	0	0	0	0	0	0	0	0	0	0	0	0	0	0	0	0	0	0	0	0	0	0	0	0	0	0	0	Ochman, H., and Selander, R.K. (1984) (PMID: 6363394)
ECOR 58	0	0	0	0	0	0	0	0	0	0	0	0	0	0	0	0	0	0	0	0	0	0	0	0	0	0	0	0	Ochman, H., and Selander, R.K. (1984) (PMID: 6363394)
ECOR 59	0	0	0	0	0	0	0	0	0	0	0	0	0	0	0	0	0	0	0	0	0	0	0	0	0	0	0	0	Ochman, H., and Selander, R.K. (1984) (PMID: 6363394)
ECOR 6	0	0	0	0	0	0	0	0	0	0	0	0	0	0	0	0	0	0	0	0	0	0	0	0	0	0	0	0	Ochman, H., and Selander, R.K. (1984) (PMID: 6363394)
ECOR 60	0	0	0	0	0	0	0	0	0	0	0	0	0	0	0	0	0	0	0	0	0	0	0	0	0	0	0	0	Ochman, H., and Selander, R.K. (1984) (PMID: 6363394)
ECOR 61	1	1	1	1	1	1	1	1	1	1	1	1	1	1	1	1	1	1	1	1	1	1	1	1	1	1	1	1	Ochman, H., and Selander, R.K. (1984) (PMID: 6363394)
ECOR 62	1	1	1	1	1	1	1	1	1	1	1	1	1	1	1	1	0	1	1	1	1	1	1	1	1	1	1	1	Ochman, H., and Selander, R.K. (1984) (PMID: 6363394)
ECOR 63	0	0	0	0	0	0	0	0	0	0	0	0	0	0	0	0	0	0	0	0	0	0	0	0	0	0	0	0	Ochman, H., and Selander, R.K. (1984) (PMID: 6363394)
ECOR 64	0	0	0	0	0	0	0	0	0	0	0	0	0	0	0	0	0	0	0	0	0	0	0	0	0	0	0	0	Ochman, H., and Selander, R.K. (1984) (PMID: 6363394)
ECOR 65	0	0	0	0	0	0	0	0	0	0	0	0	0	0	0	0	0	0	0	0	0	0	0	0	0	0	0	0	Ochman, H., and Selander, R.K. (1984) (PMID: 6363394)
ECOR 66	0	0	0	0	0	0	0	0	0	0	0	0	0	0	0	0	0	0	0	0	0	0	0	0	0	0	0	0	Ochman, H., and Selander, R.K. (1984) (PMID: 6363394)
ECOR 67	0	0	0	0	0	0	0	0	0	0	0	0	0	0	0	0	0	0	0	0	0	0	0	0	0	0	0	0	Ochman, H., and Selander, R.K. (1984) (PMID: 6363394)
ECOR 68	0	0	0	0	0	0	0	0	0	0	0	0	0	0	0	0	0	0	0	0	0	0	0	0	0	0	0	0	Ochman, H., and Selander, R.K. (1984) (PMID: 6363394)
ECOR 69	0	0	0	0	0	0	0	0	0	0	0	0	0	0	0	0	0	0	0	0	0	0	0	0	0	0	0	0	Ochman, H., and Selander, R.K. (1984) (PMID: 6363394)
ECOR 7	0	0	0	0	0	0	0	0	0	0	0	0	0	0	0	0	0	0	0	0	0	0	0	0	0	0	0	0	Ochman, H., and Selander, R.K. (1984) (PMID: 6363394)
ECOR 70	0	0	0	0	0	0	0	0	0	0	0	0	0	0	0	0	0	0	0	0	0	0	0	0	0	0	0	0	Ochman, H., and Selander, R.K. (1984) (PMID: 6363394)
ECOR 8	0	0	0	0	0	0	0	0	0	0	0	0	0	0	0	0	0	0	0	0	0	0	0	0	0	0	0	0	Ochman, H., and Selander, R.K. (1984) (PMID: 6363394)
ECOR 9	0	0	0	0	0	0	0	0	0	0	0	0	0	0	0	0	0	0	0	0	0	0	0	0	0	0	0	0	Ochman, H., and Selander, R.K. (1984) (PMID: 6363394)
LF110	0	0	0	0	0	0	0	0	0	0	0	0	0	0	0	0	0	0	0	0	0	0	0	0	0	0	0	0	Darfeuille-Michaud et al ., 2004 (PMID:15300573)
LF31	0	0	0	0	0	0	0	0	0	0	0	0	0	0	0	0	1	0	0	0	0	0	0	0	0	0	0	0	Darfeuille-Michaud et al ., 2004 (PMID:15300573)
LF50	0	0	0	0	0	0	0	0	0	0	0	0	0	0	0	0	1	0	0	0	0	0	0	0	0	0	0	0	Darfeuille-Michaud et al ., 2004 (PMID:15300573)
LF73	0	0	0	0	0	0	0	0	0	0	0	0	0	0	0	0	0	0	0	0	0	0	0	0	0	0	0	0	Darfeuille-Michaud et al ., 2004 (PMID:15300573)
LF82	0	0	0	0	0	0	0	0	0	0	0	0	0	0	0	0	0	0	0	0	0	0	0	0	0	0	0	0	Miquel et al ., 2010 (PMID:20862302)
LM33	0	0	0	0	0	0	0	0	0	0	0	0	0	0	0	0	0	0	0	0	0	0	0	0	0	0	0	0	Dufour et al., 2016 (PMID:27387322)
M1/5	0	0	0	0	0	0	0	0	0	0	0	0	0	0	0	0	0	0	0	0	0	0	0	0	0	0	0	0	Laboratory collection, gift from E. Oswald
MG1655	0	0	0	0	0	0	0	0	0	0	0	0	0	0	0	0	0	0	0	0	0	0	0	0	0	0	0	0	Laboratory collection
Mt1B1	1	1	1	1	1	1	1	1	1	1	1	1	1	1	1	1	1	1	1	1	1	1	1	1	1	1	1	1	Garzetti et al 2018 (DSM-28618)
Nissle 1917	0	0	0	0	0	0	0	0	0	0	0	0	0	0	1	0	1	0	0	0	0	0	0	0	0	0	0	0	Laboratory collection, gift from E. Oswald
NRG857c	0	0	0	0	0	0	0	0	0	0	0	0	0	0	0	0	0	0	0	0	0	0	0	0	0	0	0	0	Small et al ., 2013 (PMID:23748852)
O42	0	0	0	0	0	0	0	0	0	0	0	0	0	0	0	0	0	0	0	0	0	0	0	0	0	0	0	0	Laboratory collection, gift from C. Le Bouguénec
OP50	0	0	0	0	0	0	0	0	0	0	0	0	0	0	0	0	0	0	0	0	0	0	0	0	0	0	0	0	Laboratory collection, gift from J. Ewbank
PDP110	0	0	0	0	0	0	0	0	0	0	0	0	0	0	0	0	0	0	0	0	0	0	0	0	0	0	0	0	laboratory collection, gift from E. Denamur
PDP351	0	0	0	0	0	0	0	0	0	0	0	0	0	0	0	0	0	0	0	0	0	0	0	0	0	0	0	0	laboratory collection, gift from E. Denamur
SE15	0	1	0	0	0	0	0	0	0	0	0	0	0	0	0	0	0	0	0	0	0	0	0	0	0	0	0	0	Laboratory collection
Sp15	0	0	0	0	0	0	0	0	0	0	0	0	0	0	0	0	0	0	0	0	0	0	0	0	0	0	0	0	Laboratory collection, gift from E. Oswald
ST24	0	0	0	0	0	0	0	0	0	0	0	0	0	0	0	0	0	0	0	0	0	0	0	0	0	0	0	0	Laboratory collection
T145	0	0	0	0	0	0	0	0	0	0	0	0	0	0	0	0	1	0	0	0	0	0	0	0	0	0	0	0	laboratory collection, gift from E. Denamur
T147	0	0	0	0	0	0	0	0	0	0	0	0	0	0	0	0	0	0	0	0	0	0	0	0	0	0	0	0	laboratory collection, gift from E. Denamur
total score	11	9	8	8	8	8	8	8	8	11	8	11	11	8	8	8	17	8	8	8	8	8	8	8	8	8	8	8	

scoring

0 was given to phages that were not able to clear the lawn of bacteria with a spot of 30.000 PFU (3µL of 10^7 PFU/mL)

1 was given to phages that were able to clear the lawn of bacteria with a spot of 30.000 PFU (3µL of 10^7 PFU/mL)

Table S2 related to Table 1. Closest phage homologs to phages P3, P10 and P17.

Homologs to Phage P3 (40.1 kb)						
Description	**Max score**	**Total score**	**Query cover**	**E value**	**Identity**	**Accession**
Enterobacteria phage K1F, complete genome	26378	58105	92%	0.0	95.90%	AM084414.1
Escherichia phage vB_EcoP_F, complete genome	26092	59661	93%	0.0	95.82%	KY295894.1
Escherichia phage LM33_P1, complete genome	17570	52746	87%	0.0	94.66%	LT594300.1
Escherichia phage PE3-1, complete genome	17538	51871	84%	0.0	94.98%	KJ748011.1
Escherichia phage JSS1, complete genome	17533	51844	84%	0.0	94.98%	KX689784.2
Escherichia virus Vec13, complete genome	17457	52867	87%	0.0	94.16%	MH400309.1
Homologs to Phage P10 (45.1 kb)						
Description	**Max score**	**Total score**	**Query cover**	**E value**	**Ident**	**Accession**
Escherichia virus AAPEc6, complete genome	31124	60643	89%	0.0	92.77%	KX279892.2
Escherichia virus VEc3, complete genome	29724	53841	83%	0.0	92.75%	MG251390.1
Escherichia phage vB_EcoP_C, complete genome	27353	62103	90%	0.0	94.08%	KY295892.1
Escherichia virus mutPK1A2, complete genome	25453	59969	90%	0.0	93.81%	MG004687.1
Escherichia virus K1E, complete genome	25340	62944	89%	0.0	94.36%	KY435490.1
Escherichia phage vB_EcoP_KAW1A4500, complete genome	23865	57685	88%	0.0	92.75%	MK373773.1
Homologs to Phage P17 (150.9 kb)						
Description	Max score	Total score	Query cover	E value	Ident	Accession
Escherichia phage ESCO13, complete genome	63247	2.407e+05	93%	0.0	98.10%	KX552041.2
Escherichia phage vB_EcoM-Ro121lw, complete genome	63032	2.440e+05	94%	0.0	98.28%	MH160766.1
Escherichia phage vB_EcoM_Schickermooser, complete genome	62626	2.396e+05	93%	0.0	98.17%	MK373788.1
Escherichia phage phAPEC8, complete genome	45930	2.345e+05	91%	0.0	97.74%	JX561091.1
Escherichia phage vB_EcoM-Ro121c4YLVW, complete genome	43886	2.459e+05	94%	0.0	98.33%	MH051333.1
Escherichia phage ESCO5, complete genome	43853	2.332e+05	91%	0.0	98.29%	KX664695.2

Magablast tool from NCBI (https://blast.ncbi.nlm.nih.gov/Blast.cgi) was used to search for the closest homologs ranked in decreasing values of query cover (Last update august 2019). Only the top 6 homologs are shown.

Table S3, related to Table 1. Genome annotations of Mt1B1 phages P3, P10 and P17.
Genome annotations can be found with the following accession numbers:
GenBank: MT496969 for Mt1B1_P3
GenBank: MT496971 for Mt1B1_P10
GenBank: MT496970 for Mt1B1_P17

Table S4, related to Figure 4. Statistical analysis with a mixed-effects model of the abundance of strain Mt1B1 and PFU/CFU ratios in feces and intestinal sections.

CFU abundance in feces

ANOVA

day: testing difference between the different days

phage: effect of the phage exposure

Response:	scale(log10(CFU.g))		
	Chisq	Df	Pr(>Chisq)
day	13.6891	3	0.0033
phage	29.0024	1	7.23E-08
day:phage	1.6313	3	0.4423

Post-hoc tests Comparison between "phage" and "no phage" at the different time points

	contrast	estimate	SE	df	t.ratio	p.value
Day=15	no phage vs. phage	1.247	0.306	91.9	4.071	0.0001
Day=16	no phage vs. phage	0.976	0.306	91.9	3.185	0.002
Day=17	no phage vs. phage	0.708	0.306	91.9	2.311	0.023

ANOVA

groups: testing the difference between groups at day 14 before phage application

Response:	scale(log10(CFU.g))		
	Chisq	Df	Pr(>Chisq)
groups	1.1798	1	0.2774

Bacterial abundance (CFU) as a function of time (day) and exposure to phages.

Random effects include individual IDs, experiments, as well as the cage in which they were reared. Overall analysis of variance (ANOVA) reveals significant effects of day (p=0.0033), phage (p=7.23E-08) and their interaction (p=0.4423).

The post-hoc Tukey comparisons displayed below were performed between mice exposed to phage and not exposed within each day (d15, p=0.0001; d16, p=0.002, d17, p=0.023).

Random effects include experiment, as well as the cage in which they were reared. Overall analysis of variance (ANOVA) reveals no significant effects on groups (p=0.2774).

CFU abundance in sections

ANOVA/ANODE

	scale(log10(CFU.g+1))		
	Chisq	Df	Pr(>Chisq)
section	77.354	4	6.33E-16
phage	25.713	1	3.96E-07
section:phage	10.113	4	0.0385

Post-hoc tests

Comparison between "phage" and "no phage" in the different sections

	contrast	estimate	SE	df	t.ratio	p.value
ileum_lumen	no phage vs. phage	1.0723044	0.2959727	110.16	3.623	0.0004
ileum_mucosa	no phage vs. phage	0.9855932	0.2959727	110.16	3.33	0.0012
colon_lumen	no phage vs. phage	0.525542	0.2959727	110.16	1.776	0.0786
colon_mucosa	no phage vs. phage	1.2514249	0.2959727	110.16	4.228	<.0001

Bacterial abundance (CFU) as a function of gut section and exposure to phages.

Random effects include individual IDs, experiments, as well as the cage in which they were reared. Overall analysis of variance (ANOVA) reveals significant effects of *gut section* (p<6.33E-16), *phage* (p=3.96E-07) and their *interaction* (p=0.0385).

The post-hoc Tukey comparisons displayed below were performed between the mice exposed to phage and not exposed within each section (il. lum, p<0.0004; il. muc, p=0.0012; col. lum, p=0.0786; col muc, p<0.0001)

PFU/CFU ratios

ANOVA – ANODE

Response:	scale(L.ratio)		
	Chisq	Df	Pr(>Chisq)
gut section	2.4925	2	0.2875
part[a]	9.7241	1	0.0018
section:part	0.7109	1	0.3991

[a] group= luminal or mucosal

Post-hoc test

organ	contrast	estimate	SE	df	t.ratio	p.value
ileum	lumen-mucosa	0.9637997	0.3440682	62.13	2.801	0.0068
colon	lumen-mucosa	0.5535417	0.3440682	62.13	1.609	0.1127

The ratios of phages over bacteria abundance (PFU/CFU) as a function of gut section and part (mucosa or lumen).

Random effects include individual IDs, experiments, as well as the cage in which they were reared. Overall analysis of variance (ANOVA) reveals no significant effect of the *gut sections* (p=0.2875) and section vs parts (luminal or mucosal, p=0.3991), but a significant difference of *parts (luminal or mucosal,*

The post-hoc Tukey comparisons were performed between the luminal and mucosal data and revealed a significant difference for the ileum (p=0.0068) but not for the colon (p=0.1127).

Table S5, related to Figure 4. p-values associated with the mixed models applied to the abundance of the 12 strains assessed from qPCR data.

day 14: variations within samples day 14				
day 17: variations within samples day 17				
experiment: variations taking in account the 3 days (0, 14 and 17)				
phage: variations caused by phage exposition				
ref#	I48	YL44	YL27	YL32
Strain name	*Bacteroides caecimuris*	*Akkermansia muciniphila*	*Muribaculum intestinale*	*Clostridium clostridioforme*
day 14	0.238	0.354	0.403	0.182
day 17	0.45	0.01	0.838	0.01
experiment	0.078	0.862	0.442	0.179
phage	0.28	0.071	0.867	0.275
ref#	I46	I49	YL58	YL45
Strain name	*Clostridium innocuum*	*Lactobacillus reuteri*	*Blautia coccoides*	*Turicimonas muris*
day 14	0	0.279	0	0.55
day 17	0.782	0.256	0.022	0.035
experiment	0.509	0.556	0.338	0.295
phage	0.269	0.269	0.434	0.434
ref#	KB1	YL31	YL2	KB18
Strain name	*Enterococcus faecalis*	*Flavonifractor plautii*	*acterium longum subsp. a*	*Acutalibacter muris*
day 14	0.022	0.078	NA	NA
day 17	0.269	0.011	NA	NA
experiment	0.112	0.684	NA	NA
phage	0.403	0.579	NA	NA
The model tested variations within day 14, within day 17 and also variations on the samples taking into account days 0, 14 and 17.				
The model also tested variations on each strain taking into account the phage exposure.				

Table S6, related to Figure 5. Statistical analysis with a mixed-effects model of the abundance of strain 55989 and PFU/CFU ratios in feces and intestinal sections.

CFU abundance in feces

ANOVA

day: testing difference between the different days

phage: effect of the phage exposure

Response:	scale(log10(CFU.g))		
	Chisq	Df	Pr(>Chisq)
day	11.837	3	0.0079
phage	4.898	1	0.0268
day:phage	0.1911	3	0.9088

Post-hoc tests — Comparison between "phage" and "no phage" at the different time points

	contrast	estimate	SE	df	t.ratio	p.value
Day=8	no phage vs. phage	0.497	0.379	105	1.311	0.1926
Day=9	no phage vs. phage	0.344	0.379	105	0.907	0.3666
Day=10	no phage vs. phage	0.565	0.379	105	1.49	0.1391

ANOVA

groups: testing the difference between groups at day 7 before phage application

Response:	scale(log10(CFU.g))		
	Chisq	Df	Pr(>Chisq)
groups	0.5245	1	0.4689

Bacterial abundance (CFU) as a function of time (day) and exposure to phages.

Random effects include individual IDs, experiments, as well as the cage in which they were reared. Overall analysis of variance (ANOVA) reveals significant effects of day (p=0.0079), phage (p=0.0268) and their interaction (p=0.9088).

The post-hoc Tukey comparisons displayed below were performed between mice exposed to phage and not exposed within each day (d8, p=0.1926; d9, p=0.3666, d10, p=0.1391).

Random effects include experiment, as well as the cage in which they were reared. Overall analysis of variance (ANOVA) reveals no significant effects on groups (p=0.4689).

CFU abundance in sections

ANOVA/ANODE

	scale(log10(CFU.g+1))		
	Chisq	Df	Pr(>Chisq)
gut section	206.950	4	< 2.2E-16
phage	18.987	1	1.31E-05
gut section:pha	18.550	4	0.0009

Post-hoc tests — Comparison between "phage" and "no phage" in the different sections

	contrast	estimate	SE	df	t.ratio	p.value
ileum_lumen	no phage vs. phage	1.18250	0.244	121	4.838	<.0001
ileum_mucosa	no phage vs. phage	0.7306	0.244	121	2.978	0.0035
colon_lumen	no phage vs. phage	0.7935	0.244	121	3.158	0.0020
colon_mucosa	no phage vs. phage	0.0881	0.244	121	-0.030	0.9761

Bacterial abundance (CFU) as a function of gut section and exposure to phages.

Random effects include individual IDs, experiments, as well as the cage in which they were reared. Overall analysis of variance (ANOVA) reveals significant effects of *gut section* (p<2.2E-16), *phage* (p=1.31E-05) and their *interaction* (p=0.0009).

The post-hoc Tukey comparisons displayed below were performed between the mice exposed to phage and not exposed within each section (il. lum, p<0.0001; il. muc, p=0.0035; col. lum, p=0.002; col muc, p=0.9761)

PFU/CFU ratios

ANOVA – ANODE

Response:	scale(L.ratio)		
	Chisq	Df	Pr(>Chisq)
gut section	0.2531	1	0.6149
part[a]	6.2674	1	0.0123
section:part	0.4592	1	0.498

[a] part= luminal or mucosal

Post-hoc test

organ	contrast	estimate	SE	df	t.ratio	p.value
ileum	lumen-mucosa	0.929	0.41	44	2.261	0.0287
colon	lumen-mucosa	0.53	0.418	44.5	1.269	0.2112

The ratios of phages over bacteria abundance (PFU/CFU) as a function of gut section and part (mucosa or lumen).

Random effects include individual IDs, experiments, as well as the cage in which they were reared. Overall analysis of variance (ANOVA) reveals no significant effect of the *gut sections* (p=0.6149) and section vs parts (luminal or mucosal, p=0.498), but a significant difference of *parts (luminal or mucosal,*

The post-hoc Tukey comparisons were performed between the luminal and mucosal data and revealed a significant difference for the ileum (p=0.0287) but not for the colon (p=0.2112).

Table S7, related to Figure 5. Frequencies of CLB_P2 resistant clones

Group	Mice / Sample	Nb of 55989 cells	Nb of phage-resistant	Frequency	Mean
CLB_P2	NM2	2,00E+05	9,00E+00	4,50E-04	7,50E-04
	OD2	2,83E+05	4,00E+00	1,41E-04	
	NM6	3,42E+05	1,00E+01	1,63E-03	
	OD6	1,75E+05	2,30E+01	7,80E-04	
PBS	NM4	4,92E+04	8,00E+00	2,93E-04	9,76E-04
	OD4	1,67E+05	1,30E+01	1,31E-03	
	NM7	2,25E+04	1,00E+00	4,44E-04	
	OD7	9,17E+04	1,70E+01	1,85E-03	
55989	Tube 1 (n=4)	3,83E+05	5,10E+01	2,66E-04	8,10E-04
			5,00E+01	2,61E-04	
			2,70E+01	1,41E-03	
			2,50E+01	1,30E-03	

Table S8, related to Figure 6. Statistical analysis of the amount of fluorescence in histological samples

Fluorescence (red channel) in sections						
ANOVA						
	scale(log10(CFU.g))					
	Chisq	Df	Pr(>Chisq)			
organ	28.3714	3	3.04E-06			
phage	0.024	1	0.8768			
organ:phage	4.2361	3	0.2371			
Post-hoc tests						
	Comparison between “phage” and “no phage” in the different sections					
	contrast	estimate	SE	df	t.ratio	p.value
ileum_lumen	no phage vs. phage	-0.768	0.565	8.24	-1.358	0.2106
ileum_mucosa	no phage vs. phage	-0.269	0.565	8.24	-0.476	0.6463
colon_lumen	no phage vs. phage	0.216	0.557	8.86	0.387	0.7078
colon_mucosa	no phage vs. phage	0.602	0.557	8.86	1.081	0.3084
The fluorescence (red channel) density per pixel as a function of organ and expsure to phages.						
Random effect include individual IDs as well as cage in which mice were reared. Overall analysis of variance (ANOVA) reveals significant effect of organ (p=3.04E-06) but not of phage (p=0.8768) and their interaction (p=0.2371).						
The post-hoc test of Tukey comparisons displayed below were performed between mice exposed and not exposed to phage CLB_P2 for each organ.						
Ratios of the fluorescence (red channel) in mucosal over luminal parts.						
ANOVA						
	ratio muc/lum					
	Chisq	Df	Pr(>Chisq)			
organ	2.7542	1	0.097			
phage	2.4938	1	0.1143			
organ:phage	0.1911	1	0.662			
Post-hoc tests	Comparison between “phage” and “no phage” in the different sections					
	contrast	estimate	SE	df	t.ratio	p.value
ileum	no phage vs. phage	0.966	0.681	14	1.1419	0.1779
colon	no phage vs. phage	0.6	0.681	14	0.881	0.393
Ratios of the fluorescence (red channel) in mucosal over luminal parts as a function of organ and exposure to phages.						
Random effect include individual IDs as well as cage in which mice were reared. Overall analysis of variance (ANOVA) reveals no significant effect of organ (p=0.097) of phage (p=0.1143) and their interaction (p=0.662).						
The post-hoc test of Tukey comparisons were performed between mice exposed and not exposed to phages for each organ.						

II – Caractériser les effets de l'acide biliaire épimérisé, UDCA, sur une inflammation intestinale induite par un entéropathogène

Les acides biliaires sont produits par le foie sous forme d'acides biliaires primaire qui sont métabolisés en acides biliaires secondaires par les bactéries du microbiote intestinal. Ces acides biliaires secondaires possèdent de nombreuses fonctions dans dont celle de facilité la digestion des lipides ou encore comme molécules de signalisation en agissant comme hormone.

L'acide ursodéoxycholique (UDCA) est un acide biliaire secondaire obtenu par l'épimérisation de l'acide chénodésoxycholique. Les effets anti-inflammatoires de l'UDCA ont été caractérisés *in vitro* (1,2) et *in vivo* dans des souris présentant une inflammation induite par du DSS (1). Cependant, l'étude des effets des acides biliaires *in vivo* est complexe en raison de leur métabolisation par le microbiote intestinal.

Afin de s'affranchir de cet écueil, nous avons choisi d'utiliser des souris OMM^{12}. En effet, le consortium OMM^{12} présente l'avantage de ne pas métaboliser les acides biliaires, convenant ainsi à leur étude *in vivo* (3). Dans un deuxième temps, nous avons mis au point un modèle d'inflammation induite par un entéropathogène, *Citrobacter rodentium*. A l'aide de ce nouveau modèle expérimental, nous avons étudié les effets anti-inflammatoires de l'UDCA *in vivo*. L'ajout d'UDCA dans la nourriture des souris OMM^{12} infectées par *C. rodentium* a permis d'observer une inhibition de la voie de l'IL-22, une cytokine clé de la réponse inflammatoire contre *C. rodentium*.

Dans ce projet, j'ai pris part à l'ensemble des expériences animales avec l'aide de Thierry Pédron, Quentin Lamy-Besnier et Marie Titécat. J'ai mis au point et réalisé les expériences in vitro. J'ai effectué l'analyse statistique des données, réalisé les figures et rédigé le manuscrit.

1. Ward JBJ, Lajczak NK, Kelly OB, O'Dwyer AM, Giddam AK, Ní Gabhann J, et al. Ursodeoxycholic acid and lithocholic acid exert anti-inflammatory actions in the colon. Am J Physiol Gastrointest Liver Physiol. 1 juin 2017;312(6):G550-8.

2. Ko WK, Lee SH, Kim SJ, Jo MJ, Kumar H, Han IB, et al. Anti-inflammatory effects of ursodeoxycholic acid by lipopolysaccharide-stimulated inflammatory responses in RAW 264.7 macrophages. PLoS One. 2017;12(6):e0180673.

3. Studer N, Desharnais L, Beutler M, Brugiroux S, Terrazos MA, Menin L, et al. Functional Intestinal Bile Acid 7α-Dehydroxylation by Clostridium scindens Associated with Protection from Clostridium difficile Infection in a Gnotobiotic Mouse Model. Front Cell Infect Microbiol. 2016;6:191.

Title

Ursodeoxycholic acid inhibits IL-22 pathway of bacterial-induced gut inflammation in isobiotic OMM[12] mice.

Authors

Lorenzo Chaffringeon[1,2,3], Quentin Lamy-Besnier[1], Marie Titecat[1,4], Loic Brot[2], Thierry Pédron[1], Luisa De Sordi[2,3], Jean-Pierre Grill[2,3], and Laurent Debarbieux[1]

Affiliations

1 Institut Pasteur, Université Paris Cité, CNRS UMR6047, Bacteriophage Bacterium Host, Paris F-75015 France

2 Sorbonne Université, INSERM, Centre de Recherche St Antoine, UMRS_938, Paris, France

3 Paris Center for Microbiome Medicine (PaCeMM) FHU, AP-HP, Paris, Ile-de-France, France

4 Université de Lille, INSERM, CHU Lille, U1286-INFINITE-Institute for Translational Research in Inflammation, F-59000 Lille, France

INTRODUCTION

Primary bile acids, such as chenodeoxycholic acid (CDCA), are molecules synthesized by the liver that are excreted in the digestive tract where they are metabolized by intestinal bacteria in a family of molecules called secondary bile acids. Secondary bile acids exert a large panel of functions from the emulsification of lipids during digestion to signalization through bile acid receptors. Ursodeoxycholic acid (UDCA) is an epimerized bile acid metabolised from chenodeoxycholic acid (CDCA) by bacteria in the colon and is used in the treatment of primary sclerosing cholangitis, a form of inflammation of the bile duct (1). In this condition, the anti-inflammatory property of UDCA leads to the stimulation of the hepatobiliary secretion that reduces the hydrophobicity and toxicity of the bile (1). It was also reported that the level of UDCA is reduced in colorectal cancer (2) and increased in remittent patients with inflammatory bowel diseases (3).

The anti-inflammatory and anti-apoptotic properties of UDCA have been studied with several *in vitro* systems such as the murine macrophage RAW264.7 stimulated with LPS (4), the human intestinal cells T84 stimulated with poly IC (5), or the primary culture of monocyte induced with TNFα (6). Using a DSS induced colitis model in conventional mice the anti-inflammatory capacity of UDCA was confirmed *in vivo* (5,7). Likewise, the intestinal inflammation driven by the pathogen *Clostridiodes difficile* was reduced by UDCA (8,9) . However, in these studies UDCA was transformed into lithocholic acid (LCA) by the gut microbiota of the mice (5,7). Finally, UDCA was found to exacerbate the intestinal inflammation of rats treated with indomethacin (10). Therefore, the demonstration and the mechanism of action of UDCA per se as a molecule reducing bacterial pathogen-induced intestinal inflammation remains to be demonstrated.

Animal models of pathogen-induced intestinal inflammation often rely on lethal pathogens (e.g., *Salmonella* or *C. difficile*) that offers a narrow window of observation to study the kinetics of anti-inflammatory compounds. The alternatives are pathogens that induce on a transitory inflammation such as the murine pathogen *Citrobacter rodentium*, which provokes a intestinal inflammation in mice that resolves itself by the combined action of the immune response and the niche competition provided by the resident microbiota. This murine enteropathogen is widely used to model several human infectious and inflammatory intestinal disorders (11–13). The infection process of *C. rodentium* in conventional mice includes four steps (14,15): (i) a caecal colonisation within the first 3 days post-gavage during which bacteria adapt to the gastro-intestinal environment of the host; (ii) a colonic expansion associated to a rarefaction of

anaerobes commensals (14,16); (iii) a peak of the bacterial load followed by a plateau and (iv) a clearance phase within the 3 weeks post infection. Conventionally, *C. rodentium* induces a self-limiting infection, triggers robust colitis, colonic crypt hyperplasia and dysbiosis (17,18).

One way to circumvent the metabolization of UDCA by the intestinal microbiota would be to use animals lacking bacteria encoding enzymes required for this transformation. This can be achieved through the use of gnotobiotic animals such as the OMM^{12} mice, which are axenic mice colonized by 12 bacteria representative of the five most abundant phyla of the murine gastrointestinal tract (19–21). In these animals, bile acids are not metabolized beyond their deconjugation, making them suitable to study secondary bile acids such as UDCA (22).

Here we first investigated the anti-inflammatory properties of UDCA *in vitro* on the human epithelial cell line Caco/Tc7 co-incubated with the human pathogen enteroaggregative *E. coli* strain 55989. Second, we developed and characterized *C. rodentium* induced intestinal inflammation in isobiotic OMM^{12} mice. Third, we assessed the anti-inflammatory impact of UDCA in *C. rodentium*-induced inflamed OMM^{12} mice and found that it relies on the IL-22 pathway.

RESULTS

UDCA reduces IL-8 secretion induced by the enteroaggregative *E. coli* strain 55989

To study the impact of UDCA on the intestinal inflammation induced by a bacterial pathogen, we incubated Caco2-Tc7 human epithelial cells with increasing concentration of UDCA (10^{-4}M, $2x10^{-4}$M, $5x10^{-4}$M, 10^{-3}M) for 18h before addition of the enteropathogenic *E. coli* strain 55959. We observed a UDCA dose-dependent reduction of the level of the inflammatory marker IL-8 (CXCL8) (Fig. 1A). Neither the LDH nor the *E. coli* levels measured in the supernatant at final time points were affected by the presence of UDCA compared to the control (Fig. 1B,1C). Moreover, the assessment of the ratio of free bacteria in the supernatant over adherent bacteria in presence/absence of UDCA (Fig. 1D) revealed no significant difference. Therefore, the presence of UDCA reduces the inflammatory response induced by a bacterial pathogen, without affecting cell viability as well as bacteria-cell interactions.

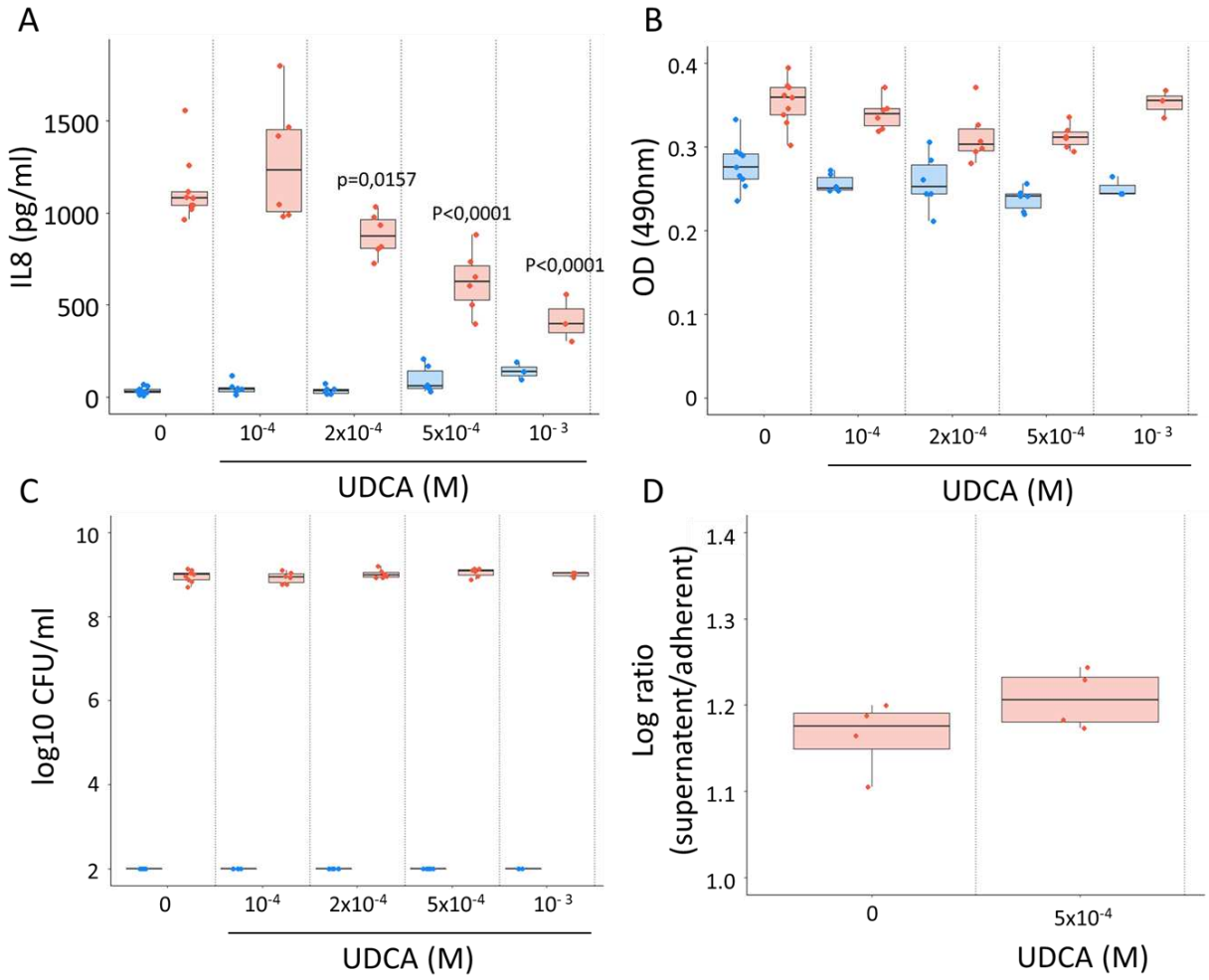

Figure 1: UDCA reduces IL-8 production by Caco2-Tc7 cells in the presence of *E. coli* strain 55989.

Caco2-Tc7 cells were incubated for 24h with concentrations of UDCA ranging from 0 to 10^{-3}M added in the medium prior to a 6 h incubation with (red) or without (blue) the bacteria *E. coli* strain 55989 (10^6CFU/ml). **A.** IL-8 concertation (pg/ml) at end point, **B.** LDH level and **C.** Bacteria concentration in the supernatant of cells culture after the co-incubation (n=3 to 9). **D.** Log ratio of free bacteria over adherent bacteria in the supernatant after a 6h co-incubation (n=4). p-value are compared to control condition in presence of *E. coli* strain 55959.

Citrobacter rodentium colonizes the gut of OMM^{12} mice without severe symptoms

Moving towards the evaluation of UDCA in a suitable murine model, we developed a *C. rodentium*-induced inflammation model in isobiotic OMM^{12} mice.

To determine the relationship between the infectious dose and the rate of infection we orally administered mice with decreasing doses of *C. rodentium* (10^7, 10^5, 10^3 and 10 CFU) and followed the fecal counts over 20 days as well monitored weight and health status.

The progressive increase of *C. rodentium* counts in feces reached the highest density (around 10^8 CFU/g) in all animals but was faster for mice that received the higher dose (day 6 post-gavage) than the lowest dose (day 10 post-gavage) (Fig. 2A). Accordingly, the body weight and the clinical status of these animals varied over time in function of the infectious dose (Fig. S1, Table S1). This demonstrates that OMM^{12} mice are highly permissive to *C. rodentium*, which colonization dynamic is dose-dependent. We also noticed that after reaching a peak the fecal levels of *C. rodentium* decreased in all groups by approximately 2-log during the next 5 days and then remained stable around 10^6 CFU/g up to day 20.

Fecal lipocalin-2 levels were measured at multiple time points to record the progression of intestinal inflammation (23) over time. The overall trend of an expected increase followed by a decline (according to the fecal levels of *C. rodentium*) was observed for all groups with variations being faster for the group that received the highest dose (Fig. 2B). These data showed that the fecal level of lipocalin-2 is linked to the fecal density of *C. rodentium*. The *C. rodentium* density in intestinal organs collected at day 20 showed no difference between the groups (Fig. 2C). This suggests that the host response controlling the intestinal colonization is unaffected by the initial dose of *C. rodentium*.

C. rodentium infection does not alter the OMM^{12} resident microbiota nor the population of induced prophages

The infectious process of *C. rodentium* in mice is well known (24). To evaluate whether this process was affected in OMM^{12} mice, we administered 10^7 CFU of *C. rodentium* to mice and monitored them mice during 20 days (Fig. 3A). The combination of three independent experiments consolidated the colonization kinetics that peaked at day 8 post-infection with *C. rodentium* levels reaching around 10^9 CFU/g of feces (Fig. 3B). Then, between day 8 and day 15, these levels decreased by approximately 3-log before they stabilized around 10^6 CFU/g of feces up to day 20 (Fig. 3B). These clearly show that in contrast to conventional mice *C. rodentium* is not eliminated from the gut of OMM^{12} within 20 days post.

The monitoring of weight and clinical signs of an intestinal disease revealed that animals slightly lose weight during the first 10 days post-infection and subsequently gained weight (Fig. S2), while symptoms were reported in all animals only between days 8 and 17 (Fig. S3).

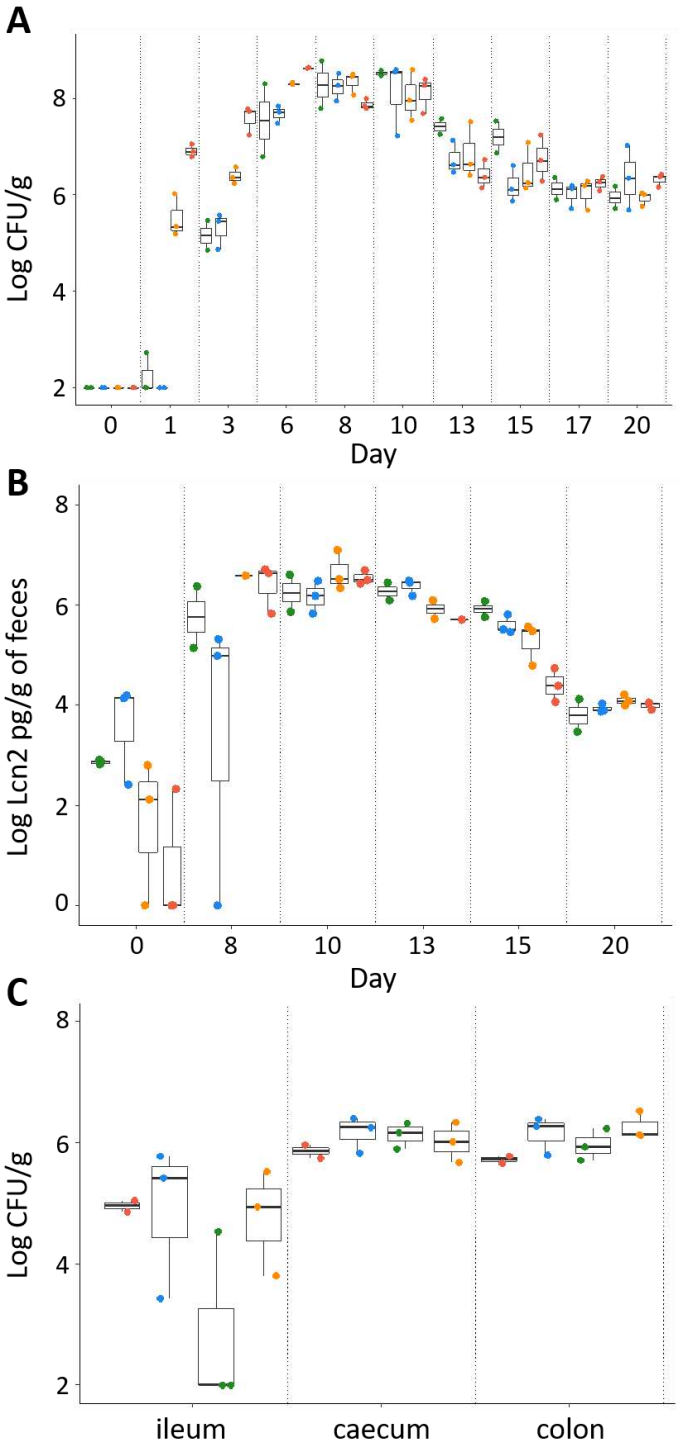

Figure 2: OMM[12] are permissive to *C rodentium* infection.
Mice were fed different doses of *C. rodentium*: green, 10 CFU (n=3); blue, 10^3 CFU (n=3); orange, 10^5 CFU (n=3); red, 10^7 CFU (n=3). **A.** Fecal levels of *C. rodentium* (CFU/g). **B.** Fecal lipocalin-2 levels (pg/g) over time. **C.** Levels of *C. rodentium* (CFU/g) in organs at day 20 post infection.

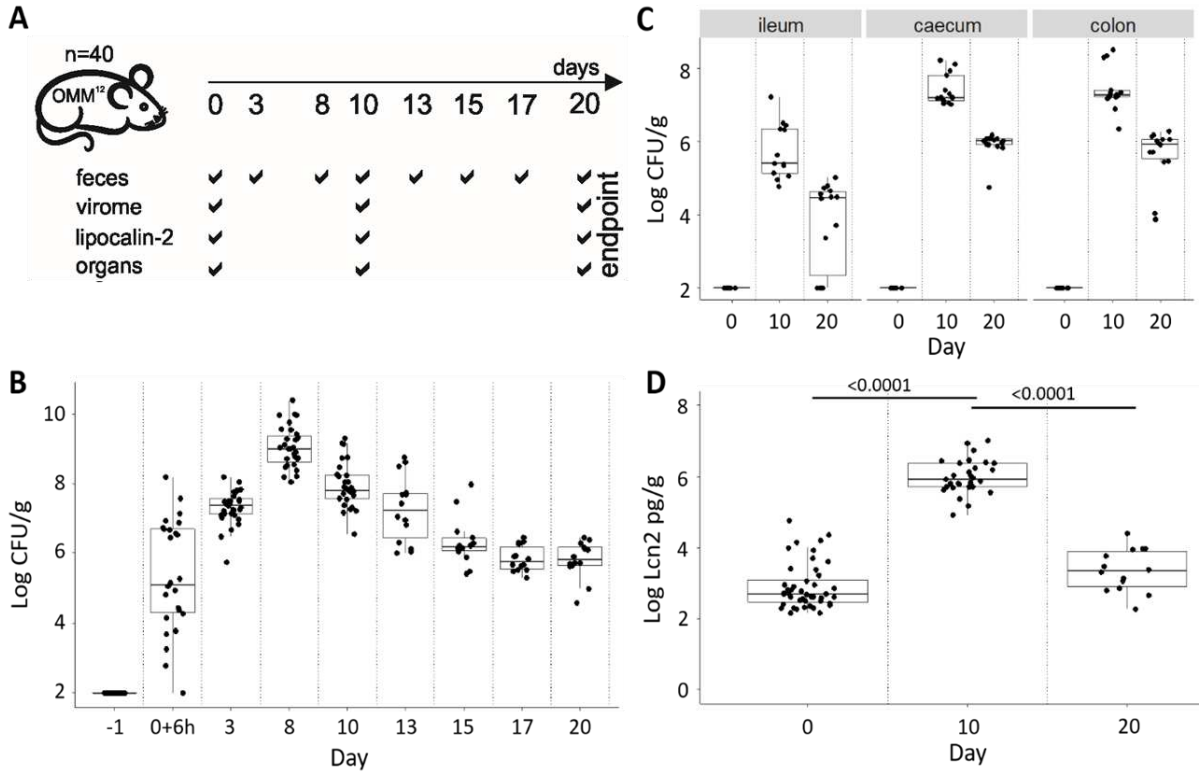

Figure 3: *C. rodentium* colonizes and cause inflammation in OMM[12] mice
A. Experimental design. **B.** Amount of *C. rodentium* (CFU/g) in fecal samples. **C.** Amount of *C. rodentium* (CFU/g) in intestinal organs. **D.** Levels of fecal lipocalin-2 (pg/g) over time.

C. rodentium is known to induce a dysbiosis while inflammation has previously been shown to induce prophage induction in a mice model (24,25), thus we studied the effect of *C. rodentium*-induced inflammation on the OMM[12] consortium and abundance of the prophages of the OMM[12] strains.

Next, we monitored in fecal samples collected at day 0, 10 and 20 the microbial and viral composition of the intestinal microbiota by performing 16S sequencing and virus-like particles (VLP) sequencing (see Methods). We found that the composition of the bacterial community between the three time points was highly similar with the obvious exception of the abundance of *C. rodentium* that rose at day 10 and decreased at day 20 (Fig 4A). The virome analysis showed that the population of induced prophages was similar at the three time points, for the nine strains for which sufficient data could be obtained (Fig. 4B). In particular, no region was found to be uniquely induced at any time point. A slight variation of the coverage depth of the prophages of *B. caecimuris* and *F. plautii* was observed in presence of *C. rodentium* compared to uninfected mice, which would require deeper investigation to be confirmed. Moreover, we

could not find any evidence of the induction of prophages from the *C. rodentium* strain, which contains 10 putative prophages. Therefore, the *C. rodentium* infection of the OMM[12] mice is highly reproducible and does not affect the relative abundance of the 12 resident bacteria nor the resident prophages, making it a robust bacterial-driven inflammatory model.

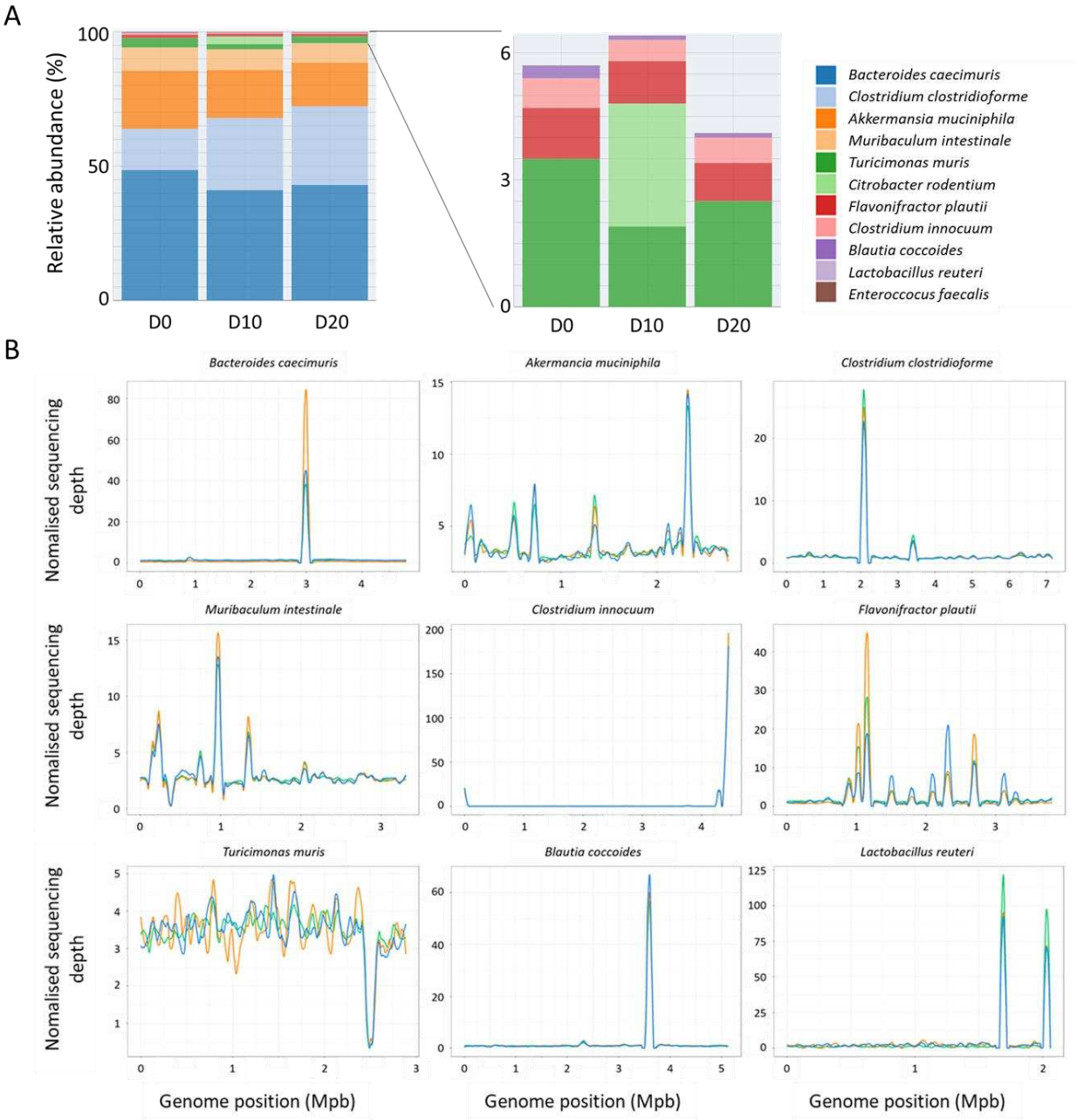

Figure 4: *C. rodentium* infection does not affect microbiota composition nor prophage induction of OMM[12] mice.

A. Relative abundance of the bacteria present in the OMM[12] consortium and *C. rodentium* assessed by 16S sequencing performed on the feces of the mice at days 0, 10, 20. **B.** Virome sequencing was performed on six mice at days 0, 10 and 20. The reads obtained were mapped on the 12 OMM[12] strains, and the resulting sequencing depth was merged per day. The resulting data for the three days are represented on the same graph for each strain: green, day 0; orange, day 10; blue, day 20. Two of 12 strains, *Acutalibacter muris* and *Bifidobacterium longum* subs. *animalis* were below the detection threshold.

In-depth characterization of the intestinal inflammation of *C. rodentium*-infected OMM^{12} mice

From the same set of experiments reported above, lipocalin-2 levels were measured at days 0, 10 and 20 and showed a 4-log increase between days 0 and 10 followed by a return to basal levels at day 20 post-infection (Fig. 3C, Table S2).

On day 0 (n=8), 10 (n=13) and 20 (n=14), intestinal organs (ileum, caecum, colon) were collected and *C. rodentium* CFUs counted. *C. rodentium* is present in all organs being more abundant in the caecum and colon compared to ileum, as expected for this pathogen (Fig. 3C). The bacterial load was approximately 2-log higher at day 10 compared to day 20, as expected from fecal counts.

Next, we measured the weight-to-size ratio of the colon, which has been reported to increase upon *C. rodentium* colonization (26). Our results indicated a significant increase of this ratio between day 0 and day 10 for the colon (Fig 5A, Table S3) but not for the ileum (Fig. S4) nor the caecum (Fig. S5).

Then, we measured the cell proliferation in the colon, which was significantly higher on day 10 compared to both day 0 and day 20 (Fig. 5B, Table S4). In addition, we measured crypt length in colon samples and observed again an increase at day 10 compared to both day 0 and day 20 (Fig. 5C, Table S5). We also quantified the lectin binding to goblet cells as a proxy of mucus abundance, which is decreased during *C. rodentium* infection (18). While mucus production tended to decrease between day 0 and day 10 (no significant difference) (Fig. 5D, Table S6), we noted a significant increase between day 10 and day 20. These observations were accompanied by a decrease in the number of goblet cells per crypt on day 10 compared to days 0 and 20 (Fig. 5E, Table S7).

Finally, from independent colon samples collected at day 0 (n=6), 10 (n=6) and 20 (n=6) post-*C. rodentium* infection, we performed qPCR to investigate the role of IL-17 and IL-22 pathways known to be involved in the immune response against *C. rodentium* in conventional mice. We observed an increased level of IL-17 and IL-22 at day 10 compared day 0 and day 20 (Fig. 6A and 6B). Next, we assessed the levels of the anti-microbial peptide REG3γ, the pro-inflammatory cytokines TNFα and IL1β and the chemokines CXCL1, 2 and 3 that all exhibit the same pattern as IL-17 and IL-22 (Fig. 6E-I). The level of the anti-inflammatory cytokines, TGFβ, IFNγ and IL-10 were either unchanged or tend to a reduction on day 10 compared to day 0 and day 20 (Fig. S5A-C).

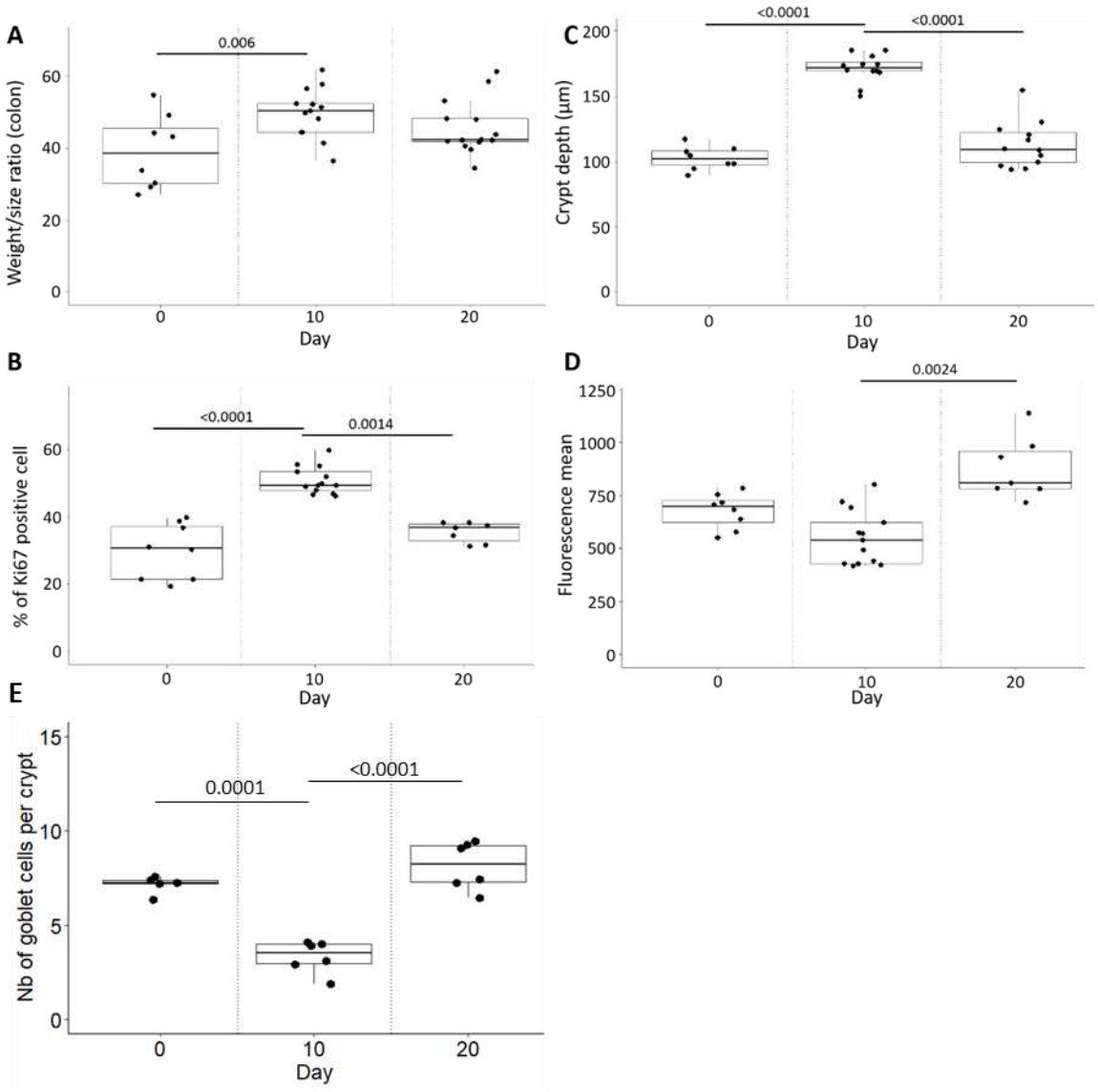

Figure 5: Macroscopic and cellular alterations of the colon of *C. rodentium*-infected OMM[12] mice
The colon of OMM[12] mice collected at day 0, 10 and 20 post *C. rodentium* infection was examined to evaluate **A.** Weight/size ratio; **B.** Percentage of Ki67 positive cells; **C.** Crypt depth (µm) and **D.** lectin staining of goblet cells (fluorescence mean). **E.** Mean number of goblet cells per crypt.

The expression of the anti-microbial peptides: cryptidin-1 and 4, CRAMP and LZP and the main protein of the mucus, Muc2, were also not increased on day 10 (Fig. S5D-H). The level of IL23, a cytokine necessary for the induction of the production of IL22, was surprisingly low on day 10 (Fig. 6 I). However, it should be noted that the expression of IL23 in the response against *C. rodentium* takes places in the early days of the infection (24).

Altogether, the results show that the *C. rodentium* infection process in OMM[12] mice is highly similar towards the host response, being much closer to conventional mice than axenic mice. These data demonstrate that *C. rodentium*-infected OMM[12] mice are a suitable model to assess the property of anti-inflammatory compounds towards intestinal bacterial infections.

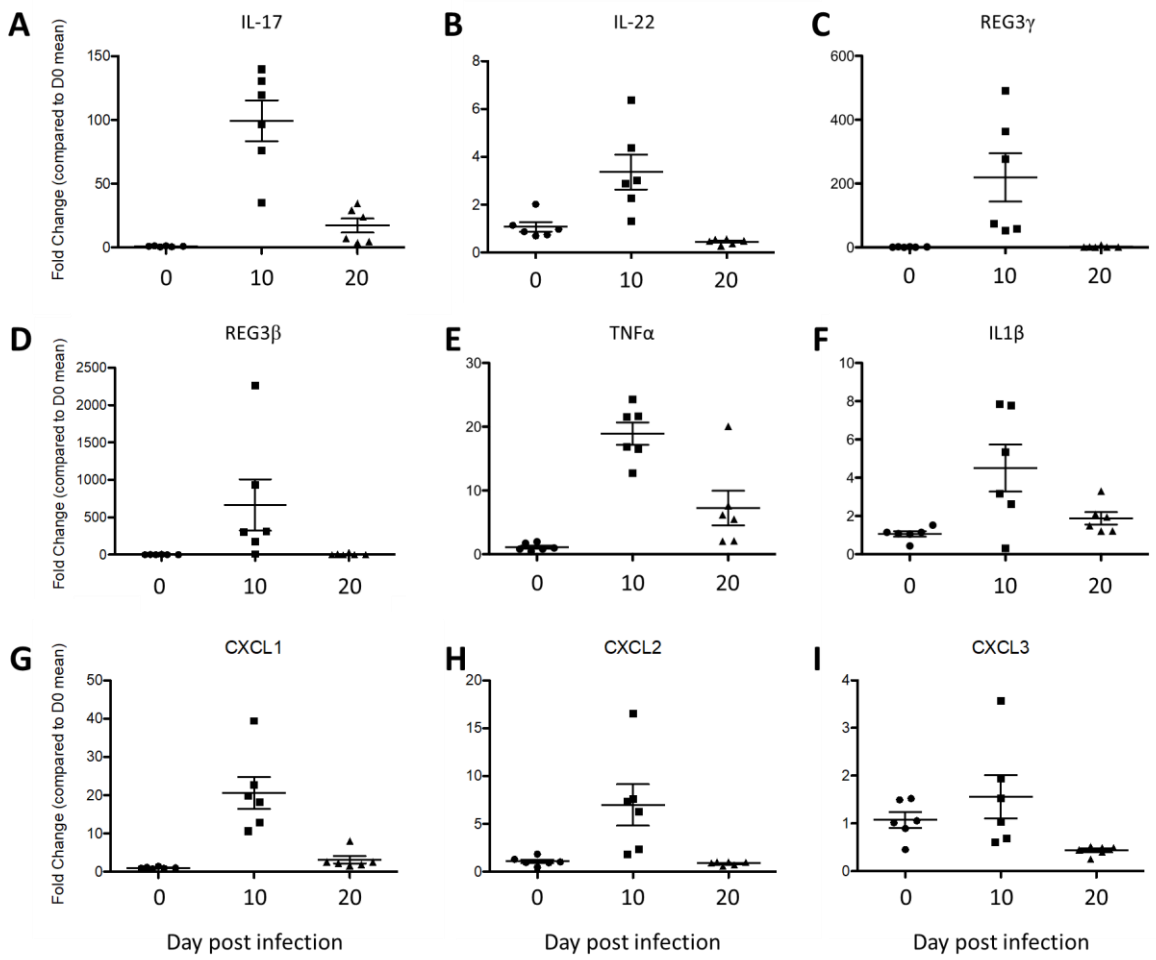

Figure 6: The *C. rodentium* infection upregulates the expression of genes involved in the IL-17 and IL-22 pathways.
OMM[12] mice colonized by *C. rodentium* were sacrificed at day 0 (n=6), day 10 (n=6) and day 20 (n=6). **A-I.** Relative expression level of the indicated genes in the colon at days 10 and 20 compared to day 0.

UDCA inhibits the IL-22 pathway in the colon of mice infected by *C. rodentium*

To assess the anti-inflammatory potential of UDCA *in vivo*, three groups of mice received a diet completed with either 0 (n=4), 0.5 (n=6) or 1 g/kg (n=6) of UDCA four days before *C. rodentium* infection.

The fecal concentration of UDCA was determined one day before as well as three and nine days after its addition. We observe a sharp concentration dependent increase of UDCA concentration on day -1 and day 9 both compared to day -4 (Fig. 7A). The conjugated forms of UDCA, glycoursodeoxycholic (GUDCA) and tauroursodeoxycholic (TUDCA) followed the same variations as UDCA, showing that UDCA enters the entero-hepatic circulation (Fig7B and C). The level sulfated derivative of UDCA, ursodeoxycholic acid 3-sulfate (UDCA 3S) was increased on day -1 and day 9 both compared to day -4, but with a high variability between

animals (Fig. 7D). We also confirmed the UDCA was not metabolized into LCA or its derivative (Fig. 7E-G).

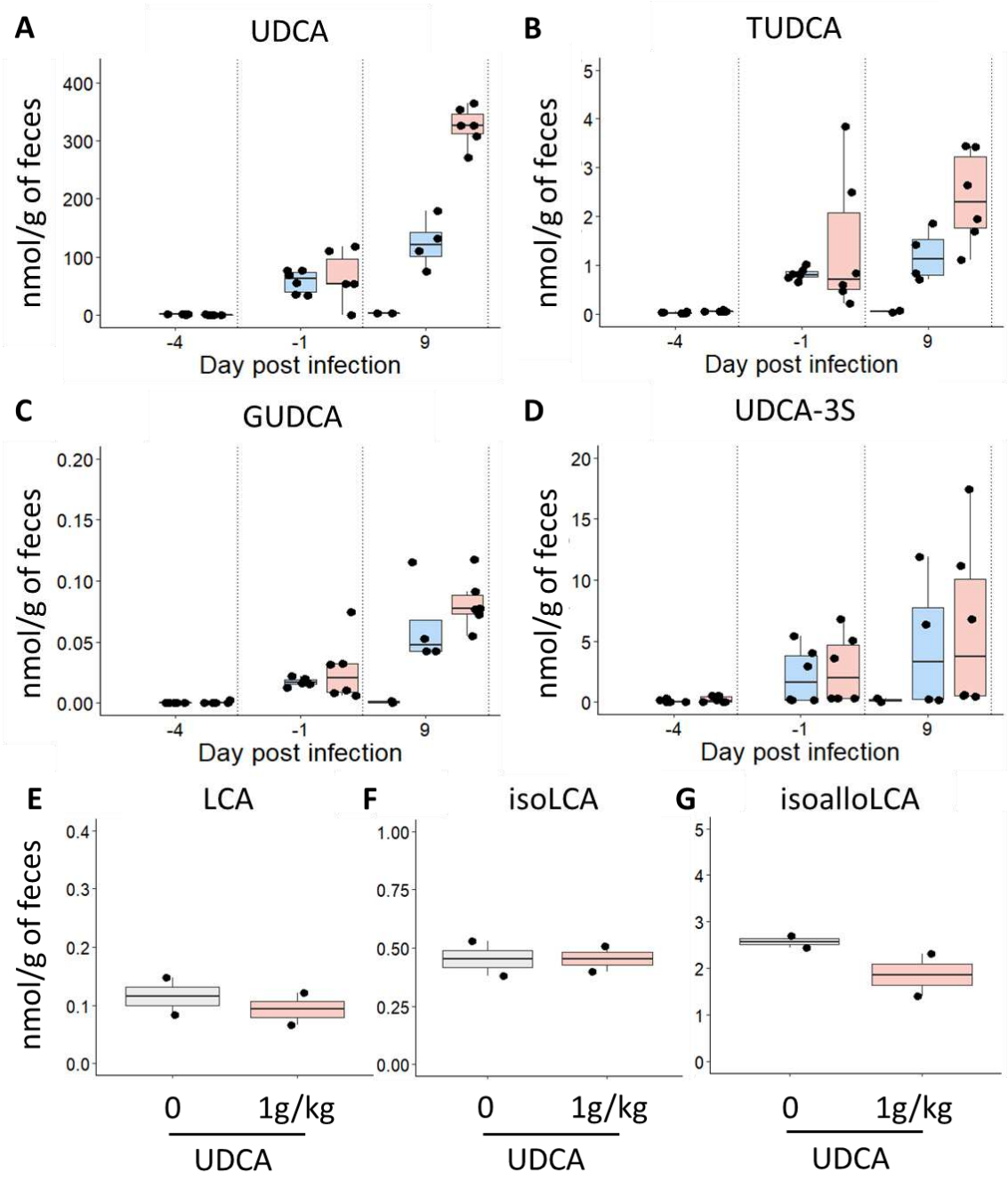

Figure 7: UDCA incorporated in the food is assimilated by OMM[12] mice and reaches the enterohepatic circulation.

OMM[12] mice were fed with 0 (grey; n=4), or 0.5 (blue; n=6) or 1 g/kg (red; n=6) of UDCA four days before the infection by *C. rodentium* (10^7 CFU) initiated at day 0. Fecal samples were taken at the indicated time points to measure **A.** UDCA levels and **B-D.** its derivatives. On day 9, **E.** LCA level and **F-G** its derivatives were measured. GUDCA: glycoursodeoxycholic; TUDCA: tauroursodeoxycholic; UDCA 3S: ursodeoxycholic acid 3-sulfate. IsoLCA: isolithocholic acid ; isoalloLCA: isoallolithocholic acid

During the course of these experiments the fecal levels of *C. rodentium* colonization were unaffected by the presence of UDCA (Fig. 8A) nor was the level of lipocalin 2 (Fig. 7C). Moreover, the density of *C. rodentium* in gut sections (ileum, caecum, colon) collected 10 days post-infection was undistinguishable between the three groups (Fig 8B) and very similar to those observed previously (Fig. 3B). Accordingly, the weight variation of all animals remains within 10% of their initial weight (Fig. 8D). Therefore, the addition of UDCA in the food of mice led to its assimilation reaching the liver where it is conjugated, but any of the two doses had an impact on the colonization pattern of *C. rodentium* in OMM^{12} mice, neither on fecal lipocalin-2 levels. Nevertheless, we performed qPCR quantification of the expression of genes related to IL-17 and IL-22 pathways. While no change was observed on the IL-17 pathway (Fig. 9A), the levels of genes coding for IL-22, REG3γ and REG3β were all decreased in the two groups that received UDCA compared to the control group (Fig 9B-D). Therefore, UDCA lowers the activation of the IL-22 pathway in the colon of OMM^{12} mice infected by *C. rodentium*. An attempt with a higher dose of UDCA (5 g/kg) was initiated but the mice showed a prolonged loss of weight that affected the *C. rodentium* infection, suggesting that this elevated dose of UDCA is toxic (data not shown).

DISCUSSION

Inflammatory bowel disease is a multifactorial affection for which there is no treatment providing a definitive relapse (27). Experimental models of intestinal inflammation are then pivotal to decipher the molecular mechanisms involved as well as to develop anti-inflammatory treatments. Amongst the recent advances in treatment, a particular attention was given to the immunomodulatory effect of secondary bile acids. These molecules are metabolised by the gut microbiota to produce a family of secondary bile acids with both pro- and anti-inflammatory properties (28,29). However, the study of these molecules *in vivo* has been jeopardized by their metabolisation by the gut microbiota of conventional murine model. On the other hand, axenic mice are not suitable as they provide a perturbed inflammatory response.

The inability of the OMM^{12} isobiotic mice to metabolise bile acids makes it a candidate to assess their property *in vivo*. Moreover, these mice have been shown to be permissive to intestinal pathogens such as *Salmonella enterica* serovar Typhimurium(30). Here, we showed that a single administration of as low as 10 CFU of *C. rodentium* to OMM^{12} mice is sufficient to

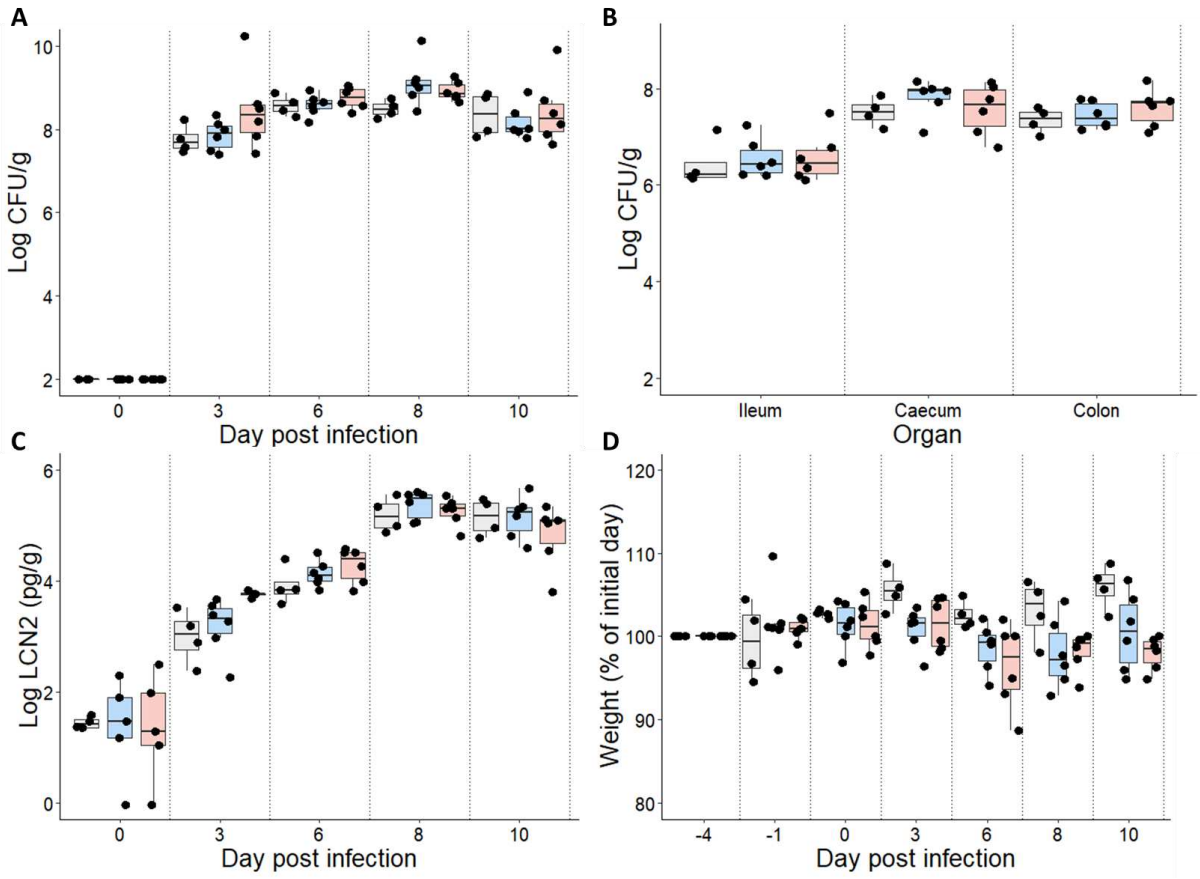

Figure 8: UDCA does not affect the colonization of *C. rodentium*.

OMM^{12} mice were fed with 0 (grey; n=4), or 0.5 (blue; n=6) or 1 g/kg (red; n=6) of UDCA four days before the infection by *C. rodentium* (10^7 CFU) initiated at day 0. **A.** Fecal levels of *C. rodentium* (Log CFU/g). **B.** Levels of *C. rodentium* (Log CFU/g) in organs collected at day 10 post infection. **C.** Fecal lipocalin-2 levels (Log pg/g) over time. **D.** Variation of the OMM^{12} mice weight over time (% of their initial weight).

induce a non-lethal intestinal infection. This infection kinetic is highly reproducible and leads to a peak of intestinal inflammation as witnessed by macroscopic damages and induced immune response (IL-17 and IL-22 pathways). Interestingly, this process is not associated with variations of neither the resident bacteria nor the resident induced prophages. The latest is surprising since it was shown that the context of IBD increases the proportion of temperate compared to virulent phages (31). Furthermore, an experimental assay showed that intestinal inflammation driven by a bacterial infection boosts the prophage transfert from one *Salmonella* strain to another, suggesting that intestinal inflammation induces prophage excision (32). As the lipocalin-2 levels observed in Salmonella-infected OMM^{12} is mice was about 100 fold higher than those obtained with *C. rodentium*, it remains possible that is intestinal inflammation was strong enough to induce additional prophages.

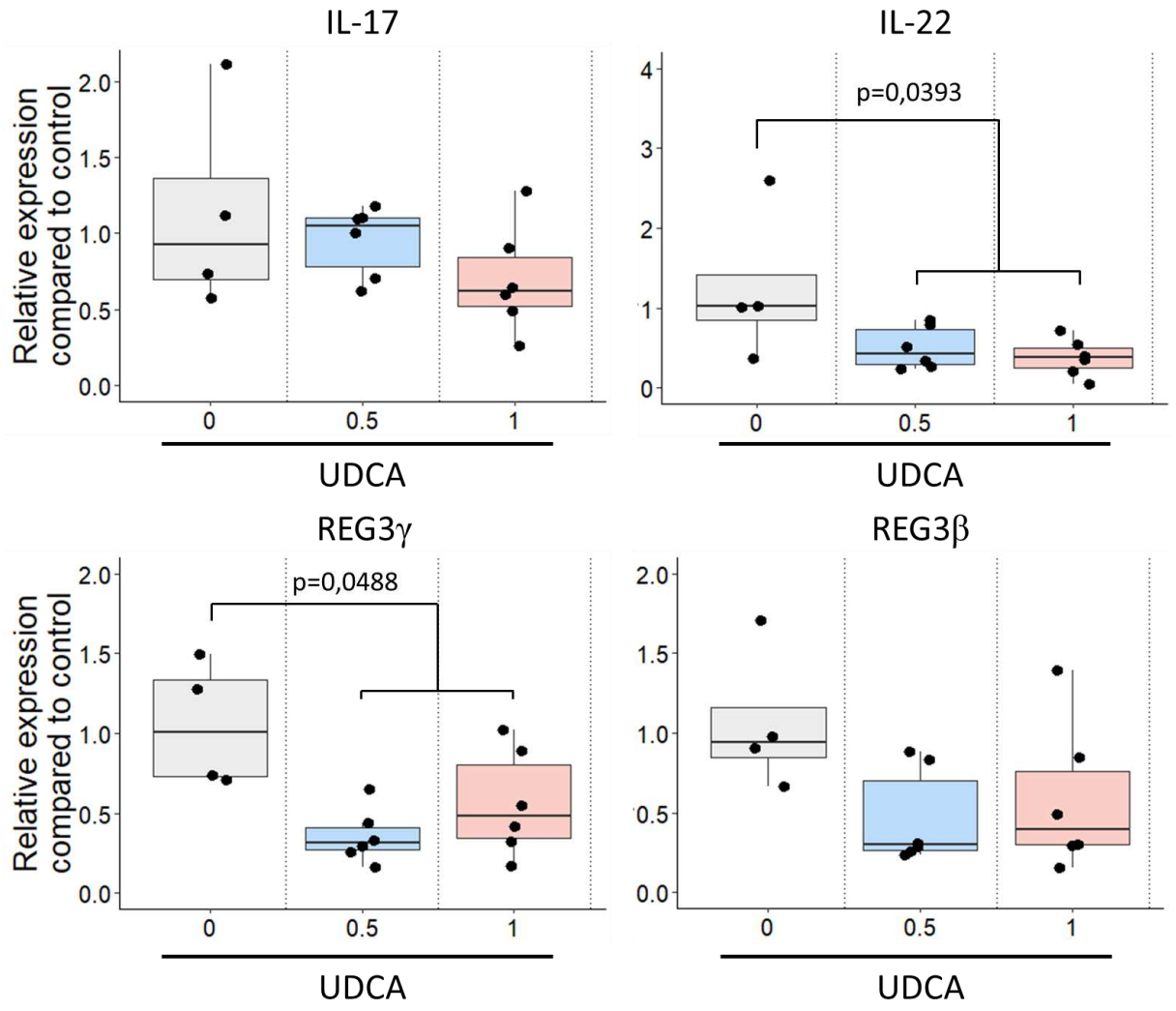

Figure 9: UDCA inhibits the IL-22 pathways in *C. rodentium*-infected OMM[12] mice.
OMM[12] mice were fed with 0 (grey; n=4), or 0.5 (blue; n=6) or 1 g/kg (red; n=6) of UDCA four days before the infection by *C. rodentium* (10^7 CFU) initiated at day 0. Colon samples were collected at day 10 and mRNA extracted to quantify the relative expression level of the indicated genes in the two UDCA groups compared to the group without UDCA. **A-D.**

We observed one key difference in the process of *C. rodentium* infection in OMM[12] compared to conventional mice. This pathogen is not eliminated after the induction of the host response. It is proposed that in conventional mice the inflammation drives the reduction of *C. rodentium* that is further eliminated by the competition provided by resident bacteria. Here, due to the low, if not the lack, of competition provided by the 12 strains, the level of *C. rodentium* stabilizes around 10^6 CFU/g of feces. This observation revealed that the host response of OMM[12] mice is effective to reduce the colonization by 3 log but no more. It opens new questions such as how, post-inflammation, *C. rodentium* is not anymore perceived as an intestinal pathogen, which may uncover how bacteria can transition from intestinal pathogens to commensal-like

colonization. It also opens the possibility to individually test the role of commensal bacteria that were proposed to be competing with *C. rodentium* colonization (33,34).

While the anti-inflammatory effects of UDCA have been known for a long time, its mechanism of action to putatively modulate intestinal inflammation *in vivo* remains unclear. UDCA was shown to affect antigen-presenting cell by repressing the major histocompatibility complex of class II (35) and to inhibit the cyclooxygenase 2 (36).

Using *C. rodentium*-infected OMM^{12} mice, we assessed the immunomodulatory property of UDCA and found that it does not reduce the fecal level of lipocaline-2, but lowers the IL-22 response, which is critical for the control of *C. rodentium*. Indeed, IL22 reinforces the epithelial barrier and induces the production of antimicrobial peptides such as REG3γ, REG3β, and lipocalin-2 (37). Surprisingly, the level of IL-17 that is often co-regulated with IL-22, was not decreased in the presence of UDCA (18). Since IL-17 also induces the production of lipocalin-2, this could explain why UDCA had no impact on lipocaline-2 levels. Both cytokines are produced by the innate lymphoid cells 3 (ILC3) and the T-lymphocyte Th17. However, the sub-population of ILC3 NKp46^{+}, important in the early reaction against attaching effacing pathogens like *C. rodentium*, displays a production of IL-22 without affecting the production of IL-17, which fits with our observations (38). The level of IL-22 can also be modulated by the IL-22 binding protein (IL-22PB) which blocks the activity of IL-22. IL-22PB is highly expressed by the dendritic cells in the colon (39) and its production could be affected by the presence of UDCA that affects antigen-presenting cell by repressing the major histocompatibility complex of class II.

To conclude, we characterized an original murine model to study the immunomodulatory property of UDCA and highlight its mechanism of action via the inhibition of the IL-22 response independently of the IL-17 pathway. This model could be used to study other bile acids and potentially any other drugs that could lower the intestinal inflammation induced by the pathogen *C. rodentium*. It also provides opportunities to test the bacterial competition between commensal and pathogens in absence of animal mortality.

MATERIAL AND METHODS

Ethics statement

All animal experiments were approved by the committee on animal experimentation at the Institut Pasteur (Paris, France) and by the French Ministry of Research. A total of 86 OMM^{12} (C57Bl/6J) mice from seven to nine-weeks old bred at Institut Pasteur were used.

Bacterial strains and culture conditions

Citrobacter rodentium strain ICC180, derived from strain DBS100 (14), and *Escherichia coli* strain 55989, described in (40), were used and routinely cultured in lysogeny broth (LB), LB agar or Drigalski agar (Bio-Rad, Hercules, CA) plates, at 37°C. For oral administration of ICC180, an overnight liquid culture in LB (around 1 x 10^9 CFU/mL) and subsequently diluted in sucrose bicarbonate buffer (20% sucrose and 2.6% sodium bicarbonate, pH 8).

IL-8 secretion of Caco2/Tc7 exposed to *E. coli* strain 55989

Caco-2/TC7 cells were seeded at 10^5 cells/well in 6-well plastic culture plates and maintained in high glucose medium (DMEM GlutaMAX 4.5 g/L glucose, ThermoFisher Scientific Waltham, MA, USA) supplemented with 20% heat-inactivated fetal calf serum (FCS, GE Healthcare, Life Science, Chicago, IL, USA), 1% non-essential amino acids NEAA, and 1% penicillin-streptomycin (ThermoFisher Scientific, Waltham, MA, USA). The cells were cultured at 37 ◦C in a 10% CO2/air atmosphere. The media were changed every day. Confluency was reached on day 6. On day 19, the cells were serum-starved, and supplemented with doses of UDCA from 0 to 10^{-3}M. The cells were incubated for 18 h before the addition of 20µL of an exponential culture of *E. coli* strain 55989 grown in LB and adjusted to OD600nm of 0.125 into the each well. 20µL of LB were added in control wells. After a 6 h co-incubation, the supernatants were collected, and stored at −80 ◦C before IL-8 quantification by ELISA (Duoset Human CXCL8/IL-8, R&D Systems, Minneapolis, MN, USA), according to manufacturer's instructions. Cytotoxicity was monitored via the dosage of LDH released. LDH assays (Roche, Basel, Switzerland) were performed immediately before freezing. Serial dilutions in PBS were performed and plated onto LB plates for *E. coli* quantification (CFU) in the supernatant. For the quantification of adherent bacteria, each well was washed three times with 1ml of PBS, then scratch and resuspended in 1ml of PBS to harvest the adherent cells. The suspension was homogenized by pipetting then serial dilutions were platted on LB agar.

C. rodentium infection of OMM^{12} mice

In all experiments, mice were randomly assigned to a group and each group included approximately the same number of male and female animals kept in separate cages. Mice were observed at least once every two days, weighed and feces were collected at indicated time points. Fecal pellets were then transferred in pre-weighed, sterile 2 mL tubes, weighed and then resuspended in 1 mL of PBS. An aliquot was centrifuged, and the supernatant was stored at -20°C. Serial dilutions in PBS of the resuspended pellets were performed and plated onto Drigalski plates for *C. rodentium* quantification (CFU/g of feces).

200 µL of *Citrobacter* (1 x 10^7, 1 x 10^5, 1 x 10^3 or 10 CFU) was administered by oral gavage to the mice. Control mice received 200 µL of PBS instead. At the end of all experiments, mice were sacrificed by cervical dislocation and intestinal sections (i.e., ileum, caecum, and colon) were collected. These sections were weighted (ileum, caecum, colon) and measured (ileum, colon) and a section was taken for histology examination. The residual organs were weighted and homogenized in PBS using gentleMACS^{TM} OctoDissociator (Miltenyi Biotec), serially diluted in PBS and plated on Drigalski plates. 5 mice were used for control in the first set of experiment and no organ were recovered from them.

UDCA (Sigma-Aldrich, St. Louis, MO) was added to the standard chow (Safe digest, R03-40) by mixing food pellet into powder. UDCA powder was then mixed at the final concentration of 0.1% or 0.05% (weight/weight). Food pellets were reformed with the addition of sterile water, dried and subsequently treated with X-ray (1100Gy with Faxitron).

Bile acids analysis

Mice feces were weighted (around 50mg) and supplemented with acidified water (1% formic acid) to a final concentration of 100 mg/mL. Feces were homogenised using ceramic beads and the « soft » program of the Precellys Evolution instrument until complete homogenization. For the extraction, a volume equivalent to 20 mg feces (200 µl homogenate) was supplemented with deuterated internal standards and 1400 µL acetonitrile for protein precipitation. Mixture was vortexed and centrifuged at 10 000 g, for 1 minute and left at 4 C for 1 h for total precipitation. Mixture was centrifuged at 20 000 g for 20 min at 4 C and 100 µL of the upper phase collected dried and resuspended in 100 µL methanol/water 50-50 v/v)

An LC MS/MS analysis of UDCA and UDCA derived bile acids was then performed. UDCA, TUDCA, UDCA 3S and GUDCA were analysed by LC ESI/MS/MS using a Prominence UFLC

and a QTrap 4000 mass spectrometer. Sample (4 µL) was injected to a Ascentis Express C 18 column 2.1 x 150. Mobile phases consisted of water and acetonitrile containing 0 1 formic acid and 2 mM ammonium acetate. Bile acids were detected using scheduled multiple reaction monitoring sMRM in the negative ion mode.

Lipocalin-2 assay

Frozen supernatants of fecal samples were thawed before lipocalin-2 quantification using a commercial ELISA kit (#DY1857, R&D Systems), according to the manufacturer's instructions.

Histological analysis

The distal colon sample (1 cm) was fixed overnight in Carnoy (ethanol/chloroform/acetic acid 60:30:10) at 4°C for mucus preservation, dehydrated, and embedded in paraffin. All the stainings were done on dewaxed 8-µm sections by submersing them in Xylene twice for 10 min, 100% ethanol (EtOH) twice for 10 min, 90% EtOH once for 10 min, 70% EtOH once for 10 min, and PBS once for 10 min. Sections were then stained with hematoxylin and eosin (H&E) or processed for immunofluorescence (IF). In IF experiments, sections were then heated for 20 min in demasking solution (citric acid buffer, 10 mM, pH 6, in distilled H_2O). Once cooled, slides were first blocked with 100 µL of Protein Block, Serum-Free (Agilent, #X090930-2) for 30 min in a humid chamber before being incubated with primary antibody diluted in PBS with 10% Protein Block overnight at 4°C. The primary rabbit polyclonal anti-*C. rodentium* antibody (Covalab) was diluted 1:200, rabbit anti-Ki67 (abcam, #ab16667) was diluted 1:100. For goblet cells detection, a combination of fluorescent lectins WGA-FITC and UEA1-FITC, each diluted 1:500, (Vector Laboratories, #FLK-2100) were used. Slides were rinsed twice for 10 min each time in PBS, followed by incubation with goat anti-rabbit A555 diluted 1:100 (Fischer Scientific, #15636746) for 2 h at room temperature. After two washing steps slides were incubated with DAPI (4',6-diamidino-2-phenylindole) diluted 1:1000 for 5 min (ThermoFisher Scientific, #D1306). Washing steps were repeated before slides were mounted with ProLong Gold antifade reagent (ThermoFisher Scientific, #P36930).

H&E-stained sections were analyzed on the IX81 Olympus microscope. At least 20 well-oriented crypts from each gut section per individual mouse were examined and staining was measured. Similarly, Ki67 staining was also measured by this method and divided by the total number of cells to calculate the percentage of Ki67 cells per crypt. The density of goblet cells

was calculated by measuring the fluorescence mean of the lectin staining. All images were analyzed using ImageJ (Fiji) (41).

RNA Extraction and cDNA synthesis

One centimeter of distal colon was homogenized in 1 mL Trizol. After extraction with chloroform, precipitation with isopropanol and washings with 70% (vol/vol) ethanol, extracted RNA was resuspended in 100 µL of sterile distilled water. A clean-up of the RNA was performed with the RNEasy Mini kit (Qiagen). cDNA synthesis was performed from 2 µg of RNA using oligo-dT (Promega) and SuperScript II (Life Technologies).

RT-qPCR Analysis of Colonic Cell Gene Expression

Colonic RNAs were analyzed by RT-qPCR. The list of the genes detected using the SYBR Green PCR system and the primers associated are listed in Table S9. Differences were calculated using the comparative 2-ΔΔCt method (42). Results obtained with the QuantStudio 7 Flex Real-Time PCR System, 384-well (Life Technologies) were normalized to those for the Gapdh gene and compared with the mean target gene expression in uninfected mice.

Virome preparation and sequencing

Fecal samples (2 pellets minimum) were frozen at -20°C upon collection and subsequently thawed and resuspended in 14 mL Tris 10 mM, pH 8 and centrifuged for 10 min at 5,200g, 4°C. The supernatant was then filtered (0.45 µm and then 0.22 µm) and ultracentrifuged for 3 h at 270,000 g. Pellets were resuspended in 500 µL of TN buffer (10 mM Tris, 150 M, pH 7.5). To remove free DNA and RNA, 4 U of Turbo DNaseI (Ambion, #AM2239) and 10 µL of RNAse (A/T1 mix, ThermoFisher, #EN0551) were added for 30 min at 37°C. EDTA (15 mM final), proteinase K (100 µg/mL, Eurobio) and SDS (10% final) were added and samples were incubated 30 min at 37°C. The viral DNA was extracted by adding a volume of phenol-chloroform-isoamyl alcohol (25:24:1). After vortexing for 30 sec and a centrifugation for 5 min at 12,000 g, the aqueous phase was recovered and treated again with phenol-chloroform-isoamyl alcohol similarly. Sodium acetate (300 mM final), 2 volumes of 100% EtOH and glycogen (1 µL) were added to recovered DNA. The sample was mixed by inversion and incubated for 2 h at -80°C before centrifugation for 20 min at 15,000 g, 4°C. The supernatants were discarded, and pellets were dried and then resuspended in 20 µL Tris 10 mM, pH 8. The

DNA concentration was measured with Qubit (Invitrogen). Libraries were prepared using TruSeq Nano DNA Sample Preparation Kit (Illumina) and were sequenced on a MiSeq (Illumina, #20015964), 2 x 150 nucleotides, paired end.

Prophage annotation

Prophage annotation for *Citrobacter rodentium* strain ICC180 was realized with Phaster (43).

Virome read analysis

The quality of the reads was assessed with FastQC (44). The reads were cleaned with fastp, with default parameters (45). They were then mapped against the most recent version of each of the 12 reference genomes of the OMM^{12} (46). The resulting mapping files were used to generate the sequencing depth at each position of the genomes using SAMtools (47). This depth was added for the six mice for each bacterium and time point and was then normalized by the total sequencing depth. The depth was then averaged in 1 kb windows, and then three time points (day 0, 10 and 20) were plotted in the same graph. Bacteria for which less than 100 reads per sample mapped on their genome were excluded from the analysis. Two of 12 strains, *Acutalibacter muris* and *Bifidobacterium longum* subs. *animalis* were below the detection threshold.

16S rRNA gene analysis

Resuspended fecal samples (500 µL) were centrifuged at 8,000 g for 10 min, and the supernatant removed. Pellets were resuspended in 500 µL of lysis buffer (500 mM NaCl, 50 mM Tris-HCl, pH 8.0, 50 mM EDTA, 4% sodium dodecyl sulfate) and incubated for 15 min at 50°C (40). Then, 100 µL of lysozyme (25 mg/mL) was added and samples were incubated at 37°C for 2 h. DNA extraction was performed using the Maxwell 16 tissue DNA purification kit (Promega). Amplicon libraries targeting the V3-V4 16S rRNA gene region were then constructed using Illumina primers (forward primer, 5'-TCGTCGGCAGCGTCAGA TGTGTATAAGAGACAGCCTACGGGNGGCWGCAG-3', and reverse primer, 5'-GTCTCGTGGGCTCGGAGATGTGTATAAGAGACAGGACTACHVGGGTATCTAATCC -3') and amplified by PCR for 25 cycles. The libraries were sequenced on an Illumina MiSeq instrument (2x300 bp). FastQC (http://www.bioinformatics.babraham.ac.uk/projects/ fastqc/) was used for the quality control of the reads. Read filtering, operational taxonomic unit (OTU) clustering, and annotation were performed with the MASQUE pipeline

(https://github.com/aghozlane/masque). All statistical analyses were performed with SHAMAN (http://shaman.c3bi.pasteur.fr) as previously described (48).

ACKNOWLEDGMENTS

We thank the members of the Centre for Gnotobiology Platform of the Institut Pasteur (Thierry Angélique, Eddie Maranghi, Martine Jacob, and Marisa Gabriela Lopez Dieguez) for their help with the animal work. We thank G M. Haustant, L. Lemée, Biomics Platform, C2RT, Institut Pasteur, Paris, France, supported by France Génomique (ANR-10-INBS-09-09) and IBISA for the 16S sequencing. LC is funded by a PhD fellowship from the Ministère de l'Enseignement Supérieur et de la Recherche, France, Ecole Doctorale 394. QLB is funded by École Doctorale FIRE - Programme Bettencourt. MT received a fellowship from Fondation DigestScience. LD receives fundings from ANR-20-CE92-0048, and LDS receives fundings from the Agence Nationale de la Recerche (ANR) and the Societé Nationale Française de Gastro-Ente´ rologie (SNFGE).

AUTHOR CONTRIBUTIONS

Conceptualization, J-P.G, L.C., L.D., and L.D.S.; Methodology, , J-P.G, L.C., L.D., and L.D.S.; Investigation, L.B., L.C., M.T., Q.L.-B., and T.P.; Formal Analysis, L.C., ; Writing – Original Draft, J-P.G., L.C., L.D. and L.D.S. ; Writing – Review & Editing, J-P.G., L.C., L.D., L.D.S. and T.P.; Funding Acquisition, J-P. G, L.D., and L.D.S.; Resources J-P.G, L.D., and L.D.S.; Supervision, J-P.G., L.D. and L.D.S.

DECLARATION OF INTERESTS

The authors declare no competing interests.

REFERENCES

1. Vesterhus M, Karlsen TH. Emerging therapies in primary sclerosing cholangitis: pathophysiological basis and clinical opportunities. J Gastroenterol. 1 juin 2020;55(6):588-614.

2. Weir TL, Manter DK, Sheflin AM, Barnett BA, Heuberger AL, Ryan EP. Stool microbiome and metabolome differences between colorectal cancer patients and healthy adults. PLoS One. 2013;8(8):e70803.

3. Lee JWJ, Plichta D, Hogstrom L, Borren NZ, Lau H, Gregory SM, et al. Multi-omics reveal microbial determinants impacting responses to biologic therapies in inflammatory bowel disease. Cell Host Microbe. 11 août 2021;29(8):1294-1304.e4.

4. Ko WK, Lee SH, Kim SJ, Jo MJ, Kumar H, Han IB, et al. Anti-inflammatory effects of ursodeoxycholic acid by lipopolysaccharide-stimulated inflammatory responses in RAW 264.7 macrophages. PLoS One. 2017;12(6):e0180673.

5. Ward JBJ, Lajczak NK, Kelly OB, O'Dwyer AM, Giddam AK, Ní Gabhann J, et al. Ursodeoxycholic acid and lithocholic acid exert anti-inflammatory actions in the colon. Am J Physiol Gastrointest Liver Physiol. 1 juin 2017;312(6):G550-8.

6. O'Dwyer AM, Lajczak NK, Keyes JA, Ward JB, Greene CM, Keely SJ. Ursodeoxycholic acid inhibits TNFα-induced IL-8 release from monocytes. American Journal of Physiology-Gastrointestinal and Liver Physiology. août 2016;311(2):G334-41.

7. Lajczak-McGinley NK, Porru E, Fallon CM, Smyth J, Curley C, McCarron PA, et al. The secondary bile acids, ursodeoxycholic acid and lithocholic acid, protect against intestinal inflammation by inhibition of epithelial apoptosis. Physiol Rep. juin 2020;8(12):e14456.

8. Palmieri LJ, Rainteau D, Sokol H, Beaugerie L, Dior M, Coffin B, et al. Inhibitory Effect of Ursodeoxycholic Acid on Clostridium difficile Germination Is Insufficient to Prevent Colitis: A Study in Hamsters and Humans. Front Microbiol. 2018;9:2849.

9. Winston JA, Rivera AJ, Cai J, Thanissery R, Montgomery SA, Patterson AD, et al. Ursodeoxycholic Acid (UDCA) Mitigates the Host Inflammatory Response during Clostridioides difficile Infection by Altering Gut Bile Acids. Infect Immun. 20 mai 2020;88(6):e00045-20.

10. Uchida A, Yamada T, Hayakawa T, Hoshino M. Taurochenodeoxycholic acid ameliorates and ursodeoxycholic acid exacerbates small intestinal inflammation. Am J Physiol. mai 1997;272(5 Pt 1):G1249-1257.

11. Higgins LM, Frankel G, Douce G, Dougan G, MacDonald TT. Citrobacter rodentium Infection in Mice Elicits a Mucosal Th1 Cytokine Response and Lesions Similar to Those in Murine Inflammatory Bowel Disease. Infect Immun. juin 1999;67(6):3031-9.

12. Mundy R, MacDonald TT, Dougan G, Frankel G, Wiles S. Citrobacter rodentium of mice and man. Cell Microbiol. déc 2005;7(12):1697-706.

13. Borenshtein D, McBee ME, Schauer DB. Utility of the Citrobacter rodentium infection model in laboratory mice. Curr Opin Gastroenterol. janv 2008;24(1):32-7.

14. Wiles S, Clare S, Harker J, Huett A, Young D, Dougan G, et al. Organ specificity, colonization and clearance dynamics in vivo following oral challenges with the murine pathogen Citrobacter rodentium. Cell Microbiol. oct 2004;6(10):963-72.

15. Wiles S, Pickard KM, Peng K, MacDonald TT, Frankel G. In vivo bioluminescence imaging of the murine pathogen Citrobacter rodentium. Infect Immun. sept 2006;74(9):5391-6.

16. Crepin VF, Collins JW, Habibzay M, Frankel G. Citrobacter rodentium mouse model of bacterial infection. Nat Protoc. oct 2016;11(10):1851-76.

17. Luperchio SA, Schauer DB. Molecular pathogenesis of Citrobacter rodentium and transmissible murine colonic hyperplasia. Microbes Infect. avr 2001;3(4):333-40.

18. Mullineaux-Sanders C, Sanchez-Garrido J, Hopkins EGD, Shenoy AR, Barry R, Frankel G. Citrobacter rodentium-host-microbiota interactions: immunity, bioenergetics and metabolism. Nat Rev Microbiol. 2019;17(11):701-15.

19. Brugiroux S, Beutler M, Pfann C, Garzetti D, Ruscheweyh HJ, Ring D, et al. Genome-guided design of a defined mouse microbiota that confers colonization resistance against Salmonella enterica serovar Typhimurium. Nat Microbiol. 21 nov 2016;2:16215.

20. Garzetti D, Brugiroux S, Bunk B, Pukall R, McCoy KD, Macpherson AJ, et al. High-Quality Whole-Genome Sequences of the Oligo-Mouse-Microbiota Bacterial Community. Genome Announc. 19 oct 2017;5(42):e00758-17.

21. Lagkouvardos I, Pukall R, Abt B, Foesel BU, Meier-Kolthoff JP, Kumar N, et al. The Mouse Intestinal Bacterial Collection (miBC) provides host-specific insight into cultured diversity and functional potential of the gut microbiota. Nat Microbiol. 8 août 2016;1(10):16131.

22. Studer N, Desharnais L, Beutler M, Brugiroux S, Terrazos MA, Menin L, et al. Functional Intestinal Bile Acid 7α-Dehydroxylation by Clostridium scindens Associated with Protection from Clostridium difficile Infection in a Gnotobiotic Mouse Model. Front Cell Infect Microbiol. 2016;6:191.

23. Chassaing B, Srinivasan G, Delgado MA, Young AN, Gewirtz AT, Vijay-Kumar M. Fecal lipocalin 2, a sensitive and broadly dynamic non-invasive biomarker for intestinal inflammation. PLoS One. 2012;7(9):e44328.

24. Mullineaux-Sanders C, Sanchez-Garrido J, Hopkins EGD, Shenoy AR, Barry R, Frankel G. Citrobacter rodentium–host–microbiota interactions: immunity, bioenergetics and metabolism. Nat Rev Microbiol. nov 2019;17(11):701-15.

25. Diard M, Bakkeren E, Cornuault JK, Moor K, Hausmann A, Sellin ME, et al. Inflammation boosts bacteriophage transfer between Salmonella spp. Science. 17 mars 2017;355(6330):1211-5.

26. Warda AK, de Almeida Bettio PH, Hueston CM, Di Benedetto G, Clooney AG, Hill C. Oral Administration of Heat-Treated Lactobacilli Modifies the Murine Microbiome and Reduces Citrobacter Induced Colitis. Front Microbiol. 2020;11:69.

27. Ng SC, Shi HY, Hamidi N, Underwood FE, Tang W, Benchimol EI, et al. Worldwide incidence and prevalence of inflammatory bowel disease in the 21st century: a systematic review of population-based studies. Lancet. 23 déc 2017;390(10114):2769-78.

28. Cai J, Sun L, Gonzalez FJ. Gut microbiota-derived bile acids in intestinal immunity, inflammation, and tumorigenesis. Cell Host & Microbe. 9 mars 2022;30(3):289-300.

29. Bromke MA, Krzystek-Korpacka M. Bile Acid Signaling in Inflammatory Bowel Disease. International Journal of Molecular Sciences. janv 2021;22(16):9096.

30. Brugiroux S, Beutler M, Pfann C, Garzetti D, Ruscheweyh HJ, Ring D, et al. Genome-guided design of a defined mouse microbiota that confers colonization resistance against Salmonella enterica serovar Typhimurium. Nat Microbiol. févr 2017;2(2):16215.

31. Clooney AG, Sutton TDS, Shkoporov AN, Holohan RK, Daly KM, O'Regan O, et al. Whole-Virome Analysis Sheds Light on Viral Dark Matter in Inflammatory Bowel Disease. Cell Host Microbe. 11 déc 2019;26(6):764-778.e5.

32. Diard M, Bakkeren E, Cornuault JK, Moor K, Hausmann A, Sellin ME, et al. Inflammation boosts bacteriophage transfer between Salmonella spp. Science. 17 mars 2017;355(6330):1211-5.

33. Kamada N, Kim YG, Sham HP, Vallance BA, Puente JL, Martens EC, et al. Regulated virulence controls the ability of a pathogen to compete with the gut microbiota. Science. 8 juin 2012;336(6086):1325-9.

34. Mullineaux-Sanders C, Carson D, Hopkins EGD, Glegola-Madejska I, Escobar-Zepeda A, Browne HP, et al. Citrobacter amalonaticus Inhibits the Growth of Citrobacter rodentium in the Gut Lumen. mBio. 12(5):e02410-21.

35. Tanaka H, Makino Y, Miura T, Hirano F, Okamoto K, Komura K, et al. Ligand-independent activation of the glucocorticoid receptor by ursodeoxycholic acid. Repression of IFN-gamma-induced MHC class II gene expression via a glucocorticoid receptor-dependent pathway. J Immunol. 15 févr 1996;156(4):1601-8.

36. Golden JM, Escobar OH, Nguyen MVL, Mallicote MU, Kavarian P, Frey MR, et al. Ursodeoxycholic acid protects against intestinal barrier breakdown by promoting enterocyte migration via EGFR- and COX-2-dependent mechanisms. American Journal of Physiology-Gastrointestinal and Liver Physiology. août 2018;315(2):G259-71.

37. Silberger DJ, Zindl CL, Weaver CT. Citrobacter rodentium: a model enteropathogen for understanding the interplay of innate and adaptive components of type 3 immunity. Mucosal Immunol. sept 2017;10(5):1108-17.

38. Jarade A, Di Santo JP, Serafini N. Group 3 innate lymphoid cells mediate host defense against attaching and effacing pathogens. Current Opinion in Microbiology. 1 oct 2021;63:83-91.

39. Huber S, Gagliani N, Zenewicz LA, Huber FJ, Bosurgi L, Hu B, et al. IL-22BP is regulated by the inflammasome and modulates tumorigenesis in the intestine. Nature. 8 nov 2012;491(7423):259-63.

40. Mossoro C, Glaziou P, Yassibanda S, Lan NTP, Bekondi C, Minssart P, et al. Chronic Diarrhea, Hemorrhagic Colitis, and Hemolytic-Uremic Syndrome Associated with HEp-2 Adherent Escherichia coli in Adults Infected with Human Immunodeficiency Virus in Bangui, Central African Republic. J Clin Microbiol. août 2002;40(8):3086-8.

41. Schindelin J, Arganda-Carreras I, Frise E, Kaynig V, Longair M, Pietzsch T, et al. Fiji: an open-source platform for biological-image analysis. Nat Methods. 28 juin 2012;9(7):676-82.

42. Livak KJ, Schmittgen TD. Analysis of relative gene expression data using real-time quantitative PCR and the 2(-Delta Delta C(T)) Method. Methods. déc 2001;25(4):402-8.

43. Arndt D, Grant JR, Marcu A, Sajed T, Pon A, Liang Y, et al. PHASTER: a better, faster version of the PHAST phage search tool. Nucleic Acids Res. 8 juill 2016;44(W1):W16-21.

44. Babraham Bioinformatics - FastQC A Quality Control tool for High Throughput Sequence Data [Internet]. [cité 20 sept 2021]. Disponible sur: https://www.bioinformatics.babraham.ac.uk/projects/fastqc/

45. Chen S, Zhou Y, Chen Y, Gu J. fastp: an ultra-fast all-in-one FASTQ preprocessor. Bioinformatics. 1 sept 2018;34(17):i884-90.

46. Lamy-Besnier Q, Koszul R, Debarbieux L, Marbouty M. Closed and High-Quality Bacterial Genome Sequences of the Oligo-Mouse-Microbiota Community. Microbiol Resour Announc. 29 avr 2021;10(17):e01396-20.

47. Li H, Handsaker B, Wysoker A, Fennell T, Ruan J, Homer N, et al. The Sequence Alignment/Map format and SAMtools. Bioinformatics. 15 août 2009;25(16):2078-9.

48. Volant S, Lechat P, Woringer P, Motreff L, Campagne P, Malabat C, et al. SHAMAN: a user-friendly website for metataxonomic analysis from raw reads to statistical analysis. BMC Bioinformatics. 10 août 2020;21(1):345.

SUPPLEMENTARY FIGURES

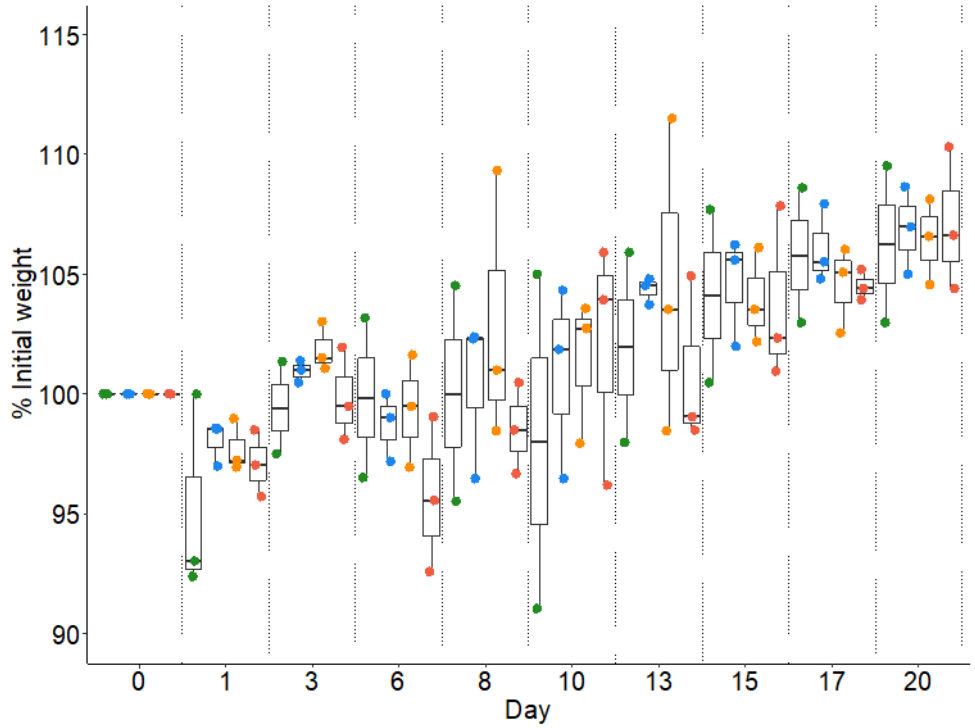

Figure S1: Variation over time of the weight of OMM^{12} mice infected by different doses of *C. rodentium*

OMM^{12} mice were fed different doses (Green, 10 CFU (n=3); blue, 10^3 CFU (n=3); orange, 10^5 CFU (n=3); red, 10^7 CFU (n=3)) of *C. rodentium* at day 0, and their weight was measured at the indicated timepoints.

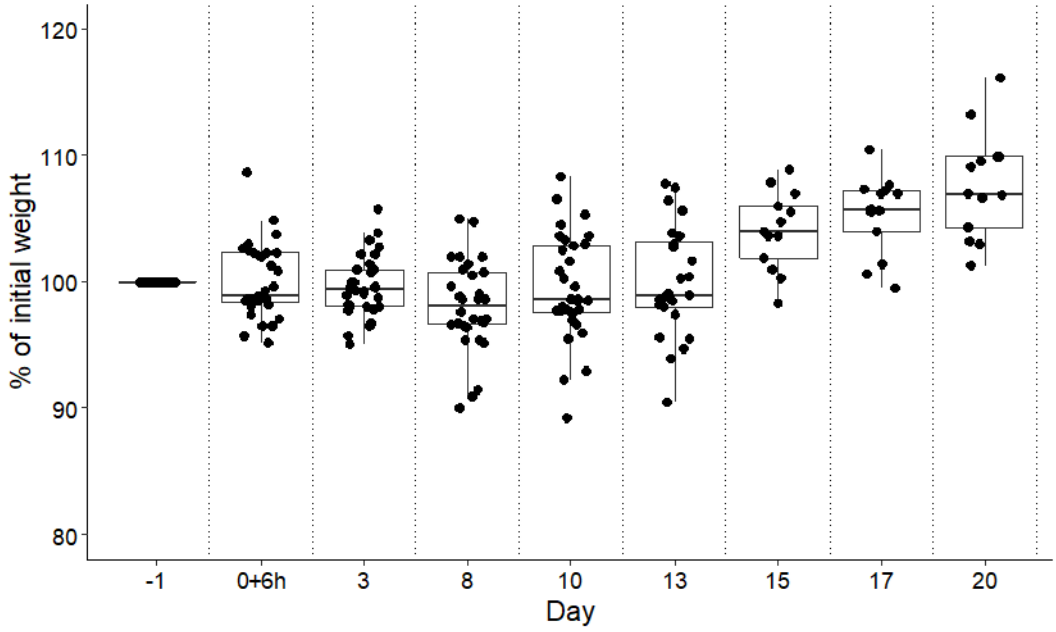

Figure S2: Weight variation of OMM^{12} mice infected by *C. rodentium*

OMM^{12} mice (n=40) were infected with 2 x 10^7 CFU of *C. rodentium.* At day 0 (n=8), day 10

(n=13) and day 20 (n=14), mice were sacrificed for the analysis of their gut content.

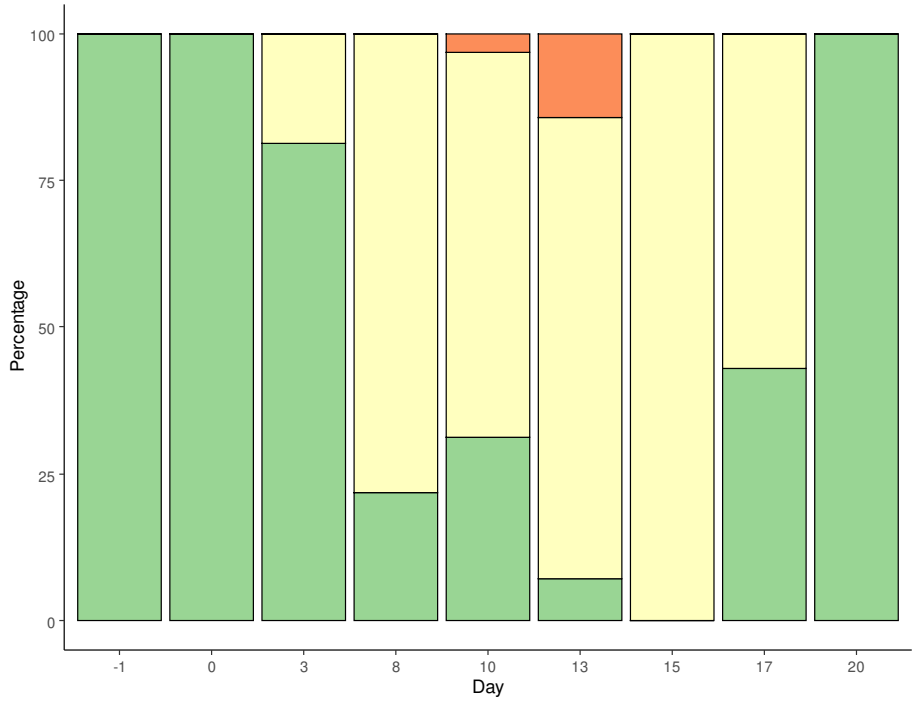

Figure S3: Clinical symptoms of OMM^{12} mice infected by *C. rodentium*
Clinical signs and symptoms of mice over time (days 0 to 20) were scored based on animal behavior (e.g., activity, hunching) and consistency of fecal pellets (e.g., formed/no liquid, formed/liquid, liquid). Green, normal; yellow, mild signs of disease; red, severe signs of disease (see methods).

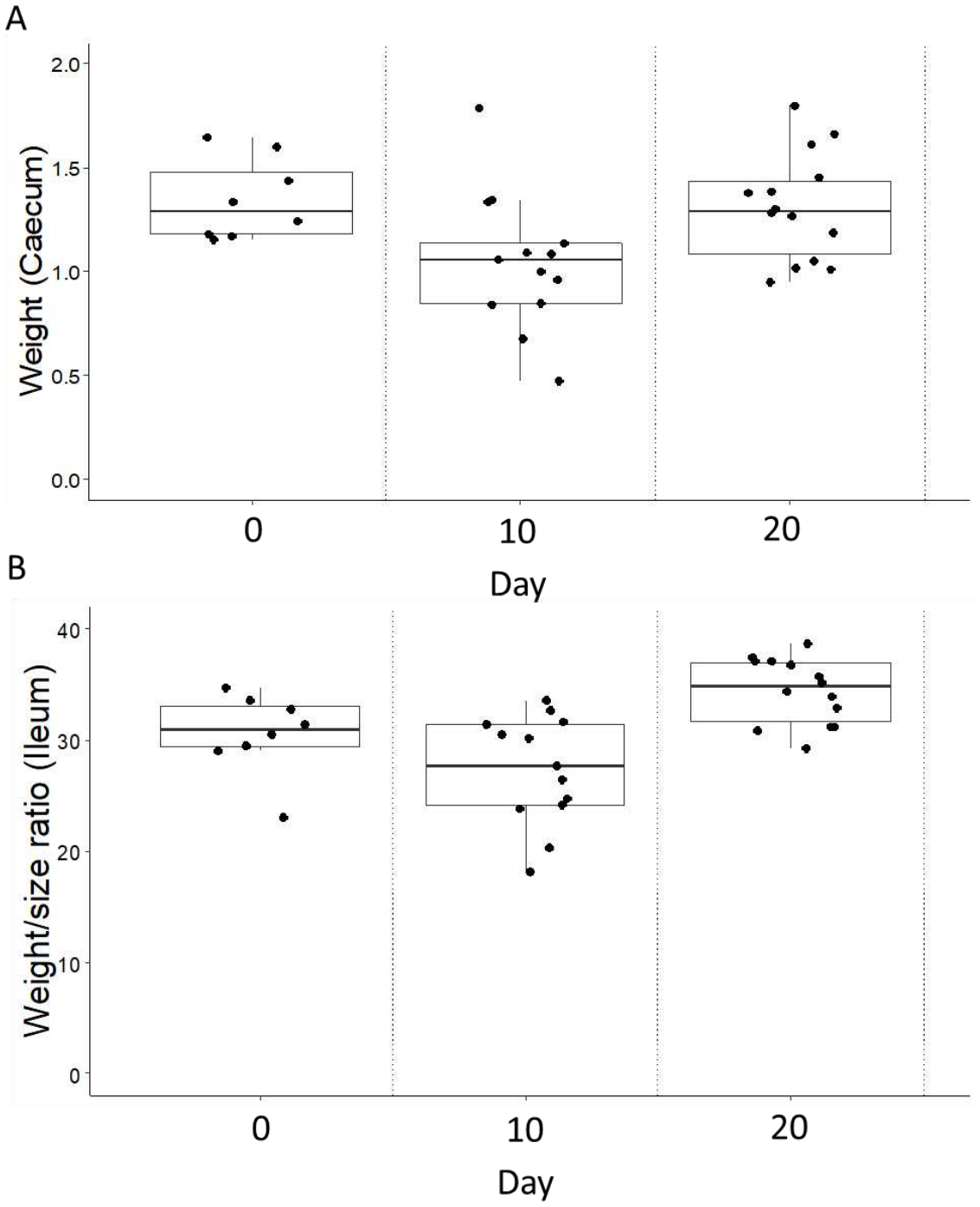

Figure S4: Dimention of the ileum and caecum of OMM[12] mice infected by *C. rodentium*

A. The ileum sections and **B.** caecum were obtained from OMM[12] mice sacrificed at day 0 (n=8), day 10 (n=13) and day 20 (n=14) after *C. rodentium* introduction.

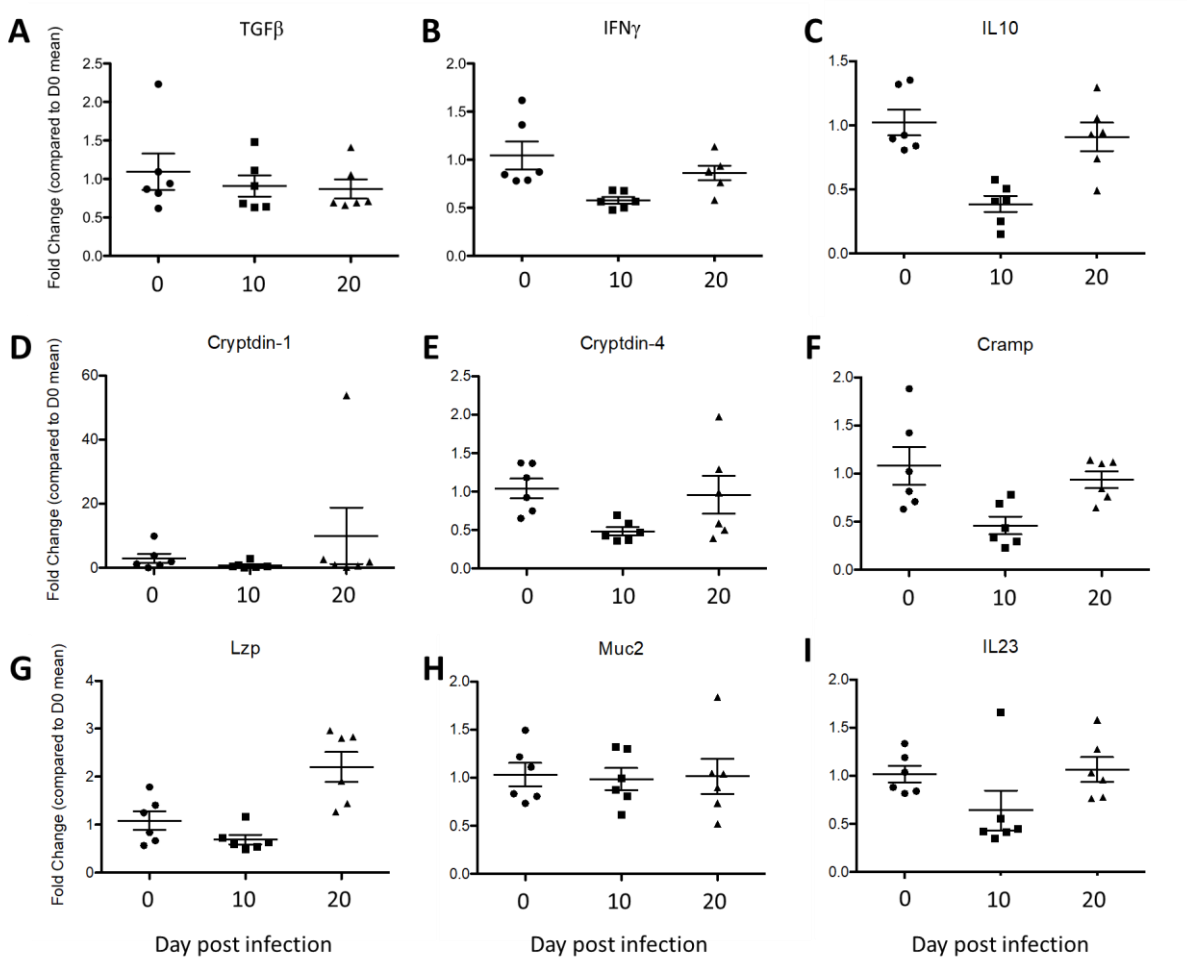

Figure S5: Expression level of genes downregulated or with an unchanged expression in the response against *C. rodentium*.

OMM[12] mice colonized by *C. rodentium* were sacrificed at day 0 (n=6), day 10 (n=6) and day 20 (n=6). **A-I.** Relative gene expression level in the colon of mice infected by *C. rodentium* compared to the mean of D0 post-infection.

SUPPLEMENTARY TABLES

	Mouse	D0	D1	D3	D6	D8	D10	D13	D15	D17	D20
10^7 CFU	NM1										
	OD1										
	OG1										
10^5 CFU	NM2										
	OD2										
	OG2										
10^3 CFU	NM3										
	OD3										
	OG3										
10 CFU	NM4										
	OD4										
	OG4										

Table S1: Clinical status of mice infected by different doses of *C. rodentium*.
Clinical signs and symptoms over time (days 0 to 20) are scored based on animal behavior (e.g., activity, hunching) and consistency of fecal pellets (e.g., formed/no liquid, formed/liquid, liquid). Green, normal; yellow, mild signs of disease; red, severe signs of disease. Mice OD4 died inadvertently on day 2

ANOVA					
testing difference between the different days					
Response:	scale(log10(CFU.g))				
	Chisq	Df	Pr(>Chisq)		
day	526.5	2	< 2.2e-16	***	
Post-hoc tests					
Comparison between days					
contrast	estimate	SE	df	t.ratio	p.value
d0 vs. d10	-2.006	0.0932	54.8	-21.528	<.0001
d0 vs. d20	-0.317	0.1331	52.7	-2.378	0.0541
d10 vs. d20	1.690	0.1289	58.6	13.109	<.0001

Table S2: Statistical analysis of the log10 concentration lipocalin-2 in feces

ANOVA					
testing difference between the different days					
Response:	scale(log10(CFU.g))				
	Chisq	Df	Pr(>Chisq)		
day	13.524	2	0.001157	**	
Post-hoc tests					
Comparison between days					
contrast	estimate	SE	df	t.ratio	p.value
d0 vs. d10	-11.028	3.27	27.6	-3.376	0.0060
d0 vs. d20	-10.701	3.77	29.8	-2.838	0.0214
d10 vs. d20	0.326	3.30	28.0	0.099	0.9946

Table S3: Statistical analysis of the weight/size ratio of the colon samples

ANOVA					
testing difference between the different days					
Response:	scale(log10(CFU.g))				
	Chisq	Df	Pr(>Chisq)		
day	83.524	2	< 2.2e-16	***	
Post-hoc tests					
Comparison between days					
contrast	estimate	SE	df	t.ratio	p.value
d0 vs. d10	-20.90	2.50	20.8	-8.353	<.0001
d0 vs. d20	-5.58	3.88	16.6	-1.437	0.3455
d10 vs. d20	15.32	3.53	15.9	4.345	0.0014

Table S4: Statistical analysis of the Ki67 staining of colon samples

ANOVA					
testing difference between the different days					
Response:	scale(log10(CFU.g))				
	Chisq	Df	Pr(>Chisq)		
day	162.5	2	< 2.2e-16	***	
Post-hoc tests					
Comparison between days					
contrast	estimate	SE	df	t.ratio	p.value
d0 vs. d10	-68.8	6.41	25.1	-10.733	<.0001
d0 vs. d20	-10.3	8.94	12.1	-1.156	0.4999
d10 vs. d20	58.4	7.69	14.0	7.595	<.0001

Table S5: **Statistical analysis of the crypt depth of the colon samples**

ANOVA					
testing difference between the different days					
Response:	scale(log10(CFU.g))				
	Chisq	Df	Pr(>Chisq)		
day	32.245	2	9.956e-8	***	
Post-hoc tests					
Comparison between days					
contrast	estimate	SE	df	t.ratio	p.value
d0 vs. d10	126	56.8	20.8	2.222	0.0907
d0 vs. d20	-201	88.2	16.6	-2.275	0.0876
d10 vs. d20	-327	80.1	15.9	-4.084	0.0024

Table S6: Statistical analysis of the mean fluorescence of lectins staining of colon samples

ANOVA						
day: testing difference between the different days						
Response:	scale(log10(CFU.g))					
	Chisq	Df	Pr(>Chisq)			
Day	85.639	2	<2.2e-16	***		
Post-hoc tests						
Comparison between days						
contrast	estimate	SE	df	t.ratio	p.value	
D0 vs. D10	3.827	0.603	13.9	6.346	0.0001	***
D0 vs. D20	-0.988	0.667	12.4	-1.481	0.3327	
D10 vs. D20	-4.815	0.643	13.3	-7.488	<.0001	***

Table S7. Statistical analysis of the number of goblet cells per colon crypt

IL22						
ANOVA						
testing difference between the different days						
Response:	scale(log10(CFU.g))					
	Chisq	Df	Pr(>Chisq)			
Traetment	8.5717	1	0.003414	**		
Post-hoc tests						
Comparison between days						
contrast	estimate	SE	df	t.ratio	p.value	
Control vs UDCA	0.812	0.277	4.3	2.928	0.0393	*
REG3γ						
ANOVA						
testing difference between the different days						
Response:	scale(log10(CFU.g))					
	Chisq	Df	Pr(>Chisq)			
Traetment	8.3421	1	0.003874	**		
Post-hoc tests						
Comparison between days						
contrast	estimate	SE	df	t.ratio	p.value	
Control vs UDCA	0.597	0.207	3.72	2.888	0.0488	

Table S8. Statistical analysis of the gene expression level of gene involved in the response against *C. rodentium* with UDCA

Gene		Sequence
mGAPDH	Forward	CTTATCAGGCCAAGTATGATG
mGAPDH	Reverse	CAACCTGGTCCTCAGTGTAGC
IL-1β	Forward	GATCCACACTCTCCAGCTGCA
IL-1β	Reverse	CAACCAACAAGTGATATTCTCCATG
IL-10	Forward	CCACAAAGCAGCCTTGCA
IL-10	Reverse	AGTAAGAGCAGGCAGCATAGCA
IL-17	Forward	CCACGTCACCCTGGACTCTC
IL-17	Reverse	CTCCGCATTGACACAGCG
IL-22	Forward	CAATCTTCCAGCAGCCATACA
IL-22	Reverse	TCCTTAGCACTGACTCCTCG
IL-23	Forward	CCTTCTCCGTTCCAAGATCCT
IL-23	Reverse	ACTAAGGGCTCAGTCAGAGTTGCT
IFNγ	Forward	TCAAGTGGCATAGATGTGGAAGAA
IFNγ	Reverse	TGGCTCTGCAGGATTTTCATG
TNFα	Forward	CCCTCACACTCAGATCATCTTCT
TNFα	Reverse	GCTACGACGTGGGCTACAG
CXCL1	Forward	ACCCAAACCGAAGTCATAGC
CXCL1	Reverse	TGGGGACACCTTTTAGCATC
CXCL2	Forward	AGCCTGGATCGTACGTACCTGATG
CXCL2	Reverse	TAACAACATCTGGGCAATGG
CXCL3	Forward	CAAGGGTTGATTTTGAGACC
CXCL3	Reverse	GGCAAACTTCTTGACCATCC
TGFβ	Forward	GGACTCTCCACCTGCAAGAC
TGFβ	Reverse	GACTGGCGAGCCTTAGTTTG
cryptdin1	Forward	AAGAGACTAAAACTGAGGAGCAGC
cryptdin1	Reverse	CGACAGCAGAGCGTGTA
cryptdin4	Forward	AAGAGACTAAAACTGAGGAGCAGC
cryptdin4	Reverse	CGGCGGGGGCAGCAGTA
Reg3γ	Forward	TTCCTGTCCTCCATGATCAAAA
Reg3γ	Reverse	CATCCACCTCTGTTGGGTTCA
Cramp	Forward	GCCGCTGATTCTTTTGACAT
Cramp	Reverse	GCCAAGGCAGGCCTACTACT
Lzp	Forward	GAGACCGAAGCACCGACTATG
Lzp	Reverse	CGGTTTTGACATTGTGTTCGC
MUC2	Forward	GTCCGAAGTGTTACCCTGGAAT
MUC2	Reverse	CAGCTCTCGATGTGTGTGTAGGT
Reg3β	Forward	CTCCTGCCTGATGCTCTTAT
Reg3β	Reverse	TTGTTACTCCATTCCCATCC

Table S9. List of qPCR primers used in this study

Discussion et Perspectives

Lors de ce travail de thèse nous avons pu observer la complexité des interactions entre les différents acteurs du microbiote intestinal à travers trois projets dont les résultats ont été discutés individuellement. Ici, nous présenterons des résultats préliminaires qui complètent et étendent les discussions précédentes.

I – Comprendre comment *Citrobacter rodentium* se comporte dans l'intestin des souris OMM^{12}

A) Identifier le mécanisme de la persistance de *C. rodentium* dans les souris OMM^{12}

Lors de la colonisation des souris OMM^{12} par *Citrobacter rodentium*, nous avons pu reproduire une infection proche de celle retrouvée dans des souris conventionnelles (1). Nous avons observé ainsi une colonisation rapide du tube digestif, un pic de colonisation atteignant 10^9 CFU/g de fèces au jour huit, suivi d'un pic d'inflammation. Les caractéristiques de l'inflammation causée par *C. rodentium* sont également présentes avec une hyperplasie des cryptes, une augmentation de la prolifération cellulaire, une production de cytokines pro-inflammatoires telles que l'IL-22 et l'IL-17 et des peptides antimicrobiens comme la lipocaline-2, REG3γ et REG3β. Cette forte réponse inflammatoire est accompagnée d'une baisse de la colonisation de *C. rodentium.* Cependant, après une baisse d'un facteur 100 à 1000, le titre de *C. rodentium* se stabilise entre 10^6 et 10^7 CFU/g de fèces, ce qui n'est jamais observé avec des souris conventionnelles où la baisse de colonisation se poursuit par l'élimination de *C. rodentium* par compétition de bactéries commensales métaboliquement proches (2). L'absence d'entérobactérie dans le consortium OMM^{12} pourrait donc expliquer cette persistance de *C. rodentium* dans l'intestin. Afin de tester cette hypothèse, nous avons colonisé des souris OMM^{12} avec la souche *Escherichia coli* dn15.6244.1 (dn15), dont il a déjà été démontré qu'elle entre en compétition nutritionnelle avec *C. rodentium* dans l'intestin de souris axénique (2). Sept jour après la colonisation de la souche dn15 dans les souris OMM^{12}, nous avons gavé ces animaux avec *C. rodentium* et suivi la colonisation des deux souches au cours du temps (Fig. 17).

La colonisation initiale de *C. rodentium* est similaire dans les souris contrôles et dans les souris colonisées par *E. coli* dn15, avec un léger retard de colonisation en présence de *E. coli* dn15. À partir du jour 15 post infection par *C. rodentium*, la concentration de *C. rodentium* dans les fèces des animaux colonisés par la souche dn15 diminue drastiquement jusqu'à passer sous

le seuil de détection dans plusieurs souris, alors qu'elle est stable dans le groupe contrôle. Ces données indiquent que cette souche d'*E. coli* permet de retrouver une compétition nutritionnelle vis-à-vis de *C. rodentium*.

Nous pouvons alors faire le lien avec une autre étude publiée par Brugiroux *et al.* Dans ce travail, les auteurs ont pu observer que les souris OMM^{12} sont susceptibles à une infection par *Salmonella enterica* serovar Typhimurium, mais que la présence de la souche *E. coli* Mt1B1 introduite chez des souris OMM^{12}, protégeait les souris contre la colonisation de *S.* Typhimurium (3). Ces différentes observations démontrent l'existence d'une niche écologique disponible pour les entérobactéries dans les souris OMM^{12} pouvant servir de modèle d'étude de la compétition bactérienne au sein de l'intestin.

Cette compétition est particulièrement importante à étudier *in vivo* afin de comprendre quel sont les mécanismes de résistance à la colonisation. Par exemple, au cours de la première phase de colonisation dans des souris conventionnelles, *C. rodentium* utilise un système de sécrétion de type 6 (T6SS) afin d'éliminer les bactéries en compétition pour la même niche écologique. La souche *E. coli* Mt1B1 peut se défendre activement également grâce à un T6SS (4). Ainsi les bactéries possédant un T6SS semblent favorisées dans cet environnement, notamment en présence d'autres bactéries possédant un T6SS. Nous pouvons même aller jusqu'à nous demander si l'accumulation de bactéries avec un T6SS pourraient engendrer un microbiote plus hostile à la colonisation de nouvelles bactéries.

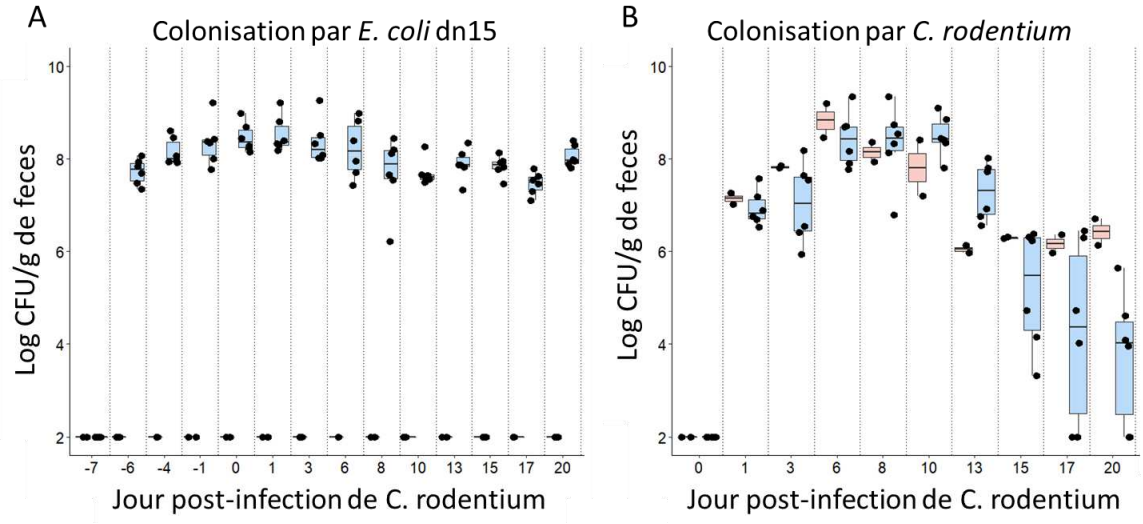

Figure 17 : Suivi de la colonisation de *C. rodentium* en présence de *E. coli* dn15
Des souris OMM^{12} ont été gavées par une suspension de *E. coli* dn15 ou par du PBS puis sept jours plus tard, toutes les souris ont été gavées par *C. rodentium*. Suivi de la colonisation de **A.** *E. coli* dn15 et **B.** de *C. rodentium* en présence (en bleu, n=6) ou en absence (en rouge, n=2) de *E. coli* dn15 au cours du temps.

B) Le contrôle de la colonisation de *C. rodentium* n'est pas lié à une perte de virulence

La persistance de *C. rodentium*, dans l'intestin des souris OMM^{12} soulève d'autres questions. Nous observons au jour 20 post-infection une concentration entre 10^6 et 10^7 CFU/g de fèces, alors que la plupart des marqueurs de l'inflammation sont revenus à un niveau pré-infection.

Des travaux réalisés dans des souris axéniques ont déjà montré que *C. rodentium* pouvait maintenir un niveau de colonisation de 10^{10} CFU/g de fèces sur plusieurs semaines (2). Mais bien que la colonisation reste stable, un changement de phénotype est observé. À partir du jour 12 post infection, l'expression du locus d'effacement entérocytaire (LEE) est diminuée. Lorsque ces clones ayant une expression abaissée de LEE sont transférés dans des souris conventionnelles, ils parviennent à les coloniser et déclenchent tout de même une inflammation. Ceci montre que ces clones sont toujours virulents et que c'est l'hôte qui contrôle l'inflammation. Cependant, ces observations ont été faites dans des souris axéniques disposant d'un système immunitaire déficient. Cela soulève également une nouvelle question qui est de savoir par quoi est provoquée cette baisse d'expression de LEE. Sachant que le système adaptatif produit des IgG anti-LEE, une hypothèse serait que ces immunoglobulines contre-sélectionneraient les bactéries exprimant LEE, donnant ainsi l'avantage aux bactéries qui expriment moins ce facteur de virulence

Nous nous sommes tout d'abord demandé si nous pouvions reproduire ces observations dans les souris OMM^{12}. Nous avons donc colonisé un premier groupe de souris avec *C. rodentium* puis attendu 20 jours afin que l'inflammation soit résolue avant d'introduire un nouveau groupe de souris OMM^{12} naïves dans les cages contenant le premier groupe. Les souris étant coprophages, elles se sont alors infectées en ingérant les fèces des souris préalablement colonisées par *C. rodentium*. Nous avons alors suivi le transfert de *C. rodentium* des souris colonisées vers des souris naïves (Fig. 18).

Nous observons que la colonisation de *C. rodentium* dans le premier groupe suit le pattern retrouvé dans les études précédentes, avec une un pic puis une baisse de la colonisation. Lorsque le deuxième groupe de souris est transféré dans les cages 21 jours après que le premier groupe a été infecté, le même pattern avec un pic de colonisation au jour huit puis une baisse de la concentration en *C. rodentium* dans les fèces des souris est observée du deuxième groupe. De plus, la colonisation de *C. rodentium* dans le premier groupe à la suite du pic de colonisation au jour huit dans le second groupe n'est pas modifiée.

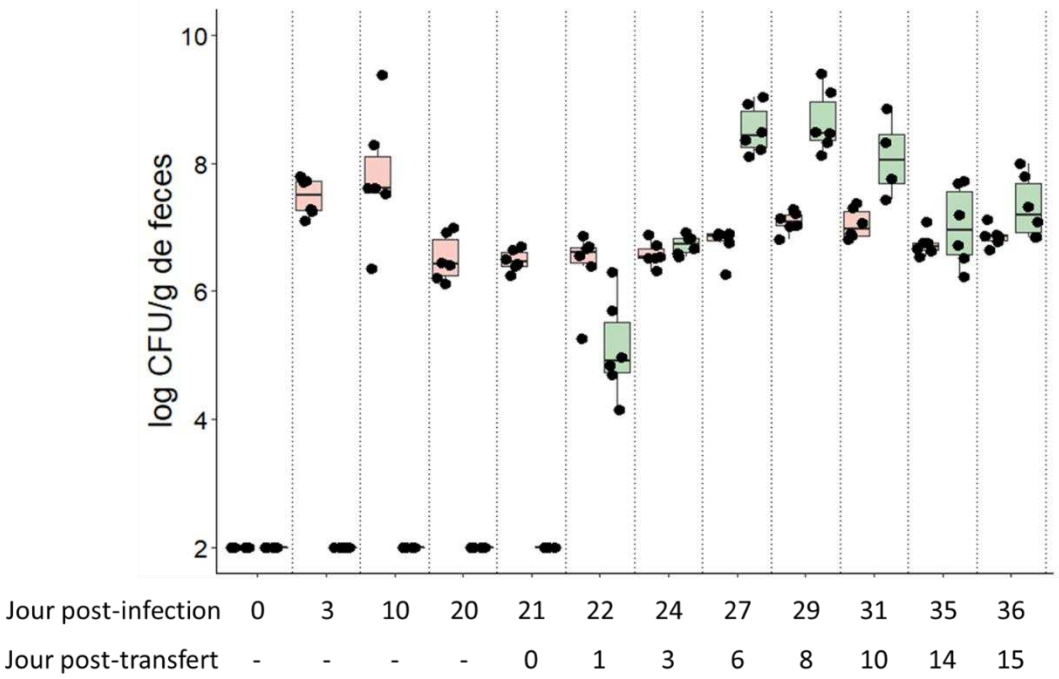

Figure 18 : Suivi de la colonisation lors du transfert de souris OMM^{12} naïves dans des cages hébergeant des souris infectées par *C. rodentium*
Un premier groupe (rouge, n=6) de souris OMM^{12} a été gavé avec *C. rodentium* 21 jour avant le transfert d'un second groupe (vert, n=6) de souris OMM^{12} dans les mêmes cages.

Ainsi, lorsque les souris du premier groupe sont exposées à une dose plus importante de *C. rodentium,* cela ne se traduit pas par une augmentation du niveau de colonisation, ce qui signifie que l'hôte a mis en place une réponse ayant pour objectif de limiter le niveau de colonisation de *C. rodentium.*

Pour confirmer définitivement cette hypothèse, nous avons prévu d'effectuer un premier gavage dans des souris OMM^{12} avec *C. rodentium* suivi d'un un second gavage 20 jours plus tard, cette fois avec le même clone ancestral.

Ces résultats ouvrent la voie à une étude des acteurs et mécanismes de la réponse de l'hôte. Sachant que si le système immunitaire des souris OMM^{12} est proche de celui des souris conventionnelles, nous pouvons proposer qu'un défaut de maturation des lymphocytes Th17 est impliqué en raison de l'absence de bactéries filamenteuses segmentées (5).

II – Explorer les rôles de l'UDCA dans la physiologie intestinale

A) L'effet immunomodulateur de l'UDCA est peu compris

Dans la troisième partie de ce travail de thèse, nous avons observé que l'UDCA inhibait la voie de l'IL-22. Ce résultat n'était pas attendu et révèle le manque de compréhension de l'effets immunomodulateur de l'UDCA.

Les acides biliaires secondaires présentent une fonction de molécule de signalisation chez l'hôte par l'intermédiaire de récepteurs spécifiques et peuvent par ce biais avoir une action immunomodulatrice (6). Cependant l'UDCA fait figure d'exception, ne présentant qu'une affinité faible pour le récepteur GPBAR1, voire nulle pour FXR ou VDR (7–9). Des études *in vitro* ont tout de même montré que l'UDCA, malgré sa faible affinité pour GPBAR1, pouvait agir selon cette voie (13), mais son importance *in vivo* reste à démontrer. En revanche son précurseur, le CDCA, présente une meilleure affinité que l'UDCA pour GPBAR1et FXR (10).

L'UDCA présente tout de même une activité immunomodulatrice et même anti-inflammatoire dans de nombreux modèles *in vitro* et *in vivo* (11–13) et est même utilisé en clinique dans le traitement de la cholangite biliaire primitive (14). Ceci implique une interaction, directe ou indirecte, avec l'hôte, mais les mécanismes restent encore très flous. Une ancienne étude a montré que l'UDCA réprimait l'expression du complexe majeur d'histocompatibilité *via* le récepteur aux glucocorticoïdes (15). Plus récemment, des travaux ont montré que l'UDCA inhibait la cyclooxygénase 2 (COX2) et stimulait ainsi la régénération épithéliale (16). On ne peut pas exclure que l'UDCA interagisse avec d'autres acteurs clés de la réponse immunitaire. De récents travaux ont par exemple démontré que le le 3-oxoLCA et l'isoalloLCA pouvaient se lier au facteur de transcription retinoid-related orphan receptor-γt (RORγt) et inhibait d'une part la différenciation des lymphocytes Th17 et favorisaient d'autre part la différenciation de lymphocytes Treg (17,18).

B) La balance CDCA - UDCA dans la physiologie intestinale

Le CDCA est un acide biliaire primaire pouvant être métabolisé en UDCA par épimérisation ou en LCA par déshydroxylation par le microbiote (19). Outre les effets directs de l'UDCA sur le système immunitaire, nous pourrions également nous intéresser à l'effet de cette épimérisation qui diminue le ratio CDCA/UDCA. Lors d'études préliminaires, nous nous sommes intéressés au caractère cytotoxique de l'UDCA et du CDCA (Fig. 19).

Nous avons observé qu'une dose intermédiaire ($5x10^{-4}$M) de CDCA provoquait une forte libération de lactate déshydrogénase (LDH) dans le surnageant, ce qui n'était pas le cas pour l'UDCA. Une forte dose d'UDCA (10^{-3}M) semblait malgré tout entrainer une mort cellulaire. L'épimérisation du CDCA en UDCA pourrait alors être bénéfique à deux niveaux, en réduisant d'un côté la concentration en CDCA et en augmentant de l'autre celle de l'UDCA (Fig. 19).

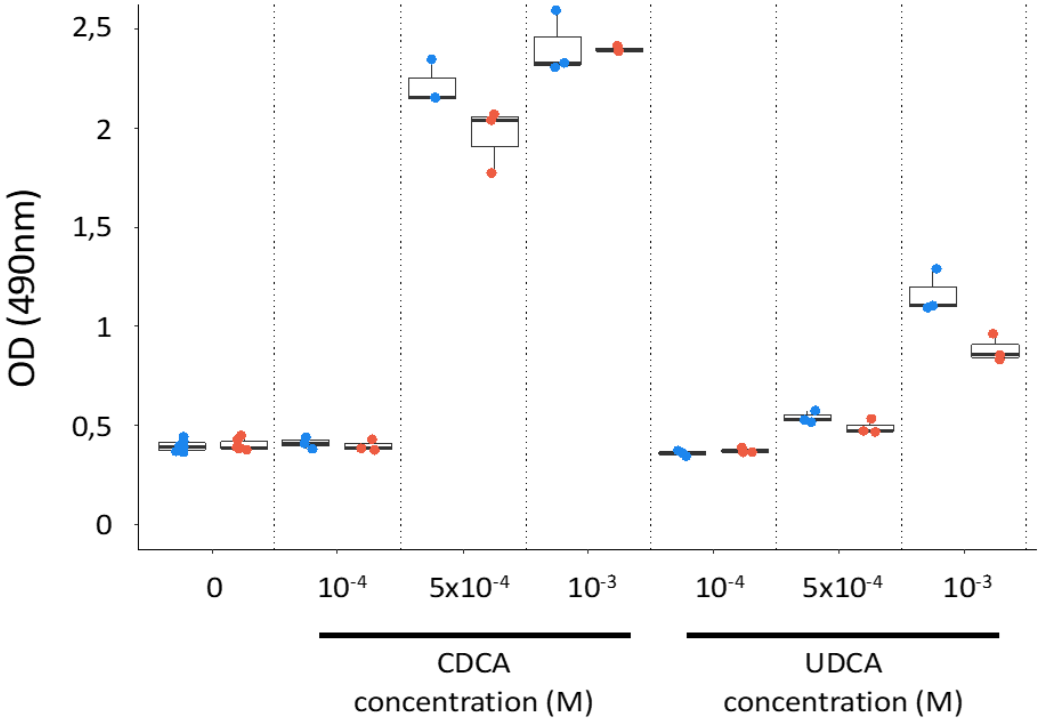

Figure 19 : Le CDCA est cytotoxique à plus faible concentration que l'UDCA

Densité optique (490nm) mesurée dans le surnageant de cellule RAW 264.7 à la suite d'une induction (en rouge, n=3 par condition) ou non (en bleu, n=3 par condition) par un mélange d'IFNγ et de LPS en présence de doses croissantes de CDCA et d'UDCA.

Ce caractère cytotoxique doit aussi prendre en compte les bactéries du microbiote intestinal et non seulement les cellules de l'hôte. De la même manière nous avons observé qu'une forte concentration d'UDCA (5g/kg de nourriture) pouvait impacter le microbiote intestinal des souris OMM[12] avec notamment une baisse significative de l'abondance de *Muribaculum intestinale* et de *Clostridium clostridrioforme*. Parallèlement, le pattern de colonisation *C. rodentium* a été

radicalement modifié avec une concentration de près de 10^{10}CFU/g de fèces au jour 3 post-infection et restant à ce niveau pendant les jours suivant. Cette dysbiose a ainsi pu directement influencer la capacité de *C. rodentium* à coloniser les souris OMM[12].

Comme nous avions observé *in vitro* une plus grande cytotoxicité du CDCA, nous nous sommes demandé si le CDCA pouvait également affecter la croissance bactérienne des souches OMM[12] et notamment de *M. intestinale* et *C. clostridioforme* (Fig. 20).

Nous observons que l'UDCA perturbe faiblement la croissance à 24h de *C. clostridioforme* et de *M. intestinale* à des concentrations de 0.5 et 1mM. De manière surprenante, à une concentration en UDCA de 2mM, la croissance est égale au milieu sans UDCA. Cette observation pourrait s'expliquer par une réponse non linéaire, ou la formation de cristaux à une forte concentration d'UDCA dans un milieu acidifié par les bactéries. Le CDCA en revanche impacte fortement la croissance de ces deux souches, notamment aux plus fortes concentrations (Fig. 20).

On peut se demander alors si la balance CDCA/UDCA peut entraîner des répercussions sur la colonisation de *C. rodentium* dans les souris OMM[12]. L'ajout de CDCA dans la nourriture des souris OMM[12] pourrait entrainer un dysbiose qui faciliterait la colonisation de *C. rodentium*. Plus largement, cela souligne l'intérêt de caractériser les acides biliaires dans leur ensemble et non pas uniquement une molécule à la fois. En effet, les acides biliaires sont capables de moduler la composition du microbiote intestinal et sont eux-même métabolisés par le microbiote, ce qui entraine des dynamiques des populations complexes. La stabilité de la composition du microbiote au sein d'un individu implique l'existence de mécanismes d'autorégulation, qu'ils soient médiés par les bactéries du microbiote ou par l'hôte.

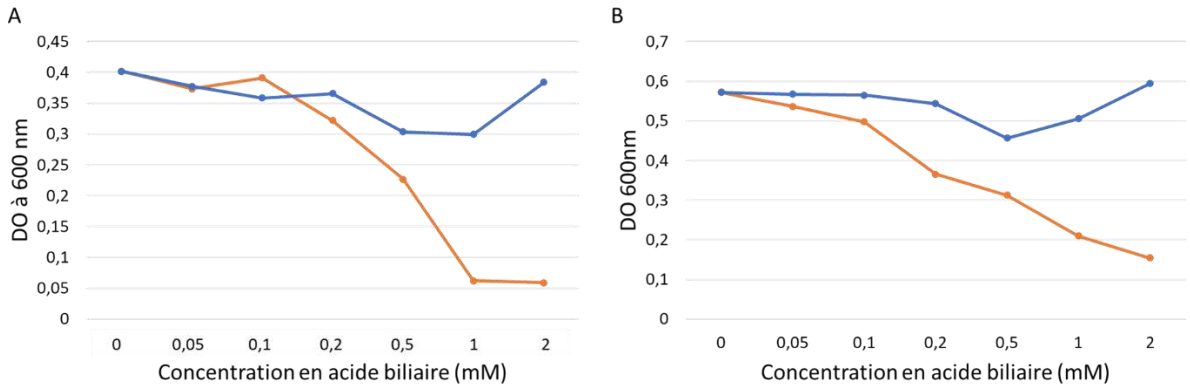

Figure 20 : Le CDCA, mais pas l'UDCA, inhibe la croissance de bactéries du consortium OMM[12]
Densité optique (600nm) mesurée à l'issue de 24h de culture à 37°C dans du milieu LYBHI en anaérobie **A.** de *C. clostridioforme* ou **B.** de *M. intestinale* en présence d'UDCA (en bleu) ou de CDCA (en orange) à différentes concentrations

III – Les interactions bactériophages - bactéries dans un contexte inflammatoire

A) L'importance de l'environnement dans les interactions bactériophages – bactéries

Les interactions bactériophages virulents – bactéries, extensivement caractérisées *in vitro*, sont encore mal comprises *in vivo* et notamment dans l'intestin. Lors de la première partie de ce travail de thèse, nous avons étudié le rôle de l'environnement intestinal dans les interactions bactériophages - bactéries.

Dans une première étude, nous nous sommes intéressés aux différences d'expression génétique des bactéries dans l'intestin. En effet, les bactéries doivent s'adapter à ce milieu très compétitif avec des conditions physico-chimiques particulières. Pour cela les bactéries modifient l'expression génétique de certains gènes par rapport à un milieu de culture simple. Nous avons retrouvé de nombreux gènes sur- ou sous-exprimés, impliqué dans l'acquisition de fer, la respiration aérobie et anaérobie, le métabolisme des glucides, la mobilité, l'adhésion, l'agrégation, la formation de biofilm et la biosynthèse du LPS. Nous avons alors identifié quatre gènes (*bss*R, *lsr*C, *fli*A et *rfa*L) et confirmé leur implication dans les interactions bactériophages – bactéries .

Dans une seconde étude, nous avons pu observer que l'hétérogénéité spatiale de l'environnement intestinal permettait la formation de réservoirs de bactéries au sein du mucus, peu accessibles aux bactériophages. Cela a pour conséquence le maintien d'une population bactérienne sensible aux bactériophages, car n'étant pas au contact de ceux-ci; mais cela permet aussi de maintenir des bactériophages qui se multiplient au détriment des bactéries qui diffusent depuis la partie mucosale vers la lumière intestinale.

Nous avons pu voir dans la première partie de ce travail de thèse que l'environnement jouait un rôle majeur. Nous pouvons alors nous demander si une perturbation de l'environnement intestinal pourrait entraîner des conséquences sur les interactions bactériophages – bactéries.

B) Étudier les interactions bactériophages - bactéries dans l'intestin lors d'une perturbation

L'inflammation dans l'intestin modifie grandement l'environnement intestinal. Selon l'origine de l'inflammation, nous pouvons observer une augmentation de la concentration en oxygène, d'espèces réactives de l'oxygène et une perturbation de la barrière intestinale (1,20) par une augmentation de sa perméabilité (21). Ces facteurs peuvent d'une part modifier l'expression des gènes bactériens dans l'intestin et d'autre part altérer la localisation des bactéries, le tout modulant potentiellement les interactions bactériophages-bactéries.

Bien que complexe, il est critique d'étudier les bactériophages dans de tels environnements. Il a été remarqué que l'abondance et la diversité des différentes populations de bactériophages est perturbée dans différentes pathologies comme les MICI (22,23). Mais ces études ne sont qu'observationnelles et ne permettent pas de comprendre comment interagissent les bactéries, les bactériophages et l'hôte dans ces circonstances. Notamment, des liens de causalité ne peuvent pas être déterminés.

C'est dans ce cadre que nous avons initié une étude des interactions bactériophages - bactéries chez des souris infectées par *C. rodentium*. Nous avons isolé et testé *in vivo* plusieurs bactériophages virulents qui se comportent tous de la même manière. Tout d'abord les bactériophages ne se répliquent pas durant la phase précoce de la colonisation dans les patchs du ceacum (au jour deux post-infection) ni dans à la phase tardive de l'infection lorsque l'inflammation est résolue dans le colon. Lors de la colonisation du colon (à partir du jour quatre post-infection) et au pic de colonisation (au jour huit post-infection), les différents bactériophages se répliquent et réduisent modérément la colonisation fécale de *C. rodentium*. L'absence d'efficacité des bactériophages aux jours précoces et tardifs peut être sujette à différents facteurs. Par exemple, le ceacum pourrait ne pas être propices à la réplication des bactériophages virulents testés. *C. rodentium* voit aussi son activité transcriptomique grandement modifiée lors de la progression de l'infection, ce qui pourrait entraîner des répercussions sur sa susceptibilité aux bactériophages, comme cela a été observé dans le premier article présenté dans cette thèse. Un autre facteur est que la densité des bactéries est réduite, limitant les possibilités de contact entre les deux populations antagonistes, ce qui pourrait s'avérer problématique pour une utilisation thérapeutique des bactériophages.

L'autre intérêt d'étudier les bactériophages dans un contexte pathologiques est l'élaboration de traitements antibactériens. Le développement de la phagothérapie dans l'intestin est aujourd'hui infructueux du fait de la complexité des interactions bactériophages-bactéries dans l'intestin. En effet, nous avons pu observer dans la première étude qu'un bactériophage

efficace *in vitro* ne le sera pas forcément *in vivo*. Et même si le bactériophage se réplique dans l'intestin, des réservoirs de bactéries pourront se former, comme nous l'avons montré dans la seconde étude. Cependant, le fait de connaitre ces limitations nous permet de commencer à trouver des solutions. Par exemple, des bactériophages avec une forte affinité pour le mucus pourraient permettre de mieux éliminer les réservoirs bactériens qui s'y trouvent (24). L'administration prophylactique de bactériophages pourrait aussi améliorer la résistance à la colonisation de bactéries pathogènes (25).

Dans le travail présenté en annexe, nous avons ainsi traité quotidiennement prophylactiquement des souris OMM[12] infectées par *Salmonella enterica* Serovar Typhimurium. Le traitement (un cocktail commercial de bactériophages) était maintenu après le gavage des souris par *S.* Typhimurium. Nous avons observé que ce traitement permettait de retarder la colonisation de la bactérie pathogène, mais pas d'empêcher une infection (26).

L'élimination d'une population bactérienne de l'intestin par l'utilisation uniquement de bactériophages semble donc difficile. Mais l'association de bactériophages avec un probiotique pourrait permettre de décoloniser un pathogène plus facilement et ainsi favoriser la colonisation par la souche compétitrice. La double pression de sélection dans ce milieu très compétitif pourrait alors être suffisante pour remplacer une souche par une autre. Ceci pourrait constituer une avancée vers la modification ciblée du microbiote intestinal afin, par exemple, de limiter la susceptibilité a certaines pathologies.

Enfin, la combinaison de l'effet antibactérien des bactériophages et de l'effet anti-inflammatoire des acides biliaires pourrait être envisagée. Cette perspective s'inscrit dans une nouvelle approche du traitement des maladies inflammatoires intestinales, qui vise à agir à la fois sur l'hôte et le microbiote intestinal. Très peu de données sont actuellement disponibles sur cette combinaison et les effets des acides biliaires sur les interactions bactériophages – bactéries restent encore à étudier (27).

Références

1. Mullineaux-Sanders C, Sanchez-Garrido J, Hopkins EGD, Shenoy AR, Barry R, Frankel G. Citrobacter rodentium–host–microbiota interactions: immunity, bioenergetics and metabolism. Nat Rev Microbiol. nov 2019;17(11):701-15.

2. Kamada N, Kim YG, Sham HP, Vallance BA, Puente JL, Martens EC, et al. Regulated virulence controls the ability of a pathogen to compete with the gut microbiota. Science. 8 juin 2012;336(6086):1325-9.

3. Brugiroux S, Beutler M, Pfann C, Garzetti D, Ruscheweyh HJ, Ring D, et al. Genome-guided design of a defined mouse microbiota that confers colonization resistance against Salmonella enterica serovar Typhimurium. Nat Microbiol. févr 2017;2(2):16215.

4. Serapio-Palacios A, Woodward SE, Vogt SL, Deng W, Creus-Cuadros A, Huus KE, et al. Type VI secretion systems of pathogenic and commensal bacteria mediate niche occupancy in the gut. Cell Reports. 26 avr 2022;39(4):110731.

5. Sano T, Huang W, Hall JA, Yang Y, Chen A, Gavzy SJ, et al. An IL-23R/IL-22 Circuit Regulates Epithelial Serum Amyloid A to Promote Local Effector Th17 Responses. Cell. 8 oct 2015;163(2):381-93.

6. Cai J, Sun L, Gonzalez FJ. Gut microbiota-derived bile acids in intestinal immunity, inflammation, and tumorigenesis. Cell Host & Microbe. 9 mars 2022;30(3):289-300.

7. Wang H, Chen J, Hollister K, Sowers LC, Forman BM. Endogenous Bile Acids Are Ligands for the Nuclear Receptor FXR/BAR. Molecular Cell. 1 mai 1999;3(5):543-53.

8. Kawamata Y, Fujii R, Hosoya M, Harada M, Yoshida H, Miwa M, et al. A G Protein-coupled Receptor Responsive to Bile Acids *. Journal of Biological Chemistry. 14 mars 2003;278(11):9435-40.

9. Schaap FG, Trauner M, Jansen PLM. Bile acid receptors as targets for drug development. Nat Rev Gastroenterol Hepatol. janv 2014;11(1):55-67.

10. Ticho AL, Malhotra P, Dudeja PK, Gill RK, Alrefai WA. Bile Acid Receptors and Gastrointestinal Functions. Liver Res. mars 2019;3(1):31-9.

11. Ward JBJ, Lajczak NK, Kelly OB, O'Dwyer AM, Giddam AK, Ní Gabhann J, et al. Ursodeoxycholic acid and lithocholic acid exert anti-inflammatory actions in the colon. Am J Physiol Gastrointest Liver Physiol. 1 juin 2017;312(6):G550-8.

12. O'Dwyer AM, Lajczak NK, Keyes JA, Ward JB, Greene CM, Keely SJ. Ursodeoxycholic acid inhibits TNFα-induced IL-8 release from monocytes. American Journal of Physiology-Gastrointestinal and Liver Physiology. août 2016;311(2):G334-41.

13. Lajczak-McGinley NK, Porru E, Fallon CM, Smyth J, Curley C, McCarron PA, et al. The secondary bile acids, ursodeoxycholic acid and lithocholic acid, protect against intestinal inflammation by inhibition of epithelial apoptosis. Physiol Rep. juin 2020;8(12):e14456.

14. Suraweera D, Rahal H, Jimenez M, Viramontes M, Choi G, Saab S. Treatment of primary biliary cholangitis ursodeoxycholic acid non-responders: A systematic review. Liver Int. déc 2017;37(12):1877-86.

15. Tanaka H, Makino Y, Miura T, Hirano F, Okamoto K, Komura K, et al. Ligand-independent activation of the glucocorticoid receptor by ursodeoxycholic acid. Repression of IFN-gamma-induced MHC class II gene expression via a glucocorticoid receptor-dependent pathway. J Immunol. 15 févr 1996;156(4):1601-8.

16. Golden JM, Escobar OH, Nguyen MVL, Mallicote MU, Kavarian P, Frey MR, et al. Ursodeoxycholic acid protects against intestinal barrier breakdown by promoting enterocyte migration via EGFR- and COX-2-dependent mechanisms. American Journal of Physiology-Gastrointestinal and Liver Physiology. août 2018;315(2):G259-71.

17. Paik D, Yao L, Zhang Y, Bae S, D'Agostino GD, Zhang M, et al. Human gut bacteria produce TH17-modulating bile acid metabolites. Nature. mars 2022;603(7903):907-12.

18. Hang S, Paik D, Yao L, Kim E, Trinath J, Lu J, et al. Bile acid metabolites control TH17 and Treg cell differentiation. Nature. déc 2019;576(7785):143-8.

19. Ridlon JM, Bajaj JS. The human gut sterolbiome: bile acid-microbiome endocrine aspects and therapeutics. Acta Pharmaceutica Sinica B. 1 mars 2015;5(2):99-105.

20. Hartog G den, Chattopadhyay R, Ablack A, Hall EH, Butcher LD, Bhattacharyya A, et al. Regulation of Rac1 and Reactive Oxygen Species Production in Response to Infection of Gastrointestinal Epithelia. PLOS Pathogens. 13 janv 2016;12(1):e1005382.

21. Ahmad R, Sorrell MF, Batra SK, Dhawan P, Singh AB. Gut permeability and mucosal inflammation: bad, good or context dependent. Mucosal Immunol. mars 2017;10(2):307-17.

22. Clooney AG, Sutton TDS, Shkoporov AN, Holohan RK, Daly KM, O'Regan O, et al. Whole-Virome Analysis Sheds Light on Viral Dark Matter in Inflammatory Bowel Disease. Cell Host Microbe. 11 déc 2019;26(6):764-778.e5.

23. Norman JM, Handley SA, Baldridge MT, Droit L, Liu CY, Keller BC, et al. Disease-Specific Alterations in the Enteric Virome in Inflammatory Bowel Disease. Cell. 29 janv 2015;160(3):447-60.

24. Green SI, Gu Liu C, Yu X, Gibson S, Salmen W, Rajan A, et al. Targeting of Mammalian Glycans Enhances Phage Predation in the Gastrointestinal Tract. mBio. 12(1):e03474-20.

25. Almeida GMF, Laanto E, Ashrafi R, Sundberg LR. Bacteriophage Adherence to Mucus Mediates Preventive Protection against Pathogenic Bacteria. mBio. 10(6):e01984-19.

26. Lamy-Besnier Q, Chaffringeon L, Lourenço M, Payne RB, Trinh JT, Schwartz JA, et al. Prophylactic Administration of a Bacteriophage Cocktail Is Safe and Effective in Reducing Salmonella enterica Serovar Typhimurium Burden in Vivo. Microbiology Spectrum. 9(1):e00497-21.

27. Scanlan JG, Hall AR, Scanlan PD. Impact of bile salts on coevolutionary dynamics between the gut bacterium Escherichia coli and its lytic phage PP01. Infect Genet Evol. sept 2019;73:425-32.

Annexes

Liste des figures

Liste des tables

Liste des abréviations

αMCA : α-MuriCholic Acid
βMCA : β-MuriCholic Acid
A/E : Attachement/Effacement
AGCC : Acide Gras à Chaine Courte
AhR : Aryl hydrocarbon Receptor
AIEC : Adherent-Invasive *Escherichia coli*
ADN : Acide DésoxyriboNucléique
AMP : Adénosine MonoPhosphate
ARN : Acide RiboNucléique
BSH : Bile Salt Hydrolase
CA : Cholic acid
CBASS : Cyclic oligonucleotide Based Anti-phage Signalling System
CAR : Constitutive Androstane Receptor
CAS : CRISPR Associated Protein
CD : Cluster de Différenciation
CDCA : ChenoDeoxyCholic Acid
CEI : Cellule Epithéliale Intestinale
COX2 : CycloOXygénase 2
CRISPR : Clustered Regularly Interspaced Short Palindromic Repeats
DAEC : Diffusely-Adherent *Escherichia coli*
DCA : DeoxyCholic Acid
DSS : Dextran Sulfate Sodium
EAEC : Enteroaggregative *Escherichia coli*
EHEC : EnteroHemorrhagic *Escherichia coli*
EIEC : EnteroInvasive *Escherichia coli*
EPEC : EnteroPathogenic *Escherichia coli*
ETEC : EnteroToxinegic *Escherichia coli*
FXR : Farnesoid X Receptor
G-CDCA : GlycoChenoDeoxyCholic Acid
G-CA : GlycoChenoCholic Acid
GALT : Gut Associated Lymphoid Tissue
GLP1 : Glucagon-Like Peptide 1
GMP : Guanosine MonoPhosphate
GPBAR1 : G-Protein-coupled Bile Acid Receptor 1
ICTV : International Committee for the Taxonomy of Viruses
IFNγ : Interféron- γ
Ig : Immunoglobuline
IL : InterLeukine
ILC : Innate Lymphoid Cell
JPI : Jour Post-Infection
LCA : LitoCholic Acid
LCN2 : Lipocaline-2
LEE : Locus of Enterocyte Effacement
LPS : LipoPolySaccharide
MALT : Mucosal Associated Lymphoid Tissue
MAM : Microbial Anti-inflammatory Molecule
MAMP : Microbial Associated Molecular Pattern
MICI : Maladies Inflammatoires Chroniques de l'Intestin
NF-κB : Nuclear Factor κ-light-chain-enhancer of activated B cells
NLR : Node Like Receptor
OMM^{12} : Oligo Mouse Model 12
PAM : Peptides Anti-Microbien

PAMP : Pathogen Associated Molecular Pattern
PICIs : Phage-Inducible Chromosomal Islands
PRR : Pattern Recognition Receptor
PXR : Pregnane X Receptor
SP1R2 : Sphingosine 1-Phosphate Receptor
REG3 : Regenerating islet-derived protein 3
RORγt : retinoid-related orphan receptor γt
SHIME : Simulator of the Human Intestinal Microbial Ecosystem
SPF : Specific Pathogen Free
stx : shigatoxine
T3SS : Type III Secretion System
T6SS : Type VI Secretion System
T-CA : TauroChenoCholic Acid
T-CDCA : TauroChenoDeoxyCholic Acid
Th : T-helper
TLR : Toll Like Receptor
Treg : T régulateur
UDCA : UrsoDeoxyCholic Acid
UFC : Unité Formant Colonie
UFP : Unité Formant Plage
VDR : Vitamin D Receptor
ZO : Zonula Occludens

Publication supplémentaire

AMERICAN SOCIETY FOR MICROBIOLOGY | Microbiology Spectrum

RESEARCH ARTICLE

Prophylactic Administration of a Bacteriophage Cocktail Is Safe and Effective in Reducing *Salmonella enterica* Serovar Typhimurium Burden *in Vivo*

Quentin Lamy-Besnier,[a,b] Lorenzo Chaffringeon,[a,c] Marta Lourenço,[a,d] Rayford B. Payne,[e] Jimmy T. Trinh,[e] Jennifer A. Schwartz,[e] Alexander Sulakvelidze,[e] Laurent Debarbieux[a]

[a]Department of Microbiology, Institut Pasteur, Paris, France
[b]Université de Paris, Paris, France
[c]Sorbonne Université, INSERM, Centre de Recherche St Antoine, UMRS_938, Paris, France
[d]Sorbonne Université, Collège Doctoral, Paris, France
[e]Intralytix, Inc., Columbia, Maryland, USA

ABSTRACT Nontyphoidal *Salmonella* bacteria are the causative agent of salmonellosis, which accounts for the majority of foodborne illness of bacterial etiology in humans. Here, we demonstrate the safety and efficacy of the prophylactic administration of a bacteriophage preparation termed FOP (foodborne outbreak pill), which contains lytic phages targeting *Salmonella* (SalmoFresh phage cocktail), Shiga toxin-producing *Escherichia coli* (STEC), and *Listeria monocytogenes*, for lowering *Salmonella* burdens in OMM^{12} gnotobiotic mice. Prophylactic administration of FOP significantly reduced the levels of *Salmonella* in feces and in intestinal sections compared to the levels in controls. Moreover, the overall symptoms of the disease were also considerably lessened. Dose-dependent administration of FOP showed that phage amplification reached similarly high levels in less than 48 h independent of dose. In addition, 16S rRNA gene analysis showed that FOP did not alter the intestinal microbiota of healthy OMM^{12} mice and reduced microbiota perturbations induced by *Salmonella*. FOP maintained its full potency against *Salmonella* in comparison to that of SalmoFresh, its *Salmonella*-targeting component phages alone. Altogether, the data support that preventive administration of FOP may offer a safe and effective approach for reducing the risk of foodborne infections caused by *Salmonella* and, potentially, other foodborne bacteria (namely, STEC and *L. monocytogenes*) targeted by the FOP preparation.

IMPORTANCE Foodborne bacterial infections cause worldwide economic loss. During an epidemic, the use of antibiotics to slow down the spread of the disease is not recommended because of their side effects on the resident microbiota and the selection of antibiotic-resistant bacteria. Here, we investigated the potential for the prophylactic administration of bacteriophages (viruses infecting bacteria) to reduce the burden of *Salmonella in vivo* using mice colonized by a synthetic microbiota. We found that the repeated administration of bacteriophages was safe and efficient in lowering the *Salmonella* burden. Perturbations of the microbiota by the *Salmonella* infection were also reduced when mice received bacteriophages. Altogether, these data support the use of bacteriophages as a prophylactic intervention to lower the spread of foodborne epidemics.

KEYWORDS foodborne disease, gnotobiotic model, epidemic, prevention, food-borne disease

Foodborne illnesses are a major cause of morbidity and mortality, with an estimated 600 million foodborne infections and >400,000 deaths worldwide in 2010 (1, 2). The majority of foodborne disease (FBD) is caused by bacterial pathogens, where nontyphoidal *Salmonella* (NTS) strains are among those most commonly associated with invasive disease

Citation Lamy-Besnier Q, Chaffringeon L, Lourenço M, Payne RB, Trinh JT, Schwartz JA, Sulakvelidze A, Debarbieux L. 2021. Prophylactic administration of a bacteriophage cocktail is safe and effective in reducing *Salmonella enterica* serovar Typhimurium burden *in vivo*. Microbiol Spectr 9:e00497-21. https://doi.org/10.1128/Spectrum.00497-21.

Editor Daria Van Tyne, University of Pittsburgh School of Medicine

Address correspondence to Laurent Debarbieux, laurent.debarbieux@pasteur.fr.

Received 4 June 2021
Accepted 29 July 2021
Published 25 August 2021

(3) and gastroenteritis (4). NTS infections are consistently the leading cause of an estimated 80 million cases of FBD worldwide, and approximately 1 million cases of FBD occur in the United States each year. NTS strains are Gram-negative, facultative, anaerobic bacteria consisting of multiple serovars of *Salmonella enterica* subsp. *enterica*. *Salmonella* infections (i.e., salmonellosis) in humans typically are acquired during transmission from the consumption of contaminated food or water, often from animal sources (5, 6).

Salmonellosis, a form of gastroenteritis, is often self-limiting, resulting in nausea, abdominal cramps, vomiting, and diarrhea that, while often lasting several days in healthy individuals, can lead to serious and deadly complications in vulnerable populations, such as the immunocompromised, elderly, or very young (7, 8). Salmonellosis may be treated using broad-spectrum antibiotics, but recent developments, including antibiotic resistance, have exposed limitations and risks with this approach (9–13). Thus, considerable effort is increasingly directed at finding prevention strategies to lower the dissemination of foodborne pathogens in a more specific manner (14).

Bacteriophages (or phages) offer one such approach. Phages are bacterial viruses that, unlike antibiotics, are highly specific and effective at killing their targeted host bacteria. In addition, the mechanisms by which antibiotics and phages kill bacteria and, conversely, the mechanisms of bacterial resistance to antibiotics or phages are fundamentally different (15–17). There is a long history of using phages to treat bacterial infections in humans, namely, phage therapy (18, 19), and currently, the number of successful compassionate treatments is increasing worldwide (20, 21). In contrast, the prophylactic use of phages remains underevaluated, in particular in the field of FBD.

Here, we utilize gnotobiotic mice (OMM^{12}) to examine the tolerability and efficacy of the prophylactic administration of a phage preparation to target an intestinal foodborne pathogen. The OMM^{12} mice harbor a defined and stable intestinal community composed of 12 bacterial strains of mouse origin, which represent the five most prevalent and abundant phyla of the native laboratory mouse intestine (22). Importantly, when challenged by the human foodborne pathogen *Salmonella enterica* subsp. *enterica* serovar Typhimurium, OMM^{12} mice exhibited symptoms similar to those of salmonellosis in humans, without the need to use an antibiotic treatment to favor intestinal colonization, making these mice a relevant model for assessing the prophylactic impact of phages (22, 23).

We evaluated two phage preparations, SalmoFresh and FOP (foodborne outbreak pill), that target *Salmonella* Typhimurium. SalmoFresh is a cocktail of 6 phages targeting multiple *Salmonella* strains, and FOP is a cocktail of 15 phages that includes those from SalmoFresh, 6 phages targeting *Listeria monocytogenes* strains, and 3 phages targeting Shiga toxin-producing *Escherichia coli* (STEC) strains, including *E. coli* O157:H7 (24). FOP was equally as effective as SalmoFresh in reducing the *Salmonella* burden in feces and intestinal sections and in reducing symptoms of the disease. The prophylactic administration of FOP to healthy mice did not perturb the native gut microbiome, and FOP alone did not induce a gut inflammatory response as measured by the biomarker lipocalin-2. Altogether, these observations show that the prophylactic administration of FOP is both safe and effective to reduce *Salmonella* burdens *in vivo*.

RESULTS

SalmoFresh delays the burden of *Salmonella* in OMM^{12} mice. To assess the impact of the prophylactic administration of phage products on the burden of *Salmonella in vivo*, we first evaluated SalmoFresh, a product that contains six lytic phages (Fig. 1A and Table 1) (24, 25). Animals (3 groups) received for 2 days (days 0 and 1) either phosphate-buffered saline (PBS) (1 group) or SalmoFresh (2 groups) administered twice a day by oral gavage to reduce variability between animals and to ensure appropriate dosing and efficient delivery of the treatments and control. On day 2, the PBS group and one of the SalmoFresh groups received a single administration of *Salmonella* Typhimurium strain ST784 (1×10^8 CFU by oral gavage) (referred to as the ST784 PBS and ST784 SalmoFresh groups), while the other SalmoFresh group received PBS as a SalmoFresh control (referred to as the PBS SalmoFresh group). SalmoFresh (1×10^9

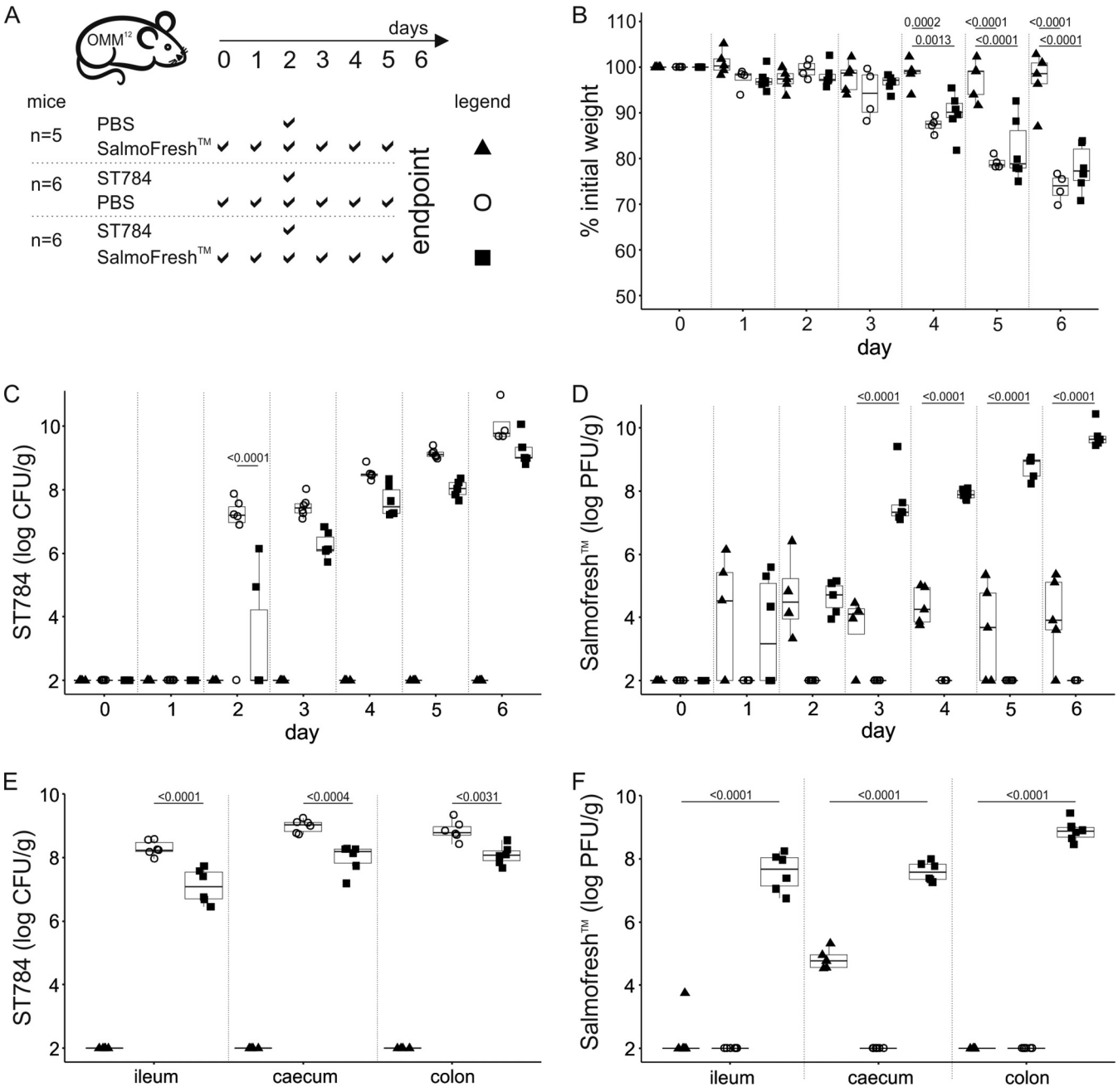

FIG 1 SalmoFresh delays the burden of *Salmonella* after challenge in OMM[12] mice. (A) Experimental design. Groups of 4 to 6 OMM[12] mice were orally administered PBS or SalmoFresh (1×10^9 PFU) on the indicated days. On day 2, mice were challenged with ST784 (1×10^8 CFU) or a PBS control as indicated. (B) Mice were weighed daily. Shown are the percentages of weight loss compared to starting weights of OMM[12] mice over time. (C and D) The amounts of ST784 (CFU) (C) and phages (PFU) (D) in OMM[12] mouse feces were quantitated daily (day 2 corresponds to 3 h after ST784 challenge). (E and F) Intestinal organs were collected on day 6 and homogenized, and the amounts of ST784 (CFU) (E) and phage (PFU) (F) were quantitated. Statistical analyses are described in Materials and Methods and reported in Table S1.

PFU/dose, quantified on strain ST784 prior to use) and PBS were then administered to the respective groups by oral gavage twice a day for an additional 4 days (from day 2 to day 5). Of note, four of the six phages included in SalmoFresh infect strain ST784 with similar efficiencies *in vitro* (see Materials and Methods). The single oral administration of ST784 in OMM[12] mice receiving PBS (ST784 PBS group) led to a significant loss of weight compared to the weight loss in uninfected mice (PBS SalmoFresh group), starting 48 h post-ST784 administration and lasting two more days before animals reached the experimental endpoint (loss of 25% of their initial weight) (Fig. 1B and

TABLE 1 SalmoFresh reduces disease symptoms associated with the burden of *Salmonella* in OMM[12] mice

	No. of mice that were[b]:		Treatment		Challenge		Clinical signs and symptoms on day[d]:						
Treatment group[a]	M	F	SF[c]	PBS	ST784	PBS	0	1	2	3	4	5	6
ST784 SalmoFresh	2	−	+	−	+	−	None	None	None	None	None	*Mild*	Mod
	−	4	+	−	+	−	None	None	None	None	None	None	Mod
PBS SalmoFresh	2	−	+	−	−	+	None	None	None	None	None	None	None
	−	3	+	−	−	+	None	None	None	None	None	None	None
ST784 PBS	2	−	−	+	+	−	None	None	None	None	None	Mod	Mod
	−	4	−	+	+	−	None	None	None	None	Mod	Mod	**Sev**

[a]Treatment groups were as shown in Fig. 1A.
[b]M, male; F, female.
[c]SF, SalmoFresh.
[d]Clinical signs and symptoms over time (days 0 to 6) are scored based on animal behavior (e.g., activity, hunching) and consistency of fecal pellets (e.g., formed/no liquid, formed/liquid, liquid) as follows: None, no signs of disease; *Mild*, 50% of animals in group exhibited mild signs of disease; Mod, all animals in group exhibited moderate disease; **Sev**, all animals in group exhibited severe disease.

Table S1). Infected animals that received SalmoFresh twice a day (ST784 SalmoFresh group) displayed significant weight loss compared to the weight loss in uninfected mice (PBS SalmoFresh group). No significant weight variations were observed between ST784 PBS and ST784 SalmoFresh groups post-ST784 administration (Fig. 1B and Table S1). Additionally, symptoms of the disease (fur appearance, mobility, weight loss, and fecal consistency) were delayed in ST784 SalmoFresh animals compared to the onset in the ST784 PBS controls (Table 1). Concomitant to these observations, the levels of *Salmonella* in fecal samples increased steadily over time in both infected groups (Fig. 1C and Table S1). However, this increase was delayed by approximately 24 h in the ST784 SalmoFresh group and trended lower than in the ST784 PBS group (Fig. 1C and Table S1). This suggests that phages were able to infect ST784 *in vivo*, which was confirmed by the highly significant difference in the fecal phage levels when comparing uninfected and infected groups receiving SalmoFresh, which culminated with a 4-log difference by day 6 (Fig. 1D). Intestinal gut sections (ileum, cecum, and colon) were collected at day 6, and the *Salmonella* and phage levels were measured (Fig. 1E and F). Significant differences in *Salmonella* counts between the ST784 SalmoFresh and ST784 PBS groups were confirmed in all gut sections (Fig. 1E and Table S1). Phage levels in all three gut sections from ST784 SalmoFresh mice reached 10^8 PFU/g of feces, while in PBS SalmoFresh mice, the levels only reached 10^4 PFU/g in the cecum and were below the threshold of detection in both the ileum and colon (Fig. 1F). Phages were undetectable in the gut sections of the ST784 PBS group. These data demonstrate that the prophylactic administration of phages delays the burden of *Salmonella* in OMM[12] mice. They are congruent with results previously obtained when testing SalmoFresh to reduce *Salmonella* contamination on fresh products (25). Additionally, the repeated administration of SalmoFresh in uninfected mice (PBS SalmoFresh group) did not impact their overall health (i.e., behavior and weight), showing that in the absence of their bacterial target, phages are innocuous.

FOP strongly reduces *Salmonella* burden *in vivo*. Using an experiment similar to the one described above, we next assessed the impact of FOP, which contains a combination of products including SalmoFresh (Fig. 2A and Table 2). In two independent experiments, two groups of mice were administered by oral gavage either FOP (1×10^9 PFU/dose; $n = 14$) or PBS ($n = 11$) twice a day for 6 days. Both groups were challenged with ST784 (1×10^8 CFU) on day 2 (ST784 PBS and ST784 FOP groups). We observed in both groups a median weight loss of approximately 10% of their initial weights within 24 h after *Salmonella* administration (Fig. 2B and Table S2). During the following 3 days (days 3 to 5), the median weight loss increased to 20% in the ST784 PBS group, while it stayed roughly stable in the ST784 FOP group (Fig. 2B and Table S2). Fecal pellets collected 3 h after *Salmonella* administration showed that in the ST784 PBS group, *Salmonella* levels reached 10^6 CFU/g of feces in all but two mice (Fig. 2C and Table S2). This was in sharp contrast to the ST784 FOP group, in which only 6 of 14 mice had *Salmonella* levels above the detection threshold (Fig. 2C and Table S2). During the next 4 days (days 3 to 6), the initial impact of the FOP product was significantly

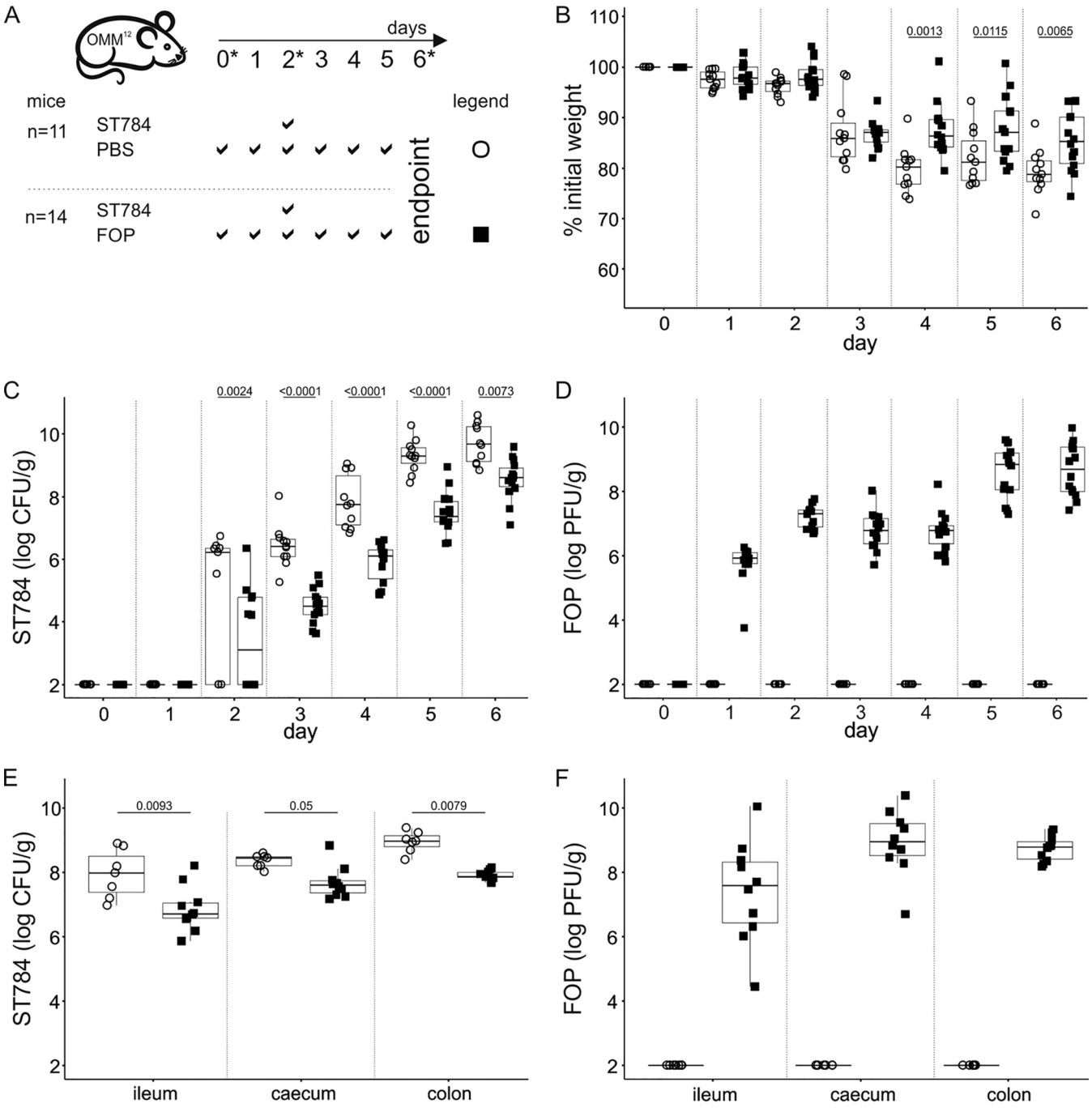

FIG 2 FOP reduces *Salmonella* burden *in vivo*. (A) Experimental design. OMM^{12} mice were orally administered PBS or FOP (1×10^9 PFU) on the indicated days. On day 2, all mice were challenged with strain ST784 (1×10^8 CFU). Stars indicate the time points at which samples were taken for the 16S rRNA gene analysis reported in Fig. 3. (B) Mice were weighed daily. Shown are the percentages of weight loss compared to starting weights of OMM^{12} mice over time. (C and D) The amounts of ST784 (CFU) (C) and phages (PFU) (D) in OMM^{12} mouse feces were quantitated daily (day 2 corresponds to 3 h after ST784 challenge). (E and F) Intestinal organs were collected on day 6, and the amounts of ST784 (CFU) (E) and phages (PFU) quantitated. Statistical analyses are described in Materials and Methods and reported in Table S2.

maintained, despite a progressive increase of fecal *Salmonella* levels, where the *Salmonella* burden in the ST784 FOP group was >1-log lower than in the ST784 PBS group (Fig. 2C and Table S2). Additionally, clinical signs and symptoms were significantly reduced and delayed in the ST784 FOP group compared to the clinical signs and symptoms in the ST784 PBS group (Table 2). Fecal phage levels were approximately 10^7 PFU/g 3 h after *Salmonella* administration, remained stable during the next 2 days (days 3 and 4), and increased up to 10^8 to 10^{10} PFU/g during the last 2 days (days 5 and 6), which is a pattern expected from continuous

TABLE 2 FOP reduces disease symptoms associated with the burden of *Salmonella* in OMM[12] mice

Treatment group[a]	No. of mice that were[b]:		Treatment		Clinical signs and symptoms on day[c]:						
	M	F	FOP	PBS	0	1	2	3	4	5	6
ST784 FOP	6	−	+	−	None	None	None	None	None	None	*Mild*
	−	8	+	−	None	None	None	None	None	None	*Mild*
ST784 PBS	6	−	−	+	None	None	None	None	None	Mod	**Sev**
	−	5	−	+	None	None	None	None	*Mild*	Mod	Mod

[a]Treatment groups were as shown in Fig. 2.

[b]M, male; F, female.

[c]Clinical signs and symptoms over time (days 0 to 6) are scored based on animal behavior (e.g., activity, hunching) and consistency of fecal pellets (e.g., formed/no liquid, formed/liquid, liquid) as follows: None, indicates no signs of disease; *Mild*, indicates 50% of animals in group exhibited mild signs of disease; Mod, indicates all animals in group exhibited moderate disease; **Sev**, indicates 50% of animals in group exhibited severe disease.

infection of increasing levels of *Salmonella* in the intestine (Fig. 2D). The levels of both *Salmonella* and phages in gut sections examined at day 6 were in agreement with the observations presented in Fig. 2C and D, where smaller amounts of *Salmonella* were measured in the ST784 FOP group than in the ST784 PBS group (Fig. 2E and Table S2), together with concomitant elevated levels of phages (Fig. 2F).

An independent experiment was performed with uninfected OMM[12] mice to assess the safety of repeated administration of FOP, evaluated by observation of mouse behavior and measures of weight and fecal levels of lipocalin-2, a marker of intestinal inflammation (26), over time (Fig. S1A). When comparing groups of mice that received either FOP or PBS, we observed that all animals lost a slight amount of weight in both groups, which was attributed to repeated handling (i.e., twice-daily gavage) (Fig. S1B). No changes in overall health were observed (i.e., fur appearance, mobility, and fecal consistency). Fecal levels of phages were high and remained stable over time (Fig. S1C). Fecal levels of lipocalin-2 were quantitated before and 24 h and 96 h after FOP or PBS administration (Fig. S1D). Overall, lipocalin-2 levels remained below the threshold of inflammation (5 ng/g of feces [26]), and no increases were observed in the FOP group compared to the PBS group, indicating that FOP does not induce gastrointestinal tract inflammation (Fig. S1D).

The FOP treatment lowers *Salmonella*-induced perturbation of the bacterial consortium of the OMM[12] mice. We next assessed whether the prophylactic administration of the FOP product to *Salmonella*-infected OMM[12] mice would affect the relative abundances of the resident bacteria of the gut. Fecal DNA was extracted from samples (Fig. 2C) at three time points: before FOP or PBS administrations (day 0), before ST784 challenge (day 2), and before sacrifice on day 6. Samples were subjected to 16S rRNA gene amplification and sequencing (Fig. 3A). No significant differences in bacterial abundance were seen between day 0 and day 2 for each of the PBS and FOP groups of animals. Additionally, no significant differences in bacterial abundance were seen between the FOP or PBS groups on day 2 prior to the bacterial challenge (Fig. 3B and Table S3). As expected, *Salmonella* bacteria were substantially more abundant in day 6 samples but significantly lower in ST784 FOP than in ST784 PBS samples, further demonstrating the efficacy of FOP in reducing *Salmonella* burdens *in vivo* (Fig. 3B). In the ST784 PBS group (day 6 versus day 0), the relative abundances of four strains (*Clostridium clostridioforme*, *Muribaculum intestinale*, *Lactobacillus reuteri*, and *Enterococcus faecalis*) were altered by the presence of *Salmonella* (Tables S3). Interestingly, in ST784 FOP samples, the abundances of *C. clostridioforme* and *M. intestinale* were not significantly altered, while the abundances of *L. reuteri* and *E. faecalis* were. These results indicate that the latter two strains were strongly associated with the burden of *Salmonella*, while the other two were not, suggesting that FOP prevented their variation (Table S3). These data are consistent with those previously obtained with an *in vitro* human model system (24) showing that FOP administration does not alter the resident gastrointestinal microbial community.

Decreasing the FOP dose does not reduce its *in vivo* efficacy. To assess whether there was a dose-dependent effect on the ability of FOP to reduce *Salmonella in vivo*, three groups of 4 to 6 OMM[12] mice were orally administered FOP twice a day for 7 days

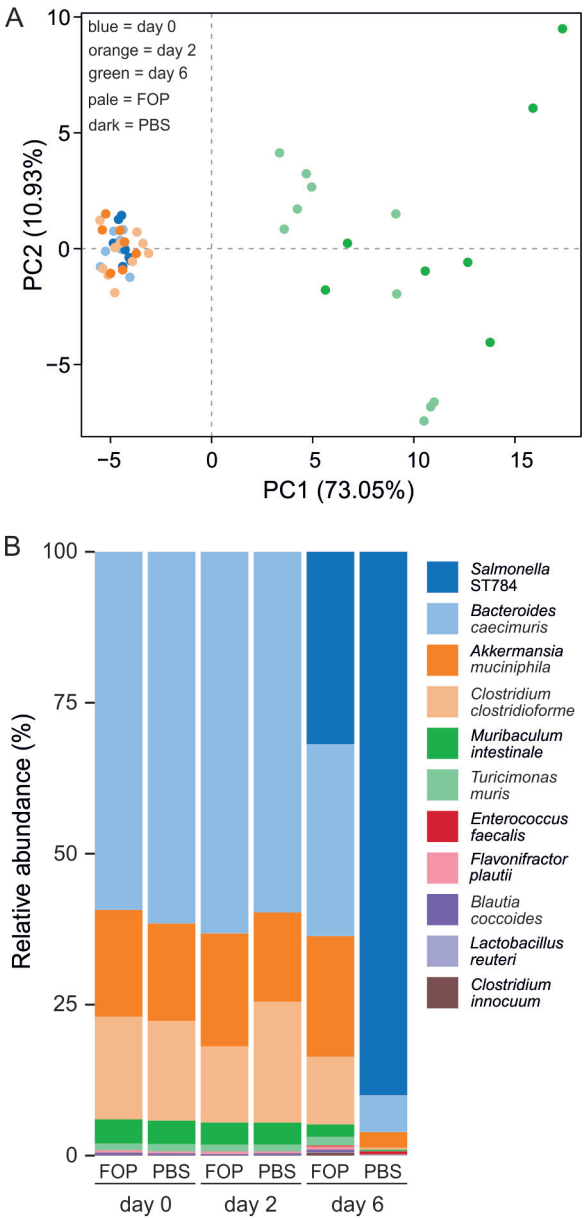

FIG 3 *Salmonella* infection disturbs the microbiota in OMM^{12} mice but FOP does not. (A) Shown is a principal-component analysis (PCA) plot of 16S rRNA gene data obtained from fecal pellets taken at days 0 (baseline), 2 (just before the ST784 challenge), and 6 (before sacrifice) from OMM^{12} mice that received FOP ($n = 10$) or PBS ($n = 7$). All animals were infected with strain ST784 on day 2 (see Fig. 2A for the experimental design). (B) The relative abundances of the ST784 challenge strain and OMM^{12} mouse origin bacteria from the fecal samples are shown. A comparison of $\log_2$-fold changes of 16S rRNA gene read abundances between days and conditions with statistical values is given in Table S3. Note that only 10 of the 12 mouse origin bacteria are detectable by either 16S rRNA gene or quantitative PCR (qPCR), as reported previously (31).

at different doses with 10-fold reductions between doses, ranging from 1×10^9 to 1×10^7 PFU (Fig. 4A). All animals received a single dose of ST784 (1×10^8 CFU) on day 2. No differences in mouse behavior or weight were observed between the three groups (Fig. 4B and Table S4). At 3 h post-*Salmonella* administration, all mice that received the lowest dose of FOP (1×10^7 PFU) had detectable levels of *Salmonella* in feces, while only one mouse in the group receiving the middle dose (1×10^8 PFU) and none receiving the highest dose (1×10^9 PFU) had detectable ST784 counts (Fig. 4C and Table S4). This indicates that the highest prophylactic dose of FOP had a stronger impact on the ST784 inoculum. During the

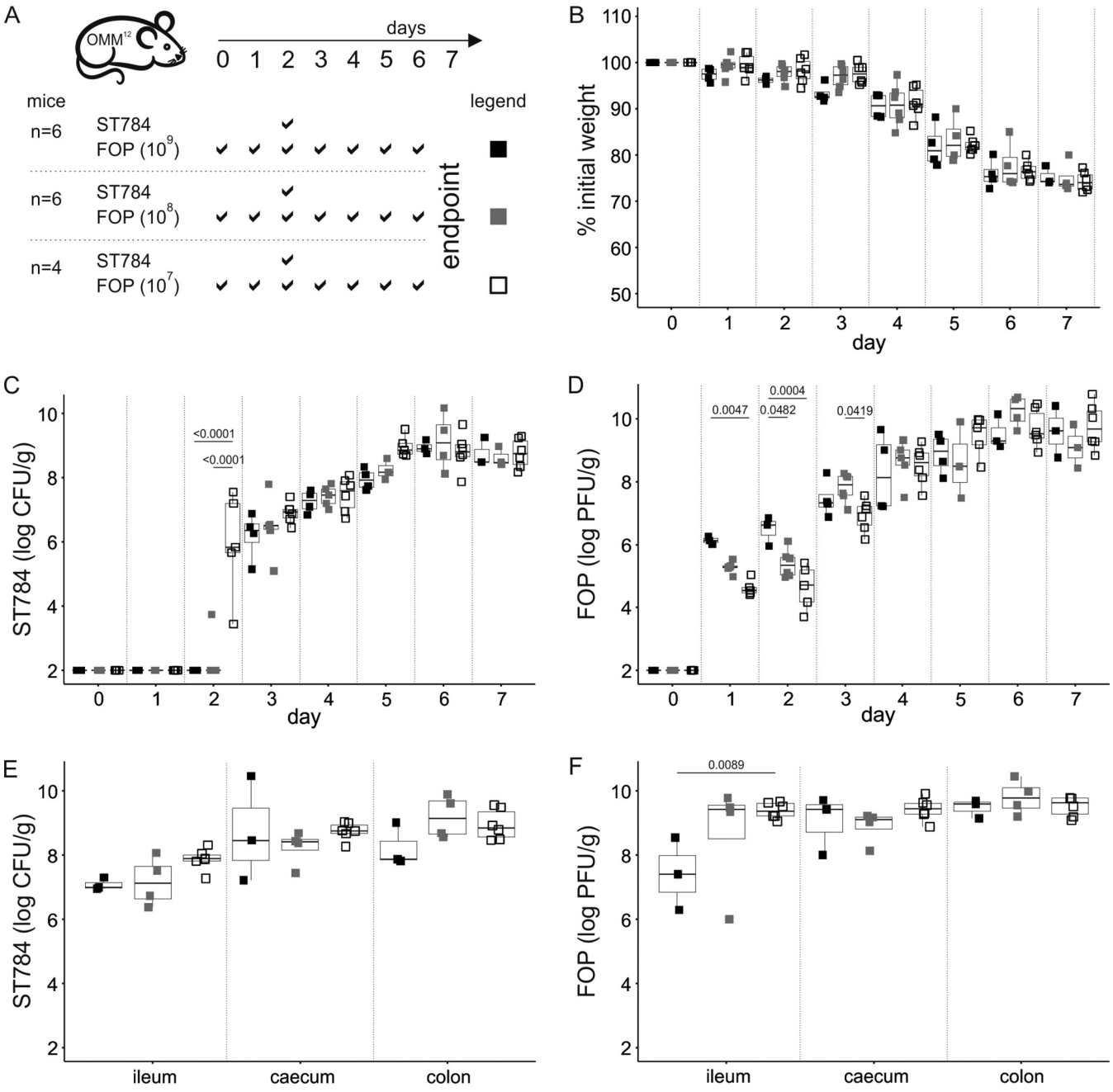

FIG 4 Dose dependence of effect of FOP on ST784 burden in OMM^{12} mice. (A) Experimental design. OMM^{12} mice ($n = 4$ to 6) were orally administered the indicated doses of FOP (10^7 PFU, white squares; 10^8 PFU, gray squares; 10^9 PFU, black squares) on the indicated days. On day 2, all mice were challenged with strain ST784 (1×10^8 CFU). (B) Mice were weighed daily. Shown are the percentages of weight loss compared to starting weights of OMM^{12} mice over time. (C and D) The amounts of ST784 (CFU) (C) and phages (PFU) (D) in OMM^{12} mouse feces were quantitated daily (day 2 corresponds to 3 h after ST784 challenge). (E and F) Intestinal organs were collected on day 6, and the amounts of ST784 (CFU) (E) and phages (PFU) quantitated. Statistical analyses are described in Materials and Methods and reported in Table S4.

next 3 days (days 3 to 5), fecal levels of *Salmonella* rose in all three groups with no significant differences; however, the levels trended inversely proportional to the FOP dose (Fig. 4C and Table S4). During the last 2 days (days 5 and 6), *Salmonella* levels reached a median value of 10^8 CFU/g in feces and the difference between the groups vanished. Fecal levels of phages showed initial differences between the three groups on days 1 and 2 in agreement with the administered doses. Then, over the next several days, phage levels progressively increased, mirroring *Salmonella* fecal levels, with diminishing differences between the dosing groups until reaching a plateau where the median phage level was approximately 10^9 PFU/g

(Fig. 4D and Table S4). We measured *Salmonella* (Fig. 4E) and phage (Fig. 4F) levels from gut sections on day 7 (1 day later than the experiments whose results are shown in Fig. 1 and 2). No significant differences in levels of ST784 between the three gut compartments were discerned, as expected from fecal contents (Fig. 4C), while a significant difference in phage counts could only be detected in the ileum between the highest and lowest dose groups (Fig. 4F and Table S4).

DISCUSSION

Several phage products have been granted generally recognized as safe (GRAS) status by the U.S. Food and Drug Administration (FDA), which is in agreement with a large body of literature that has shown that phages are innocuous when ingested by humans (27–29). This is not surprising, given the large and diverse amount of phages already present in the human gut (10^{15}) (30). Nevertheless, the characterization of any new phage product for human applications must include information on safety as well as efficacy. Here, we evaluated the prophylactic application of FOP, a novel phage cocktail designed to target FBDs, including gut infections of *Salmonella*, which remains one of the most common causes of FBD worldwide. We attempted to mimic a real-life situation where individuals at risk, residing in the close proximity of an ongoing foodborne epidemic, would prophylactically take a phage product to lower the probability of contracting a disease. For this purpose, we used OMM^{12} mice that do not provide colonization resistance to *Salmonella* and therefore do not require antibiotic treatment (22, 23), in order to perform our study with an *in vivo* controlled-microbiota environment.

Given the expected rate of passive transit of phages in the guts of mice (31), we administered phages twice a day to maintain a high level of phages in order to maximize their impact on incoming *Salmonella* bacteria. The safety of such repetitive treatment was confirmed by the lack of any abnormal behavior or clinical symptoms, as well as the quantitation of an intestinal inflammatory marker (lipocalin-2), which remained below the threshold of inflammation. In addition, no impact on the microbiota structure was observed following 48 h of such treatment. Altogether, these data confirm that FOP is equally as safe as any of the three GRAS phage cocktails that compose it (i.e., EcoShield, ListShield, and SalmoFresh) (32).

We show that the prophylactic administration of SalmoFresh or FOP delayed the onset and lessened the most severe symptoms of *Salmonella* infection compared to the time of onset and severity of symptoms in PBS controls. Remarkably, the nearly 2-log decrease in CFU in the feces of mice that received FOP was also observed in each gut section, showing that phages can kill *Salmonella* with the same efficacy throughout the intestine. When comparing three different doses of FOP, we observed that 3 h after the ST784 challenge, the highest dose was sufficient to reduce the shedding of the inoculum to below the limit of detection. This rapid efficacy is congruent with data obtained with an *in vitro* human gut simulation model, which showed that FOP treatment killed $\geq$90% of ST784 after 5 h while simultaneously inhibiting the ability of ST784 to invade human intestinal cells (24). This strong impact on the *Salmonella* inoculum is encouraging for the prophylactic application of phages. Indeed, the *Salmonella* dose used in mice (1×10^8 CFU for a 20-g mouse) would correspond to a dose of 3.5×10^{11} CFU for a 70-kg human, which is several log higher than the infective dose for nontyphoidal salmonellosis ($<10^3$ CFU) (33, 34), as well as the most probable numbers (MPNs) of contaminating bacteria in retail settings, which are estimated to be even lower (35–37). Therefore, an FOP dose of 1×10^9 PFU would still remain several log higher than the target dose of *Salmonella*.

During all experiments, and more strikingly during the FOP dose experiments, the fecal levels of phages rose rapidly following ST784 challenge, demonstrating that orally administered FOP is actively replicating in the gut at the expense of ST784. Interestingly, during the dose experiment, within 24 h there was already no difference between the phage levels in mice that received the middle and the high doses, and within another 24 h, the phage levels resulting from the three doses were undistinguishable, while all three doses

were significantly different before the challenge. These data showed that within 48 h, a 100-fold-lower dose of FOP reached a similar density in the gut that was associated with an equivalent impact on the *Salmonella* burden.

The relative abundances of 4 of the 12 intestinal bacteria of OMM^{12} mice were altered by increased levels of ST784 *Salmonella*. However, the FOP treatment limited these variations to increased abundances of *L. reuteri* and *E. faecalis*, suggesting that these two strains benefit from the presence of *Salmonella*. These observations illustrate that the growth of a pathogen has a direct impact on microbiota structure and that a phage intervention can limit such impact. They also demonstrate that murine gnotobiotic models, despite their limitations, are suitable to study mechanisms involved in the role of the gut microbiota during infection by *Salmonella* (22) and, potentially, other intestinal pathogens.

Finally, we showed that the prophylactic administration of phage products like FOP lowers the burden of a foodborne intestinal pathogen and could represent a strategy to reduce the dissemination of FBD during an outbreak. Lowering the spread of the contamination until the identification of its source, which can last several weeks, would have direct economic impact (38). In addition, the use of phages instead of antibiotics will be beneficial to the resident microbiota and will not increase the selection for antibiotic-resistant pathogens.

MATERIALS AND METHODS

Ethics statement. All animal experiments were approved by the committee on animal experimentation at the Institut Pasteur (Paris, France) and by the French Ministry of Research. A total of 68 OMM^{12} (C57BL/6J) mice from 7 to 9 weeks old, bred at Institut Pasteur, were used.

Bacterial strains and phage products. *S. enterica* subsp. *enterica* serovar Typhimurium strain ST784 was obtained from Intralytix, Inc. (Columbia, MD), and routinely cultured in lysogeny broth (LB), on LB agar, or on Drigalski agar (Bio-Rad, Hercules, CA) at 37°C. For oral administration of ST784, an overnight liquid culture in LB was diluted 1/10 in sucrose bicarbonate buffer (20% sucrose and 2.6% sodium bicarbonate, pH 8). SalmoFresh (25, 39) and FOP (24) phage preparations were obtained from Intralytix. SalmoFresh is a commercially available phage cocktail consisting of 6 lytic phages at approximately equivalent titers targeting *Salmonella* spp., 4 of which infect strain ST784 with similar efficiencies. The FOP phage cocktail, which includes 15 phages at approximately equivalent titers, was prepared as described previously (24). It is a combination of three previously described commercial FDA-affirmed generally recognized as safe (GRAS) phage cocktails (i.e., ListShield, EcoShield PX, and SalmoFresh) that, combined, target *Listeria monocytogenes*, *E. coli* (STEC), and *Salmonella*, respectively (24). Before use, the phage cocktails were diluted in PBS to the indicated concentrations, which were calculated from the titration of these products on strain ST784. *Salmonella*-specific-phage quantification was performed by spotting serial dilutions of fecal or intestinal-section samples on LB plates overlaid with strain ST784 (24).

Murine model. In all experiments, mice were randomly assigned to a group, and each group included approximately the same numbers of male and female animals kept in separate cages. Every day, mice were observed and weighed and feces were collected. Fecal pellets were transferred into preweighed, sterile, 2 ml tubes, weighed, and then resuspended in 1 ml of PBS. Serial dilutions in PBS were performed and plated onto Drigalski plates for *Salmonella* quantitation (CFU) and onto LB plates overlaid with ST784 for phage titration (PFU).

SalmoFresh, FOP, or PBS was administered by oral gavage in 200 μl twice daily, 6 h apart. The dose of phages administered through each gavage was 1×10^9 PFU, or lower as specified. Strain ST784 (1×10^8 CFU) was administered by oral gavage in 200 μl on day 2, 3 h after the first phage gavage on that day. Control mice not receiving ST784 received PBS instead. At the end of all experiments, mice were sacrificed by cervical dislocation, and intestinal sections (i.e., ileum, cecum, and colon) were collected without the separation of luminal and mucosal contents. These sections were homogenized in PBS using the gentleMACS OctoDissociator (Miltenyi Biotec), serially diluted in PBS, and plated on both Drigalski plates and LB plates overlaid with strain ST784.

Lipocalin-2 assay. Frozen supernatants of fecal samples resuspended in PBS were thawed before lipocalin-2 quantification using a commercial enzyme-linked immunosorbent assay (ELISA) kit (catalog number DY1857; R&D Systems) according to the manufacturer's instructions. The threshold of inflammation (5 ng/g of feces) was defined according to the method in reference 26.

16S rRNA gene analysis. Resuspended fecal samples (500 μl) were centrifuged at 8,000 $\times$ *g* for 10 min, and the supernatant removed. Pellets were resuspended in 500 μl of lysis buffer (500 mM NaCl, 50 mM Tris-HCl, pH 8.0, 50 mM EDTA, 4% sodium dodecyl sulfate) and incubated for 15 min at 50°C (40). Then, 100 μl of lysozyme (25 mg/ml) was added and samples were incubated at 37°C for 2 h. DNA extraction was performed using the Maxwell 16 tissue DNA purification kit (Promega). Amplicon libraries targeting the V3-V4 16S rRNA gene region were then constructed using Illumina primers (forward primer, 5′-TCGTCGGCAGCGTCAGATGTGTATAAGAGACAGCCTACGGGNGGCWGCAG-3′, and reverse primer, 5′-GTCTCGTGGGCTCGGAGATGTGTATAAGAGACAGGACTACHVGGGTATCTAATCC-3′) and amplified by PCR for 25 cycles. The libraries were sequenced on an Illumina MiSeq instrument (2 $\times$ 300 bp). FastQC (http://www.bioinformatics.babraham.ac.uk/projects/fastqc/) was used for the quality control of the reads. Read filtering, operational taxonomic unit (OTU) clustering,

and annotation were performed with the MASQUE pipeline (https://github.com/aghozlane/masque). All statistical analyses were performed with SHAMAN (http://shaman.c3bi.pasteur.fr) as previously described (41).

Statistical analysis. Statistical analysis on the numbers of bacteria (CFU) and phages (PFU), as well as mouse weights, were carried out using the lme4 and lmerTest packages of R (42, 43). Both CFU and PFU were $\log_{10}$ transformed prior to analysis. Given the nonlinearity of responses, the day at which a measure was performed was considered a categorical variable. Linear mixed models were used to account for random experimental effects (i.e., individuals, experiments, and cage effects). Overall effects were assessed with analysis of variance (ANOVA) and *post hoc* Tukey's comparisons and were performed using the lsmeans R package (44). A P value of <0.05 was considered statistically significant.

SUPPLEMENTAL MATERIAL

Supplemental material is available online only.

SUPPLEMENTAL FILE 1, XLSX file, 0.02 MB.

SUPPLEMENTAL FILE 2, XLSX file, 0.1 MB.

SUPPLEMENTAL FILE 3, XLSX file, 0.02 MB.

SUPPLEMENTAL FILE 4, XLSX file, 0.02 MB.

SUPPLEMENTAL FILE 5, PDF file, 0.1 MB.

ACKNOWLEDGMENTS

We thank Thierry Angélique and Eddie Maranghi, members of the Centre for Gnotobiology Platform of the Institut Pasteur, for their help with the animal work. We thank Amine Ghozlane from the Bioinformatics and Biostatistics Hub, Department of Computational Biology, Institut Pasteur, for help with 16S rRNA gene analysis. We also thank Joelle Woolston (Intralytix) for editorial contributions.

Q.L.-B. was funded by École Doctorale FIRE—Program Bettencourt. L.C. was funded by a Ph.D. fellowship from the Ministère de l'Enseignement Supérieur et de la Recherche, France, Ecole Doctorale 394. M.L. belongs to the Pasteur—Paris University (PPU) international Ph.D. program funded by Institut Carnot Pasteur Maladies Infectieuses (grant number ANR 11-CARN 017-01).

The study was funded in part by Intralytix, Inc. (Columbia, MD, USA). A.S. holds an equity stake in Intralytix, Inc., a Maryland-based corporation specializing in developing and commercializing phage-based preparations, including FOP. A.S., J.A.S., J.T.T., and R.B.P. are employees of Intralytix, Inc.

A.S., J.A.S., and L.D. designed the study. Q.L.-B., L.C., and M.L. performed experiments. Q.L.-B., L.C., J.A.S., J.T.T., and L.D. analyzed the data. J.A.S., R.B.P., and L.D. drafted the paper, and all the authors contributed to and approved the submitted version.

REFERENCES

1. Ashida H, Mimuro H, Sasakawa C. 2015. Shigella manipulates host immune responses by delivering effector proteins with specific roles. Front Immunol 6:219. https://doi.org/10.3389/fimmu.2015.00219.
2. Havelaar AH, Kirk MD, Torgerson PR, Gibb HJ, Hald T, Lake RJ, Praet N, Bellinger DC, de Silva NR, Gargouri N, Speybroeck N, Cawthorne A, Mathers C, Stein C, Angulo FJ, Devleesschauwer B, World Health Organization Foodborne Disease Burden Epidemiology Reference Group. 2015. World Health Organization global estimates and regional comparisons of the burden of foodborne disease in 2010. PLoS Med 12:e1001923. https://doi.org/10.1371/journal.pmed.1001923.
3. Vugia DJ, Samuel M, Farley MM, Marcus R, Shiferaw B, Shallow S, Smith K, Angulo FJ, Emerging Infections Program FoodNet Working Group. 2004. Invasive *Salmonella* infections in the United States, FoodNet, 1996–1999: incidence, serotype distribution, and outcome. Clin Infect Dis 38(Suppl 3): S149–S156. https://doi.org/10.1086/381581.
4. Centers for Disease Control and Prevention. 2010. Preliminary FoodNet data on the incidence of infection with pathogens transmitted commonly through food—10 states, 2009. MMWR Morb Mortal Wkly Rep 59:418–422.
5. Greig J, Rajić A, Young I, Mascarenhas M, Waddell L, LeJeune J. 2015. A scoping review of the role of wildlife in the transmission of bacterial pathogens and antimicrobial resistance to the food chain. Zoonoses Public Health 62:269–284. https://doi.org/10.1111/zph.12147.
6. Levantesi C, Bonadonna L, Briancesco R, Grohmann E, Toze S, Tandoi V. 2012. *Salmonella* in surface and drinking water: occurrence and water-mediated transmission. Food Res Int 45:587–602. https://doi.org/10.1016/j.foodres.2011.06.037.
7. Havelaar AH, Garssen J, Takumi K, Koedam MA, Dufrenne JB, Van Leusden FM, De La Fonteyne L, Bousema JT, Vos JG. 2001. A rat model for dose–response relationships of *Salmonella* Enteritidis infection. J Appl Microbiol 91:442–452. https://doi.org/10.1046/j.1365-2672.2001.01399.x.
8. Scallan E, Fitzgerald M, Collins C, Crowley D, Daly L, Devine M, Igoe D, Quigley T, Robinson T, Smyth B. 2004. Acute gastroenteritis in northern Ireland and the Republic of Ireland: a telephone survey. Commun Dis Public Health 7: 61–67.
9. Asperilla MO, Smego RA, Scott LK. 1990. Quinolone antibiotics in the treatment of *Salmonella* infections. Rev Infect Dis 12:873–889. https://doi.org/10.1093/clinids/12.5.873.
10. Bartlett JG. 1992. Antibiotic-associated diarrhea. Clin Infect Dis 15: 573–581. https://doi.org/10.1093/clind/15.4.573.
11. Francino MP. 2016. Antibiotics and the human gut microbiome: dysbioses and accumulation of resistances. Front Microbiol 6:1543. https://doi.org/10.3389/fmicb.2015.01543.
12. Huddleston JR. 2014. Horizontal gene transfer in the human gastrointestinal tract: potential spread of antibiotic resistance genes. Infect Drug Resist 7:167–176. https://doi.org/10.2147/IDR.S48820.
13. Laxminarayan R, Duse A, Wattal C, Zaidi AKM, Wertheim HFL, Sumpradit N, Vlieghe E, Hara GL, Gould IM, Goossens H, Greko C, So AD, Bigdeli M, Tomson G, Woodhouse W, Ombaka E, Peralta AQ, Qamar FN, Mir F, Kariuki S, Bhutta

ZA, Coates A, Bergstrom R, Wright GD, Brown ED, Cars O. 2013. Antibiotic resistance—the need for global solutions. Lancet Infect Dis 13:1057–1098. https://doi.org/10.1016/S1473-3099(13)70318-9.
14. Ghosh C, Sarkar P, Issa R, Haldar J. 2019. Alternatives to conventional antibiotics in the era of antimicrobial resistance. Trends Microbiol 27:323–338. https://doi.org/10.1016/j.tim.2018.12.010.
15. Lu TK, Koeris MS. 2011. The next generation of bacteriophage therapy. Curr Opin Microbiol 14:524–531. https://doi.org/10.1016/j.mib.2011.07.028.
16. Merril CR, Scholl D, Adhya SL. 2003. The prospect for bacteriophage therapy in Western medicine. Nat Rev Drug Discov 2:489–497. https://doi.org/10.1038/nrd1111.
17. Sulakvelidze A, Alavidze Z, Morris JG, Jr. 2001. Bacteriophage therapy. Antimicrob Agents Chemother 45:649–659. https://doi.org/10.1128/AAC.45.3.649-659.2001.
18. Chanishvili N. 2012. Phage therapy–history from Twort and d'Herelle through Soviet experience to current approaches. Adv Virus Res 83:3–40. https://doi.org/10.1016/B978-0-12-394438-2.00001-3.
19. Kortright KE, Chan BK, Koff JL, Turner PE. 2019. Phage therapy: a renewed approach to combat antibiotic-resistant bacteria. Cell Host Microbe 25:219–232. https://doi.org/10.1016/j.chom.2019.01.014.
20. Aslam S, Lampley E, Wooten D, Karris M, Benson C, Strathdee S, Schooley RT. 2020. Lessons learned from the first 10 consecutive cases of intravenous bacteriophage therapy to treat multidrug-resistant bacterial infections at a single center in the United States. Open Forum Infect Dis 7:ofaa389. https://doi.org/10.1093/ofid/ofaa389.
21. Djebara S, Maussen C, De Vos D, Merabishvili M, Damanet B, Pang KW, De Leenheer P, Strachinaru I, Soentjens P, Pirnay JP. 2019. Processing phage therapy requests in a Brussels military hospital: lessons identified. Viruses 11:265. https://doi.org/10.3390/v11030265.
22. Brugiroux S, Beutler M, Pfann C, Garzetti D, Ruscheweyh HJ, Ring D, Diehl M, Herp S, Lötscher Y, Hussain S, Bunk B, Pukall R, Huson DH, Münch PC, McHardy AC, McCoy KD, Macpherson AJ, Loy A, Clavel T, Berry D, Stecher B. 2016. Genome-guided design of a defined mouse microbiota that confers colonization resistance against *Salmonella enterica* serovar Typhimurium. Nat Microbiol 2:16215. https://doi.org/10.1038/nmicrobiol.2016.215.
23. Herp S, Brugiroux S, Garzetti D, Ring D, Jochum LM, Beutler M, Eberl C, Hussain S, Walter S, Gerlach RG, Ruscheweyh HJ, Huson D, Sellin ME, Slack E, Hanson B, Loy A, Baines JF, Rausch P, Basic M, Bleich A, Berry D, Stecher B. 2019. Mucispirillum schaedleri antagonizes Salmonella virulence to protect mice against colitis. Cell Host Microbe 25:681–694.e688. https://doi.org/10.1016/j.chom.2019.03.004.
24. Moye ZD, Woolston J, Abbeele PVD, Duysburgh C, Verstrepen L, Das CR, Marzorati M, Sulakvelidze A. 2019. A bacteriophage cocktail eliminates *Salmonella Typhimurium* from the human colonic microbiome while preserving cytokine signaling and preventing attachment to and invasion of human cells by *Salmonella* in vitro. J Food Prot 82:1336–1349. https://doi.org/10.4315/0362-028X.JFP-18-587.
25. Woolston J, Parks AR, Abuladze T, Anderson B, Li M, Carter C, Hanna LF, Heyse S, Charbonneau D, Sulakvelidze A. 2013. Bacteriophages lytic for *Salmonella* rapidly reduce *Salmonella* contamination on glass and stainless steel surfaces. Bacteriophage 3:e25697. https://doi.org/10.4161/bact.25697.
26. Chassaing B, Srinivasan G, Delgado MA, Young AN, Gewirtz AT, Vijay-Kumar M. 2012. Fecal lipocalin 2, a sensitive and broadly dynamic non-invasive biomarker for intestinal inflammation. PLoS One 7:e44328. https://doi.org/10.1371/journal.pone.0044328.
27. Sarker SA, Brüssow H. 2016. From bench to bed and back again: phage therapy of childhood *Escherichia coli* diarrhea. Ann N Y Acad Sci 1372:42–52. https://doi.org/10.1111/nyas.13087.
28. Vandenheuvel D, Lavigne R, Brüssow H. 2015. Bacteriophage therapy: advances in formulation strategies and human clinical trials. Annu Rev Virol 2:599–618. https://doi.org/10.1146/annurev-virology-100114-054915.
29. Weiss M, Denou E, Bruttin A, Serra-Moreno R, Dillmann ML, Brüssow H. 2009. In vivo replication of T4 and T7 bacteriophages in germ-free mice colonized with Escherichia coli. Virology 393:16–23. https://doi.org/10.1016/j.virol.2009.07.020.
30. Dalmasso M, Hill C, Ross RP. 2014. Exploiting gut bacteriophages for human health. Trends Microbiol 22:399–405. https://doi.org/10.1016/j.tim.2014.02.010.
31. Lourenço M, Chaffringeon L, Lamy-Besnier Q, Pédron T, Campagne P, Eberl C, Bérard M, Stecher B, Debarbieux L, De Sordi L. 2020. The spatial heterogeneity of the gut limits predation and fosters coexistence of bacteria and bacteriophages. Cell Host Microbe 28:390–401.e395. https://doi.org/10.1016/j.chom.2020.06.002.
32. Dissanayake U, Ukhanova M, Moye ZD, Sulakvelidze A, Mai V. 2019. Bacteriophages reduce pathogenic *Escherichia coli* counts in mice without distorting gut microbiota. Front Microbiol 10:1984. https://doi.org/10.3389/fmicb.2019.01984.
33. Ryan KJ, Ray CG, Sherris JC. 2004. Sherris medical microbiology: an introduction to infectious disease, 4th ed, McGraw-Hill, New York, NY.
34. Bronze MS, Greenfield RA (ed). 2005. Biodefense: principles and pathogens. Horizon Bioscience, Wymondham, Norfolk, England.
35. Boughton C, Leonard FC, Egan J, Kelly G, O'Mahony P, Markey BK, Griffin M. 2004. Prevalence and number of Salmonella in Irish retail pork sausages. J Food Prot 67:1834–1839. https://doi.org/10.4315/0362-028x-67.9.1834.
36. Dufrenne J, Ritmeester W, Delfgou-van Asch E, van Leusden F, de Jonge R. 2001. Quantification of the contamination of chicken and chicken products in The Netherlands with Salmonella and Campylobacter. J Food Prot 64:538–541. https://doi.org/10.4315/0362-028X-64.4.538.
37. Fegan N, Vanderlinde P, Higgs G, Desmarchelier P. 2004. Quantification and prevalence of Salmonella in beef cattle presenting at slaughter. J Appl Microbiol 97:892–898. https://doi.org/10.1111/j.1365-2672.2004.02380.x.
38. Van Duynhoven YT, Isken LD, Borgen K, Besselse M, Soethoudt K, Haitsma O, Mulder B, Notermans DW, De Jonge R, Kock P, Van Pelt W, Stenvers O, Van Steenbergen J, Outbreak Investigation Team. 2009. A prolonged outbreak of Salmonella Typhimurium infection related to an uncommon vehicle: hard cheese made from raw milk. Epidemiol Infect 137:1548–1557. https://doi.org/10.1017/S0950268809002337.
39. Moye ZD, Woolston J, Sulakvelidze A. 2018. Bacteriophage applications for food production and processing. Viruses 10:205. https://doi.org/10.3390/v10040205.
40. Yu Z, Morrison M. 2004. Improved extraction of PCR-quality community DNA from digesta and fecal samples. Biotechniques 36:808–812. https://doi.org/10.2144/04365ST04.
41. Volant S, Lechat P, Woringer P, Motreff L, Campagne P, Malabat C, Kennedy S, Ghozlane A. 2020. SHAMAN: a user-friendly website for metataxonomic analysis from raw reads to statistical analysis. BMC Bioinformatics 21:345. https://doi.org/10.1186/s12859-020-03666-4.
42. Bates D, Mächler M, Bolker B, Walker S. 2015. Fitting linear mixed-effects models using lme4. J Stat Softw 67:1–48. https://doi.org/10.18637/jss.v067.i01.
43. Kuznetsova A, Brockhoff PB, Christensen RHB. 2017. lmerTest package: tests in linear mixed effects models. J Stat Softw 82:1–26. https://doi.org/10.18637/jss.v082.i13.
44. Lenth RV. 2016. Least-squares means: the R package lsmeans. J Stat Softw 69:1–33. https://doi.org/10.18637/jss.v069.i01.

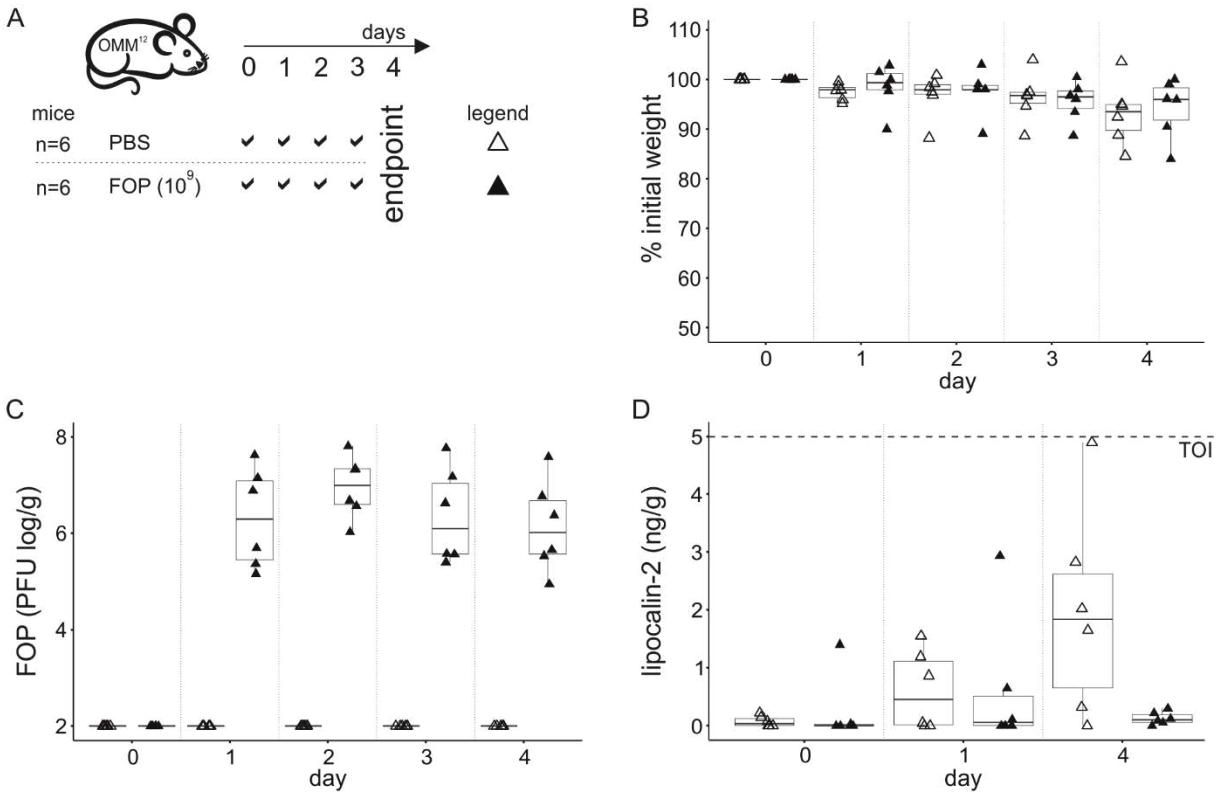

Figure S1. Repeated administration of FOP to OMM^{12} mice is safe

A. Experimental design. OMM^{12} mice (n = 6) were orally administered FOP (10^9 PFU), black triangles) or PBS (white triangles) on the indicated days. **B.** Mice were weighed daily. Shown is the percentage of weight loss compared to starting weight of OMM^{12} mice over time. **C.** The amount of phage in OMM^{12} mice feces were quantitated daily. Shown are the PFU counts in OMM^{12} mice that received the indicated doses of FOP. **D.** Fecal lipocalin-2 was quantitated (ng/g) over time. The horizontal dash line represents the threshold of inflammation (TOI) as defined in (26)**.**

Table S1. Statistical analysis of data obtained during the evaluation of SalmoFresh (related to Figure 1)

This Excel file includes 3 data sheets related to the statistical tests shown in Figure 1

Statistical analysis of the weight as a function of time (day), exposure to SalmoFresh and colonization by ST784 (related to Figure 1B)

Analysis of Deviance Table (Type II Wald chisquare tests)

day: testing difference between the different days
phage: effect of the phage exposure

Response: scale(log10(CFU.g))

	Chisq	Df	Pr(>Chisq)	
day	331.162	5	< 2.2e-16	***
Phage/ST784 administration	36.933	2	9.554e-09	***
day:phage	139.431	10	< 2.2e-16	***

Post-hoc tests: Comparison between "phage" and "no phage" at the different time points

group # 1 PBS + ST784
group # 2 SalmoFresh + ST784
group # 3 SalmoFresh + PBS

	contrast	estimate	SE	df	t.ratio	p.value
Day=1	1-2	0.143	2.48	43.8	0.058	0.9982
	1-3	-3.609	2.58	43.8	-1.399	0.3501
	2-3	-3.752	2.33	43.8	-1.612	0.2515
Day=2	1-2	1.407	2.48	43.8	0.567	0.8383
	1-3	2.338	2.58	43.8	0.907	0.6390
	2-3	0.932	2.33	43.8	0.400	0.9157
Day=3	1-2	-2.513	2.48	43.8	-1.012	0.5730
	1-3	-3.777	2.58	43.8	-1.464	0.3177
	2-3	-1.264	2.33	43.8	-0.543	0.8505
Day=4	1-2	-2.475	2.48	43.8	-0.997	0.5825
	1-3	-11.305	2.58	43.8	-4.383	0.0002
	2-3	-8.830	2.33	43.8	-3.793	0.0013
Day=5	1-2	-2.803	2.48	43.8	-1.130	0.5012
	1-3	-18.127	2.58	43.8	-7.029	<.0001
	2-3	-15.324	2.33	43.8	-6.583	<.0001
Day=6	1-2	-4.255	2.48	43.8	-1.715	0.2112
	1-3	-23.457	2.58	43.8	-9.096	<.0001
	2-3	-19.202	2.33	43.8	-8.248	<.0001

Weight (% of initial weight) as a function of time (day), exposure to phages and colonization by ST784
Random effects include individual IDs, as well as the cage in which they were reared. Overall analysis of variance (ANOVA)

The post-hoc Tukey comparisons displayed below were performed between mice exposed to phage and not exposed and

Statistical analysis of the abundance of strain ST784 in feces as a function of time (day) and exposure to SalmoFresh (related to Figure 1C)

Analysis of Deviance Table (Type II Wald chisquare tests)

day: testing difference between the different days
phage: effect of the phage exposure

Response: scale(log10(CFU.g))

	Chisq	Df	Pr(>Chisq)	
day	103.651	4	2.2e-16	***
phage	15.866	1	6.799e-05	***
day:phage	12.319	4	0.01513	*

Post-hoc tests: Comparison between "phage" and "no phage" at the different time points

	contrast	estimate	SE	df	t.ratio	p.value
Day=2	no phage \ 1.631		0.328	22.3	4.966	0.0001
Day=3	no phage \ 0.457		0.328	22.3	1.392	0.1776
Day=4	no phage \ 0.332		0.343	25.8	0.970	0.3411
Day=5	no phage \ 0.419		0.346	24.3	1.211	0.2374
Day=6	no phage \ 0.304		0.388	28.7	0.782	0.4407

Bacterial abundance (CFU) as a function of time (day) and exposure to phages.
Random effects include individual IDs, as well as the cage in which they were reared. Overall analysis of variance (ANOVA) reveals significant effects of day (p< 2.2e-16), phage (p=6.799e-05) and their interaction (p=0.01513).

The post-hoc Tukey comparisons displayed below were performed between mice exposed to phage and not exposed within each day.

Statistical analysis of the abundance of phage in feces as a function of time (day) and colonization by ST784 (related to Figure 1D)

Analysis of Deviance Table (Type II Wald chisquare tests)

day: testing difference between the different days
phage: effect of the phage exposure

Response: scale(log10(CFU.g))

	Chisq	Df	Pr(>Chisq)	
day	63.464	5	2.333e-12	***
ST784 level	105.657	1	< 2.2e-16	***
day:phage	70.603	5	7.676e-14	***

Post-hoc tests: Comparison between "Bacteria" and "no bacteria" at the different time points

	contrast	estimate	SE	df	t.ratio	p.value
Day=1	Bacteria vs -0.1963		0.281	50	-0.699	0.4876
Day=2	Bacteria vs -0.0201		0.301	50	-0.067	0.9470
Day=3	Bacteria vs 1.6490		0.301	50	5.484	<.0001
Day=4	Bacteria vs 1.4531		0.281	50	5.178	<.0001
Day=5	Bacteria vs 2.1354		0.294	50	7.259	<.0001
Day=6	Bacteria vs 2.3722		0.294	50	8.064	<.0001

Phage abundance (PFU) as a function of time (day) and the coloniszation by ST784.
Random effects include individual IDs, experiments, as well as the cage in which they were reared.
Overall analysis of variance (ANOVA) reveals significant effects of day (p=2.333e-12), the ST784 colonization (p< 2.2e-16) and their interaction (p=7.676e-14).

The post-hoc Tukey comparisons displayed below were performed between mice colonized with ST784 and not colonized within each day.

Statistical analysis of the abundance of strain ST784 in intestinal sections with SalmoFresh (related to Figure 1 E)

Analysis of Deviance Table (Type II Wald chisquare tests)

day: testing difference between the different days
phage: effect of the phage exposure

Response: scale(log10(CFU.g))

	Chisq	Df	Pr(>Chisq)	
day	37.6828	2	6.566e-09	***
phage	68.3591	1	< 2.2e-16	***
day:phage	2.0798	2	0.3535	

Post-hoc tests — Comparison between "phage" and "no phage" at the different time points

	contrast	estimate	SE	df	t.ratio	p.value
Ileum	no phage \ 1.42		0.299	13.3	4.753	0.0004
Caecum	no phage \ 1.08		0.299	13.3	3.604	0.0031
Colon	no phage \ 1.67		0.299	13.3	5.581	0.0001

Bacterial abundance (CFU) as a function of gut section and exposure to phages.
Random effects include individual IDs, as well as the cage in which they were reared.
Overall analysis of variance (ANOVA) reveals significant effects of *gut section* (p=6.566e-09), *phage* (p=< 2.2e-16) but not of their *interaction* (p=0.3535).

The post-hoc Tukey comparisons displayed below were performed between the mice exposed to phage and not exposed within each section.

Statistical analysis of the abundance of phage in intestinal sections with ST784 (related to Figure 1F)

Analysis of Deviance Table (Type II Wald chisquare tests)

day: testing difference between the different days
phage: effect of the phage exposure

Response: scale(log10(CFU.g))

	Chisq	Df	Pr(>Chisq)	
day	48.194	2	3.426e-11	***
ST784 level	588.053	1	< 2.2e-16	***
day:phage	158.216	2	< 2.2e-16	***

Post-hoc tests — Comparison between "Bacteria" and "no bacteria" at the different time points

	contrast	estimate	SE	df	t.ratio	p.value
Ileum	Bacteria vs 1.92		0.102	22.8	18.716	<.0001
Caecum	Bacteria vs 1.02		0.102	22.8	9.913	<.0001
Colon	Bacteria vs 2.53		0.102	22.8	24.654	<.0001

Phage abundance (PFU) as a function of gut section and the presence of ST784.
Random effects include individual IDs, as well as the cage in which they were reared.
Overall analysis of variance (ANOVA) reveals significant effects of *gut section* (p=3.426e-11), the ST784 colonization (p=< 2.2e-16) and their *interaction* (p< 2.2e-16).

The post-hoc Tukey comparisons displayed below were performed between the mice colonized with ST784 and not colonized within each section.

Table S2. Statistical analysis of data obtained during the evaluation of FOP (related to Figure 2)

This Excel file includes 3 data sheets related to the statistical tests shown in Figure 2

Statistical analysis of the weight as a function of time (day) and exposure to FOP (related to Figure 2B)

Analysis of Deviance Table (Type II Wald chisquare tests)

day: testing difference between the different days
phage: effect of the phage exposure

Response: scale(log10(CFU.g))

	Chisq	Df	Pr(>Chisq)	
day	481.4459	5	<2.2e-16	***
phage	6.8987	1	0.008626	**
day:phage	28.0246	5	3.6e-05	***

Post-hoc tests — Comparison between "phage" and "no phage" at the different time points

	contrast	estimate	SE	df	t.ratio	p.value
Day=1	no phage \ -0.1006		0.246	14.1	-0.408	0.6891
Day=2	no phage \ -0.2722		0.246	14.1	-1.106	0.2874
Day=3	no phage \ 0.0414		0.246	14.1	0.168	0.8689
Day=4	no phage \ -0.9863		0.246	14.1	-4.006	0.0013
Day=5	no phage \ -0.7151		0.246	14.1	-2.905	0.0115
Day=6	no phage \ -0.7853		0.246	14.1	-3.190	0.0065

Weight (% of initial weight) as a function of time (day) and exposure to phages.
Random effects include individual IDs, experiments, as well as the cage in which they were reared. Overall analysis of variance (ANOVA) reveals significant effects of day (p< 2.2e-16), phage (p=0.008626) but not of their interaction (p=3.6e-05).

The post-hoc Tukey comparisons displayed below were performed between mice exposed to phage and not exposed within each day.

Statistical analysis of the abundance of strain ST784 in feces as a function of time (day) and exposure to FOP (related to Figure 2C)

Analysis of Deviance Table (Type II Wald chisquare tests)

day: testing difference between the different days
phage: effect of the phage exposure

Response: scale(log10(CFU.g))

	Chisq	Df	Pr(>Chisq)	
day	410.0303	4	< 2.2e-16	***
phage	84.4760	1	< 2.2e-16	***
day:phage	3.1808	4	0.528	

Post-hoc tests — Comparison between "phage" and "no phage" at the different time points

	contrast	estimate	SE	df	t.ratio	p.value
Day=2	no phage \	0.632	0.199	59.2	3.171	0.0024
Day=3	no phage \	0.874	0.181	55.5	4.822	<.0001
Day=4	no phage \	0.889	0.187	58.7	4.749	<.0001
Day=5	no phage \	0.822	0.181	55.5	4.535	<.0001
Day=6	no phage \	0.519	0.186	55.7	2.786	0.0073

Bacterial abundance (CFU) as a function of time (day) and exposure to phages.
Random effects include individual IDs, experiments, as well as the cage in which they were reared.
Overall analysis of variance (ANOVA) reveals significant effects of day (p< 2.2e-16), phage (p<2.2e-16) but not of their interaction (p=0.528).

The post-hoc Tukey comparisons displayed below were performed between mice exposed to phage and not exposed within each day.

Statistical analysis of the abundance of strain ST784 in intestinal sections with FOP (related to Figure 2E)

Analysis of Deviance Table (Type II Wald chisquare tests)

day: testing difference between the different days
phage: effect of the phage exposure

Response: scale(log10(CFU.g))

	Chisq	Df	Pr(>Chisq)	
day	43.2895	2	3.979e-10	***
phage	20.4129	1	6.241e-06	***
day:phage	2.0188	2	0.3644	

Post-hoc tests: Comparison between "phage" and "no phage" at the different time points

	contrast	estimate	SE	df	t.ratio	p.value
Ileum	no phage - phage	1.393	0.356	5.99	3.910	0.0079
Caecum	no phage - phage	0.872	0.356	5.99	2.447	0.0500
Colon	no phage - phage	1.344	0.356	5.99	3.774	0.0093

Bacterial abundance (CFU) as a function of gut section and exposure to phages.
Random effects include individual IDs, as well as the cage in which they were reared.
Overall analysis of variance (ANOVA) reveals significant effects of *gut section* (p=3.979e-10), *phage* (p=6.241e-06) but not of their *interaction* (p=0.3644).

The post-hoc Tukey comparisons displayed below were performed between the mice exposed to phage and not exposed within each section.

Table S3. Variations of 16S reads abundance for each strain in the indicated comparisons (log2 fold change and associated p-values)

green: significantly (p-value < 0.05) more abundant strains (log2FC>2)
red: significantly (p-value < 0.05) less abundant strains (log2FC<-2)

PBS vs. FOP

Day 0

	log2FoldChan	pvalue_adjusted
Salmonella ST784	0.6	0.977
Bacteroides caecimuris	0.2	0.977
Akkermansia muciniphila	0.0	0.977
Clostridium clostridioforme	0.0	0.977
Muribaculum intestinale	0.1	0.977
Clostridium innocuum	-0.2	0.977
Flavonifractor plautii	-0.2	0.977
Turicimonas muris	0.2	0.977
Blautia coccoides	-0.2	0.977
Lactobacillus reuteri	0.0	0.977
Enterococcus faecalis	2.1	0.499

Day 2

	log2FoldChan	pvalue_adjusted
Salmonella ST784	0.1	0.975
Bacteroides caecimuris	0.1	0.975
Akkermansia muciniphila	-0.2	0.975
Clostridium clostridioforme	0.8	0.975
Muribaculum intestinale	0.2	0.975
Clostridium innocuum	-0.1	0.975
Flavonifractor plautii	0.0	0.975
Turicimonas muris	0.1	0.975
Blautia coccoides	0.2	0.975
Lactobacillus reuteri	0.2	0.975
Enterococcus faecalis	-0.3	0.975

Day 6 vs. Day 0

PBS

	log2FoldChan	pvalue_adjusted
Salmonella ST784	16.9	5.13E-96
Bacteroides caecimuris	-0.9	0.103
Akkermansia muciniphila	-0.2	0.673
Clostridium clostridioforme	-3.3	3.85E-06
Muribaculum intestinale	-2.2	0.002
Clostridium innocuum	0.3	0.673
Flavonifractor plautii	-0.5	0.363
Turicimonas muris	-1.7	0.008
Blautia coccoides	-1.2	0.103
Lactobacillus reuteri	6.8	8.54E-17
Enterococcus faecalis	8.8	2.75E-25

FOP

	log2FoldChan	pvalue_adjusted
Salmonella ST784	13.3	2.01E-65
Bacteroides caecimuris	-1.2	0.023
Akkermansia muciniphila	-0.2	0.854
Clostridium clostridioforme	-1.0	0.162
Muribaculum intestinale	-1.3	0.034
Clostridium innocuum	2.0	3.35E-05
Flavonifractor plautii	-0.1	0.918
Turicimonas muris	-0.1	0.918
Blautia coccoides	-0.1	0.918
Lactobacillus reuteri	3.1	4.32E-05
Enterococcus faecalis	6.6	1.76E-12

Day 6

	log2FoldChan	pvalue_adjusted
Salmonella ST784	4.2	1.24E-08
Bacteroides caecimuris	0.5	0.381
Akkermansia muciniphila	-0.1	0.874
Clostridium clostridioforme	-2.3	0.001
Muribaculum intestinale	-0.8	0.214
Clostridium innocuum	-1.9	0.001
Flavonifractor plautii	-0.6	0.209
Turicimonas muris	-1.5	0.019
Blautia coccoides	-1.3	0.066
Lactobacillus reuteri	3.7	8.69E-07
Enterococcus faecalis	4.3	2.60E-08

Day 2 vs. Day 0

PBS

	log2FoldChan	pvalue_adjusted
Salmonella ST	0.7	0.932
Bacteroides caec	0.1	0.932
Akkermansia muc	0.1	0.932
Clostridium clostric	-0.4	0.932
Muribaculum inte	-0.1	0.932
Clostridium innc	-0.4	0.932
Flavonifractor p	-0.1	0.932
Turicimonas m	0.0	0.998
Blautia coccoi	-0.5	0.932
Lactobacillus re	0.1	0.932
Enterococcus fa	1.1	0.932

FOP

	log2FoldChan	pvalue_adjusted
Salmonella ST	0.7	0.932
Bacteroides caec	0.1	0.932
Akkermansia muc	0.1	0.932
Clostridium clostric	-0.4	0.932
Muribaculum inte	-0.1	0.932
Clostridium innc	-0.4	0.932
Flavonifractor p	-0.1	0.932
Turicimonas m	0.0	0.998
Blautia coccoi	-0.5	0.932
Lactobacillus re	0.1	0.932
Enterococcus fa	1.1	0.932

Day 6 vs. Day 2

PBS

	log2FoldChan	pvalue_adjusted
Salmonella ST	16.7	6.98E-81
Bacteroides caec	-1.0	0.104
Akkermansia muc	-0.2	0.729
Clostridium clostric	-3.7	2.92E-07
Muribaculum inte	-2.1	0.003
Clostridium innc	0.5	0.398
Flavonifractor p	-0.5	0.347
Turicimonas m	-1.7	0.015
Blautia coccoi	-1.2	0.118
Lactobacillus re	6.5	1.28E-14
Enterococcus fa	10.1	1.86E-23

FOP

	log2FoldChan	pvalue_adjusted
Salmonella ST	12.7	5.43E-62
Bacteroides caec	-1.3	0.010
Akkermansia muc	-0.3	0.643
Clostridium clostric	-0.6	0.492
Muribaculum inte	-1.2	0.049
Clostridium innc	2.3	6.43E-07
Flavonifractor p	0.1	0.837
Turicimonas m	-0.1	0.837
Blautia coccoi	0.4	0.643
Lactobacillus re	3.0	9.91E-05
Enterococcus fa	5.5	1.88E-10

Table S4. Statistical analysis of data obtained during the evaluation of three doses of FOP (related to Figure 4)

This Excel file includes 3 data sheets related to the statistical tests shown in Figure 4

Statistical analysis of the weight as a function of time (day) and exposure to FOP dilutions (related to Figure 4B)

Analysis of Deviance Table (Type II Wald chisquare tests)

day: testing difference between the different days

phage: effect of the phage exposure

Response:	scale(log10(CFU.g))			
	Chisq	Df	Pr(>Chisq)	
day	2557.2026	6	<2e-16	***
phage dilutions	1.1293	2	0.5685	
day:phage	11.9863	12	0.4468	

Post-hoc tests — Comparison between "phage" and "no phage" at the different time points

	contrast	estimate	SE	df	t.ratio	p.value
Day=1	FOP	-0.2052	0.199	7.14	-1.029	0.5830
	FOP/10	-0.2220	0.204	6.70	-1.087	0.5523
	FOP/100	-0.0168	0.186	4.52	-0.090	0.9955
Day=2	FOP	-0.1644	0.199	7.14	-0.825	0.7006
	FOP/10	-0.2165	0.204	6.70	-1.060	0.5673
	FOP/100	-0.0520	0.186	4.52	-0.280	0.9582
Day=3	FOP	-0.3828	0.199	7.14	-1.920	0.2017
	FOP/10	-0.4430	0.204	6.70	-2.169	0.1480
	FOP/100	-0.0602	0.186	4.52	-0.324	0.9446
Day=4	FOP	-0.0237	0.199	7.14	-0.119	0.9923
	FOP/10	-0.0886	0.204	6.70	-0.434	0.9029
	FOP/100	-0.0650	0.186	4.52	-0.349	0.9359
Day=5	FOP	-0.1295	0.208	8.45	-0.621	0.8127
	FOP/10	-0.0238	0.204	6.70	-0.117	0.9925
	FOP/100	0.1056	0.196	5.54	0.540	0.8555
Day=6	FOP	-0.1881	0.208	8.45	-0.903	0.6530
	FOP/10	-0.0752	0.204	6.70	-0.368	0.9288
	FOP/100	0.1130	0.196	5.54	0.577	0.8371
Day=7	FOP	-0.0227	0.217	9.76	-0.105	0.9939
	FOP/10	0.0409	0.213	7.85	0.192	0.9799
	FOP/100	0.0636	0.196	5.54	0.325	0.9440

Weight (% of initial weight) as a function of time (day) and exposure to diffrent phage dilutions.

Random effects include individual IDs, as well as the cage in which they were reared.

Overall analysis of variance (ANOVA) reveals significant effects of day (p< 2.2e-16) but not of phage dilutions (p=0.5685) and their interaction (p=0.4468).

The post-hoc Tukey comparisons displayed below were performed between mice exposed to phage and not exposed within each day.

Statistical analysis of the abundance of strain ST784 in feces as a function of time (day) and exposure to FOP dilutions (related to Figure 4C)

Analysis of Deviance Table (Type II Wald chisquare tests)

day: testing difference between the different days

phage: effect of the phage exposure

Response:	scale(log10(CFU.g))			
	Chisq	Df	Pr(>Chisq)	
day	678.522	5	< 2.2e-16	***
phage dilution	43.963	2	2.842e-10	***
day:phage	133.812	10	< 2.2e-16	***

Post-hoc tests — Comparison between "phage" and "no phage" at the different time points

	contrast	estimate	SE	df	t.ratio	p.value
Day=2	FOP	-0.23923	0.208	46.5	-1.150	0.4887
	FOP/10	-2.27317	0.216	48.0	-10.518	<.0001
	FOP/100	-2.03394	0.178	35.8	-11.417	<.0001
Day=3	FOP	-0.10554	0.188	41.7	-0.561	0.8413
	FOP/10	-0.27565	0.190	39.5	-1.450	0.3256
	FOP/100	-0.17011	0.170	30.6	-0.998	0.5837
Day=4	FOP	-0.06516	0.196	43.8	-0.332	0.9411
	FOP/10	-0.08276	0.190	39.5	-0.435	0.9010
	FOP/100	-0.01760	0.179	33.6	-0.098	0.9947
Day=5	FOP	-0.11060	0.225	51.5	-0.491	0.8760
	FOP/10	-0.39078	0.197	43.8	-1.984	0.1283
	FOP/100	-0.28018	0.217	48.0	-1.290	0.4076
Day=6	FOP	-0.06612	0.225	51.5	-0.294	0.9536
	FOP/10	0.05106	0.210	44.6	0.243	0.9679
	FOP/100	0.11718	0.191	39.5	0.614	0.8136
Day=7	FOP	0.04846	0.242	53.9	0.200	0.9782
	FOP/10	-0.00343	0.210	44.6	-0.016	0.9999
	FOP/100	-0.05189	0.211	44.6	-0.246	0.9672

Bacterial abundance (CFU) as a function of time (day) and exposure to different phage dilutions.

Random effects include individual IDs, as well as the cage in which they were reared.

Overall analysis of variance (ANOVA) reveals significant effects of day (p< 2.2e-16), phage dilutions (2.842e-10) and their interaction (p< 2.2e-16).

The post-hoc Tukey comparisons displayed below were performed between mice exposed tovarious phage dilutions within each day.

Statistical analysis of the abundance of phage in feces as a function of time (day) and exposure to FOP dilutions (related to Figure 4D)

Analysis of Deviance Table (Type II Wald chisquare tests)

day: testing difference between the different days

phage: effect of the phage exposure

Response: scale(log10(CFU.g))

	Chisq	Df	Pr(>Chisq)	
day	758.4840	6	< 2.2e-16	***
phage dilution	4.7212	2	0.0943642	***
day:phage	37.5082	12	0.0001847	***

Post-hoc tests: Comparison between "phage" and "no phage" at the different time points

	contrast	estimate	SE	df	t.ratio	p.value
Day=1	FOP	0.4465	0.236	74.9	1.894	0.1475
	FOP/10	0.7946	0.244	74.9	3.259	0.0047
	FOP/100	0.3481	0.202	74.8	1.727	0.2020
Day=2	FOP	0.5673	0.236	74.9	2.407	0.0482
	FOP/10	0.9725	0.244	74.9	3.989	0.0004
	FOP/100	0.4052	0.202	74.8	2.010	0.1169
Day=3	FOP	-0.1917	0.214	74.7	-0.894	0.6459
	FOP/10	0.2810	0.214	74.7	1.310	0.3939
	FOP/100	0.4726	0.192	74.7	2.464	0.0419
Day=4	FOP	-0.1799	0.223	74.8	-0.806	0.7003
	FOP/10	-0.1238	0.214	74.7	-0.577	0.8327
	FOP/100	0.0561	0.201	74.8	0.279	0.9581
Day=5	FOP	0.1336	0.255	74.9	0.523	0.8601
	FOP/10	-0.3067	0.223	74.8	-1.374	0.3597
	FOP/100	-0.4404	0.245	75.0	-1.801	0.1764
Day=6	FOP	-0.3756	0.255	74.9	-1.472	0.3103
	FOP/10	-0.0900	0.236	74.9	-0.382	0.9229
	FOP/100	0.2855	0.215	74.8	1.327	0.3848
Day=7	FOP	0.2517	0.273	75.0	0.920	0.6293
	FOP/10	-0.0787	0.236	74.9	-0.334	0.9405
	FOP/100	-0.3303	0.237	75.0	-1.397	0.3479

Phage abundance (PFU) as a function of time (day) and exposure to different phage dilutions.

Random effects include individual IDs, as well as the cage in which they were reared.

Overall analysis of variance (ANOVA) reveals significant effects of day (p< 2.2e-16), phage dilutions (0.0943642) and their interaction (p=0.0001847).

The post-hoc Tukey comparisons displayed below were performed between mice exposed tovarious phage dilutions within each day.

Statistical analysis of the abundance of strain ST784 in intestinal sections with FOP dilutions (related to Figure 4E)

Analysis of Deviance Table (Type II Wald chisquare tests)

day: testing difference between the different days

phage: effect of the phage exposure

Response: e(log10(CFU.g))

	Chisq	Df	Pr(>Chisq)	
day	33.8027	2	4.569e-08	***
phage dilutions	4.0631	2	0.1311	
day:phage	5.6678	4	0.2254	

Post-hoc tests: Comparison between "phage" and "no phage" at the different time points

	contrast	estimate	SE	df	t.ratio	p.value
Ileum	FOP	-0.1021	0.557	19.1	-0.183	0.9817
	FOP/10	-0.8772	0.527	15.1	-1.665	0.2503
	FOP/100	-0.7751	0.478	12.5	-1.620	0.2737
Caecum	FOP	0.5329	0.557	19.1	0.957	0.6120
	FOP/10	-0.0389	0.527	15.1	-0.074	0.9970
	FOP/100	-0.5718	0.478	12.5	-1.195	0.4773
Colon	FOP	-1.0686	0.557	19.1	-1.919	0.1604
	FOP/10	-0.8052	0.527	15.1	-1.528	0.3061
	FOP/100	0.2634	0.478	12.5	0.550	0.8481

Bacterial abundance (CFU) as a function of gut section and exposure to different phage dilutions.

Random effects include individual IDs, as well as the cage in which they were reared.

Overall analysis of variance (ANOVA) reveals significant effects of *gut section* (p=4.569e-08) but not of the *phage dilutions* (p=0.1311) and their *interaction* (p=0.2254).

The post-hoc Tukey comparisons displayed below were performed between the mice exposed to different phage dilutions within each section.

Statistical analysis of the abundance of phage in intestinal sections with FOP dilutions (related to Figure 4F)

Analysis of Deviance Table (Type II Wald chisquare tests)

day: testing difference between the different days

phage: effect of the phage exposure

Response: scale(log10(CFU.g))

	Chisq	Df	Pr(>Chisq)	
day	19.7282	2	5.201e-05	***
phage dilutions	3.6322	2	0.16266	
day:phage	10.5874	4	0.03161	*

Post-hoc tests: Comparison between "phage" and "no phage" at the different time points

	contrast	estimate	SE	df	t.ratio	p.value
Ileum	FOP	-1.2631	0.649	20.2	-1.946	0.1517
	FOP/10	-2.0008	0.601	20.2	-3.329	0.0089
	FOP/100	-0.7377	0.549	20.2	-1.345	0.3878
Caecum	FOP	0.1604	0.649	20.2	0.247	0.9670
	FOP/10	-0.3865	0.601	20.2	-0.643	0.7983
	FOP/100	-0.5469	0.549	20.2	-0.997	0.5872
Colon	FOP	-0.3273	0.649	20.2	-0.504	0.8701
	FOP/10	-0.3661	0.601	20.2	-0.609	0.8168
	FOP/100	-0.0388	0.549	20.2	-0.071	0.9972

Phage abundance (PFU) as a function of gut section and exposure to different phage dilutions.

Random effects include individual IDs, as well as the cage in which they were reared.

Overall analysis of variance (ANOVA) reveals significant effects of *gut section* (p=5.201e-05) and their interaction (p=0.03161) but not of the *phage dilutions* (p=0.16266).

The post-hoc Tukey comparisons displayed below were performed between the mice exposed to different phage dilutions within each section.